

**School of Civil and Mechanical Engineering  
Department of Civil Engineering**

**Soil Slope Stability Techniques: A Comprehensive Analysis**

**Seyed Reza Azimi**

**This thesis is presented for the Degree of  
Master of Philosophy (Civil Engineering)  
of  
Curtin University**

**September 2016**

## **Declaration**

This thesis contains no material that has been accepted for the award of any other degree or diploma in any university.

To the best of my knowledge and belief this thesis contains no material previously published by any other person except where due acknowledgment has been made.

Signature: .....

Date: .....

## PREFACE

Slope stability is one of the most sophisticated and challenging problems for all disciplines of mining and geotechnical engineering. Over the recent decades, substantial progress in the knowledge and practice concerning slope analysis has been made. Surface failure is both a natural and artificial phenomenon, with little information known regarding the mechanisms behind this failure. The importance of slope stability analysis has increased because of a significant increase in the frequency and consequence of natural hazards.

In this thesis, the necessity of the subject area is presented in Chapter 1. New developments are presented in Chapter 2 that focuses on the latest knowledge, experiences and practices that have been introduced, highlighting several recent developments in slope stability analysis. There has been a gradual increase in the power of computers and significant progress has been made in the development of specialised software based on various methods of slope stability analysis under dynamic and static conditions. In this chapter, a list of different types of slope stability software is described, including a discussion on their advantages and limitations. This opens new windows to the potential capabilities embedded in the image processing methods that are beyond traditional software programs. Thus, a complete description of experimental attempts for shallow failures studies with imaging methods are presented in Chapter 3.

Techniques such as image processing can help researchers analyse and synthesise temporal and spatial data based on the parameters influencing slope stability, with it being necessary for analysts to be aware of new developments. Based on the key importance of uncertainty in slope stability analysis, an increasing role for image processing techniques is ensured. Image processing techniques are crucial for both regional and site-specific studies focusing on slope stability analysis. This thesis employs one of the most popular image processing techniques, so-called partial image velocimetry (PIV), to undertake slope stability investigations as presented in Chapter 4, which shows results and discussion from the experiments. The conclusions obtained from these results are shown in Chapter 5 and recommendations for further research involving this technique are discussed in Chapter 6.

## ACKNOWLEDGEMENTS

I owe my deepest gratefulness to my wife and children for their patience and encouragement. The support and ambition they gave me means a lot. Words can barely express my gratitude to my family, without whose boundless support and care this task would have never been accomplished, particularly to my parents who have been inspiring me for being hardworking and determined. They taught me how to live and appreciate life in the best way. This thesis is a dedication to their kind spirits for practicing tolerance and devotion.

The present study is the consequence of knowledge provided by teachers and lecturers in my entire study life, to whom I always appreciate. I wish to thank Prof. Hamid Nikraz, the supervisor of this research, for his useful comments and encouragement through the guideline process of this research study. He is always quick in response and available to meet. Without his precious supervision this research would never have succeeded. Furthermore, I would like to thank Dr Amin Chegenizadeh for choosing the topic that I am always enthusiastic to work on as well as for the support on the way.

It was a great opportunity to have a support, more than 25 year experience in image processing, from Prof. Peter Kovési. He spent his valuable time, gave me good insight and friendly help regarding MATLAB algorithms and analysis in the image processing chapter. I must offer my appreciation to Zeinab Hajiabolhasani for her suggestions in image processing.

I like to thank the friendly staff members at Curtin University for supporting me in this research. Many thanks to Dr Andrew Whyte, my chairperson and the head of Department of Civil Engineering, for his attention. Special thanks to Mark Whittaker in the Geotechnical Laboratory, Mick Elliss and Mirzet Sehic and Ashley Hughes for their help in manufacturing and fitting parts to equipment and Dianne Garth in administrative jobs.

I have to acknowledge my friend, Dr Alireza Rezagholilou, for sharing his knowledge with me. During the period of this research, many friends helped me to colour my life and with their assistance in many aspects that I cannot list them all because of limited space.

## TABLE OF CONTENTS

	<u>PAGE</u>
1. INTRODUCTION.....	1
1.1. Statement of Problem.....	1
1.2. Aims and Objectives .....	4
1.3. Scope of Work .....	4
2. LITERATURE REVIEW .....	6
2.1. Introduction.....	6
2.2. Limit Analysis.....	6
2.2.1. Method Based on the Extremum Principle .....	8
2.3. Limit Equilibrium Method (LEM).....	8
2.3.1. Swedish Circle Method (SCM).....	10
2.3.2. Infinite slope failures.....	11
2.3.3. Methods of Slices.....	12
2.3.3.1. The Ordinary Method of Slices.....	12
2.3.3.2. Simplified Bishop Method .....	13
2.3.4. Noncircular methods .....	14
2.3.4.1. Janbu's Simplified Method .....	14
2.3.4.2. Spencer's (1967) Method.....	15
2.3.4.3. Morgenstern and Price's (1965) Method .....	15
2.4. Numerical Modelling .....	17
2.4.1. Finite Element Method (FEM).....	17
2.4.2. Distinct Element Method (DEM).....	18
2.4.3. Rigid Element Method (REM).....	19
2.5. Empirical Design.....	20
2.6. Physical Model Tests .....	22
2.7. Probabilistic Methods .....	22

2.8. Image Processing Methods .....	23
2.8.1. Particle Image Velocimetry Analysis.....	26
2.9. Applications and Software .....	26
2.10. Literature Review Conclusions .....	34
3. EXPERIMENTAL METHOD .....	36
3.1. Material .....	37
3.1.1. Soil .....	37
3.1.2. Bentonite .....	40
3.2. Laboratory Tests .....	41
3.2.1. Particle Density .....	41
3.2.2. Direct Shear Test.....	41
3.3. PIV Apparatus Design and Manufacturing.....	44
3.3.1. Base Plate .....	45
3.3.2. Main Framework Support Structure .....	46
3.3.3. Plexiglass Container (Tank).....	48
3.3.4. Water Transmitter and Holes Map.....	48
3.3.5. Implementation Procedure .....	50
3.4. Camera .....	52
3.4.1. Camera Mount.....	54
3.5. Manufactured Apparatus.....	55
3.6. Sample Preparation .....	56
3.7. Apparatus Standardisation Test.....	57
3.8. Apparatus Alignment .....	58
3.9. Preparation before Test .....	58
3.9.1. Test Coding Method.....	58
3.9.2. Sample Coding Method .....	58
3.10. Camera Setup .....	59

3.11. Test Report Sheet .....	59
3.12. Pilot Tests.....	60
3.13. MATLAB Analysis.....	61
3.13.1. MATLAB Code .....	61
3.14. SPSS Analysis.....	66
4. EXPERIMENTAL RESULTS AND DISCUSSION .....	69
4.1. Comparison between Tests with Same Ingredients and Different Alignments ..	69
4.1.1. S-D:(A0-1, A5-1, A10-1).....	69
4.1.2. SB5-D:(A0-2, A5-2, A10-2) .....	76
4.1.3. SB10-D:(A0-3, A5-3, A10-3) .....	78
4.1.4. SB15-D:(A0-4, A5-4, A10-4) .....	81
4.1.5. SB20-D:(A0-5, A5-5, A10-5) .....	83
4.2. Tests Conducted with the Same Alignment and Different Ingredients.....	85
4.2.1. A0-1,2,3,4,5: (S, SB5 , SB10, SB15, SB20 – D) .....	85
4.2.2. A5-1,2,3,4,5: (S, SB5 , SB10, SB15, SB20 – D) .....	91
4.2.3. A10-1,2,3,4,5: (S, SB5 , SB10, SB15, SB20 – D).....	97
4.3. Summary of Results from Image Processing .....	102
4.4. SPSS Analysis Results .....	103
4.5. Calculation of Inclination and Maximum Vertical Displacement Speed.....	113
4.6. Interpretation .....	117
5. SUMMARY AND CONCLUSIONS .....	140
5.1. Influence of Bentonite.....	141
5.2. Benefits of PIV Method .....	142
5.3. Planar Failure Features.....	142
6. RECOMMENDATIONS .....	143
7. REFERENCES.....	144
8. APPENDIX.....	154

## LIST OF FIGURES

### PAGE

Figure 2-1: Slices and Forces in a Sliding Mass .....	12
Figure 2-2: Ordinary Method of Slices (a) different slices (b) forces acting on single slice (Fellenius, 1936) .....	13
Figure 2-3: Forces acting on slice in simplified Bishop method (Bishop, 1955).....	14
Figure 2-4: Janbu’s Simplified Method (Janbu, 1954) .....	14
Figure 2-5: Morgenstern and Price’s Method Effecting Forces (Pulat, 2009).....	15
Figure 2-6: Typical functional variations (Pulat, 2009).....	16
Figure 2-7: Slope height versus slope angle (Hoek & Bray, 1981) .....	21
Figure 2-8: The interaction between the radiative energy emitted by the object and environment rays.....	25
Figure 2-9: A typical telecentric illumination system (Jähne, 2004) .....	25
Figure 3-1: Schematic diagram of the experimental method .....	36
Figure 3-2: Location of the soil resource (GoogleMaps, 2016).....	37
Figure 3-3: Soil grain size distribution graph .....	39
Figure 3-4: Drained soil sample before test .....	40
Figure 3-5: Bentonite package TRUBOND brand.....	41
Figure 3-6: Mohr Circle result for sample S-D (Soil).....	42
Figure 3-7: Mohr Circle result for sample SB5-D (5% bentonite) .....	42
Figure 3-8: Mohr Circle result for sample SB10-D (10% bentonite) .....	43
Figure 3-9: Mohr Circle result for sample SB15-D (15% bentonite) .....	43
Figure 3-10: Mohr Circle result for sample SB20-D (20% bentonite) .....	44
Figure 3-11: Base plate, orthographic layout.....	45
Figure 3-12: Corner view of the main framework structure .....	46
Figure 3-13: Front view of main framework structure, base plate, and winch .....	47
Figure 3-14: Right side view of main framework structure, base plate and winch.....	47
Figure 3-15: Tank container, an orthographic layout.....	48
Figure 3-16: Water transmitter.....	49
Figure 3-17: A corner view of the water tank container .....	49
Figure 3-18: Installation of divider and water transmitter .....	50
Figure 3-19: Front view of designed apparatus .....	51



Figure 3-20: View of the apparatus and saturation driver. A – table structure, B – glass container, C – camera, D – mount camera holder, E – winch force generator, F – soil sample and G – water feeder. ....	51
Figure 3-21: View of designed apparatus with lifting up driver. A – table structure, B – glass container, C – camera, D – mount camera holder, E – winch force generator and F – soil sample. ....	52
Figure 3-22: Gopro Hero3+ camera and water-resistant cover (Hero3 Black edition, 2014)	53
Figure 3-23: Camera flexible mount (Hero3 Black edition, 2014).....	54
Figure 3-24: A front view of the manufactured apparatus.....	55
Figure 3-25: A close view of the apparatus .....	55
Figure 3-26: A view of the water section and winch in the manufactured apparatus .....	56
Figure 3-27: Schematic diagram for apparatus standardisation test .....	57
Figure 3-28: Stable sample .....	59
Figure 3-29: Sample label.....	62
Figure 3-30: Mask area designed to remove unnecessary areas .....	62
Figure 3-31: Rectangular area to optimise sample colour .....	63
Figure 3-32: Separator line shows slope line .....	63
Figure 3-33: Points coordinates for pixels generating the slope line .....	64
Figure 3-34: Setting the slope line in a sheet frame by frame .....	65
Figure 3-35: The graph generated from frame 840 to 891 .....	65
Figure 3-36: Selection of variable parameters in K-Mean cluster analysis .....	66
Figure 3-37: Determination of the number of maximum clusters.....	67
Figure 3-38: Standardisation process.....	67
Figure 3-39: Selection of variables for normalising .....	68
Figure 4-1: Changes in slope stability for different frames with alignment of 0° .....	70
Figure 4-2: Changes in slope stability for different frames with alignment of 5° .....	71
Figure 4-3: Changes in slope stability for different frames with alignment of 10° .....	72
Figure 4-4: Changes in slope stability for different frames with intervals of 50 frames .....	72
Figure 4-5: Changes in slope stability for different frames with alignment of 5° .....	73
Figure 4-6: Changes in slope stability for different frames with intervals of 50 frames .....	74
Figure 4-7: Changes in slope stability for different frames with intervals of 20 frames .....	75
Figure 4-8: Changes in slope stability for different frames with intervals of 20 frames .....	75
Figure 4-9: Changes in slope stability for different frames with alignment of 10° .....	76
Figure 4-10: Changes in slope stability for different frames with intervals of 20 frames .....	77
Figure 4-11: Changes in slope stability for different frames with alignment of 5° .....	77
Figure 4-12: Changes in slope stability for different frames with alignment of 10° .....	78
Figure 4-13: Changes in slope stability for different frames with intervals of 20 frames .....	79

Figure 4-14: Changes in slope stability for different frames with alignment of 5° .....	80
Figure 4-15: Changes in slope stability for different frames with alignment of 10° .....	80
Figure 4-16: Changes in slope geometry for different frames with intervals of 20 frames ...	81
Figure 4-17: Changes in slope geometry for different frames with alignment of 5° .....	82
Figure 4-18: Changes in slope geometry for different frames with alignment of 10° .....	82
Figure 4-19: Changes in slope geometry for different frames with intervals of 20 frames ...	83
Figure 4-20: Changes in slope geometry for different frames with alignment of 5° .....	84
Figure 4-21: Changes in slope geometry for different frames with alignment of 10° .....	84
Figure 4-22: Changes in slope geometry for different frames with intervals of 50 frames ...	85
Figure 4-23: Changes in slope geometry for different frames with 5% bentonite .....	86
Figure 4-24: Changes in slope geometry for different frames with 10% bentonite .....	86
Figure 4-25: Changes in slope geometry for different frames with 15% bentonite .....	87
Figure 4-26: Changes in slope geometry for different frames with 20% bentonite .....	87
Figure 4-27: Changes in slope geometry for different frames with alignment of 20 frames .	88
Figure 4-28: Changes in slope geometry for different frames with 5% bentonite .....	89
Figure 4-29: Changes in slope geometry for different frames with 10% bentonite .....	89
Figure 4-30: Changes in slope geometry for different frames with 15% bentonite .....	90
Figure 4-31: Changes in slope geometry for different frames with 20% bentonite .....	90
Figure 4-32: Changes in slope geometry for different frames with alignment of 5° .....	91
Figure 4-33: Changes in slope geometry for different frames with intervals of 50 frames ...	92
Figure 4-34: Changes in slope geometry for different frames with 10% bentonite .....	92
Figure 4-35: Changes in slope geometry for different frames with 15% bentonite .....	93
Figure 4-36: Changes in slope geometry for different frames with 20% bentonite .....	93
Figure 4-37: Changes in slope geometry for different frames with intervals of 20 frames ...	94
Figure 4-38: Changes in slope geometry for different frames with 5% bentonite .....	94
Figure 4-39: Changes in slope geometry for different frames with 10% bentonite .....	95
Figure 4-40: Changes in slope geometry for different frames with 15% bentonite .....	96
Figure 4-41: Changes in slope geometry for different frames with 20 % bentonite .....	96
Figure 4-42: Changes in slope geometry for different frames with alignment of 10 percent	97
Figure 4-43: Changes in slope geometry for different frames with 5% bentonite .....	98
Figure 4-44: Changes in slope geometry for different frames with 10% bentonite .....	98
Figure 4-45: Changes in slope geometry for different frames with 15% bentonite .....	99
Figure 4-46: Changes in slope geometry for different frames with 20% bentonite .....	99
Figure 4-47: Changes in slope geometry for different frames with intervals of 20 frames .	100
Figure 4-48: Changes in slope geometry for different frames with 5% bentonite .....	100
Figure 4-49: Changes in slope geometry for different frames with 10% bentonite .....	101
Figure 4-50: Changes in slope geometry for different frames with 15% bentonite .....	101

Figure 4-51: Changes in slope geometry for different frames with 20% bentonite .....	102
Figure 4-52: Changes in slope geometry for different frames with intervals of 20 frames .	104
Figure 4-53: Micro failures .....	104
Figure 4-54: Cluster5 - A0-1 - S-D - Intervals of 20 frames .....	108
Figure 4-55: Cluster4 - A0-1 - S-D - Intervals of 20 frames .....	108
Figure 4-56: Cluster9 - A0-1 - S-D - Intervals of 20 frames .....	109
Figure 4-57: Cluster1 - A0-1 - S-D - Intervals of 20 frames .....	109
Figure 4-58: Cluster8 - A0-1 - S-D - Intervals of 20 frames .....	110
Figure 4-59: Cluster6 - A0-1 - S-D - Intervals of 20 frames .....	110
Figure 4-60: Cluster10 - A0-1 - S-D - Intervals of 20 frames .....	111
Figure 4-61: Cluster7 - A0-1 - S-D - Intervals of 20 frames .....	111
Figure 4-62: Cluster2 - A0-1 - S-D - Intervals of 20 frames .....	112
Figure 4-63: Cluster3 - A0-1 - S-D - Intervals of 20 frames .....	112
Figure 4-64: Test A0-1 - S-D - output graph of F840 and F900.....	114
Figure 4-65: Test A0-1 - S-D - output graph of F840 and F900- the selected area to compare.....	114
Figure 4-66: Test A0-1 - S-D - output graph of F840 and F900 - line equation.....	115
Figure 4-67: Test A0-1 - S-D - output graph F840 and F900- Displacement mm.....	116
Figure 4-68: Variation of slope angle and angular velocity with time for test: A0-1, sample: S-D..	118
Figure 4-69: Variation of factor of safety(FOS) with time for test: A0-1, sample: S-D.....	118
Figure 4-70: Variation of slope angle and angular velocity with time for test: A0-2, sample: SB5-D .....	119
Figure 4-71: Variation of factor of safety(FOS) with time for test: A0-2, sample: SB5-D .	119
Figure 4-72: Variation of slope angle and angular velocity with time for test: A0-3, sample: SB10-D .....	120
Figure 4-73: Variation of factor of safety(FOS) with time for test: A0-3, sample: SB10-D	120
Figure 4-74: Variation of slope angle and angular velocity with time for test: A0-4, sample: SB15-D .....	121
Figure 4-75: Variation of factor of safety(FOS) with time for test: A0-4, sample: SB15-D	121
Figure 4-76: Variation of slope angle and angular velocity with time for test: A0-5, sample: SB20-D .....	122
Figure 4-77: Variation of factor of safety(FOS) with time for test: A0-5, sample: SB20-D	122
Figure 4-78: Variation of slope angle and angular velocity with time for test: A5-1, sample: S-D .....	123
Figure 4-79: Variation of factor of safety(FOS) with time for test: A5-1, sample: S-D.....	123
Figure 4-80: Variation of slope angle and angular velocity with time for test: A5-2, sample: SB5-D .....	124
Figure 4-81: Variation of factor of safety(FOS) with time for test: A5-2, sample: SB5-D .	124

Figure 4-82: Variation of slope angle and angular velocity with time for test: A5-3, sample: SB10-D .....	125
Figure 4-83: Variation of factor of safety(FOS) with time for test: A5-3, sample: SB10-D	125
Figure 4-84: Variation of slope angle and angular velocity with time for test: A5-4, sample: SB15-D .....	126
Figure 4-85: Variation of factor of safety(FOS) with time for test: A5-4, sample: SB15-D	126
Figure 4-86: Variation of slope angle and angular velocity with time for test: A5-5, sample: SB20-D .....	127
Figure 4-87: Variation of factor of safety(FOS) with time for test: A5-5, sample: SB20-D	127
Figure 4-88: Variation of slope angle and angular velocity with time for test: A10-1, sample: S-D .....	128
Figure 4-89: Variation of factor of safety(FOS) with time for test: A10-1, sample: S-D....	128
Figure 4-90: Variation of slope angle and angular velocity with time for test: A10-2, sample: SB5-D .....	129
Figure 4-91: Variation of factor of safety(FOS) with time for test: A10-2, sample: SB5-D	129
Figure 4-92: Variation of slope angle and angular velocity with time for test: A10-3, sample: SB10-D .....	130
Figure 4-93: Variation of factor of safety(FOS) with time for test: A10-3, sample: SB10-D.....	130
Figure 4-94: Variation of slope angle and angular velocity with time for test: A10-4, sample: SB15-D .....	131
Figure 4-95: Variation of factor of safety(FOS) with time for test: A10-4, sample: SB15-D .....	131
Figure 4-96: Variation of slope angle and angular velocity with time for test: A10-5, sample: SB20-D .....	132
Figure 4-97: Variation of factor of safety(FOS) with time for test: A10-5, sample: SB20-D .....	132
Figure 4-98: Variation of median (FOS) of jumps with bentonite content for all samples .	139
Figure 5-1: A schematic view of research output procedures.....	141

## LIST OF TABLES

	<u>PAGE</u>
Table 2-1: Slope stability analysis methods (Pulat, 2009).....	16
Table 2-2: Software programs and applications for slope stability analysis.....	27
Table 3-1: Gaskell concrete sand physical properties.....	38
Table 3-2: Gaskell concrete sand sieve analysis.....	39
Table 3-3: Information / Composition on Bentonite ingredients.....	40
Table 3-4: Samples ingredients for direct shear tests .....	41
Table 3-5: Results of Direct Shear tests for samples .....	44
Table 3-6: Gopro Hero3+black resolution (Hero3 Black edition, 2014).....	53
Table 3-7: Application of video resolution (Hero3 Black edition, 2014).....	54
Table 3-8: Test characters sorted by test code .....	60
Table 3-9: Test characters sorted by sample code .....	61
Table 4-1 : K-Mean cluster analysis .....	105
Table 4-2: The conversion of the frame numbers F840 and F900 to a monochrome plan..	113
Table 4-3: Calculation of inclination and maximum vertical displacement speed ..	116

## **1. INTRODUCTION**

### **1.1. Statement of Problem**

From the beginning of civilisation, humans have deliberately attempted to discover more stable areas for their domiciles. With rapid expansion of population size and industrialisation, a sharp increase in establishing infrastructure, such as railways, highways, and roads, has been necessary. To facilitate such developments, human-made cut and fill slopes are ineluctable during the construction process. In the majority of cases, the slopes strongly facilitate the convenience of humans, whereas in other situations, past disasters related to geo-technological problems has been closely related to slope instability.

Soil landslides are known as one of the most common geohazard phenomena in the world, particularly in zones with residual soils that have high potential for sliding. This phenomenon is a crucial problem in many parts of the world because it might damage houses, jeopardise continuity of mining activities, destroy roads, prevent road development projects from continuing, and even harm people and/or lead to loss of life. To protect lives and properties, it is necessary to discover affected area resulting from the failures (Chen et al., 2011). Furthermore, it can effectively help authorities to accomplish prevention measures and mitigate risk of failure or establish early warning systems.

According to the key importance associated with slope stability analysis, different models have been developed. The first mathematical model for slope stability calculation was stated by a French engineer Alexander Collin (1846), after which an influx of new techniques on slope stability analysis occurred. Several techniques such as Taylor and Wood's (1937) model utilised stability charts to evaluate slope stability conveniently and efficiently, while other techniques such as Bishop's (1955) Simplified Method of Slices employed equilibrium of moments. Following this, progress was made by Morgenstern and Price (1965) to consider the equilibrium of moments and forces simultaneously. Parallel inter-slice forces were then considered by Spencer (1967) with computations, and Janbu (1973) who refined the circular slip to be a generalised slip surface. In addition, several models have been developed to

simulate the impact of the friction angle and the fall height of materials on the collapsed volume of soil (Hsü, 1975; Scheidegger, 1973). The factor of safety (FOS) in slope stability analysis is typically employed by researchers to reflect the stability of the soil slope. This factor is defined as the ratio of the ultimate shear strength divided by the mobilised shear stress at incipient failure (Cheng & Lau, 2008). A slope is considered unstable if the FOS is less than one.

However, these models often formulate a failure phenomenon with low accuracy or high vagueness because of the complexity of factors influencing the soil slope stability; therefore, conventional models neglect to apply all available information. Consequently, they inaccurately estimate the FOS because of limited information. The merit of using the particle image velocimetry (PIV) technique is that it formulates a failure by utilising exactly the optical features of the soil slope instead of using analytical and mathematical equations. An initial review of the applications of the PIV technique was investigated by Adrian (1991), which focused on velocimetry measurements in the field of fluid mechanics.

The PIV procedure has emerged as a strong and robust tool for analyses of displacement. In the present thesis, a comprehensive comparison between different procedures is conducted by utilising identical safety factors from the PIV technique. This approach makes it possible to compare the PIV results with those of other techniques.

Despite the fact that the PIV has several drawbacks and limitations, this method is broadly employed in practice. The majority of conventional procedures are two-dimensional (2D), which assume that the failure surfaces are infinitely wide and that the three-dimensional (3D) shear forces are negligible in comparison with the overall resisting and driving forces. The main reason for the popularity of 2D procedures like Bishop's (1955) model, which is based on vertical slices, has arisen from two useful simplifications: (i) the base of each slice passes through just one type of material, and (ii) the slices are narrow enough so the slip surface at the base of each slice can be formulated by a straight line (Akhtar, 2011). Nevertheless, some slope failures have a 3D geometry and are not infinitely wide. Therefore, from a theoretical

point of view, applying a 2D procedure to a 3D problem is conservative for engineering practice.

Previous research has demonstrated that the FOS yields from 3D procedures are generally greater than that from 2D ones (Cavoundis, 1987; Hungr, 1987; Hutchinson & Sarma, 1985), when everything else is equal (Duncan, 1996). Since the shear forces along the two sides of the slide mass are ignored in the analysis of the 2D procedures, these processes might calculate the FOS sufficiently. Nonetheless, in the case of back analyses of slope failures, the results arising from 2D procedures can be significantly different from back-calculated shear strength (Stark & Eid, 1998). Therefore, 3D procedures can be important in situations where: (i) slopes are formed by corners or ridges (Giger & Krizek, 1975; Hungr et al., 1989), (ii) slopes have extra loads (Baligh & Azzouz, 1975; Hungr et al., 1989), (iii) slopes have asymmetry and faults (Stark & Eid, 1998), and (iv) slopes are curved in plan (Baligh & Azzouz, 1975).

Despite the importance of 2D analyses and the widely accepted 2D procedures, only a small amount of corresponding software has been developed, with the majority of these computer programs inferior in practice. However, the accuracy of the 2D analyses strongly depends on the degree to which the analysis reflects soil properties and slope geometry.

The main aim of this thesis was to investigate the capability of an image processing technique, namely PIV, in characterisation of the behaviour of infinite soil slopes and evaluation of their stability. The soil samples included in the study were loose sand having varying clay content that were utilised to investigate fine particles effects. As such, different compositions including without bentonite, 5% bentonite, 10% bentonite, 15% bentonite, and 20% bentonite were examined. The main aim of the research was to immediately and effectively detect and trace the threshold and shape of failures to reduce their adverse effects on slope movements.



## **1.2. Aims and Objectives**

The main aims and objectives of this research are:

- To establish a pilot plant to accomplish the required images of shallow slope stability issues within loose dry sands or sands with clay soils.
- To define a platform for repeatable and traceable tests.
- To determine in detail micro failures in terms of their accurate shapes, distribution and velocities by using PIV for minor movement and particle size analysis.
- To develop an approach that generates digital data from running the captured movies of slope failure in a 2D scale.
- To understand the importance of micro failures in shallow slope stability issues by utilising statistical investigations.

## **1.3. Scope of Work**

To achieve these aims and objectives, the following main tasks were performed:

- Review soil slope stability methods.
- Study soil properties and geometry of shallow slope failures to track the different statuses of surfaces that should be considered for modelling.
- Convert the images into numerical codes using MATLAB software.
- Verify the accuracy of the PIV model and code against real case.
- Compare the soil slope stability analyses resulting from the PIV technique with those obtained from conventional procedures.
- Study the model designed by the PIV technique.
- Analyse the threshold of failures for planar or shallow slopes.

The remainder of this thesis is organised as follows:

Chapter 2 provides a literature review of existing soil slope stability procedures.

Chapter 3 establishes an apparatus design or pilot plant for acquiring the experimental data.

Chapter 4 presents the results of the failure surfaces using PIV method, analyses the impact of shear forces on soil slope stability and discusses the findings.

Chapter 5 summarises the conclusions obtained from the PIV technique.

Chapter 6 illustrates the research contributions and provides directions for future studies.

Chapter 7 contains the reference list, resource information and links.

Chapter 8 contains the appendixes:

Appendix A presents a description of the computer code.

Appendix B shows the SPSS output for test: A0-1 and sample: S-D, for intervals of 20 frames.

Appendix C contains the Material: sand and bentonite, specifications.

Appendix D shows a test report sheet

## **2. LITERATURE REVIEW**

### **2.1. Introduction**

Analysis of slope stability is a key but risky component of civil and mining engineering. The experience of the failure surfaces can teach important lessons to not only understand the causes of failure but also comprehensively evaluate the slope stability. Therefore, methods with high capabilities of modelling sophisticated systems have been developed. Over recent decades, a gradual increase in the power of computers has occurred and significant progress in the development of technical analysis software based on both conventional and modern techniques of slope stability analysis has taken place. Nonetheless, the selection of the proper technique for slope stability assessment is crucial. To achieve this aim, a set of failure observations and field studies is required to determine failure mechanisms to select the most appropriate technique for the analysis.

Slope stability techniques can be categorised into seven sub-sections, consisting of limit analysis, limit equilibrium methods (LEM), numerical modelling, empirical design, physical model tests, probabilistic methods, and image processing techniques.

An extensive review of the literature pertaining to the present research on slope stability techniques is illustrated in this chapter.

### **2.2. Limit Analysis**

For a precise result, the equilibrium and compatibility of the slope need to be simultaneously taken into account. This means that the constitutive equations of the material, strain compatibility equations, differential equations of equilibrium, and boundary conditions of the problem under consideration are required. The limit analysis models a slope stability problem by utilising the concept of the stress-strain relationship based on the assumption that the soil is a rigid structure. Without handling a systematic elasto-plastic analysis, many problems can be solved using this analysis (Cheng & Lau, 2008), and the bound formulas of traditional plasticity concept are applied (Drucker et al., 1951).

Based on the principal concepts of limit analysis, an upper bound solution assumes the failure mechanism is systematically admissible; whereas, a lower bound solution undertakes the mechanism is statically admissible. In addition, control variables are employed to optimise the objective function. Early attempts of limit analysis were made based on systematic or direct algebraic techniques to discover the solutions for analysing the slope stability with the help of soil profile and simple geometry (Chen, 1975). However, for most practical problems, these techniques could not discover the solutions. Therefore, slice techniques have been employed for analysing the upper bound limit (Donald & Chen, 1997).

A combination of both theorems provides a strict bound on the failure include mechanism. According to the potential application of the method, an extraordinary amount of research has been conducted, including Zhao et al. (2016) who utilised the pseudo-static method and the upper bound limit analysis technique to calculate the seismic factor of safety of homogeneous slopes while considering cracks subjected to seismic loading. Gao et al. (2015) presented a kinematic method of limit analysis to assess the influence of the nonlinear failure envelope on 3D stability analysis of homogenous slopes. Lim et al. (2015) used the finite element upper and lower bound limit analysis approach to evaluate 3D slope stability of two-layered undrained clay slopes, while Tschuchnigg et al. (2015) performed slope stability analyses by combining the LEMs and limit analyses to take advantage of both methods. Nian et al. (2016) conducted slope stability analysis based on a technique that integrated the kinematic theorem of limit analysis with strength reduction concept, while Tang et al. (2015) used the upper bound limit analysis theory to analyse slope stability. The impacts of 3D conditions on reinforced structure stabilised were considered by Gao et al. (2016) who utilised a limit analysis approach to determine the length of reinforcement and the required strength. A nonlinear failure criterion based on an upper bound analysis finite element method (FEM) for assessing slope stability was developed by Yang and Chi (2013).

A new failure mechanism using the upper bound limit analysis was proposed by Huang et al. (2013) to evaluate the stability of slopes with weak interlayers. Liu et al. (2011) utilised the upper bound limit analysis to obtain the safety factor using

nonlinear constrained optimisation. Although the lower and upper bound limit analysis can bound the true failure load, this method cannot predict the displacement of the slope (Liu et al., 2011).

### **2.2.1. Method Based on the Extremum Principle**

The determination of the inter-slice force function by the user before the analysis process is the most critical limitation of the LEM. Therefore, lower bound techniques have been developed. These techniques state that any statically admissible stress field not exceeding the yield will be a lower bound of the final condition (Cheng & Lau, 2008). However, because of redistributing the internal forces to prevent failure, stability analysis of the soil mass leads to a maximum safety factor for any surface failure. This is known as the extremum principle or maximum variational. Conversely, for any given slip surface, the most likely slip surface is connected with the minimum safety factor. This is known as the minimum variational or extremum principle, corresponding to the upper bound method (Cheng & Lau, 2008). Two techniques have been developed for the implementation of the maximum extremum principle having different local and single factor of safeties.

The extremum principle technique has been applied by different researchers. Cheng et al. (2013) utilised the limit equilibrium formulations by using the extremum principle and the external and internal components to bearing capacity and slope stability issues. Xiao et al. (2011) determined potential slip surfaces in soil slopes by combining limit equilibrium theory and numerical analysis in the form of a precise method. To achieve this, the extremum principle and Coulomb's strength principle based on the ratio of the shear strength to the shear stress at any point were applied to compute the direction of the critical slip surface at that point in a slope. However, this technique is unable to investigate the displacement of the slope (Xiao et al., 2011).

### **2.3. Limit Equilibrium Method (LEM)**

The most general method in slope stability analysis is the LEM (Cheng & Lau, 2008). Based on the primary concept of the LEM, a division process of the sliding

mass into sections is required to compute a safety factor for a specific failure, which is known as the method of slices. To compute the driving or resisting force or moment, equilibrium conditions are performed for each slice. The summation of the values pertaining to all resisting and driving moments and forces are calculated for the computation of the total factor of safety. The ratio between these two sums can be defined as the safety factor,  $F$  :

$$F = \frac{\sum(\text{resisting forces})}{\sum(\text{driving forces})} \quad 2-1$$

The merit of using a FOS is that the slope stability is clearly calculated by a numerical value. Based on the safety factor equation, failure is possible when a FOS of less than one is obtained. A total FOS less than one, calculated by different failure surfaces or several potential failure modes, indicates that the slope could fail.

Based on the classical concepts of soil slope stability, the FOS is usually constant along the slip surface. Hence, the average value is utilised instead of the actual one, which might fluctuate along the failure surface. Several models have been introduced to formulate the FOS where this factor can change along the slip surface. A procedure based on the framework of the LEM for determining a variable FOS in analysing the slope stability was proposed by Chugh (1986). However, this model follows a process that employs several assumptions that have no strong theoretical background.

Conventionally, failure computations are based on the assumption that defines a circular failure. Although this assumption is accurate for many homogenous soils, the assumption cannot be accurate in many real world situations where soil is heterogeneous or a complex geometry is formed. In such situations, noncircular failures are much more likely. Several methods have been developed for computation of FOS by applying the slicing process. The LEM has been employed by different researchers, including Agam et al. (2016) who determined the impact of varying parameters values on the safety factor by using Spencer's and General Limit Equilibrium methods of slices and Mohr-Coulomb failure criterion, while Zhou and Cheng (2015) analysed the stability and the displacement of 3D creeping slopes using a novel displacement-based rigorous limit equilibrium method.

A new method combining the rigorous LEM and the pseudo-dynamic method was proposed by Zhou and Cheng (2014) to investigate stability of 3D seismic landslides, in which the force equilibrium conditions along three coordinate axes and the overall moment equilibrium conditions around three coordinate axes were all strictly satisfied. In an earlier study, Zhou and Cheng (2013) utilised inter-column forces based on six equilibrium conditions to develop the rigorous limit equilibrium column method, which includes three directional moment equilibrium conditions around three coordinate axes and three directional force equilibrium conditions along coordinate axes. Conti and Viggiani (2013) described a new pseudo-static limit equilibrium approach for analysis and design of cantilevered retaining walls for seismic loading, while Shamsabadi et al. (2013) estimated seismic earth pressures due to earthquake-induced pseudo-static body forces by using a method of slices. Wei et al. (2009) applied the LEM and the strength reduction method to analyse 3D slope stability for several cases. LEMs can be divided into three main techniques, including the Swedish circle method (SCM), methods of slices, and noncircular methods. However, there is not one codified rule to demonstrate which method is the best; however, it is generally true that noncircular methods are better because they consider the internal forces more carefully. There is a general principle that the noncircular methods will usually be better than the others are because it considers more carefully the internal forces. Despite some differences between these methods, many researchers have discovered that the results obtained are approximately the same (Cheng et al., 2008; Morgenstern, 1992).

### **2.3.1. Swedish Circle Method (SCM)**

The SCM was established on the assumption that the failure surface is a circular and the FOS is calculated by summing the moments about the centre of the circle. This method, which was first applied by Petterson in 1916 and formalised by Fellenius in 1992 (Duncan et al., 2014), assumes that the friction angle is equal to zero. Otherwise, the shear strength, mathematically shown as the following equation, only results from cohesion ( $\phi = 0 \rightarrow \tau = c_d$ ):

$$\tau = c_d + \sigma \tan \phi_d \quad 2-2$$

where,

$$c_d = \frac{c}{F} \quad 2-3$$

and

$$\tan \phi_d = \frac{\tan \phi}{F} \quad 2-4$$

The variables  $c_d$  and  $\phi_d$  represent the developed cohesion and friction angle, respectively;  $c$  and  $\phi$  are the cohesion and friction angle for the soil, respectively; and  $\sigma$  is the total normal stress on the shear plane. The SCM is an appropriate tool for analysing short-term stability of both homogeneous and heterogeneous slopes (Duncan et al., 2014).

### 2.3.2. Infinite slope failures

Shallow landslides are a type of slope failure that might be induced by rainfall infiltration, which causes changes in total suction (i.e. the sum of matric and osmotic suctions) and soil properties, such as soil shear strength and pore fluid (e.g. air, water, and dissolved air in water and menisci) properties, in a process where the mechanism of change (from unsaturation to saturation and back to unsaturation) is still not clearly understood. Extensive studies completed by numerous researchers have occurred over the years, both in the field and in the laboratory (Abramson, 2002, pp. 658–659).

A few standard codes have been developed to analyse shallow slope stability. The country of Los Angeles developed a well-known set of standard codes as follows:

$$\mathbf{FOS} = \frac{c' + (\gamma_t - \gamma_w)z_w \cos^2 \alpha \tan \Phi'}{\gamma_t z_w \sin \alpha \cos \alpha} \quad 2-5$$

Where

$c'$  = the effective cohesion;  $\Phi'$  = the effective friction angle;  $z_w$  = the vertical depth of saturated soil;  $\alpha$  = the slope angle;  $\gamma_t$  = the total unit weight; and  $\gamma_w$  = the unit weight of water.



If cohesion is neglected, then:

$$\text{FOS} = \left(1 - \frac{\gamma_w}{\gamma_t}\right) \frac{\tan\phi'}{\tan\alpha}$$

2-6

### 2.3.3. Methods of Slices

For the methods of slices, a number of solution techniques have been developed. The primary difference among all techniques arises from the equations of the considered statics, the included interslice normal and shear forces, and the presumed correlation between the inner slice forces (Krahn, 2003). A typical slice in a potential sliding mass with the forces acting on the slice is depicted in Figure 2-1. The real number of slices that is utilised is based on geometry and profile of slope earthfill (Duncan et al., 2014).

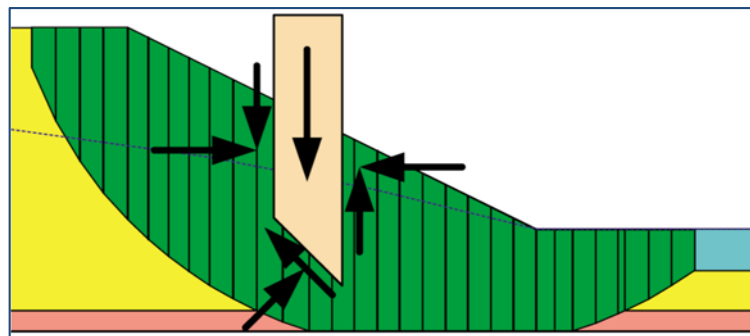


Figure 2-1: Slices and Forces in a Sliding Mass

A number of the methods of slices formulate a slope stability problem focused on the assumption that the slip surface is a circular slip surface; whereas, a noncircular slip surface is assumed by the others. The former considers the equilibrium of moments about the centre of the circle, while the latter considers the equilibrium in terms of the individual slices (Duncan et al., 2014).

#### 2.3.3.1. The Ordinary Method of Slices

This approach is also known as the Fellenius method or Swedish method of slices. This method is a procedure of slices that neglects the forces on the sides of the slices (Figure 2-2). As shown in Figure 2-2(a), the failure surface is divided into a number of imaginary upright slices. In this method, the computational method for calculating the factor of safety is simple and straightforward according to:

$$F = \frac{\sum \{c' \times l + \tan \phi' (W \times \cos(\alpha) - u \times l)\}}{\sum W \times \sin(\alpha)}$$

2-7

where  $c'$  is the effective cohesion;  $l$  denotes the slice base length;  $\phi'$  is the effective friction angle;  $W$  denotes the weight of the slice;  $u$  expresses the pore water pressure, and  $\alpha$  denotes the angle between the tangent of the center of the base of the slice and the horizon (Fellenius, 1936).

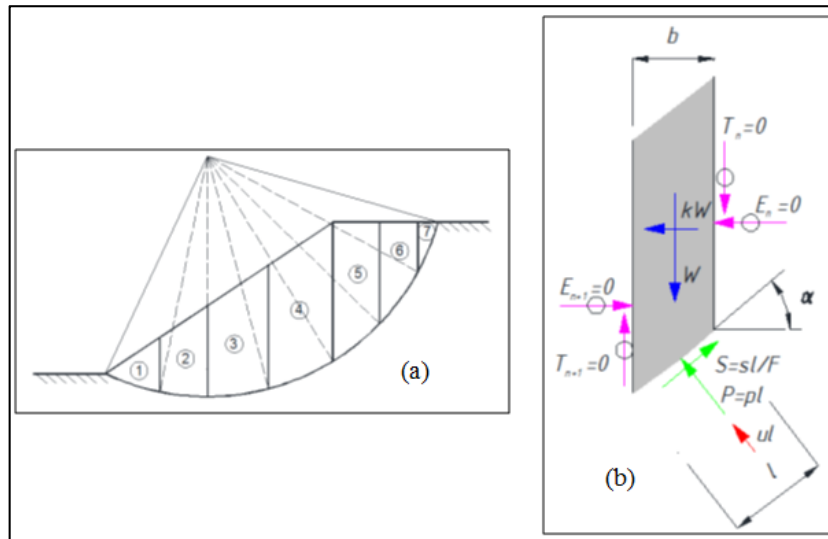


Figure 2-2: Ordinary Method of Slices (a) different slices (b) forces acting on single slice (Fellenius, 1936)

### 2.3.3.2. Simplified Bishop Method

The simplified Bishop method, proposed originally by Bishop (1955), is based on the statement that the forces on the sides of the slice are flat. Therefore, it is assumed that no shear stresses exist between slices. Figure 2-3 depicts the slice with the forces considered by the simplified Bishop method, where the total moment equilibrium about a centre of rotation and vertical force equilibrium equation of each slice are applied for determination of the unknown forces.

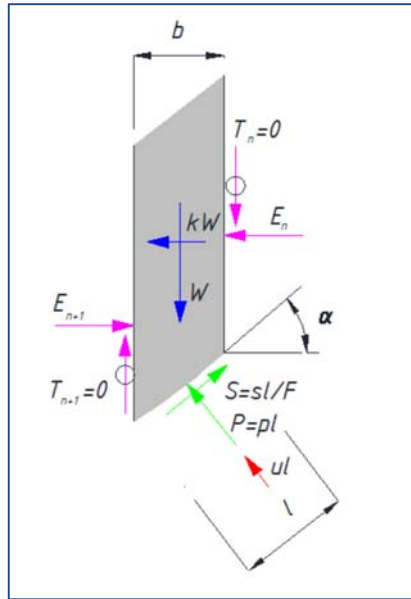


Figure 2-3: Forces acting on slice in simplified Bishop method (Bishop, 1955)

### 2.3.4. Noncircular methods

#### 2.3.4.1. Janbu's Simplified Method

Janbu's simplified method only considers total horizontal force-equilibrium, instead of total moment equilibrium (Figure 2-4). This method is similar to the Bishop method in that it only takes into account two of the three equations of the equilibrium problem. Since force equilibrium is sensitive to the forces on the sides of the slice, Janbu's simplified method which ignores these forces gives a less accurate result for circular slip surfaces.

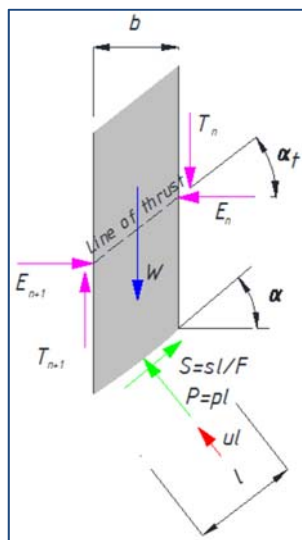


Figure 2-4: Janbu's Simplified Method (Janbu, 1954)

#### 2.3.4.2. Spencer's (1967) Method

Spencer's method, which was first developed for circular surfaces, takes into account all conditions of equilibrium, including moment equilibrium, vertical and horizontal force equilibrium. This method extends to model noncircular surfaces and assumes that all forces on the sides of the slice are parallel.

The Spencer's method separately uses the moment equilibrium and horizontal force equilibrium to derive two FOS. The FOS resulting from the moment equilibrium are close to that from the simplified Bishop technique, and from the Janbu's simplified method (Spencer, 1967).

#### 2.3.4.3. Morgenstern and Price's (1965) Method

In Morgenstern and Price's (1965) method, all normal, tangential and moment equilibrium are considered for each slice in the circular and noncircular slip surfaces. This method generates two FOS, similar to the Spencer's method, based on moment and horizontal force equilibrium. Since the Morgenstern and Price's (1965) method takes into account force and moment equilibrium, as well as the forces on the sides of slice, the results are more robust for slope stability analysis (Figure 2-5).

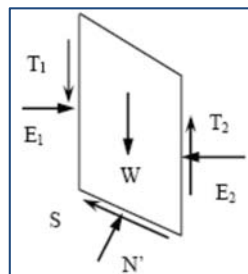


Figure 2-5: Morgenstern and Price's Method Effecting Forces (Pulat, 2009)

Morgenstern and Price's method is similar to the Spencer method if the interslice function is constant. Figure 2-6 presents the usual functional variations for the direction of the interslice force against  $x$ .

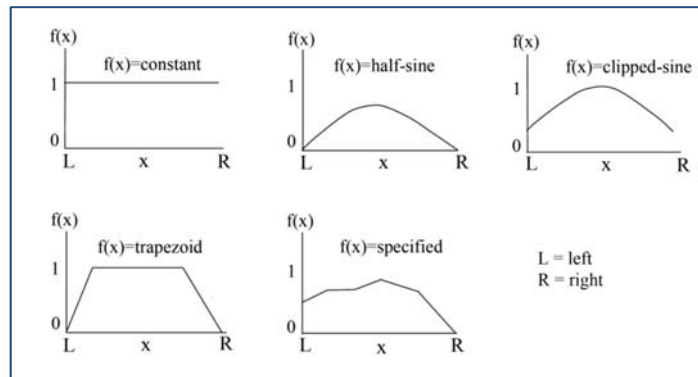


Figure 2-6: Typical functional variations (Pulat, 2009)

Table 2-1 comparative analysis between various methods of stability analyses, including the equilibrium condition of forces and moments.

Table 2-1: Slope stability analysis methods (Pulat, 2009)

No	Methods	Moment Equilibrium	Force Equilibrium	Inter Slice Normal Forces	Inter Slice Shear Forces	Moment Factor of Safety	Force Factor of Safety	Inter Slice Force Function
1	Ordinary method of slices	Yes	No	No	No	Yes	No	No
2	Simplified Bishop method	Yes	No	Yes	No	Yes	No	No
3	Janbu's Simplified method	No	Yes	Yes	No	No	Yes	No
4	Spencer's method	Yes	Yes	Yes	Yes	Yes	Yes	Constant
5	Morgenstern and Price's method	Yes	Yes	Yes	Yes	Yes	Yes	Constant Half-Sine Clipped-Sine Trapezoidal Specified

However, before using a method for slope stability assessment, it is necessary to understand its limitations. The main limitations of the LEMs for slope stability analysis are based on the assumptions that the soil mass behaves as a rigid material and that shear strength is developed simultaneously along the failure surface.

## **2.4. Numerical Modelling**

When using numerical modelling, different equations and conditions can be considered in the process of the problem formulation, including strain compatibility equations, constitutive equations for material, differential equations of equilibrium, and boundary conditions of the problem under consideration (Krahn, 2003). One of the main advantages of numerical modelling is that it computes both the displacement and the stress resulting from external loads. For the formulation of complex slope geometry, numerical modelling can result in a better result when compared to analytical models or LEMs (Bobet, 2010).

A number of numerical techniques have been developed to model the slope stability problem. The FEM, which is a continuum model, and the distinct element method (DEM), which is a discontinuum model, are two popular numerical techniques (Adhikary et al., 1996). In a continuum model, the displacement field is continuous and the focus of shear strain reflects the location of the failure surface, whereas in a discontinuum model, the geometry basic model contains discontinuities, with the location of these discontinuities, as an input, compulsory for consideration in the analysis (Shen et al., 1995).

### **2.4.1. Finite Element Method (FEM)**

Frequently, conventional methods cannot estimate the progressive failure phenomenon. To overcome this limitation, the FEM has been proposed, with two key applications developed for analysing slope stability. The first application is to apply the body force due to the soil to the slope system for accomplishing an elasto-plastic stress analysis. After determination of the stresses, the stresses and the Mohr–Coulomb criterion can then be applied for the calculation of local safety factors. In addition, the actual driving force and the ultimate shear force can be utilised to define the overall FOS. It should be noted that both the FOS and the location of the critical

failure surface from the finite element analysis are usually close to those from the limit equilibrium (Cheng & Lau, 2008). The second application is the strength reduction method (SRM), in which the gravity load vector for a material with unit weight  $\gamma_s$  can be defined as follows:

$$\{f\} = \gamma_s \int [N]^T dv \quad 2-8$$

where  $\{f\}$  indicates the equivalent body force vector and  $[N]$  represents the shape factor matrix.

The main benefits of the SRM are: (i) the critical failure surface is automatically determined from the localised shear strain arising from the application of gravity loads and the reduction of shear strength; (ii) it requires no assumption on the interslice shear force distribution; (iii) it covers many complex different soil states; and (iv) it can calculate parameters such as stresses, displacement and pore water pressures that cannot be derived using LEM (Cheng & Lau, 2008). However, the main disadvantage of the SRM is that it poorly captures the localised shear band formation.

The FEM has been employed by a number of researchers, including Shamekhi and Tannant (2015) who utilised FEMs to assess slope stability and Lu et al. (2015) who applied a numerical method using the FEM to evaluate slope stability during seismic loading. Tang et al. (2015) applied the SRM for developing an approach to assess slope stability.

#### **2.4.2. Distinct Element Method (DEM)**

The FEM, based on continuity theory, is not applicable for slope stability analysis. The DEM, however, is capable of providing a qualitative assessment to estimate the complete failure mechanism (Cheng & Lau, 2008). This method employs an approach based on a set of triangular rigid blocks or particles. However, analysing large numbers of rigid blocks or particles is a time-consuming process. Therefore, a limited number of particles or rigid blocks, ranging from 10000 to 100000, can generally be employed in the process of computations.

In the system of the FEM, the movement history of a system can be qualitatively assessed from initial displacement to an entire failure. Although it is difficult to assess a FOS using the DEM, it can assess the collapse mechanism, whereas conventional techniques are unable to assess this mechanism.

A computer program was developed by Javan (2015) to perform stability analysis of a rock slope using the DEM, while Moosavi (2009) utilised a DEM to analyse the slope stability of the west wall of a Sarcheshmeh copper mine (Moosavi, 2009). Chang (1992) presented the DEM for slope stability analysis, and Shen and Abbas (2013) used the DEM software UDEC to model the slope based on the shear strength reduction method to compute the slope stability safety factor. Botero-Jaramillo et al. (2014) used the DEM as a tool to detect stability problems in deep spillways. However, the process of the simulation of a complex problem is a cumbersome and time-consuming process.

#### **2.4.3. Rigid Element Method (REM)**

The REM, also known as the rigid body-spring model (RBSM) proposed by Kawai (1978), was initially developed from the DEM (Cundall, 1971). This technique is also known as the interface element method and rigid finite element method (RFEM). Although the process of discovering a solution for a problem in the system of the REM is similar to that in the traditional FEM, the REM employs elements and interfaces as a replacement of nodes and elements in the FEM.

The REM models a problem based on the assumption that each element is rigid. In this method, a problem is divided into an appropriate number of rigid elements bilaterally linked at the interfaces. Displacement of any point in a rigid element can be explained by a series of the sliding and rotation of the particle centroid (Cheng & Lau, 2008). Based on the high potential of the REM, different researchers have employed this technique to solve slope stability problems. Zhang and Qian (1993) developed the RFEM to model the mechanical behaviour of discontinuities structures such as bedding joints and structural discontinuities. These authors then utilised the RFEM for analysis of stability and proposed a slope stability method based on lower bound limit analysis with the rigid elements to evaluate the stability of slopes.



This method has also been applied by different practical and theoretical researchers. Liu and Zhao (2013) presented a numerical limit analysis on the slope stability using the RFEM. Zhang (1999) used the RFEM to analyse slope stability, while Merati (2015) developed a combination approach based on RFEM and limit analysis methods to assess the slope stability. Lingxi and Xiong (1995) proposed a RFEM model for the mechanical behaviour of discontinuities such as joints and beddings. However, the simulation of a sophisticated problem using the REM is a time-consuming process.

## **2.5. Empirical Design**

To analyse a simple homogeneous slope, the FOS can be extracted from a stability table or figure without using a computational process or computer software. An early attempt was made by Lutton (1970) to develop an organised classification of empirical data. According to the high potential of stability figures and tables in slope stability, several types of figures and tables have been proposed. The most famous tables and figures have been prepared by Chen (limit analysis), Morgenstern (Spencer method), Taylor (friction circle), and Cheng (2008). Generally, the stability tables and figures often obtain results that are sufficiently close to each other. However, these tables and figures are usually developed for analysing 2D problems. Hoek and Bray (1981) extended slope angle features the dataset and plotted the slope height against the slope angle as depicted in Figure 2-7.

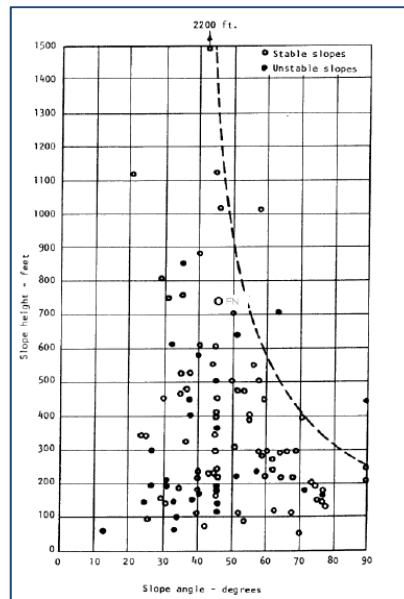


Figure 2-7: Slope height versus slope angle (Hoek & Bray, 1981)

From the figure, the dotted line estimating the upper limit for stable slopes is depicted. When the height of the slope increases, the slope angle must be decreased to maintain slope stability. However, this is not always possible as the angle of slopes is almost constant, especially when higher slopes are considered, which demonstrates that there is a limit to the slope angle. This possibly arises from the fact that there is a lack of information for higher slopes. Therefore, since several unstable slopes are located below the design curve, the design curve is somewhat arbitrary.

This method has been widely utilised by different researchers, including Jiang et al. (2016) who utilised the Hoek-Brown failure criterion to develop a chart-based seismic stability analysis method and Tang et al. (2015) who presented stability charts of homogeneous isotropic slopes to analyse slope stability.

Shen et al. (2013) presented new stability charts based on the generalised Hoek–Brown criterion for the analysis of slope stability; with these charts proposed for computing the FOS of a slope for a specified slope angle of 45°. Eid (2014) developed charts based on the results of an elaborated parametric study for evaluating the stability of homogenous earthfill slopes with nonlinear shear strength failure criterion. However, the empirical design charts only provide a general view of the slope stability analysis and cannot establish information that is more detailed.

## **2.6. Physical Model Tests**

Physical model tests have been developed for solving the problems and costs pertaining to full scale testing. These tests simulate the conditions of a real slope under a controlled environment, where the influence factors can simply vary and corresponding impacts on the slope stability are comprehensively analysed. The method provides an opportunity for studying the effects of unknown parameters that might be time-consuming and bothersome in the field (Springman, Laue, & Seward, 2010).

Since calculation of the slope angle is only possible indirectly, the physical model test is not an accurate tool. To overcome this drawback, several tests with varying slope angles have been accomplished to create a comparison analysis. A physical model is well known as a strong and successful tool that significantly increases the knowledge and understanding of possible failure modes (Springman, Laue, & Seward, 2010).

A number of researchers have used physical model tests to analyse the slope stability. Resnick and Znidarčić (1990) developed a centrifugal modelling technique to study the influence of drains on slope stability. They noted that there was good agreement between the observed phenomena and the analysis. Chen and Liu (2007) presented both modelling and laboratory means to evaluate slope stability behaviours and traditional slope stabilisation tests. However, physical model tests do not provide a precise design for the simulation of the accurate loading conditions, although they are useful for the analysis of the fundamental failure mechanism and the verification of numerical and analytical methods.

## **2.7. Probabilistic Methods**

The basic motivation for development of probabilistic approaches for slope stability analysis is to recognise the variation of factor weights based on natural variations.

Although these variations can be calculated using a sensitivity analysis, this analysis cannot quantify the chance of a slope failure. Based on the principal concepts of a

probabilistic method, the chance or probability of a slope failure is computed by means of the stochastic nature of the input components.

The chance of a slope failure is probable when the probabilities of failure are higher than the safety factors. This is more realistic than considering a certain FOS as either stable or unstable. In addition, a risk or decision analysis can be conducted using a quantitative description of the failure probability. The probabilistic methods have been broadly applied by different researchers.

Shou and Wang (2003) studied the failure of the Chiufengershan landslide and proposed a Monte Carlo analysis to investigate the residual slope. The probability tests revealed that the residual slope was more critical than the static analysis of slope and needs to be investigated carefully. A probabilistic approach was proposed by Leynaud and Sultan (2010) using a modified version of a 3D slope stability software to account for complex geometry, while Hannachi et al. (2015) presented a probability analysis using the Monte Carlo modelling approach of uncertainty. Stankovic (2013) applied two widely used methods in probabilistic analysis of slope stability in an open pit mine “Potrlica”, Pljevlja in Monte Negro, including Monte Carlo simulation and First Order Reliability Method enforced with the Response Surface Method. Low (2003) developed a practical probabilistic technique for slope stability analysis and Griffiths and Fenton (2004) studied the probability of failure of a clayey slope using various probabilistic analysis methods.

However, probabilistic methods use distribution functions that require a large amount of input data and assumptions. These methods are based on the LEM and have the same limitations as the LEM do. Likewise, practical applications of probabilistic methods are limited because of the vast amount of input data required to run such methods. However, increasing the amount of required data leads to increasing the rendering time.

## **2.8. Image Processing Methods**

Image processing is the processing of images employing mathematical methods to fulfil a set of operations on a specific image. These operations are performed for the purpose of extracting valuable information or obtaining a reduced or enhanced

image. Image processing is a typical form of signal processing whereby the input is an image (picture), a video, or a series of images and the output can be either an image or features (characteristics) pertaining to the image.

In modern technologies, image processing is a rapidly growing technique because of the increasing importance of visual sciences and large scale scientific data (Gonzalez & Woods, 2008). Image processing techniques are divided into two main methods, which are analogue and digital. The analogue method is applied to the hard copies, whereas the digital method employs computer systems to manipulate digital images. Before using a digital method, three structural analyses are conducted on all types of data, comprising pre-processing, enhancement and display. Digital image processing includes three steps: (i) importing the image via image acquisition methods; (ii) analysing and utilising the image; and (iii) reforming the resulting image or account that is based on image processing (Jain, 1989).

Image analysis is the most important phase in digital image processing. In this phase, quantitative measurements from an image are completed to develop a description and formulate a proper decision. The image analysis method requires an extraction of specific characteristics to identify the object. Quantitative measurements of object characteristics help to classify and describe the image. A digital image processing system gathers the radiative energy emitted by a certain object to make it visible (Gonzalez & Woods, 2008). The radiative energy can comprise of a flow of acoustic waves, electromagnetic waves and particles.

Generally, in the classical computer vision, the object feature of interest is analysed as a systematic approach based on what is available; whereas, in the scientific visual system, a different approach is required.

Figure 2-8 depicts that the ray emitted by an object can be influenced by environmental radiations. By refraction of the ray produced by the object, the position of the object might be changed. As shown in the figure, the scattering and absorption processes can lead to attenuation of the radiation fluctuations. As a result, the observations can be falsified. To obtain an accurate result, additional effects should be minimised (Jähne, 2005).

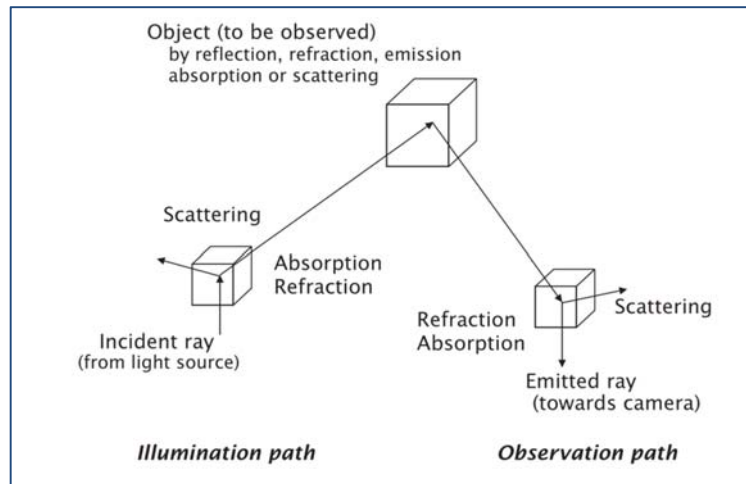


Figure 2-8: The interaction between the radiative energy emitted by the object and environment rays (Jähne, 2005)

Based on the primary concepts of image processing, the surface normal vector can describe the surface slope. An illumination system, known as telecentric, is applied for converting a radiant distribution into a set of parallel beams, with this playing a key role in surface slope measurements (Figure 2-9). From the figure, it is obvious that a parallel set of lights results from the rays emitted by a single point. The angle of the light bundle with the optical line is calculated from the location on the focal plane (Jähne, 2004).

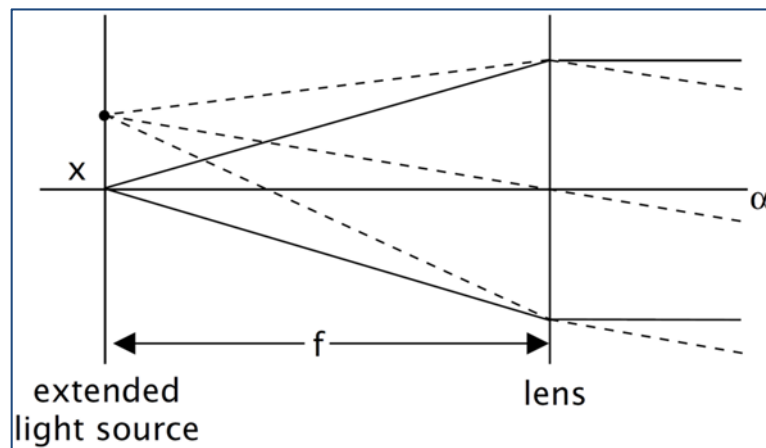


Figure 2-9: A typical telecentric illumination system (Jähne, 2004)

While techniques of flow visualisation have been used from the beginning of hydrodynamics, measurable analysis of image sequences to determine flow

parameters has only become available recently (Jähne, 2004). Particle image velocimetry (PIV) is the standard technique for analysis of flow components.

### **2.8.1. Particle Image Velocimetry Analysis**

PIV was initially developed in the 1980s to compute flow fields instantly (Adrian, 1991) and is based on design matching of two successive images irrespective of whether the pictures are obtained from a fluid or solid element (Baba & Peth, 2012). This method employs an optical evaluation system that utilises visible flow and digital images. One benefit of PIV is that it provides instantaneous high-resolution flow velocity vector data of the overall plane in the flow (Stamhuis, 2006).


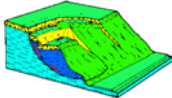
The main proposal of the PIV method is to obtain consecutive digital images from the sensors employed in digital cameras and video cameras to record standing and moving images. These images can then be analysed by a computer program to determine velocities of the tracer particles. This technique has considerable potential for observing full flow.

Although the PIV method was originally applied in fluid mechanics, based on the capability and effectiveness of the method, further research and practicality studies by engineers and researchers occurred (e.g. Adam et al., 2005; Anastasopoulos et al., 2007; Baba & Peth, 2012; Barends, 2011; Bridgwater, 2012; Cameron, 2011; Chen et al., 2011; Dejong et al., 2006; Hossain & Fourie, 2013; Hossain et al., 2005; Lu et al., 2013; Mickovski et al., 2010; Peth et al., 2010; Raffel, 2007; Schroeder et al., 2008; Take & Bolton, 2011; Tejchman, 2010; White et al., 2001, 2003, 2013; Wijewickreme et al., 2009; Win, 2012).






## **2.9. Applications and Software**






Related applications and software for analysing slope stability are presented in Table 2-2, with each of these applications designed for a specific purpose.





**Table 2-2: Software programs and applications for slope stability analysis**

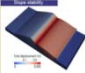


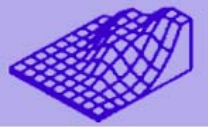

Software Name	Details
<p>SLOPE/W (Slope Stability Analysis with SLOPE/W, 2016)</p> 	<p>A software product generated by GEO-SLOPE International Ltd. Company, located in Alberta-Canada. This software analyses slope stability by calculating the safety factor of earth and rock slopes. This program can efficiently study both simple and composite failure mechanisms for a wide range of problems. The software uses limit equilibrium to model a problem under consideration by applying deterministic or probabilistic input parameters. In addition to the limit equilibrium, this software can utilise the finite element stress analysis to generate a more appropriate analysis.</p>
<p>Slope Stability Analysis Program (SSAP2010 (rel. 4.7.2 - 2016), 2016)</p> 	<p>This is a free software program that implements a series of characteristics using the LEM. The software includes different types of reinforcements, taking into account their effects in the safety computations.</p>
<p>GSTABL7 (GSTABL7 with STEDwin Gregory Geotechnical, 2016)</p>	<p>This software, developed by Gregory Geotechnical Software (2001), is powerful stability analysis software that is an extended version of the STABL program designed at Purdue University (1988). This software uses the method of slices in the form of a 2D limit equilibrium analysis to compute the safety factor using four procedures, including the modified Bishop, simplified Janbu, Spencer, and Morgenstern-Price methods, in which the first method is applied for circular failure surfaces and the last three methods are employed for circular, random, or sliding block failure surfaces.</p>



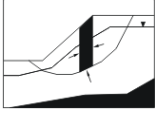





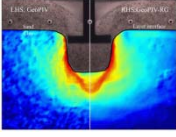

Software Name	Details
<p>ZSoil (Zace Services Ltd ZSoilPC software for geotechnics and geomechanics , 2016)</p> 	<p>Produced by Zace Services Ltd. Company in 1985 this computer software was designed for modeling rock and soil mechanics, comprising displacements, flow and dynamics. ZSoil software is written for MS-Windows environment and achieves slope stability analysis based on the finite-element method.</p>
<p>midas GTS (midas GTS NX   Geotechnical Analysis New Experience, 2016)</p> 	<p>This program was developed for geotechnical engineering applications employing finite element analysis to handle both 2D and 3D slope stability analysis.</p>
<p>GEO5 (Geotechnical Software GEO5   Fine, 2016)</p> 	<p>This software employs analytical technique and FEM to evaluate slope stability, with analytical methods helping users to design structures efficiently. The planned structure can be entered into the FEM computations so that the common analysis of the structure can be fulfilled.</p>
<p>VERSAT-2D (Wu, 2013)</p> 	<p>A software package that comprises three computer processors, including VERSAT-D2D, VERSAT-2D and VERSAT-S2D. The VERSAT-2D program is used to generate input data for VERSAT-S2D and VERSAT-D2D. The program uses the FEM to conduct slope stability analysis.</p>
<p>TAGAsoft</p>  <p>(Geotechnical Software - 3D Slope Stability – Geotechnical Software for a 3D World, 2016)</p>	<p>This was developed by Robert Pyke (1981), who is a geotechnical engineering consultant, in Berkeley, California.</p>

Software Name	Details
<p>TSLOPE (Geotechnical Software - 3D Slope Stability – Geotechnical Software for a 3D World, 2016)</p> 	<p>This is a limit equilibrium based program, which can handle slope stability analyses in either 2D or 3D.</p>
<p>SVSlope® (SoilVision Systems - Geotechnical Finite Element Software - SVSLOPE®, 2016)</p> 	<p>This is a program based on LEM that allows users to perform slope analysis by the method of slices or several stress-based methods. It uses both stress-based and LEMs for slope stability analysis. For determination of the correct location of the critical slip surface, the program employs advanced searching methods.</p>
<p>Slope (Oasys Software , 2015)</p> 	<p>This software provides a number of established methods, including the Bishop horizontal method, Fellenius or Swedish slip circle analysis, and the constant inclined method, to calculate the interslice forces. This program employs the equivalent Janbu methods to analyse the noncircular slip surfaces.</p>
<p>Plaxis (PLAXIS - Essential for geotechnical professionals, 2016)</p> 	<p>This is a finite element based program intending to conduct 2D and 3D geotechnical analysis.</p>
<p>FLAC/Slope (Engineering Consulting   Geotechnical Software   Earth Resources   An Itasca International Company, 2016)</p> 	<p>This utilises the graphical interface to model problems of slope stability under a wide variety of slope conditions, comprising arbitrary slope geometries, multiple layers, pore pressure conditions, heterogeneous soil properties, surface loading and structural reinforcement (Itasca Consulting Group, 2015).</p>

Software Name	Details
<p>CandeCAD Pro (CandeCAD, 2016)</p> 	<p>(Culvert ANalysis and DEsign inside AutoCAD)</p> <p>This software is based on the FEM that was developed under sponsorship from the United States Federal Highway Administration</p>
<p>XSLOPE (Slope stability - XSLOPE - Civil Engineering - The University of Sydney, 2016)</p> 	<p>This applies Bishop's (1955) simplified method for circular failure surfaces and Morgenstern and Price's (1965, 1967) analysis for noncircular failure surfaces. This program is a developed version of the first DOS version released in 1982.</p>
<p>ReSSA (ReSSA (3.0), 2016)</p> <p><b>ReSSA (3.0)</b></p>	<p>Capable of assessing the rotational and translational stability of slopes, this program was developed under sponsorship from the United States Federal Highway Administration</p>
<p>LimitState:Geo (LimitState:GEO - Geotechnical Analysis Software   LimitState, 2016)</p> 	<p>This is a slope stability analysis computer program that rapidly determines the failure mechanism.</p>
<p>GGU-STABILITY (GGU-STABILITY - Slope failure calculations and soil nailing, 2016)</p> 	<p>This software can use not only the Bishop or Krey methods for circular slip surfaces and the Janbu method for polygonal slip surfaces, but can also compute the dimensions of soil nailing (Geosysta, 2015).</p>

Software Name	Details
<p>SPECFEM3D GEOTECH (Computational Infrastructure for Geodynamics :: Software, 2016)</p> 	<p>This is based on the spectral-element method for 3D slope stability analysis.</p>
<p>GSLOPE (Mitre Software Corporation, 2016)</p> 	<p>This uses the LEM for slope stability analysis with soil reinforcement, unreinforced manufactured slopes, and natural slopes.</p>
<p>ReActiv (Geocentrix ReActiv - overview, 2015)</p> 	<p>This is a computer program for designing reinforced slopes in a variety of soil types, using reinforced soil or soil pins (Geosysta, 2015).</p>
<p>PCStabl (STABL -Slope Stability Analysis Software, 2016)</p>	<p>This applies the geosynthetics process to implement slope stability and reinforce soil slopes analysis.</p>
<p>STAB-3D (Biodata - Dr.D.J.Petley, 2016)</p>	<p>This is based on the LEM for 3D slope stability analysis. This program is a FORTRAN version.</p>
<p>CLARA-W (Slope Stability Analysis, 2016)</p> 	<p>This was released in 2001, a Windows version program, and has powerful capabilities for both 3D and 2D analyses.</p>
<p>GALENA (GALENA - Slope Stability Analysis, 2015)</p> 	<p>This is a powerful slope stability analysis system developed for engineers who would rather solve geotechnical problems than computer problems (Scientific Software Group, 2015).</p>

Software Name	Details
StrataSlope (StrataSlope System - Geogrid, 2016) 	This is an interactive computer program using Bishop's (1955) method for slope stability analysis.
LISA (Level I Stability Analysis) (Soil and Water Engineering - Modeling Software, 2015). 	This uses Monte Carlo simulation of the infinite slope equation to estimate a probability of slope failure for use in relative stability assessment of natural slopes.
XSTABL (XSTABL home page, 2016) 	This software, developed at Purdue University, provides an integrated environment for performing slope stability analyses.
Slide (Slide, 2016) 	This is the most comprehensive analysis software of slope stability based on the FEM. This program has the capability of performing sensitivity and probabilistic analysis.
QUAKE/W (Dynamic Earthquake Analysis with QUAKE/W - GEO-SLOPE International Ltd., 2016) 	This calculates a safety factor by calculating total shear resistance and mobilised shear stress beside the entire slip surface (www.geo-slope.com). Likewise, the software uses the Monte Carlo approach to compute the probability of failure.
CRISP (CRISP Geotechnical Finite Element Analysis Software, 2016) 	This software, written in standard FORTRAN90, was originally developed by researchers in the Cambridge University Soil Mechanics Group in the late 1970s. This software implements stability analysis by using finite element technique.

Software Name	Details
<p>GeoPIV (GeoPIV-RG, 2016)</p> 	<p>This is a MATLAB-based program, which uses the principles of image processing to gather displacement data from a set of digital images captured during the process of geotechnical tests and then implements the PIV to map the material flow. The software was written by White (2002) and Take (2002) during their PhD research.</p>
<p>ABAQUS (Abaqus/CAE User's Guide (6.14), 2016)</p> 	<p>This is a finite element based program, designed for modelling both static and dynamic structures involved in material behavior. The unique feature of ABAQUS is to conduct a wide variety of analysis such as vibration, failure analysis/fracture mechanics, heat transfer analysis, and so on. This program is applied for process optimisation, general forming analysis and material comparisons, which assists users with modelling a problem in a simple and easy manner in comparison with trial and error based techniques.</p>

## 2.10. Literature Review Conclusions

Although many slope stability techniques have been developed over recent decades, there are still some major limitations to these techniques. In this chapter, a comprehensive analysis of the different techniques in reference to applications and limitations of slope stability methods were investigated, with the LEM, limit analysis, numerical modelling, empirical design, physical model tests, probabilistic methods, and image processing techniques explored and discussed.

Several techniques including the SRM can give clear stress analysis without requiring the inter slice force assumption, although this analysis is time-consuming and there are some limitations under certain situations. In comparison with other techniques, the DEM can give better understanding about the post failure mechanism; however, this method cannot calculate the FOS. Although the lower and upper bound limit analysis can bound the true failure load, this method cannot predict the displacement of the slope. The main limitations of the LEMs for slope stability analysis are based on the assumption that the soil mass behaves as a rigid material and the shear strength is mobilised at the same time along the entire failure surface.

In the numerical methods, the simulation of smaller block sizes can lead to a lengthy and time-consuming process; therefore, it is impossible to simulate smaller block sizes. Empirical design charts only provide a general view on the slope stability analysis and cannot establish more detailed information. Physical model tests do not provide a precise design for the simulation of the accurate loading conditions, although they are useful for the analysis of the fundamental failure mechanism and the verification of numerical and analytical methods. The practical applications of the probabilistic methods are limited because of the vast amount of input data required to run such methods.

Although a number of techniques have been developed to formulate the slope stability problem (as revealed by this literature review), a novel technique based on the image processing method, which is a robust and powerful technique, for precise formulation of the behaviour of a failure mechanism is still required.

The variety of commercial software packages available for the calculation of the FOS and assessment of slope stability were briefly described to demonstrate the key importance of slope stability analysis. Although a number of computer programs have already been developed for slope stability analysis, it is still necessary to develop new computer programs for accurate and simple modelling of the behaviour of a failure mechanism. Therefore, it is proposed in this thesis to employ the high potential of the PIV method to formulate the failure mechanism in slopes and compare the results of the proposed model with those of other techniques. A typical case is micro failure modelling, which is required for the study of micro movements in natural or human-made slopes. These types of failures are dominant in dry, loose soils such as sands with fine particles. The PIV method is utilised to reveal further information regarding shallow failures and their features as a prevalent type of slope stability issue.



### 3. EXPERIMENTAL METHOD

A schematic diagram of the experimental method is depicted in Figure 3-1, which shows the stepwise process utilised to formulate the soil slope stability based on the effective parameters. All stages of the model implementation are systematically described and the results are clearly presented in the following sections of this chapter.

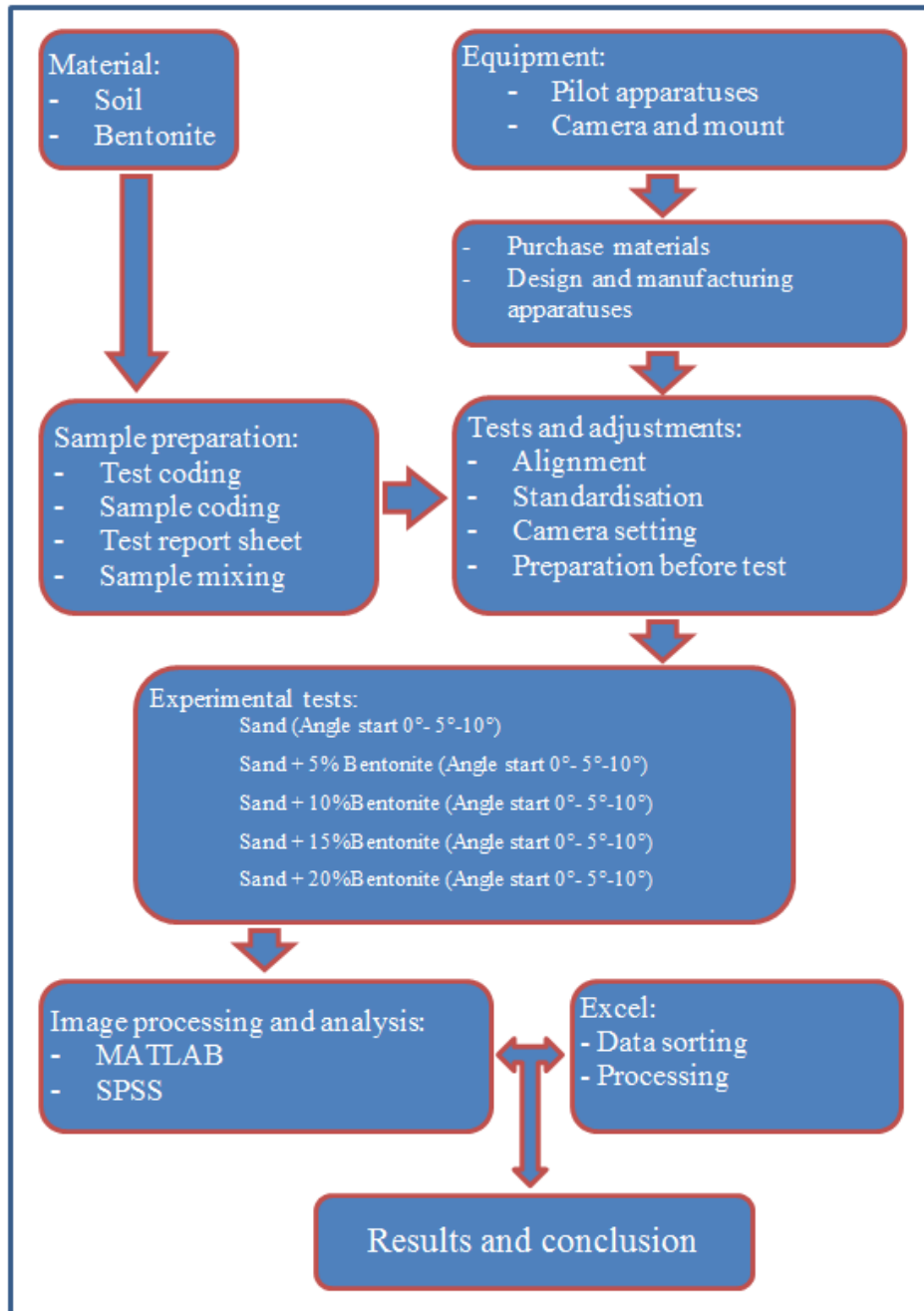


Figure 3-1: Schematic diagram of the experimental method

### 3.1. Material

#### 3.1.1. Soil

Soil samples were collected from an area of Gaskell Ave, Ellenbrook, Western Australia (Figure 3-2), which belongs to Rocla Quarry Products Pty Ltd.



Figure 3-2: Location of the soil resource (GoogleMaps, 2016)

The soil was labelled “Gaskell concrete sand” in the laboratory. To obtain a representative well-mixed sample, a standard collection (AS 1141.3.1-2012) procedure was followed, which involved establishment of a platform where the collected soil was placed and then the soil was mixed thoroughly several times. The soil pile was then divided into four parts to select one part as a representative sample and the remaining three parts were discarded. This procedure was then repeated to obtain the required quantity of soil. Next, the selected soil sample was thoroughly mixed. The discarded parts were placed into bags for transportation to the environmental engineering laboratory in Curtin University. Sand physical properties selected for slope stability analysis are presented in Table 3-1.

**Table 3-1: Gaskell concrete sand physical properties**  
(Gaskell Concrete Sand Technical Data Sheet, 2014)

Particle Density - SSD Basis	2.61 t/m <sup>3</sup>
- Dry Basis	2.59 t/m <sup>3</sup>
Water Absorption	0.8%
Dry Density - Maximum	1.86 t/m <sup>3</sup>
- Minimum	1.56 t/m <sup>3</sup>
Sodium Sulphate Soundness.	0.1 %
Light Particles	< 1
Clay and Fine Silt	3%
Gross Moisture Content	3.2%
Fineness Modulus	1.9
Alkali Reactivity At - 10 days	0.01
(CSIRO) Mortar Bar - 22 days	0.07
Material Finer than 2 micron	0.2%
Acid Soluble Salts - Cl	< 0.01%
- SO <sub>4</sub>	0.03%
Organic Impurities (N1)	Pass

### Particle size distribution

The particle size distribution strongly influences the decomposition and mechanical behaviour of soil, with particle size determinations performed using mechanical sieve analysis. In this procedure, the particles retained on each sieve were collected and transferred into an oven 105°C for the purpose of drying and weighing. Then, by dividing the weight of the sample retained on each sieve by the total weight of the sample, the percentage passing through each sieve can be calculated. Table 3-2 presents the passing percentage for each sieve. The calculation of the percent passing total for the desired sizes is as follows:

$$pp(\text{passing percent}) = \frac{\log \text{size}B - \log \text{size}C}{\log \text{size}A - \log \text{size}C} \quad 3-1$$

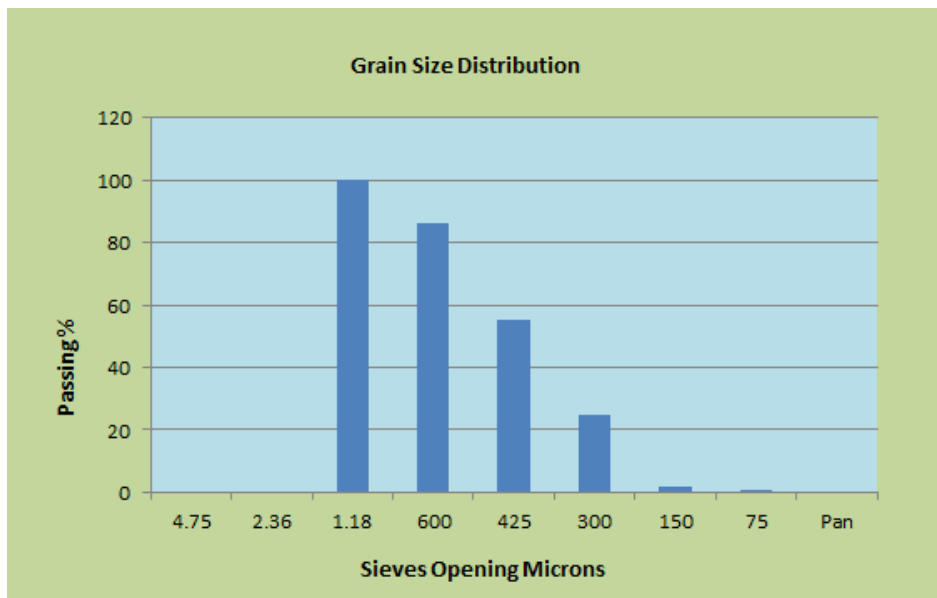
where:

A = next size larger than desired size, B = desired size, and C = next size smaller than desired size.

**Table 3-2: Gaskell concrete sand sieve analysis**  
(Gaskell Concrete Sand Technical Data Sheet, 2014)

Sieve opening ( $\mu\text{m}$ )	Passing (%)	Specification Limits
4.75 mm	–	100
2.36 mm	–	95 – 100
1.18 mm	100	90 – 100
600 $\mu\text{m}$	86	72 – 100
425 $\mu\text{m}$	55	–
300 $\mu\text{m}$	25	17 – 37
150 $\mu\text{m}$	1.7	0 – 7
75 $\mu\text{m}$	0.1	0 – 5
Pan	0	–
Clay and Fine Silt (Guide Only)	3	$\leq 4$

The grain size distribution is graphically depicted in Figure 3-3, which illustrates that the greatest size distribution was between 300  $\mu\text{m}$  and 1.8 mm, with this size accounting for greater than 97% of the total size.



**Figure 3-3: Soil grain size distribution graph**  
(Gaskell Concrete Sand Technical Data Sheet, 2014)

Soil properties and characteristics are comprehensively presented in Appendix C-1. A drained soil sample, prepared for slope stability analysis, is shown in Figure 3-4.



Figure 3-4: Drained soil sample before test

### 3.1.2. Bentonite

In this experiment, bentonite, obtained from Silbelco Australia, was mixed with the soil (soil details presented in section 3.1.1) as time progressed. Bentonite specifications are presented in Appendix C-2. Typical percentages of bentonite in the soil varied between 5 and 20%. Table 3-3 presents the typical composition of bentonite. From the table, it can be seen that Smectite is the main component of bentonite.

Table 3-3: Information / Composition on Bentonite ingredients

(Material Safety Data Sheet Sibleco Bentonite Group 2 , 2010)

Ingredients	CAS	Proportion
Smectite	12199-37-0	60–100%
Albite	-	< 2%
Quartz (Crystalline Silica)	14808-60-7	< 11%
Other information	The respirable fraction of free crystalline silica is less than 4%.	

A photograph from the bentonite trademark package in the laboratory is shown in Figure 3-5.

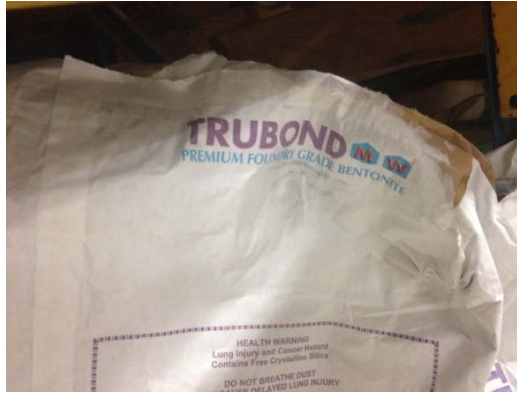


Figure 3-5: Bentonite package TRUBOND brand

### 3.2. Laboratory Tests

#### 3.2.1. Particle Density

The unit weight of the soil was obtained according to standard AS 1141.5-2000, which is the method for determining particle density, apparent particle density and water absorption of fine aggregates or the fine fraction of an aggregate. The density of sand particles in the present experiment was approximately 2.62 ton/M<sup>3</sup>

#### 3.2.2. Direct Shear Test

The direct shear test was performed according to standard AS 1289.6.2.2-1998, which is the standard approach for determining the shear strength of a soil (in terms of effective stress) by direct shearing in a shear box.

After extraction, normal stress results for five samples with ingredients presented in Table 3-4 and the Mohr Circle calculations are shown in Figure 3-6 (sample S-D), Figure 3-7 (samples SB5-D), Figure 3-8 (samples SB10-D), Figure 3-9 (samples SB15-D) and Figure 3-10 (samples SB20-D). Because following Mohr circle graphs exported from edited macro excel file half circle is shown.

Table 3-4: Samples ingredients for direct shear tests

Sample code	Batching proportions	
	Sand%	Bentonite%
S-D	100	0
SB5-D	95	5
SB10-D	90	10
SB15-D	85	15
SB20-D	80	20

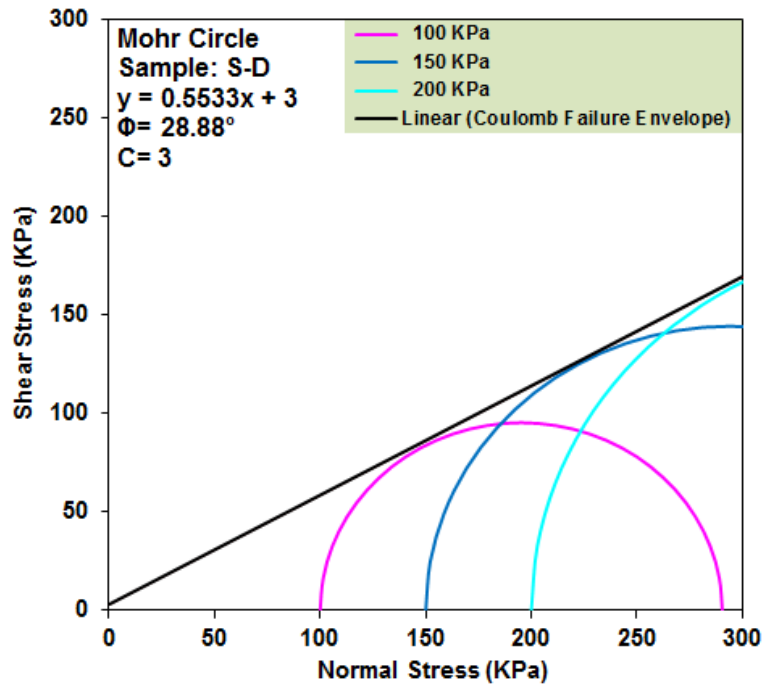


Figure 3-6: Mohr Circle result for sample S-D (Soil)

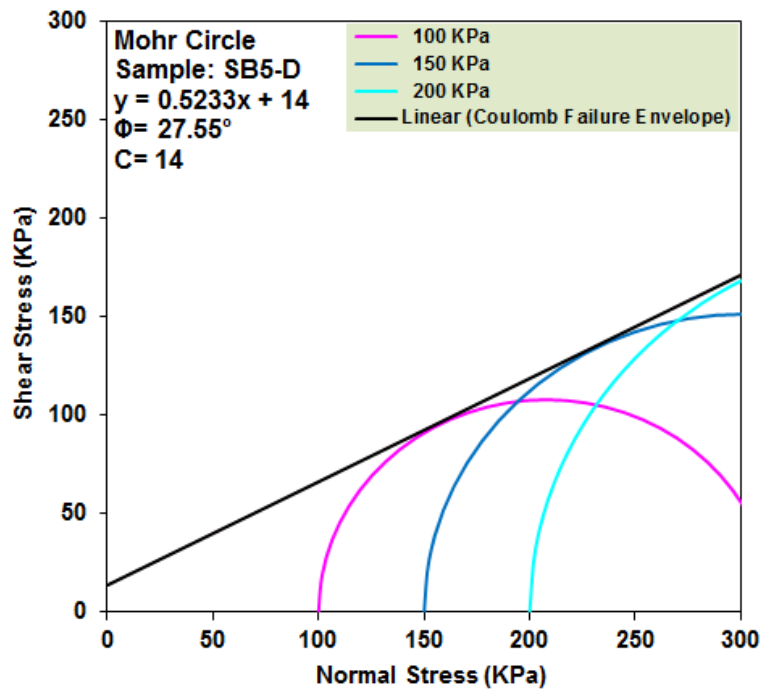


Figure 3-7: Mohr Circle result for sample SB5-D (5% bentonite)

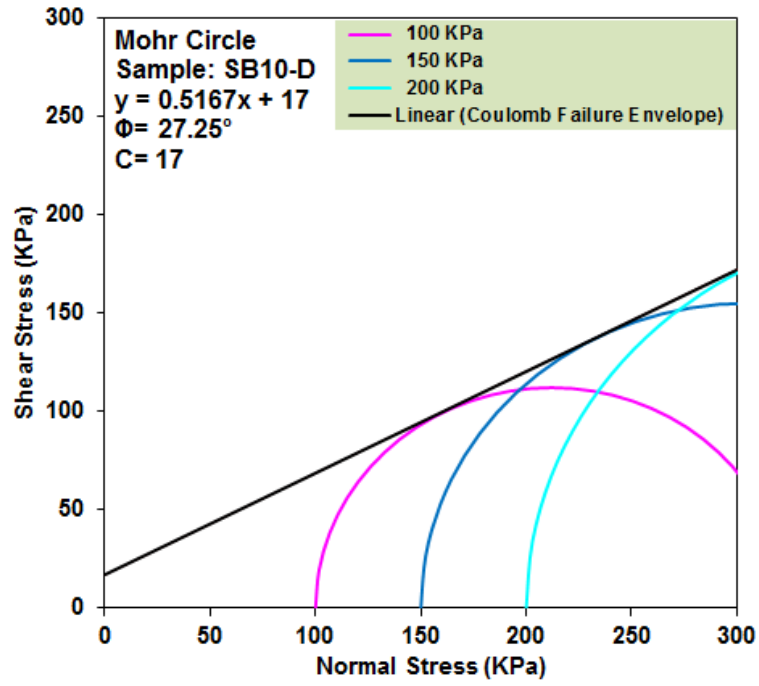


Figure 3-8: Mohr Circle result for sample SB10-D (10% bentonite)

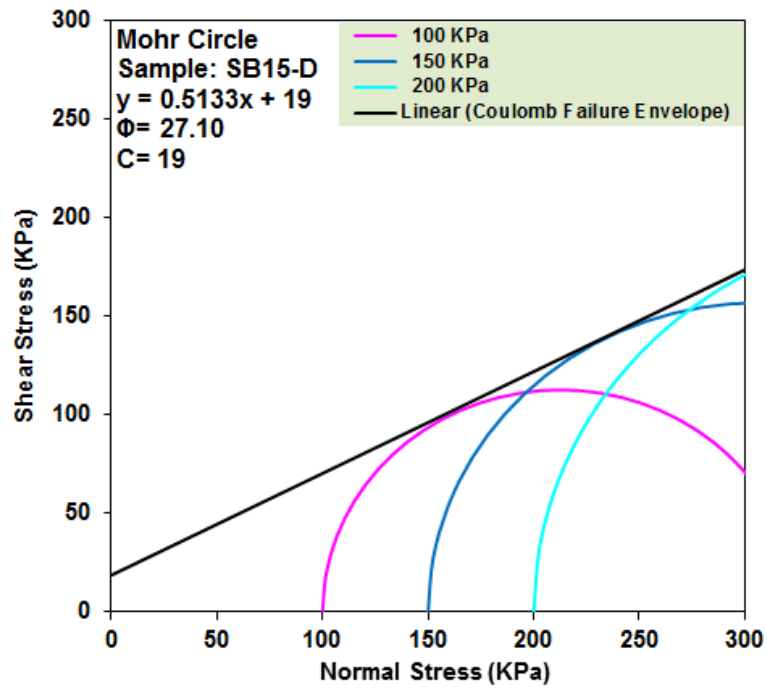


Figure 3-9: Mohr Circle result for sample SB15-D (15% bentonite)



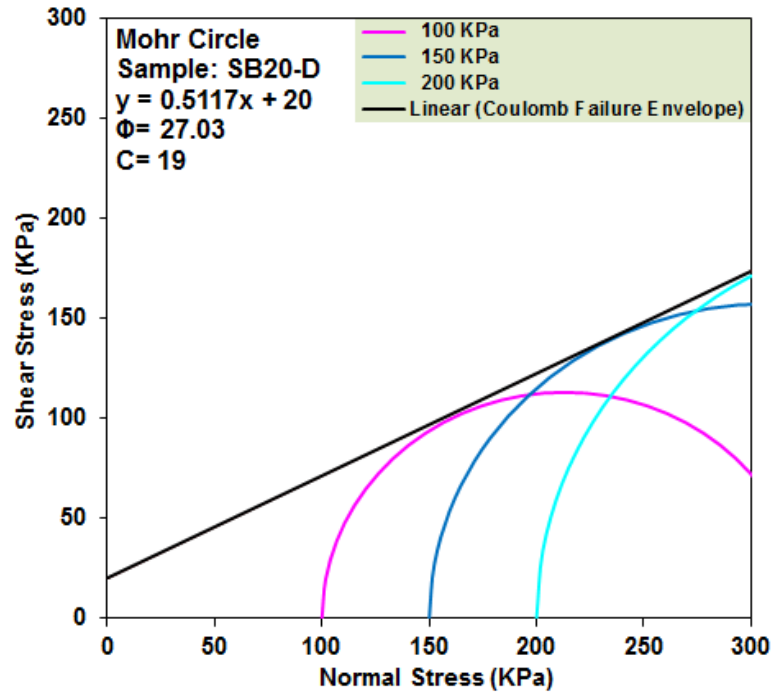


Figure 3-10: Mohr Circle result for sample SB20-D (20% bentonite)

The direct shear results are summarised in Table 3-5 and cohesion amount 3 result in soil sample is negligible it is affected by tiny elements and clay.

Table 3-5: Results of Direct Shear tests for samples

Sample	Bentonite%	Tan (Φ)	Φ (Degree)	Cohesion (KPa)
S-D	0	0.5533	28.88	3
SB5-D	5	0.5233	27.55	14
SB10-D	10	0.5167	27.25	17
SB15-D	15	0.5133	27.10	19
SB20-D	20	0.5117	27.03	20

### 3.3. PIV Apparatus Design and Manufacturing

An apparatus design is a small-scale industrial system that helps researchers formulate the behavioural patterns of a system or sub-system for use in the design of a full-scale facility. The apparatus design can be built in different sizes, although it is a relative term in the case that the apparatus is naturally smaller than the full-scale facility. The apparatus design is usually a system established in the laboratory using

a stock of laboratory materials. Researchers interchangeably utilise the terms apparatus design and pilot plant, but an apparatus design is usually smaller in comparison to a pilot plant.

An apparatus design can be comprised of the following components:

- 1- A main framework support structure onto which parts are assembled.
- 2- A tank container with a clear wall to observe movement of particles inside the tank.
- 3- A base plate under the tank that lifts from one side and is connected with a hinge on the other side.
- 4- Several specialised parts to prevent the tank from sliding on the table when one side is lifted.
- 5- A force generator like a winch or jack to lift one side of the table.
- 6- A regulator under the legs for alignment purposes.

### 3.3.1. Base Plate

A base plate is a solid piece of material that functions as the surface that other items are attached to, and it must be sturdy and strong enough to bear the weight of the tank and contained sample. Figure 3-11 shows an orthographic layout of the base plate used for the experiment in this thesis.

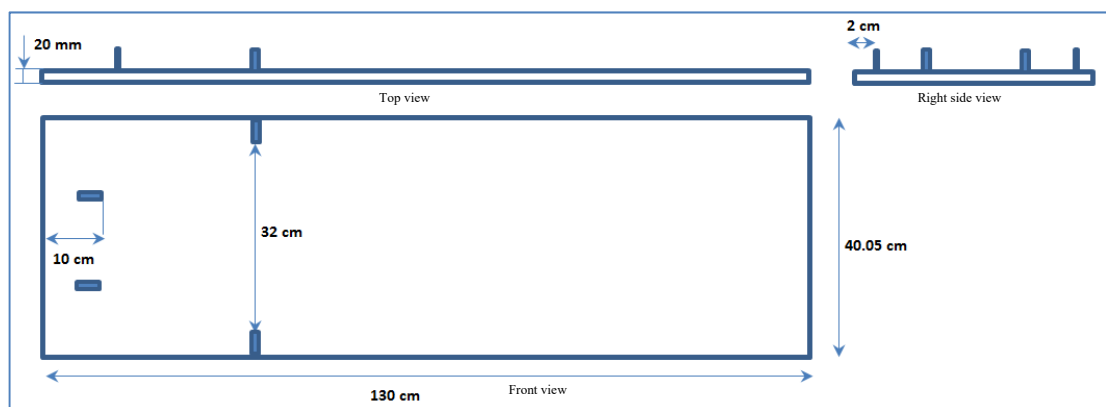


Figure 3-11: Base plate, orthographic layout

### 3.3.2. Main Framework Support Structure

A corner view of the main framework support structure is shown in Figure 3-12.

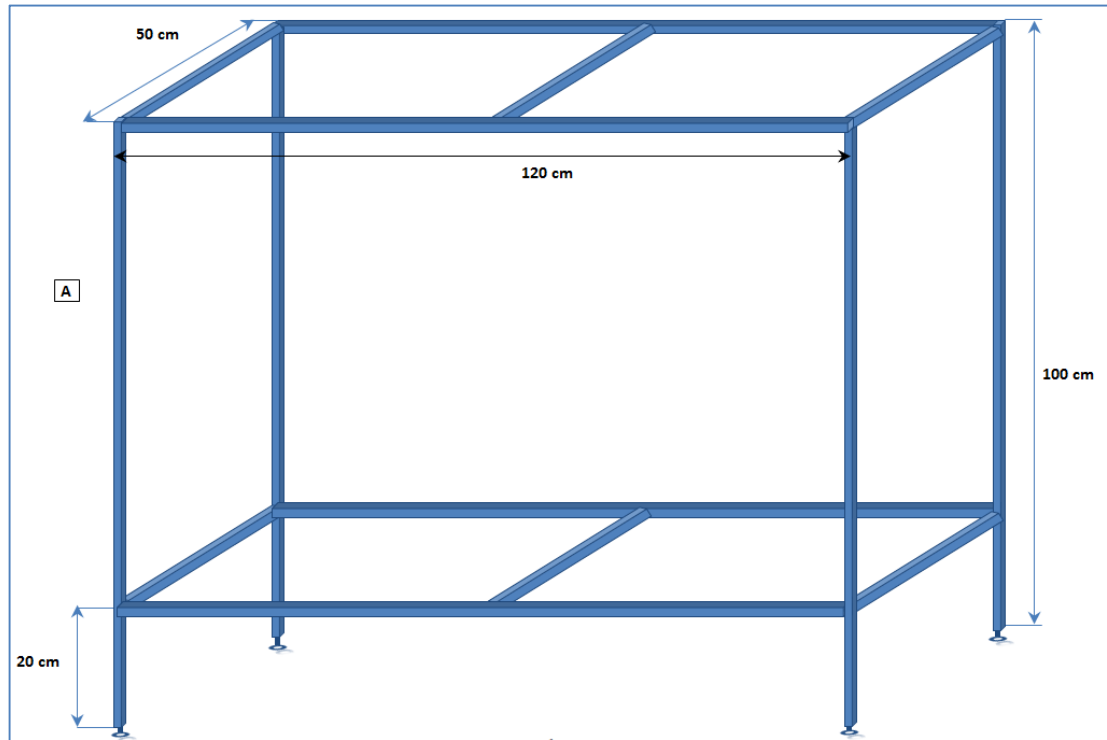


Figure 3-12: Corner view of the main framework structure

The front and right side views of the main framework are depicted in Figure 3-13 and Figure 3-14 based on the final design decision after several meetings with the workshop team helping with the experimental design utilised in this thesis.

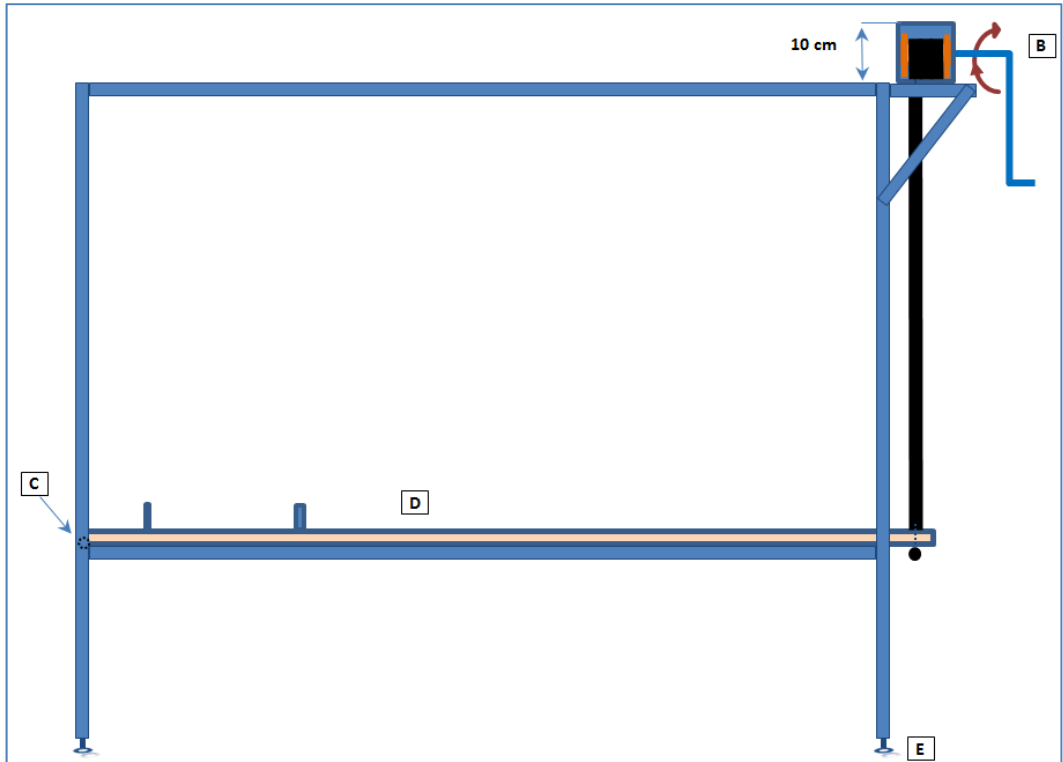


Figure 3-13: Front view of main framework structure, base plate, and winch

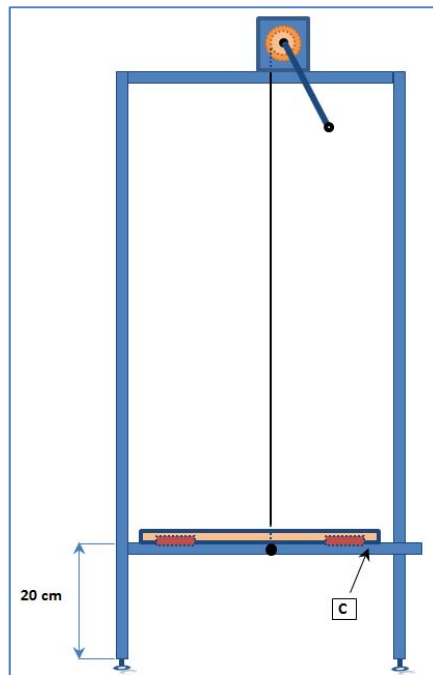


Figure 3-14: Right side view of main framework structure, base plate and winch

The main parts included in the design of the apparatus and purchased (and that appear in these figures) were the following:

- A- Steel Handyman RHS Painted  $25 \times 25 \times 1.6$ mm.
- B- Cadet Winch Webbing S Hook 300 kg.
- C- Hinge Butt Fp Zenit Th 63 mm Brass Cd2 1065.
- D- Pine Dar Fj Clear  $405 \times 19$  mm 1.8 m.
- E- Glide Screw on Romark  $3/8 \times 1.1/2$  in white 386020.

### 3.3.3. Plexiglass Container (Tank)

The tank container must be clear, with the material utilised for this study being plexiglass of 10 mm thickness. The divider section enables the tank to be separated into two sections, as shown in Figure 3-15.

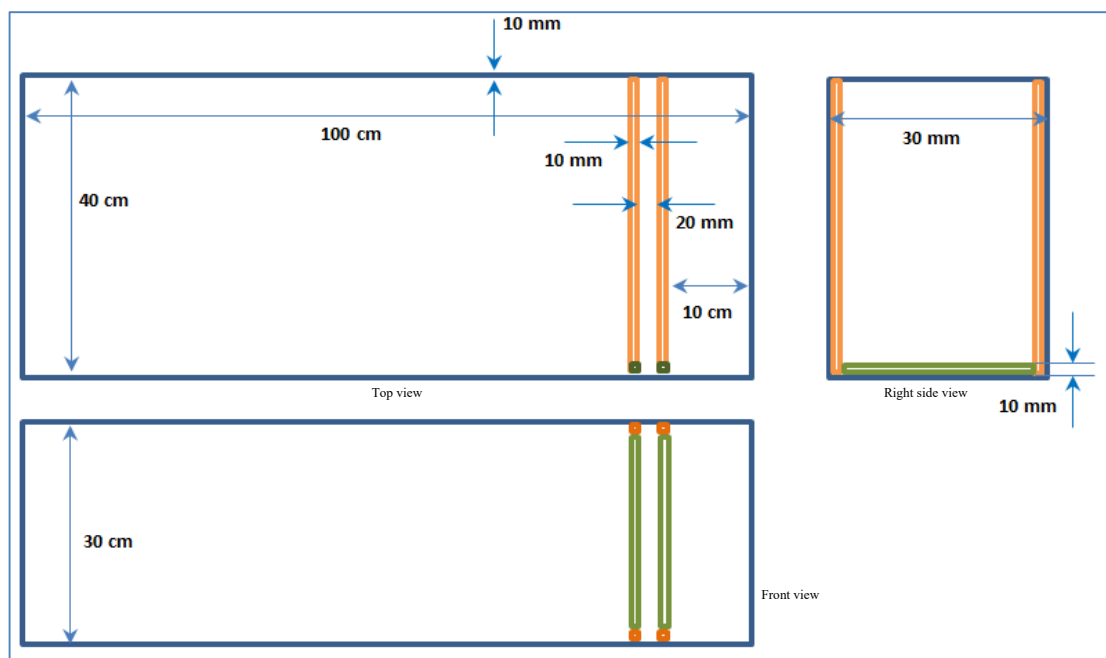


Figure 3-15: Tank container, an orthographic layout

### 3.3.4. Water Transmitter and Holes Map

The water transmitter component includes two plates: a holed plate as shown in the left hand side of Figure 3-16 and a plate of sponge as depicted in the right hand side

of Figure 3-16. The plexiglass plate having a thickness of 5 mm holds the backside of the soil.

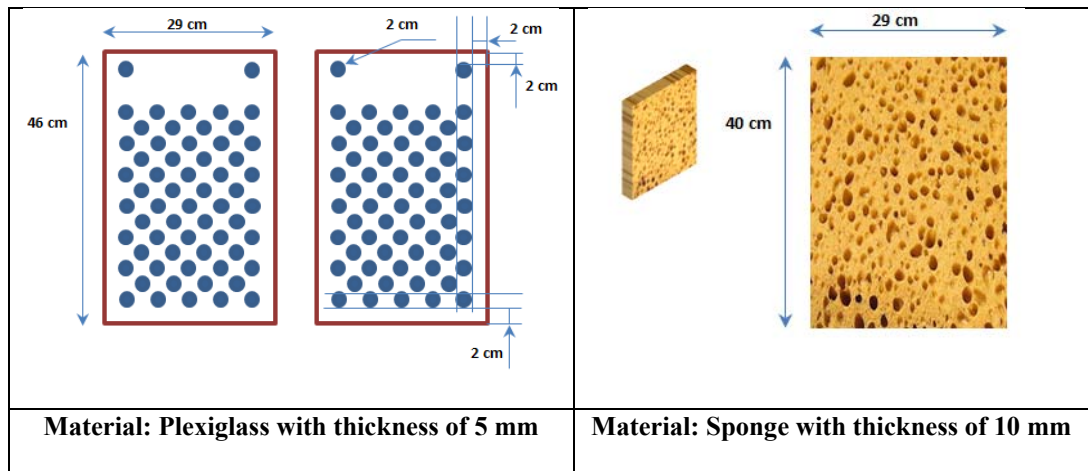


Figure 3-16: Water transmitter

The technique of installing the water transmitter component is clearly presented in Figure 3-17 and Figure 3-18.



Figure 3-17: A corner view of the water tank container

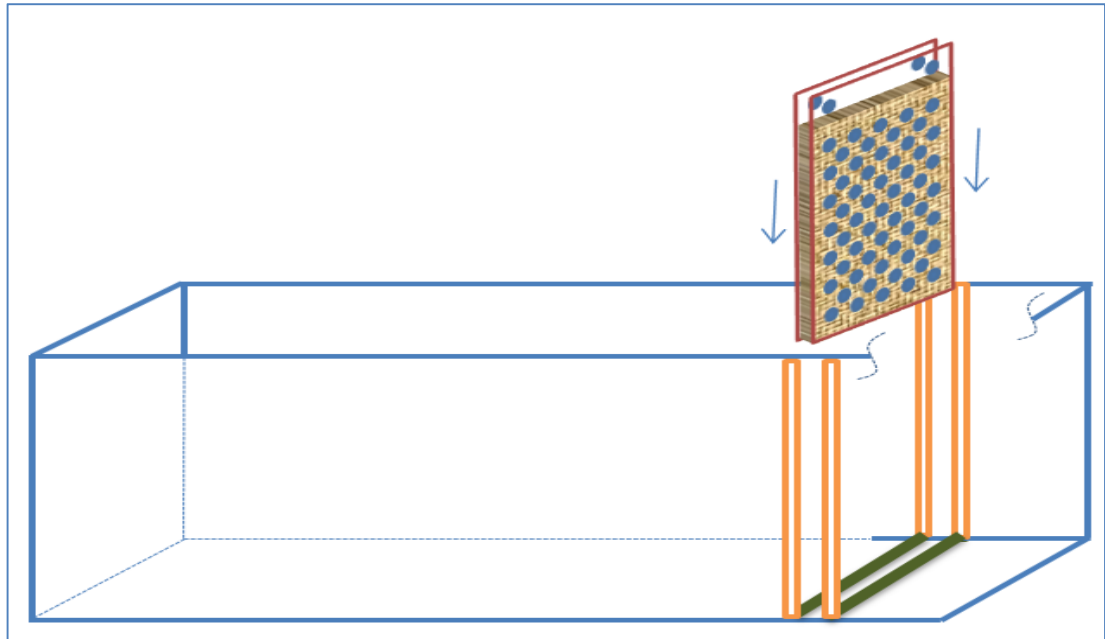


Figure 3-18: Installation of divider and water transmitter

### 3.3.5. Implementation Procedure

Before implementing a series of tests, it was necessary to accomplish an alignment process via establishing small regulators on the end of the legs and checking the level of the system with a level aligner device. Figure 3-19 and Figure 3-20 illustrate the final apparatus designed for the process of slope stability investigation that was utilised in this experiment.

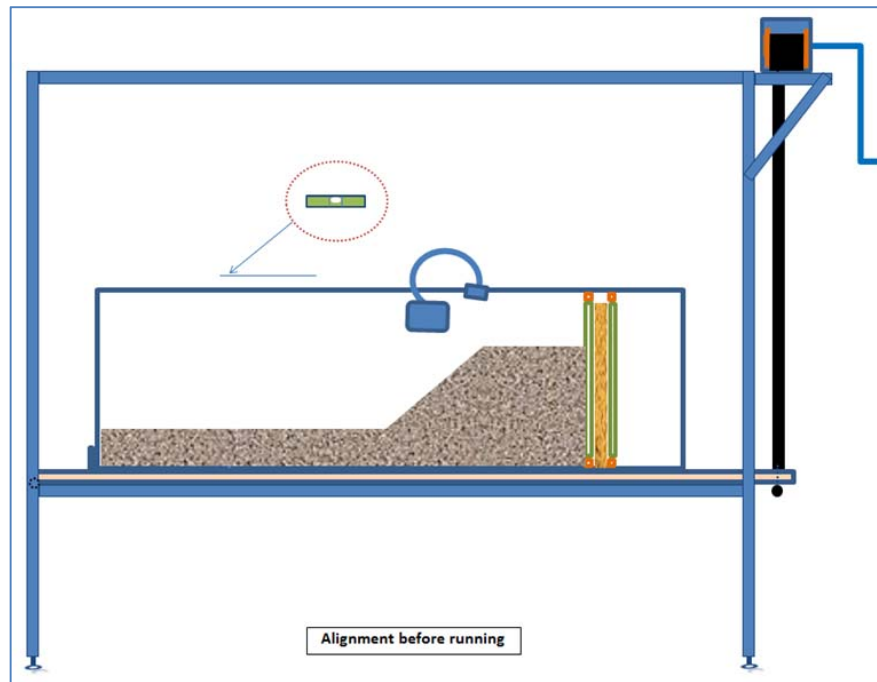


Figure 3-19: Front view of designed apparatus

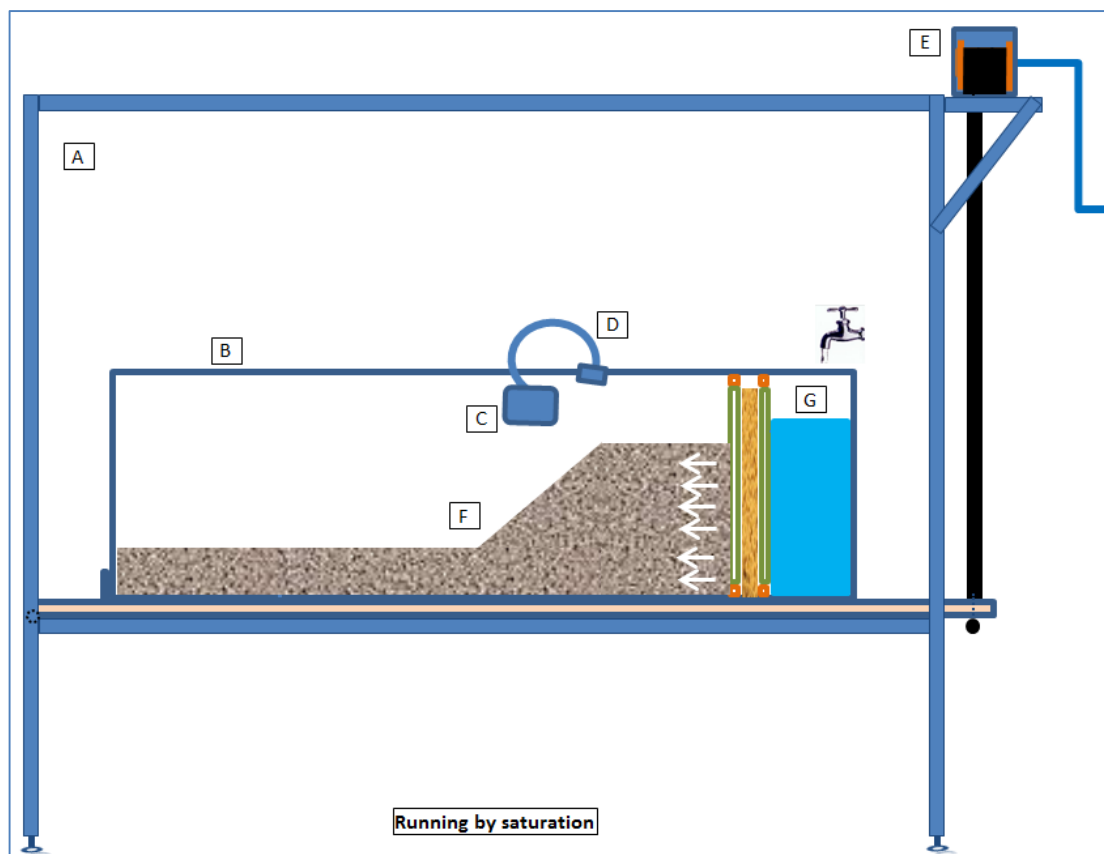


Figure 3-20: View of the apparatus and saturation driver. A – table structure, B – glass container, C – camera, D – mount camera holder, E – winch force generator, F – soil sample and G – water feeder.



A view of the designed apparatus with the lifting up driver attached is depicted in Figure 3-21.

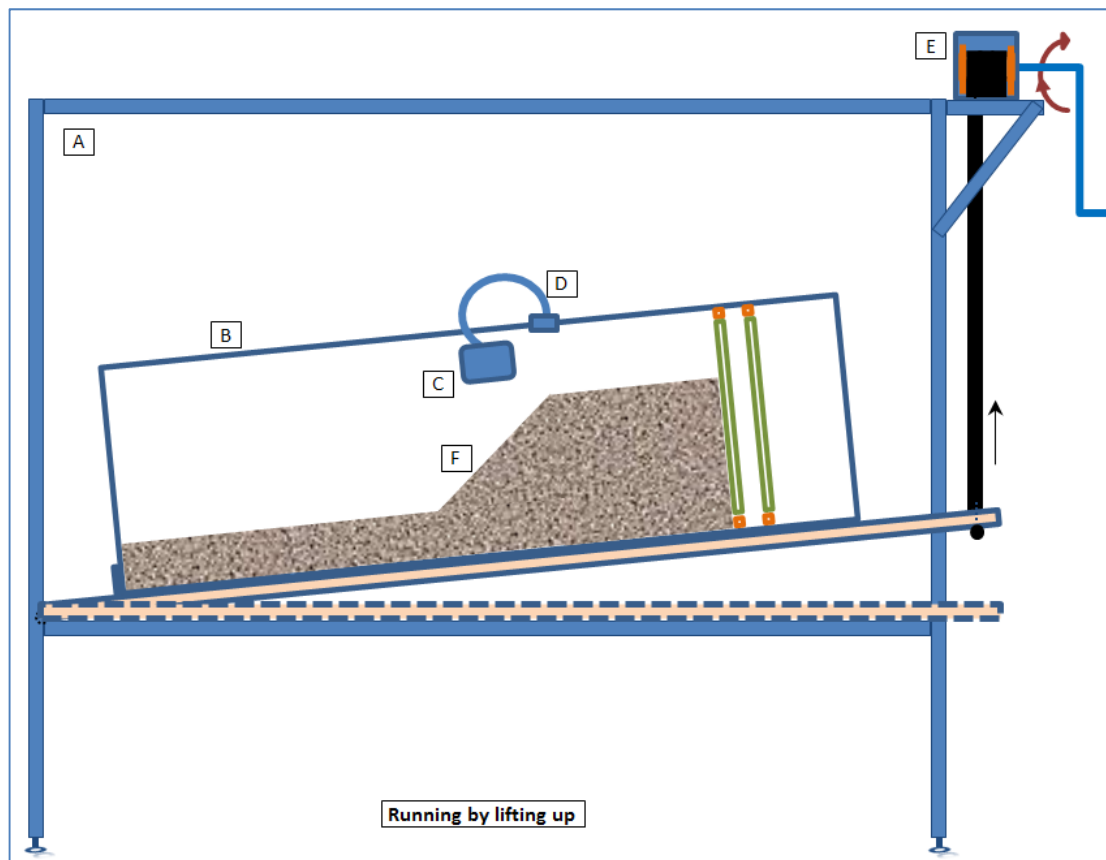


Figure 3-21: View of designed apparatus with lifting up driver. A – table structure, B – glass container, C – camera, D – mount camera holder, E – winch force generator and F – soil sample.

### 3.4. Camera

A camera is a device for capturing or recording images and videos. A camera, similar to the human eye, can capture an object without contacting it physically. In this research, a Gopro Hero3+ Black camera, which is a user friendly and 60 frames per second system, was selected (Hero3 Black edition, 2014). In Figure 3-22, the Gopro Hero3+ camera and water-resistant cover are shown.

Table 3-6 presents the camera's features and characteristics, while Table 3-7 shows the resolution instructions on how to achieve the best quality image.



Figure 3-22: GoPro Hero3+ camera and water-resistant cover (Hero3 Black edition, 2014)

Table 3-6: GoPro Hero3+black resolution (Hero3 Black edition, 2014)

Video Resolution	NTSC fps	PAL fps	Protune	Field of View (FOV)	Screen Resolution
4K /	15	12.5	Yes	Ultra Wide	3840×2160, 16:9
4K 17:9	12	12			4096×2160, 17:9
2.7K /	30	25	Yes	Ultra Wide	2704×1524, 16:9
2.7K 17:9	24	24		Medium	2704×1440, 17:9
1440p	48	48	Yes	Ultra Wide	1920×1440, 4:3
	30	25			
	24	24			
1080p	60	50	Yes	Ultra Wide	1920×1080, 16:9
	48	48		Medium	
	30	25		Narrow	
	24	24			
1080p SuperView*	60	50	Yes	Ultra Wide	1920×1080, 16:9
	48	48			
	30	25			
	24	24			
960p	100	100	Yes	Ultra Wide	1280×960, 4:3
	60	50	Yes		
	48	48	No		
720p	120	100	Yes	Ultra Wide	1280×720, 16:9
				Medium**	
	60	50	Yes	Narrow	
720p SuperView*	100	100	Yes	Ultra Wide	1280×720, 16:9
	60	50	Yes		
	48	48	No		
WVGA	240	240	No	Ultra Wide	848×480, 16:9

\*SuperView delivers the world's most immersive field of view.

\*\*720p 120 and 720p 100 only support Ultra Wide and Narrow FOV.

**Note:** Protune mode is only possible in select Video resolutions.

**Table 3-7: Application of video resolution (Hero3 Black edition, 2014)**

<b>Video Resolution</b>	<b>Best Use</b>
4K / 4K 17:9	Stunning high-resolution video with professional low-light performance. Pull 8MP stills from video. Recommended for tripod or fixed position shots.
2.7K / 2.7K 17:9	16:9 / 17:9 resolution video downscales to provide stunning, cinema-quality results for professional productions. Recommended for tripod or fixed position shots.
1440p	Recommended for body-mounted shots as larger viewing area and high frame rate yield the smoothest, most immersive results for high-action capture.
1080p	1080p60 is great for all shots as high resolution and frame rate yield stunning results. Tripod or fixed mounting for 1080p48 and 30 fps and 1080p24 is ideal for television and film productions.
1080p SuperView	Recommended for body- or gear-mounted shots. More vertical 4:3 content is automatically stretched to full-screen 16:9 for greater viewing enjoyment.
960p	Use for body-mounted shots and when slow motion is desired. Provides large viewing area and smooth results for high action capture.
720p	Good for handled shots and when slow motion is desired.
720p SuperView	Good for body- or gear-mounted shots. More vertical 4:3 content is automatically stretched to full-screen 16:9 for greater viewing enjoyment.
WVGA	Good when super slow motion is desired and standard definition is acceptable.

### 3.4.1. Camera Mount

The camera mount utilised in this experiment, as shown in Figure 3-23, was flexible and easy to fit onto the plexiglass tank.



**Figure 3-23: Camera flexible mount (Hero3 Black edition, 2014)**

### 3.5. Manufactured Apparatus

The apparatus was manufactured as depicted in Figure 3-24, with Figure 3-25 and Figure 3-26 showing information that is more detailed.



Figure 3-24: A front view of the manufactured apparatus

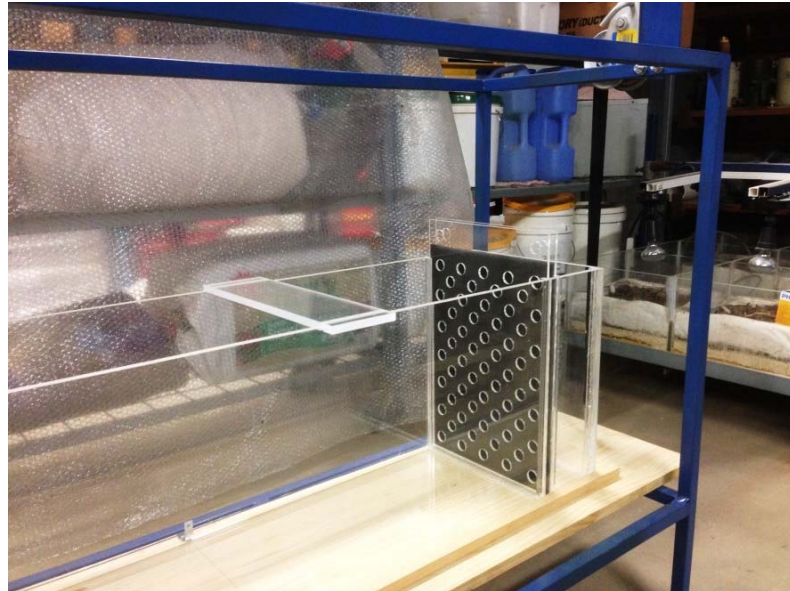


Figure 3-25: A close view of the apparatus



Figure 3-26: A view of the water section and winch in the manufactured apparatus

### 3.6. Sample Preparation

As mentioned in the Material section, the main sample considered for testing was sand extracted from Gaskell Avenue. This is the greatest area of in Western Australia; the sand is smooth and, because of considerable impurity effects, bentonite was added. A study by Ata et al. (2015) also utilised a component soil and bentonite because of coherence effect (more details are presented in section 3.2.2 Direct Shear Test). Hashemi et al. (2015) used 10, 15 and 20 % bentonite in their tests, and Wong et al. (2013) studied further the effectiveness of bentonite in incoherence. For a drained test, the soil sample should be kept in an oven at a temperature of 105 °C for 24 h.

### 3.7. Apparatus Standardisation Test

Figure 3-27 presents a schematic diagram of the process of the apparatus standardisation test. One major factor when attempting to solve a problem using image processing is to conduct the test in the dark to prevent light reflection.

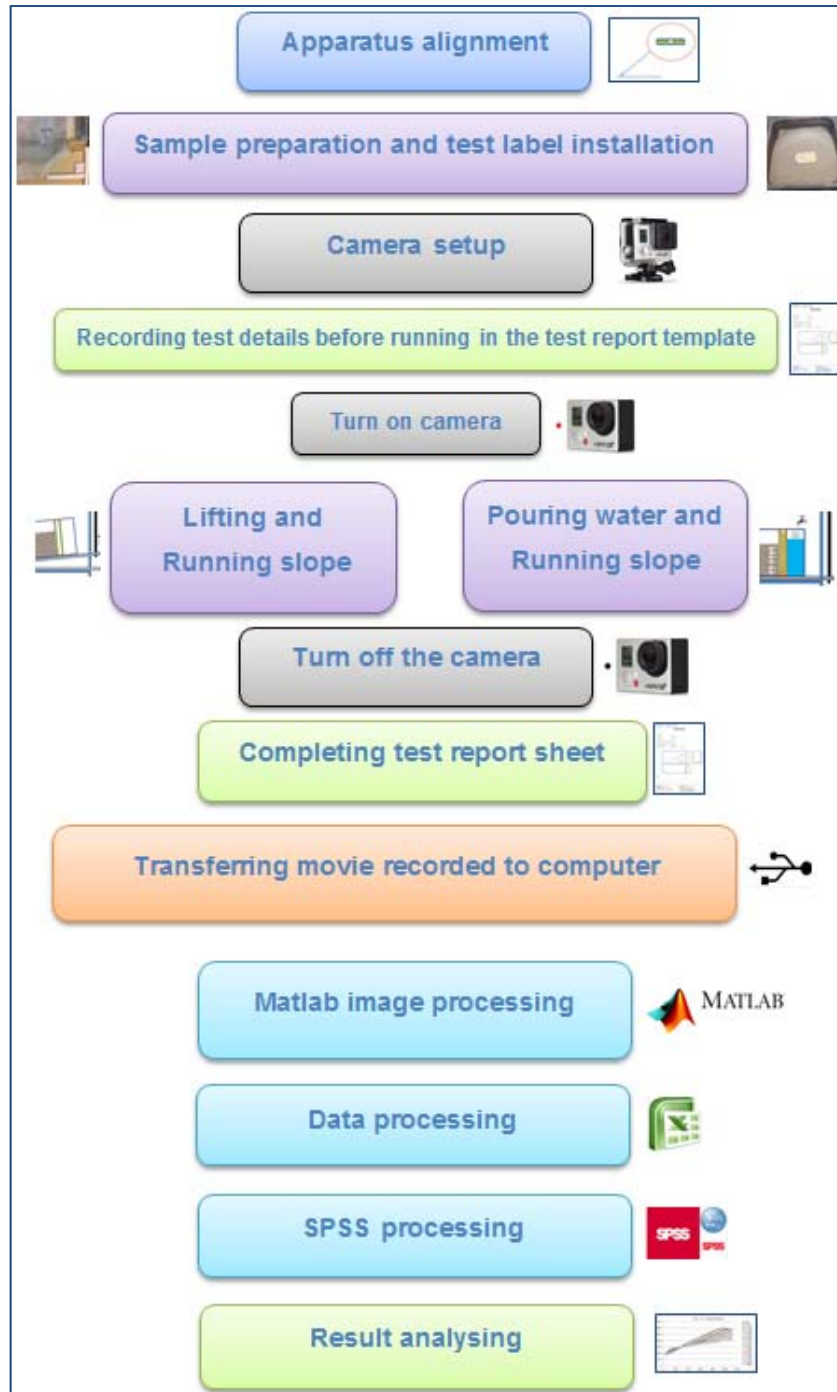


Figure 3-27: Schematic diagram for apparatus standardisation test

### **3.8. Apparatus Alignment**

The main framework and tank were initially aligned in an attempt to begin the tests from different initial slopes to replicate the effect of sub-bottom hard layers in nature. Thus, for each test three aligned angles ( $0^\circ$ ,  $5^\circ$  and  $10^\circ$ ) were assumed.

### **3.9. Preparation before Test**

To achieve repeatability of tests and identical conditions, all tests were prepared in a similar way, as clarified in Figure 3-28. In the first step, the soil sample was made in a container, with attempts at composing a loose and dry slope to replicate natural sand slopes. In the second step, the head of the slope was trimmed and flattened. Several techniques were employed to increase the quality of tests, namely the light was decreased to accomplish the test in a night situation and an anti-streak spray was applied to decrease the sticking property of the particles to the wall. An inclinometer, vertical and horizontal rulers, test code and sample codes were stuck to the glassy tank to help with any measurement during the tests and analysing the result. A coding system for tests and samples makes it easy to manage and categorise the results (see below for details).

#### **3.9.1. Test Coding Method**

A (Alignment differentiation) and S (Saturation method):

A0, A5, A10, S – 1, 2, 3

Where the letters and numbers stand for:

A0: Begin alignment at  $0^\circ$ ; A5: Begin alignment at  $5^\circ$ ; A10: Begin alignment at  $10^\circ$ ;  
and S: Saturated

#### **3.9.2. Sample Coding Method**

S, SB5, SB10, D, W5, W10

Where the letters and numbers stand for:

S: Sand; SB5: Sand + 5% Bentonite; SB10: Sand + 10% Bentonite;

D: Dry; W5: 5% Water; W10: 10% Water

For example: A10-SB5 indicates that the test type is the alignment process beginning with angle  $10^\circ$ , and the sample is sand containing 5% bentonite. In this research, the lifting process was only utilised in the process of evaluation and the saturated tests were neglected. After sample preparation for the test, a sample label was installed on the corner of the tank as shown in Figure 3-28, which enables easier checking of the videos for analysing purposes.

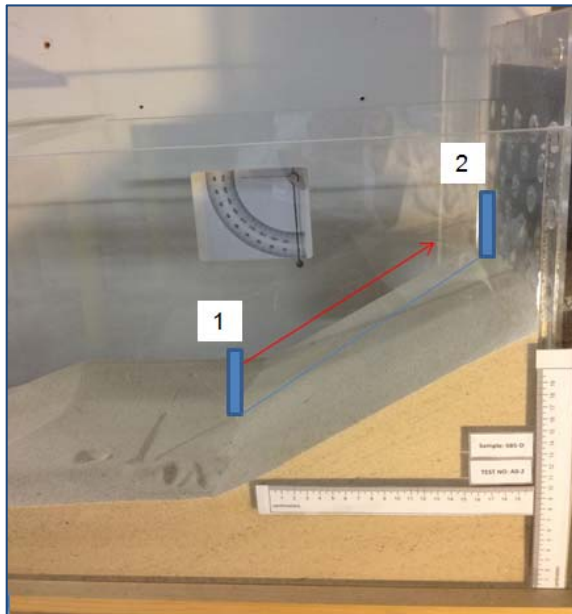


Figure 3-28: Stable sample

### 3.10. Camera Setup

The camera was installed with a mount on the container and moved with the container. Similar to above, the test was conducted in a dark room, the film resolution was set to  $720 \times 1280$  pixels and the lens was in the medium orientation to cover all surfaces of the test area. Before beginning the test, the quality of light and the covered capture area were checked through repeating and monitoring by the computer.

### 3.11. Test Report Sheet

For the data recording system, a test report sheet was designed (Appendix D – Test Report Sheet), which helped to establish the test characteristics and track the file



name associated with each file description and any information required during data analysis data.

### 3.12. Pilot Tests

A total of 15 pilot tests were conducted with the following sample ingredients:

- Sand (Angle start 0°; 5°; 10°)
- Sand + 5% bentonite (Angle start 0°; 5°; 10°)
- Sand + 10% bentonite (Angle start 0°; 5°; 10°)
- Sand + 15% bentonite (Angle start 0°; 5°; 10°)
- Sand + 20% bentonite (Angle start 0°; 5°; 10°)

The test characteristics from the report sheet and categories are presented in Table 3-8 and Table 3-9, sorted by test code and sample code, respectively.

**Table 3-8: Test characters sorted by test code**

Test Code	Sample Code	Tank Angle before test
A0-1	S-D	0
A0-2	SB5-D	0
A0-3	SB10-D	0
A0-4	SB15-D	0
A0-5	SB20-D	0
A5-1	S-D	5
A5-2	SB5-D	5
A5-3	SB10-D	5
A5-4	SB15-D	5
A5-5	SB20-D	5
A10-1	S-D	10
A10-2	SB5-D	10
A10-3	SB10-D	10
A10-4	SB15-D	10
A10-5	SB20-D	10

Table 3-9: Test characters sorted by sample code

Test Code	Sample Code	Tank Angle Before test
A0-1	S-D	0
A5-1	S-D	5
A10-1	S-D	10
A0-2	SB5-D	0
A5-2	SB5-D	5
A10-2	SB5-D	10
A0-3	SB10-D	0
A5-3	SB10-D	5
A10-3	SB10-D	10
A0-4	SB15-D	0
A5-4	SB15-D	5
A10-4	SB15-D	10
A0-5	SB20-D	0
A5-5	SB20-D	5
A10-5	SB20-D	10

### 3.13. MATLAB Analysis

MATLAB is a computational software program that utilises parallel calculations to model complex equations. This software is employed by millions of engineers and scientists worldwide to analyse and design systems and has a large number of modules for engineering and scientific applications, such as image processing, pattern recognition and optimisation. In this research, an attempt was made to find a specific character in the captured movie to cluster the output into several groups. To achieve this aim, the colour and image pixels were employed as the main parameters and the videos were converted into separate frames. The process of changing videos into corresponding frames is presented systematically in the MATLAB code lines.

#### 3.13.1. MATLAB Code

The MATLAB program uses several functions obtained from a website designed by Kovesi (2000) to code the algorithm under consideration, with the approach to the program coding in this research as follows:

A- Open video file and read it is a frame selected (Figure 3-29).

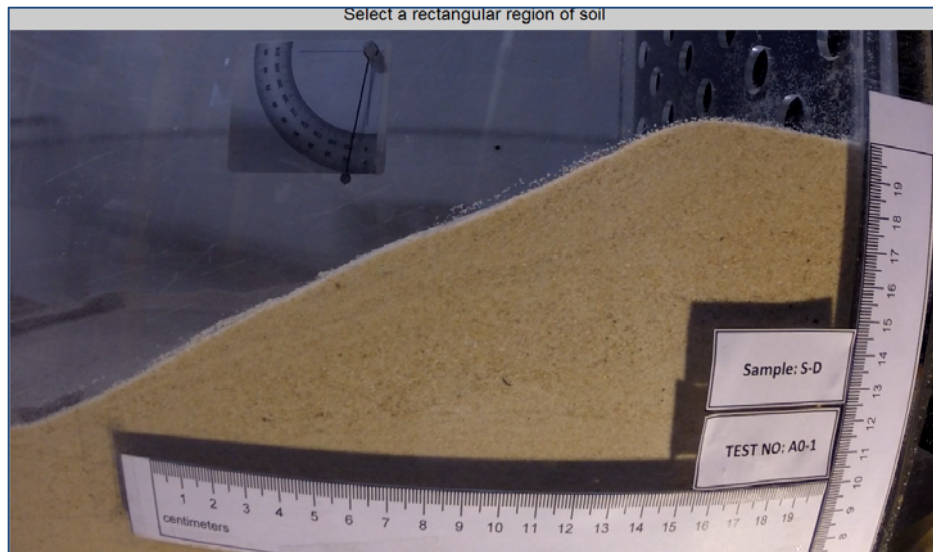


Figure 3-29: Sample label

B- Define a mask area to remove any extra surface and eliminate soil boundaries (Figure 3-30).

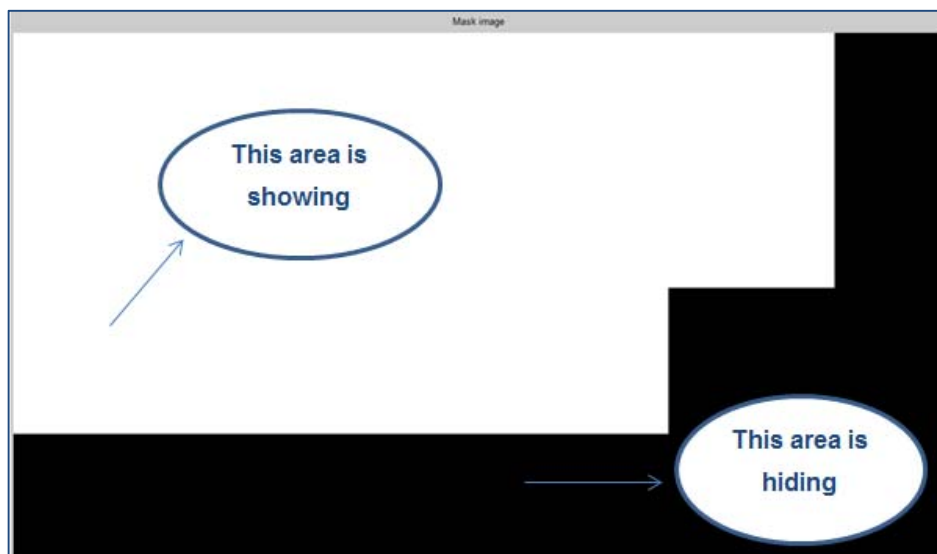


Figure 3-30: Mask area designed to remove unnecessary areas

C- Apply the colour difference threshold to remove holes in the monochrome picture.

D- Select a rectangular area on the soil section and then determine its colour value (Figure 3-31)

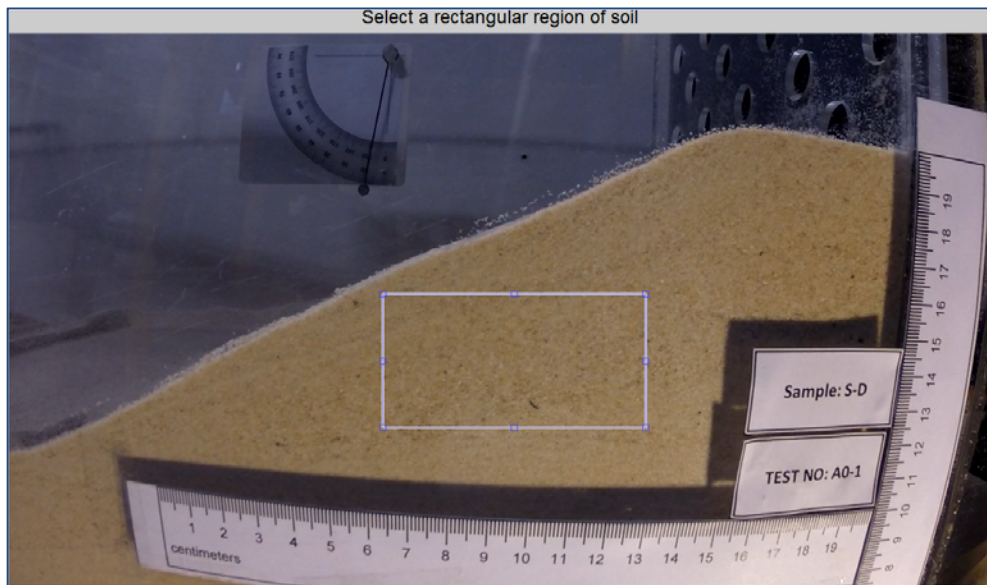


Figure 3-31: Rectangular area to optimise sample colour

E- Convert the soil region RGB values to lab colour space (monochrome) (Figure 3-32).

F- Define the inclinometer region as shown in Figure 3-32.

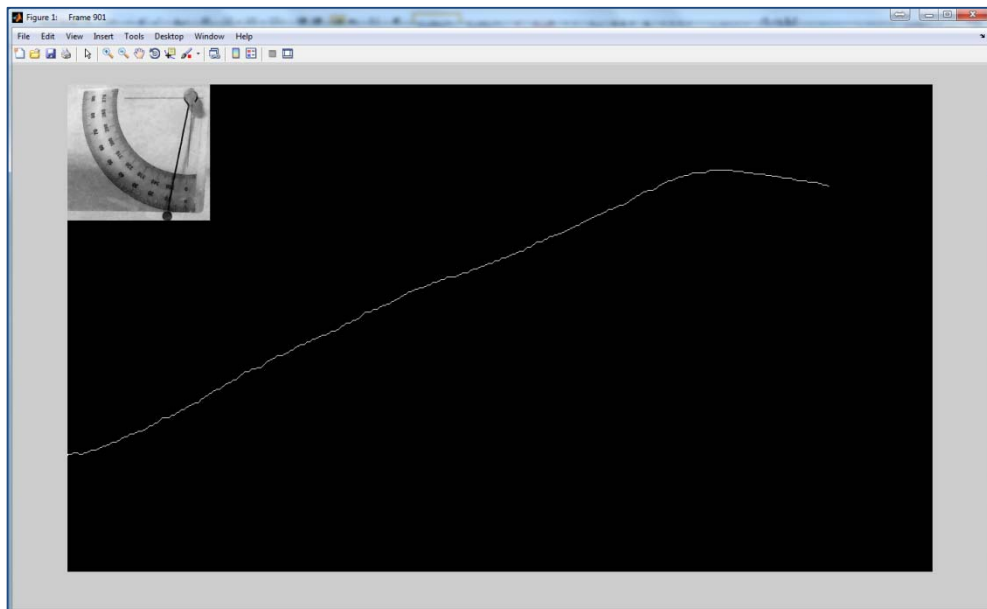


Figure 3-32: Separator line shows slope line

- G- Process the movie frames through the loop.
- H- Select and find the longest edge list and assume it is the surface profile.
- I- Generate an Excel file and export the pixel coordinates into this file where the name of the file is the same as the frame name (Figure 3-33).

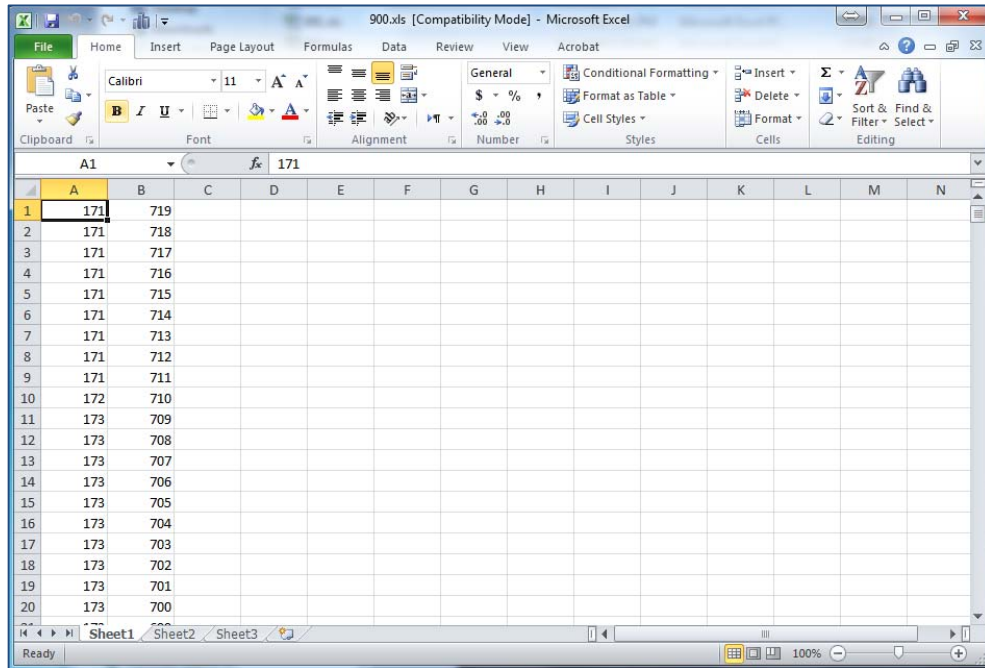


Figure 3-33: Points coordinates for pixels generating the slope line

- J- Import all data into the Excel file using a macro (Figure 3-34).

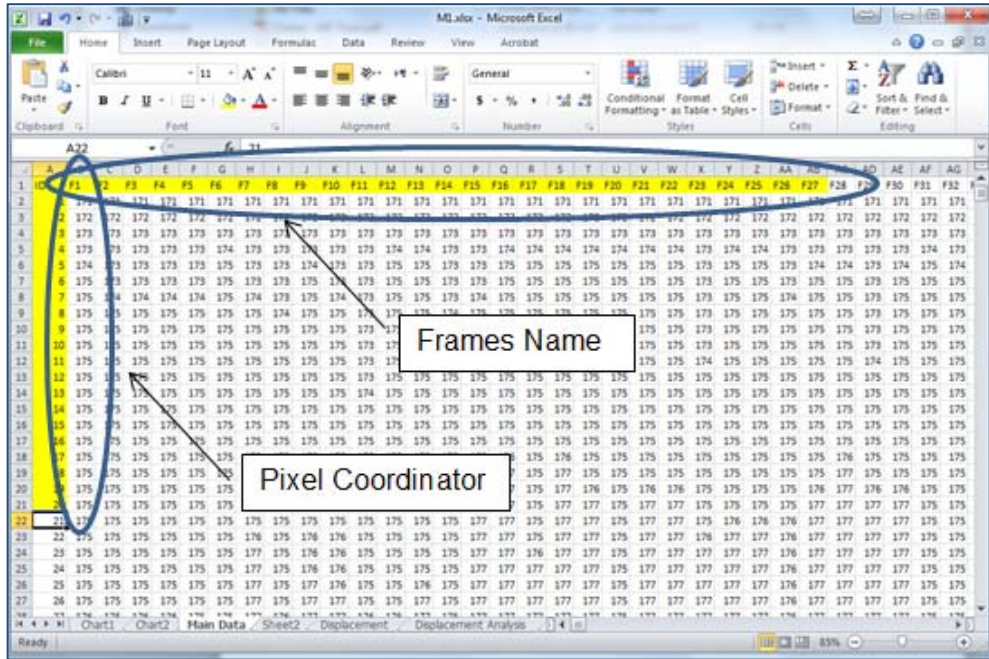


Figure 3-34: Setting the slope line in a sheet frame by frame

K- Conduct a data analysis process with Excel and SPSS software (Figure 3-35).

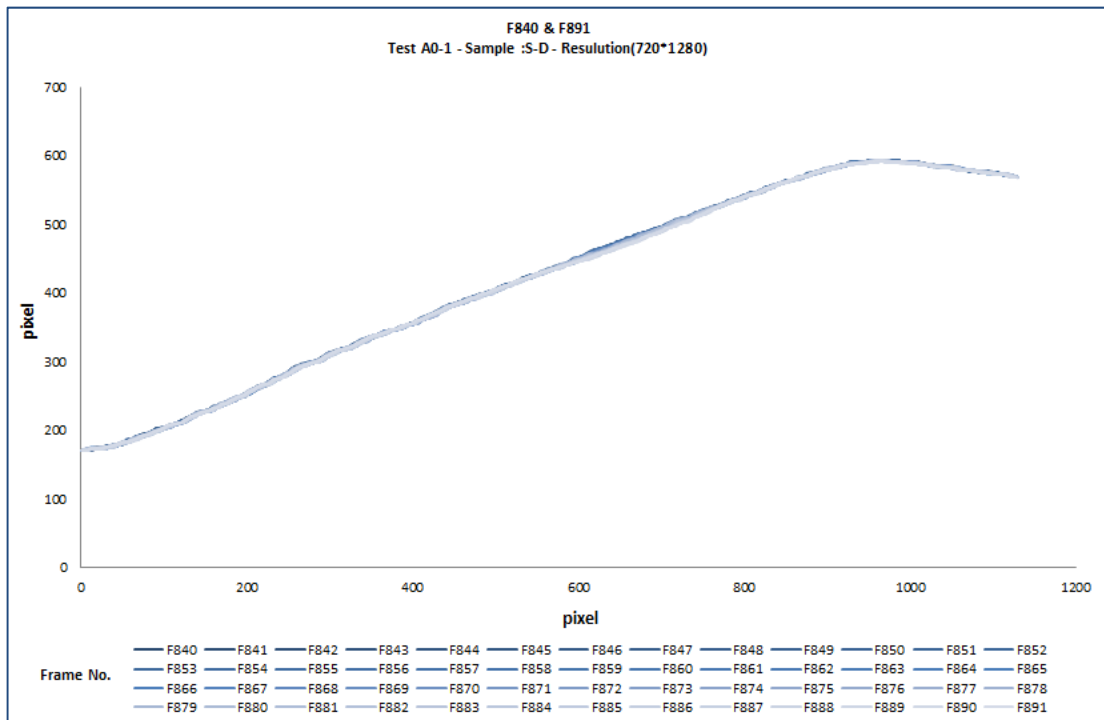


Figure 3-35: The graph generated from frame 840 to 891

The MATLAB coded program is presented in Appendix A.

### 3.14. SPSS Analysis

A comprehensive software package employed for statistical analysis is SPSS. Using the numerical data extracted from the MATLAB software, a comprehensive analysis was accomplished using SPSS software (see Figure 3-36). This software is capable of classifying data with the same characteristics into similar categories. In this research, K-Mean cluster analysis, one of the best classification methods, was applied (IBM, 2013) to analyse the frame category and determine the slope movement jumping in specific frame intervals.

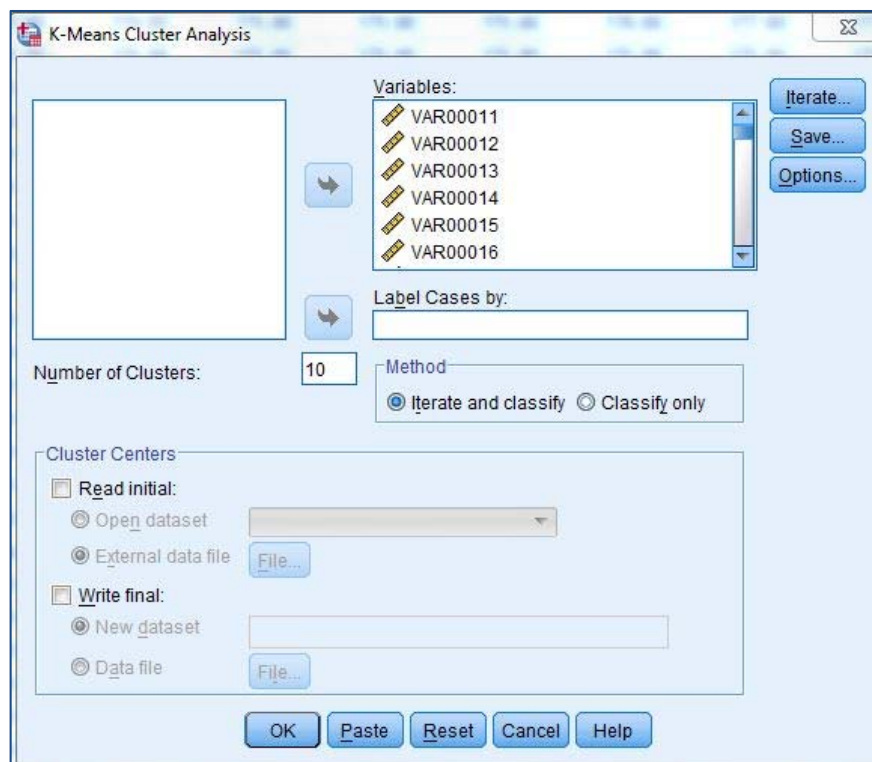


Figure 3-36: Selection of variable parameters in K-Mean cluster analysis

In addition, it was possible to change the clusters numbers to obtain different results. In this research, the number 10 was considered for clusters (Figure 3-37).

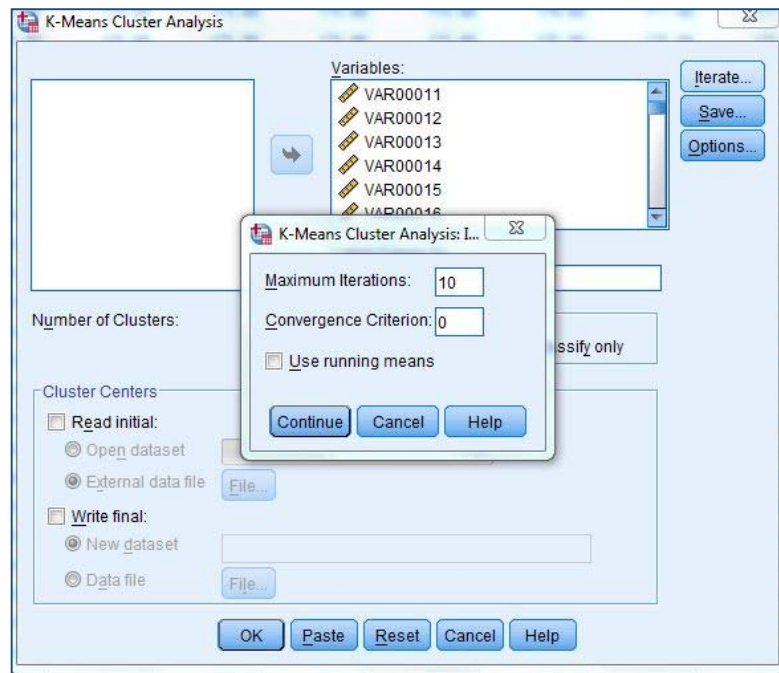


Figure 3-37: Determination of the number of maximum clusters

Before implementing data analysis by the K-Mean method, it was necessary to standardise the data by the following procedures (Figure 3-38):

- 1- Select Descriptive... from Analyze /Descriptive Statistics

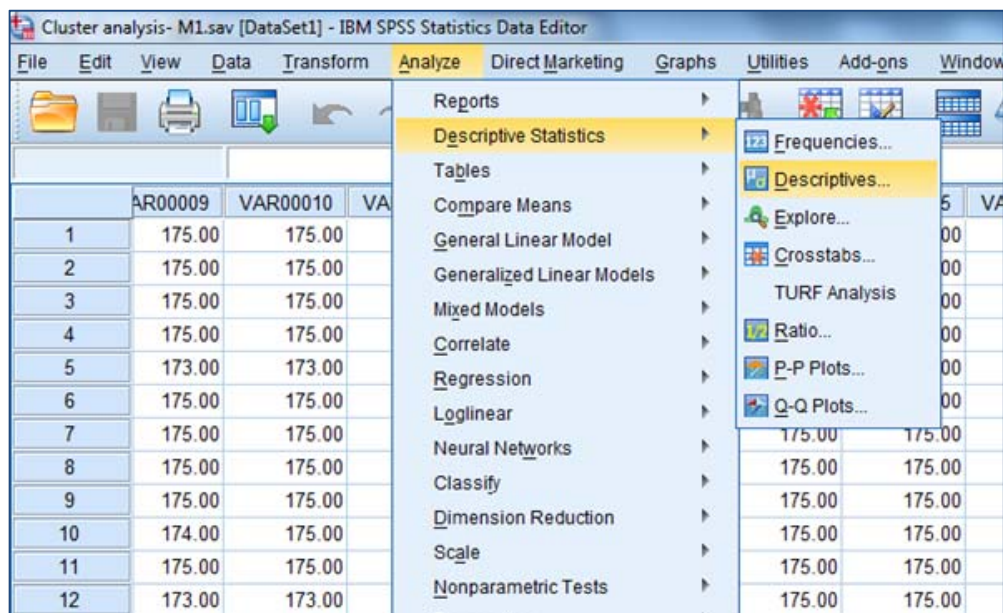


Figure 3-38: Standardisation process

- 2- Select the variables and save standardised values as variables to generate the standardised data (Figure 3-39).



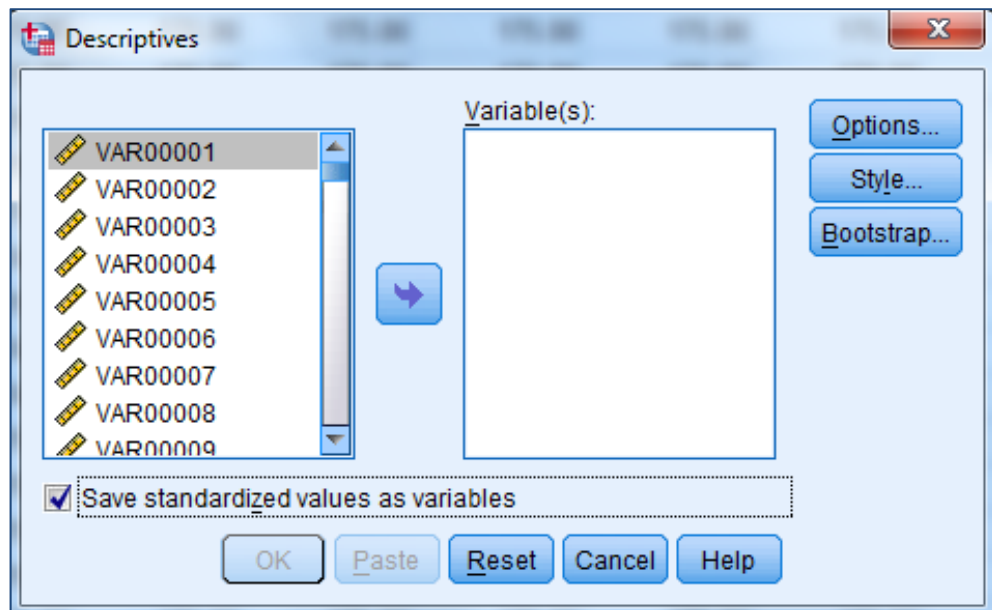


Figure 3-39: Selection of variables for normalising

This SPSS analysis was done to clarify relation between separated lines in slope lines presented for the test.

## **4. EXPERIMENTAL RESULTS AND DISCUSSION**

In this chapter, the following procedures for the interpretation and implementation of the test outcomes has been taken into account:

- MATLAB was run for 15 movies and the outputs were automatically entered into the Excel files for post-processing analysis.
- The Excel files were merged into a single Excel sheet for data analysing by SPSS software.
- The tests were categorised for comparisons as follows:
  - Same ingredients with different alignments:  
S-D:(A0-1, A5-1, A10-1)  
SB5-D:(A0-2, A5-2, A10-2)  
SB10-D:(A0-3, A5-3, A10-3)  
SB15-D:(A0-4, A5-4, A10-4)  
SB20-D:(A0-5, A5-5, A10-5)
  - Same alignment with different ingredients  
A0-1,2,3,4,5: (S, SB5 , SB10, SB15, SB20 – D)  
A5-1,2,3,4,5: (S, SB5 , SB10, SB15, SB20 – D)  
A10-1,2,3,4,5: (S, SB5 , SB10, SB15, SB20 – D)

### **4.1. Comparison between Tests with Same Ingredients and Different Alignments**

#### **4.1.1. S-D:(A0-1, A5-1, A10-1)**

In this test, three different categories were investigated as follows:

- Intervals of 100 frames
- Intervals of 50 frames
- Intervals of 20 frames

To compare soil slopes stability assuming the same ingredients, the displacement value of the soil was computed using the PIV procedure in the MATLAB software program.

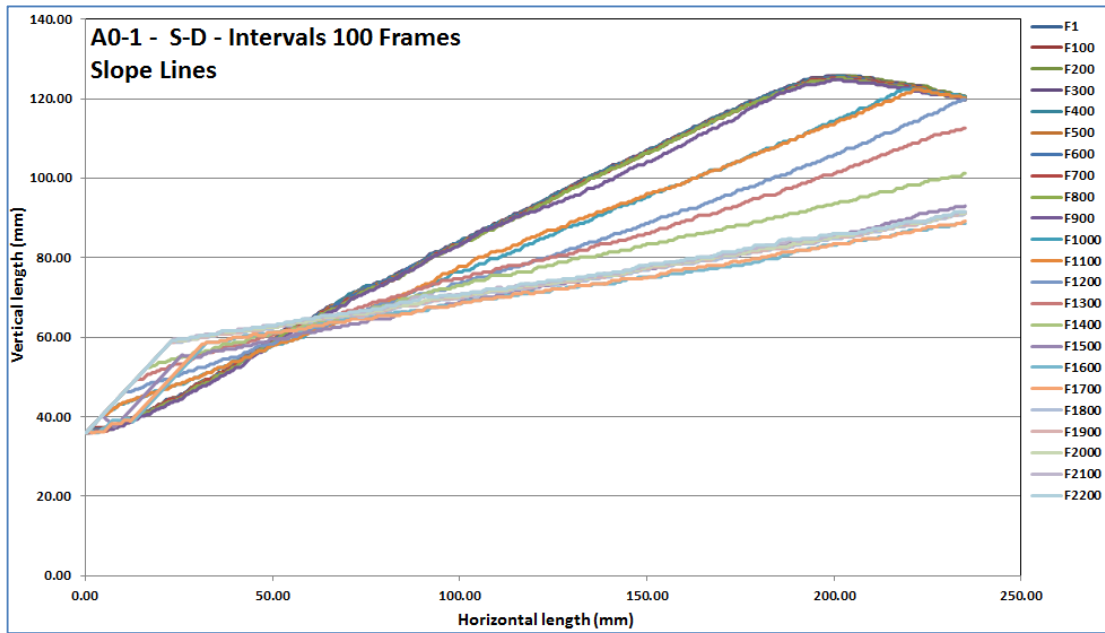


Figure 4-1: Changes in slope stability for different frames with alignment of 0°

Figure 4-1 depicts the some curves of slope stability when the frame numbers change along the test time with an interval of 100 and shows that the slope angle steadily decreased with a gradual increase in the frame numbers or rotation of the tank. This figure illustrates how slope stability can change when the frame numbers are varied or the tank moved upward at a constant rate of 5 mm/s vertically or 0.95 deg/s rotationally. A movement resistance in the initial frame can be seen followed by a jump in rotations, which can be called the failure threshold.

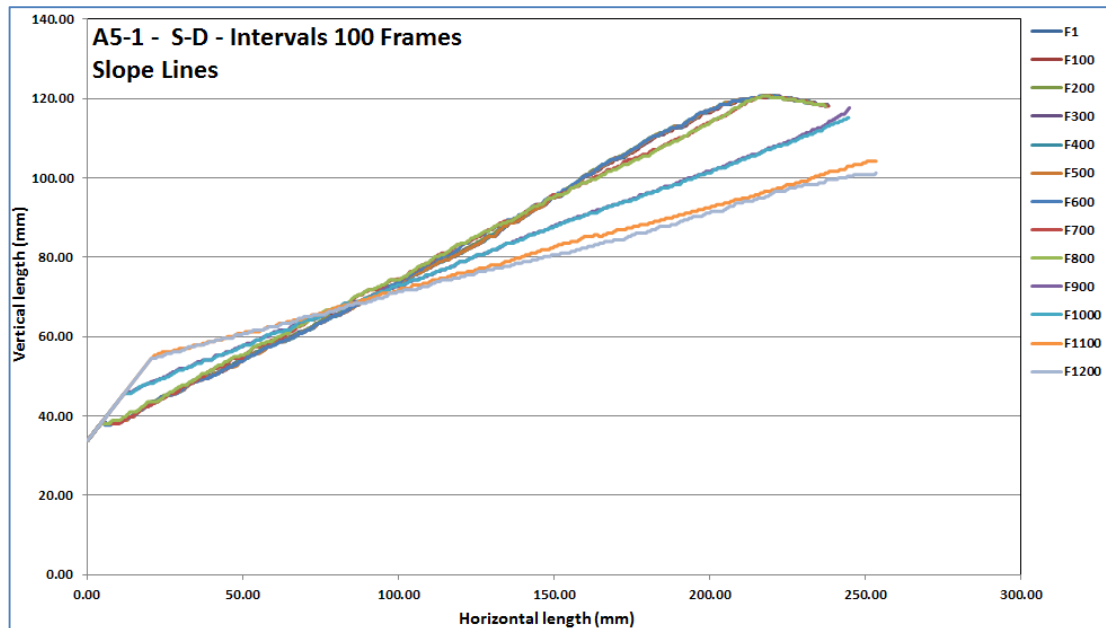


Figure 4-2: Changes in slope stability for different frames with alignment of 5°

Figure 4-2 presents changes in slope stability for different frames with alignment of 5°. The failure threshold can be clearly seen, where F900 has considerable movement compared with slopes changes in the initial frames. From the figure, the test results reveal a slight difference in slope angle with variation of the frame number initially. However, as the frame numbers increase, their corresponding slope angles decrease mainly after the failure threshold has been reached. An increase in the frame number creates more potential for slip surfaces and less potential for stability. Therefore, the test results demonstrate that the slope movements are not the same rate as loading rates induced by tank rotation.

One important result is that failures do not show planar and transitional slides. Instead, they are rotating around a point that is located along nearly one third of the slope.

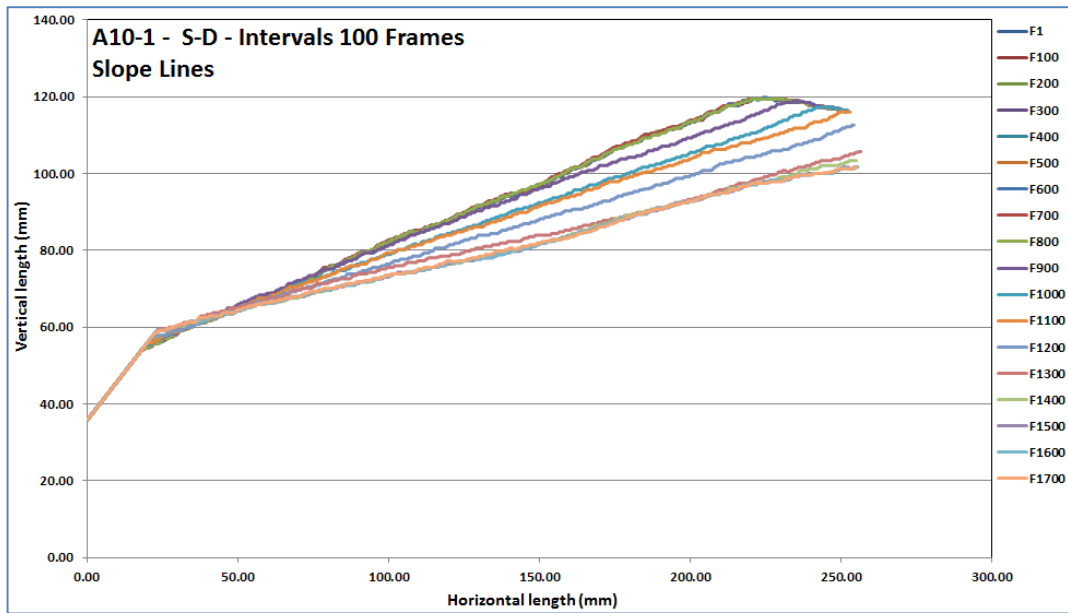


Figure 4-3: Changes in slope stability for different frames with alignment of 10°

Figure 4-3 shows variations in the slope stability for different frames with alignment of 10°, illustrating the convergence of all curves as the frame number increases. These test results confirm previous results. Hence, the relationship between the frame number and slope stability is a reverse function; therefore, the slope angle is decreased by failure when the frame number is increased.

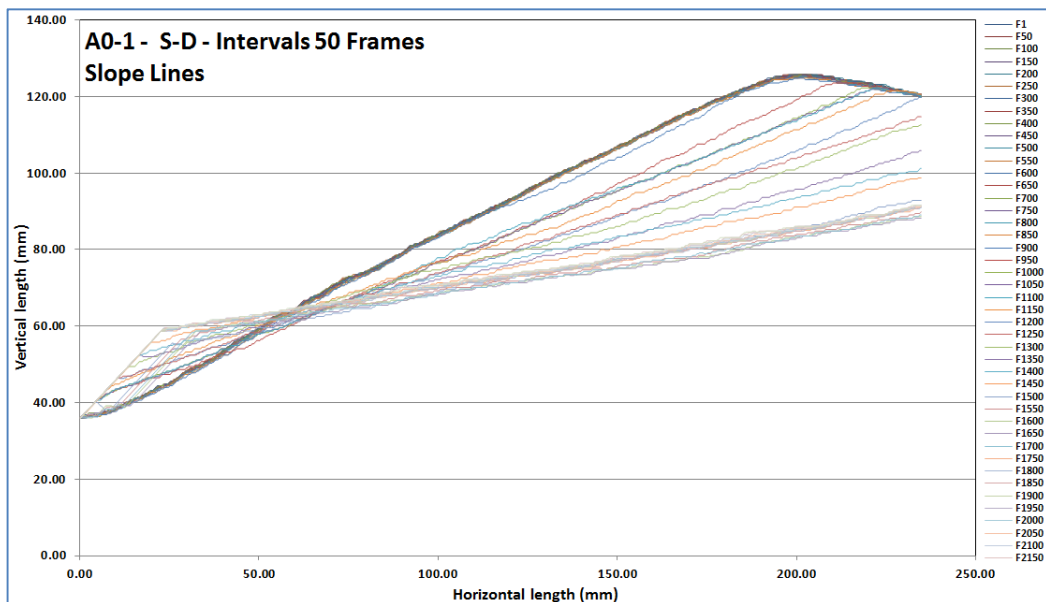


Figure 4-4: Changes in slope stability for different frames with intervals of 50 frames

Slope stabilities of the samples for eighteen frames with intervals of 50 frames are depicted in Figure 4-4. This figure illustrates how slope stability alters when the frame number varies, and reveals from the curves that there is an almost uniform rotation or movement after the first jump in frame F950. Therefore, the slope angle decreases steadily after failure.

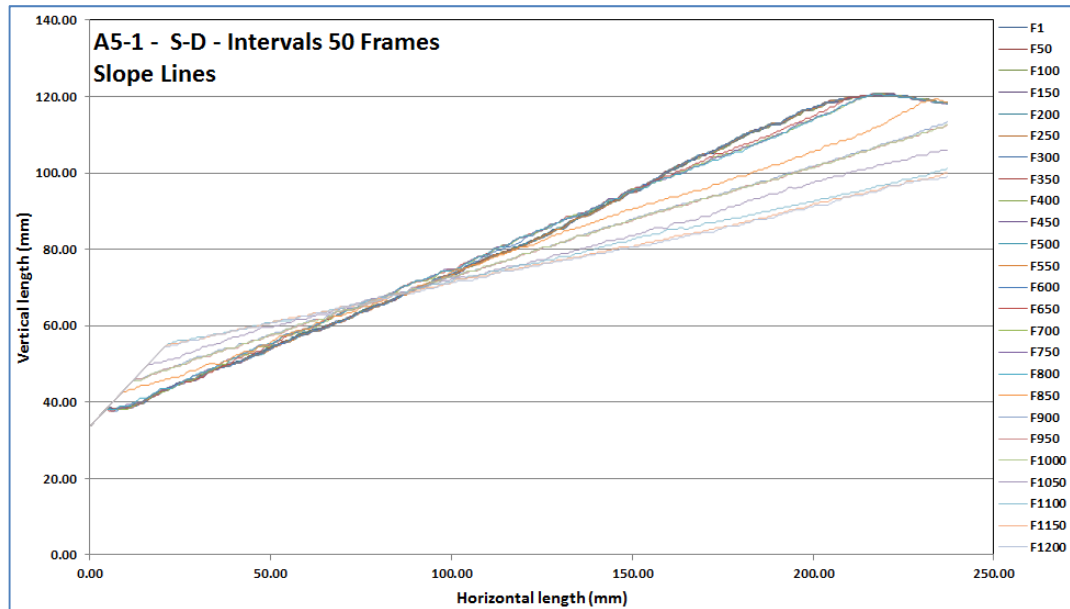


Figure 4-5: Changes in slope stability for different frames with alignment of 5°

Slope angles based on several frames with alignment of 5° are shown in Figure 4-5. When curves change from lower frame to higher frame, the angle decreases, i.e. the slope angle decreases when the frame number increases.

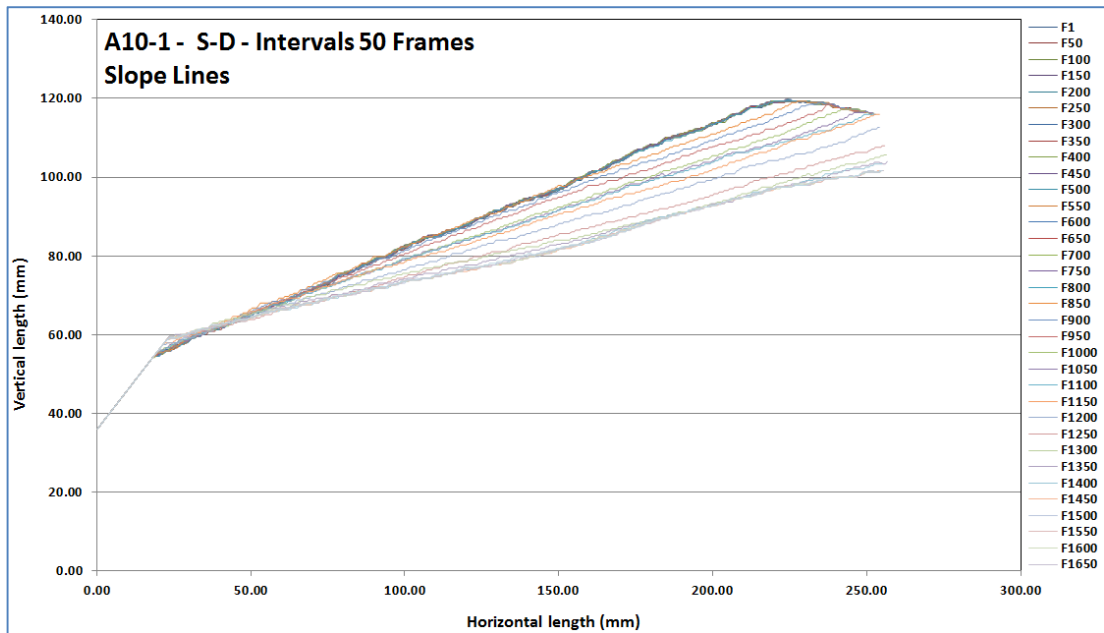


Figure 4-6: Changes in slope stability for different frames with intervals of 50 frames

Figure 4-6 shows the effect of frame numbers on slope stability for ten laboratory tests. From the figure, it is difficult to locate the jump and statistical analysis of the movement rates is required. The curves present a uniform convergence of slope stability lines by increasing the frame number, which is similar to the previous analysis that demonstrates an increase in the frame numbers leads to a decrease in slope angle.

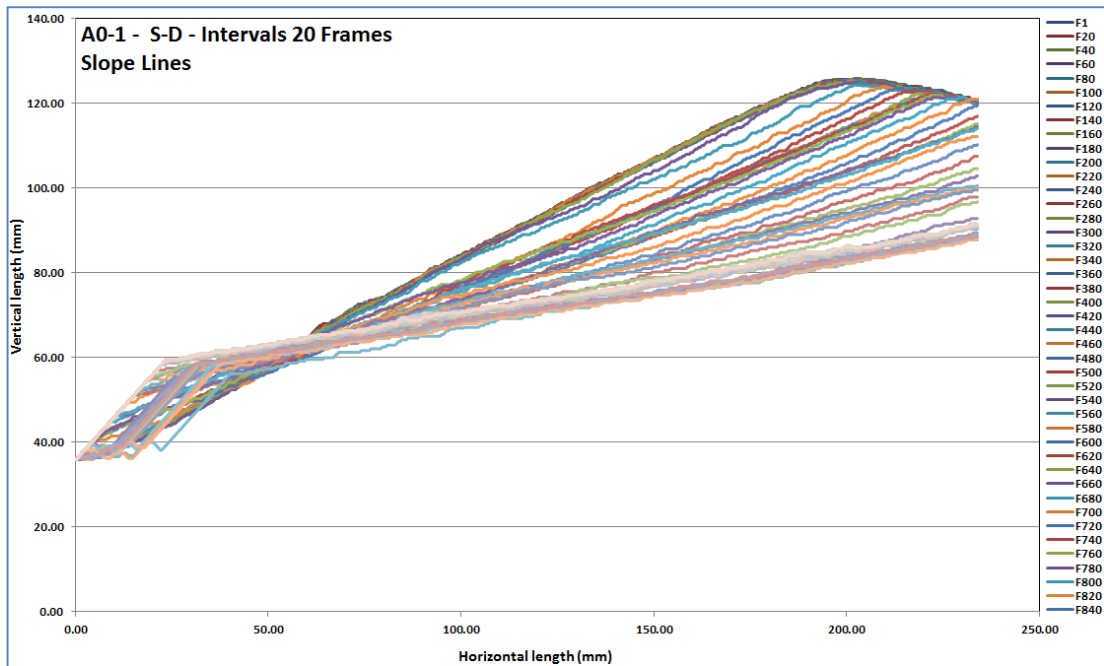


Figure 4-7: Changes in slope stability for different frames with intervals of 20 frames

Figure 4-7 shows how slope stability changes as a function of the frame numbers with intervals of 20 frames. The relationship of the slope angle and frame number changes appears to be opposite, i.e., the slope angle increases as the frame number decreases in a steady manner. However, delineating of the failure surface is not as easy as that shown in Figure 4-1 to Figure 4-7.

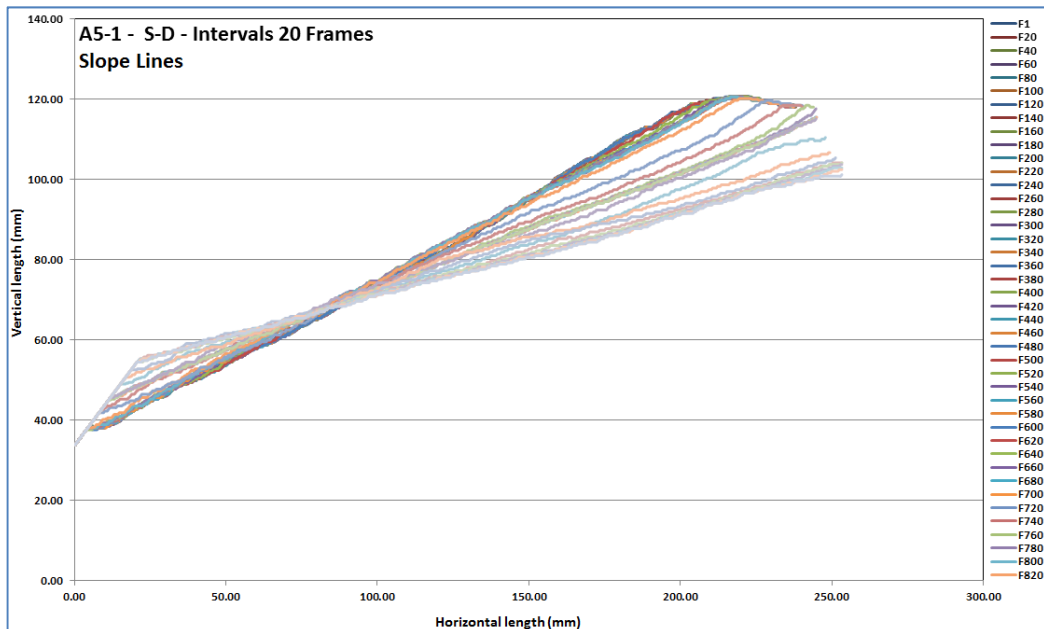


Figure 4-8: Changes in slope stability for different frames with intervals of 20 frames



The effect of the frame numbers on slope angles are presented in Figure 4-8, which reveals a slight difference between the lines resulting from slip surfaces. However, the slope angle varies with an insignificant change in the frame number; therefore, statistical analysis might be necessary to distinguish the yielding frames.

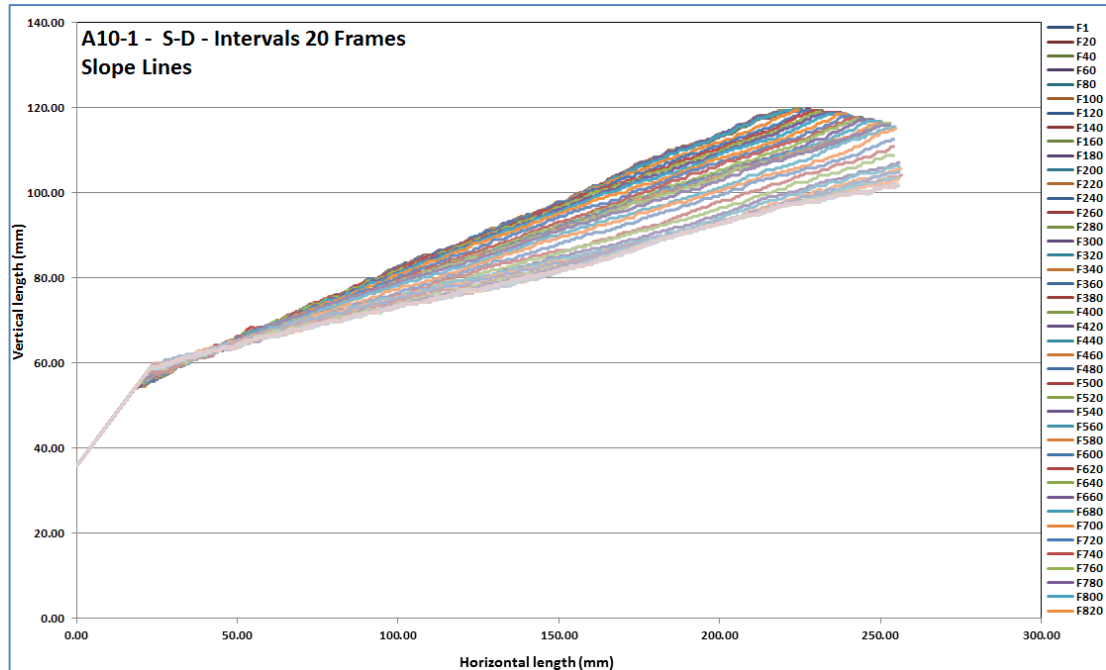


Figure 4-9: Changes in slope stability for different frames with alignment of 10°

The role of frame numbers in surface failures is depicted in Figure 4-9, where it is confirmed that the frame numbers play a significant role in the slope stability process. From the figure, it is clear that the effects of frame numbers on slope angles for several tests are converged with increasing frame number.

#### 4.1.2. SB5-D:(A0-2, A5-2, A10-2)

The following section describes the results obtained when bentonite was added to the soil in varying percentages..

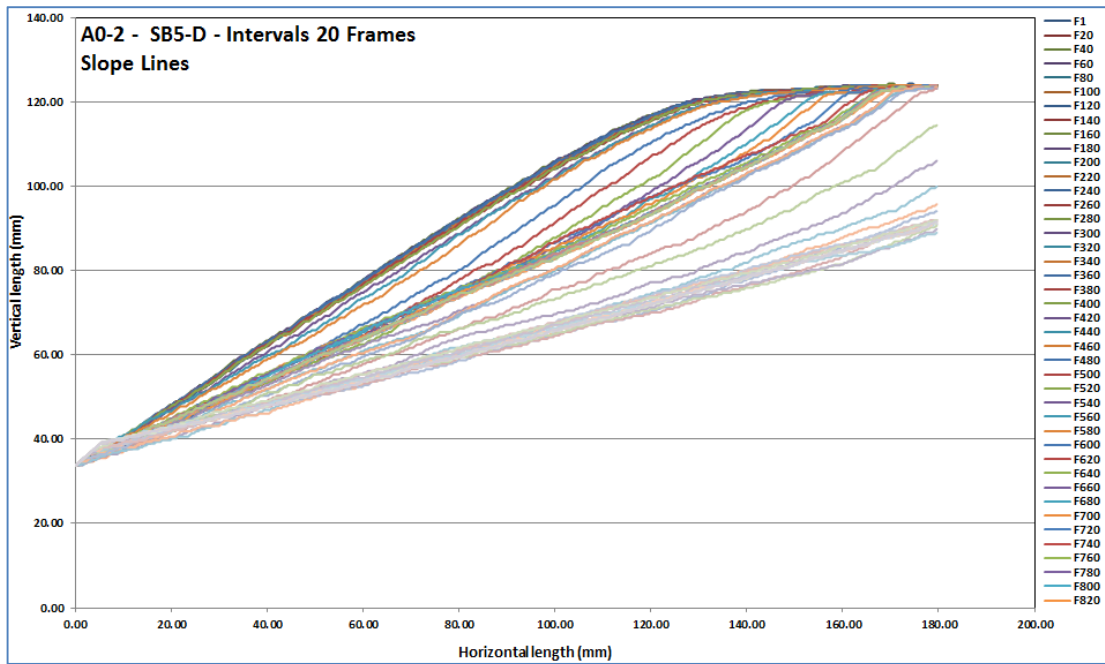


Figure 4-10: Changes in slope stability for different frames with intervals of 20 frames

Figure 4-10 shows a range of variations in slope stabilities with intervals of 20 frames, which is in agreement with previous analyses that demonstrated significant influence of frame numbers on slope angles. The figure illustrates that a decrease in the frame numbers leads to an increase in the slope angle.

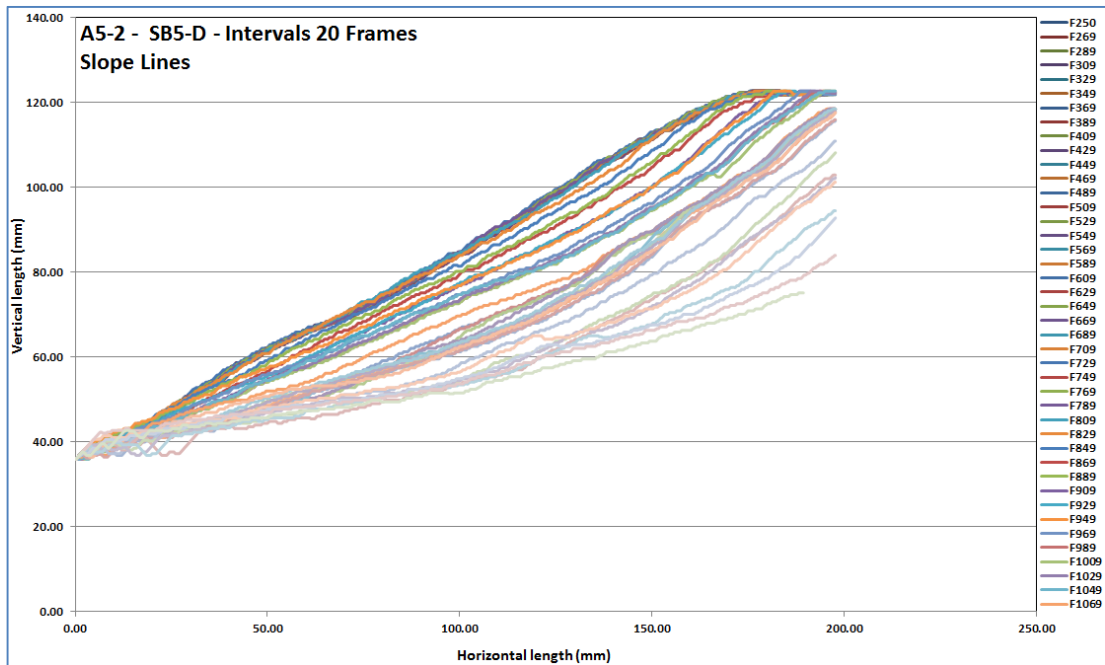


Figure 4-11: Changes in slope stability for different frames with alignment of 5°

Figure 4-11 depicts the effect of the frame numbers on slope angle under alignment of  $5^\circ$ , with a relative difference between the curves indicating that the slope angle continuously increased with decreasing frame numbers. However, overall the same trends for all curves were observed.

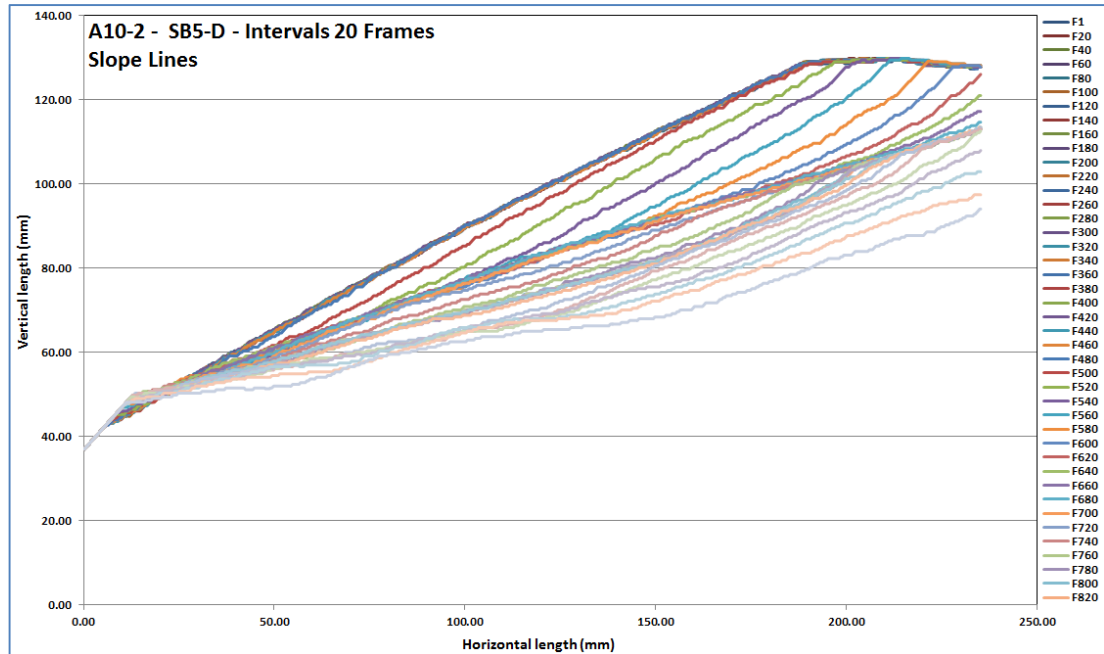


Figure 4-12: Changes in slope stability for different frames with alignment of  $10^\circ$

The changes in slope angle with the frame numbers under alignment of  $10^\circ$  are depicted in Figure 4-12, with all curves converged in F120. However, the slope angle declines with increasing frame numbers.

#### 4.1.3. SB10-D:(A0-3, A5-3, A10-3)

By addition of 10% bentonite to the saturated soil, a series of laboratory tests were conducted to determine the impact of this new composition on slope stability. The results of these tests are schematically depicted and technically described in the following section.

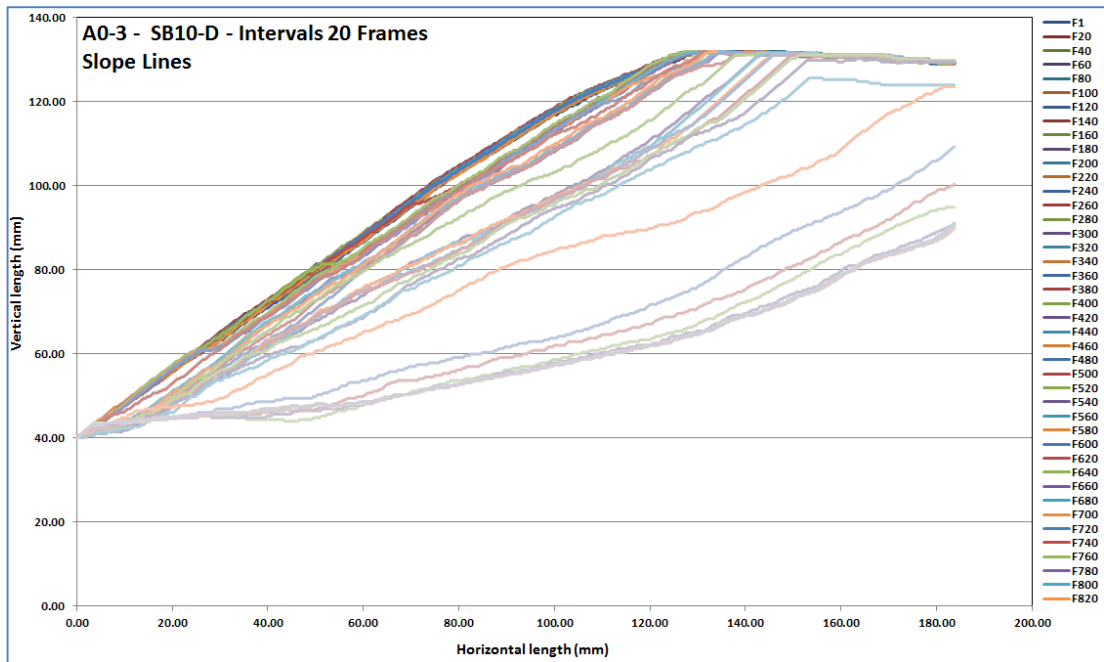


Figure 4-13: Changes in slope stability for different frames with intervals of 20 frames

The effect of several frame numbers on the slope angles is observable as shown in Figure 4-13 by varying the bentonite percentage content, with there being obvious significant differences between the slope stability lines. However, by decreasing the frame numbers, the slope angles substantially increased.

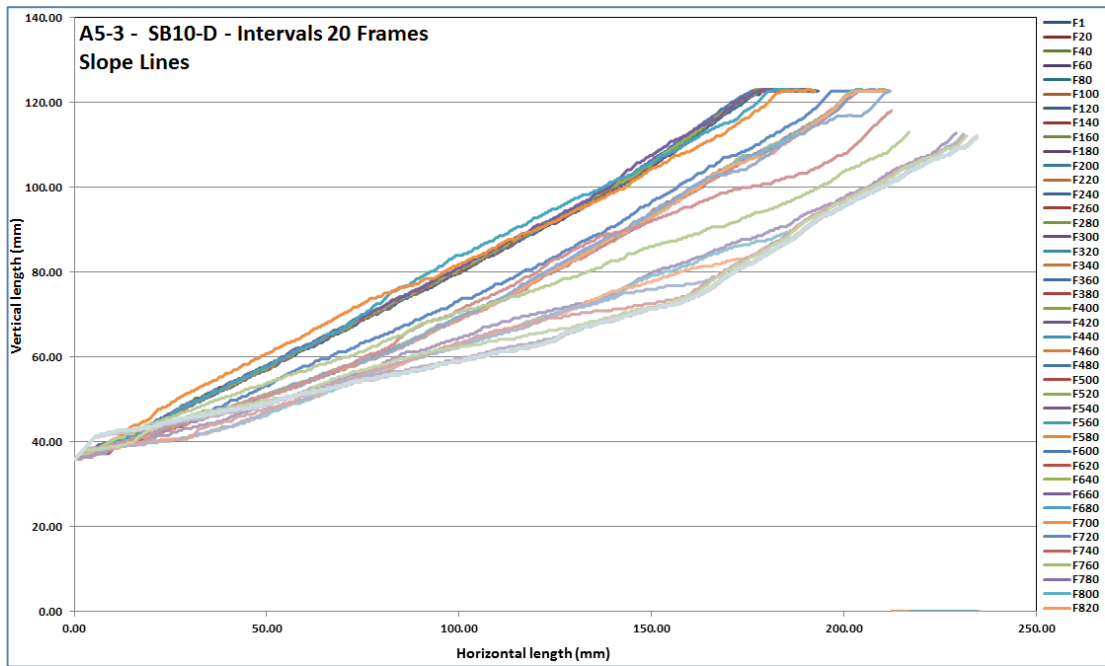


Figure 4-14: Changes in slope stability for different frames with alignment of 5°

The impact of the frame number on slope angle is depicted in Figure 4-14, which illustrates that an increase in frame numbers leads to a decrease in slope angle.

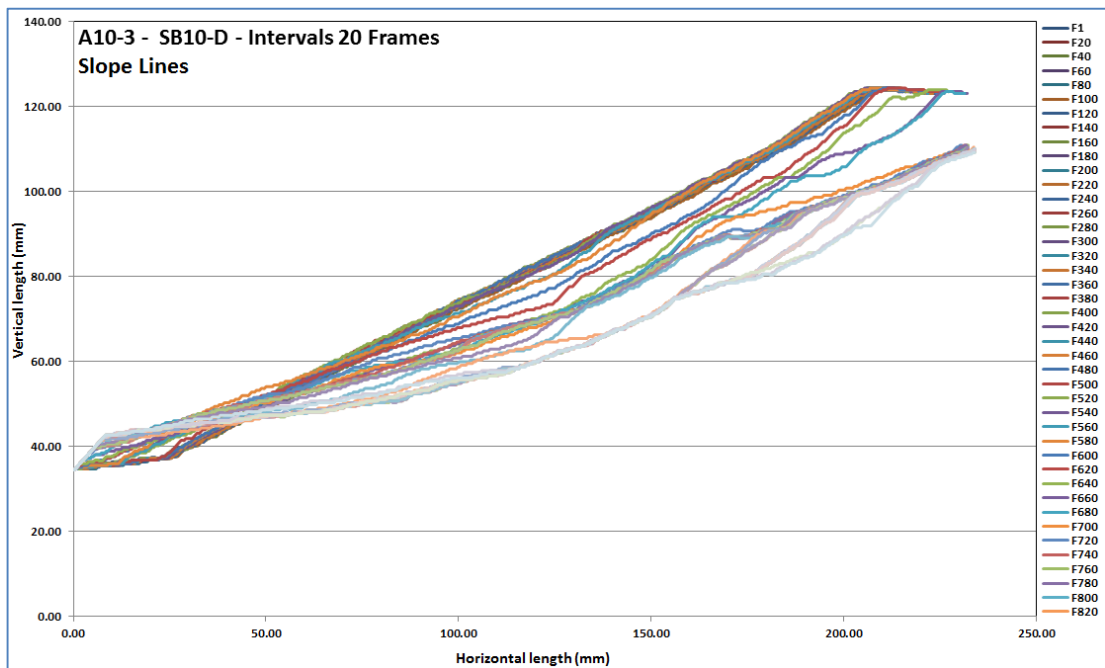


Figure 4-15: Changes in slope stability for different frames with alignment of 10°

The effect of the frame number on slope inclination under alignment of 10° is shown in Figure 4-15, which illustrates the curves are close to each other and approximately present the same behaviour.

#### 4.1.4. SB15-D:(A0-4, A5-4, A10-4)

By addition of 15% bentonite, the following patterns were extracted from the laboratory tests.

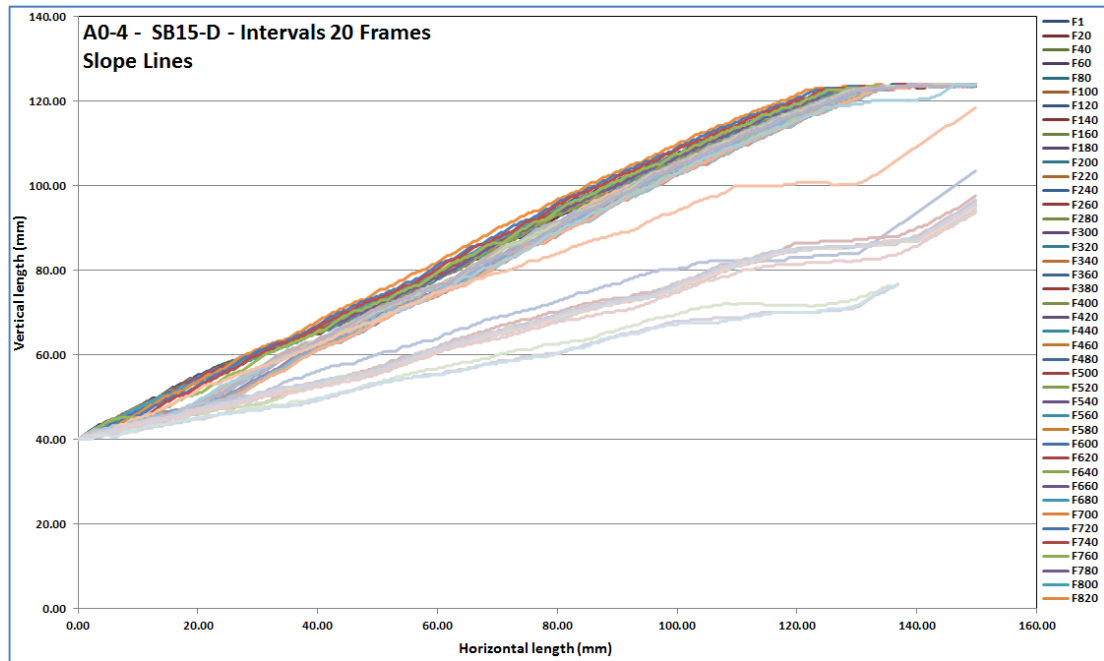


Figure 4-16: Changes in slope geometry for different frames with intervals of 20 frames

Figure 4-16 reflects the behaviour of slope inclination when altering the frame numbers and shows a significant relationship between slope inclination and frame numbers. Therefore, the slope angle decreases when the frame number considerably increases.

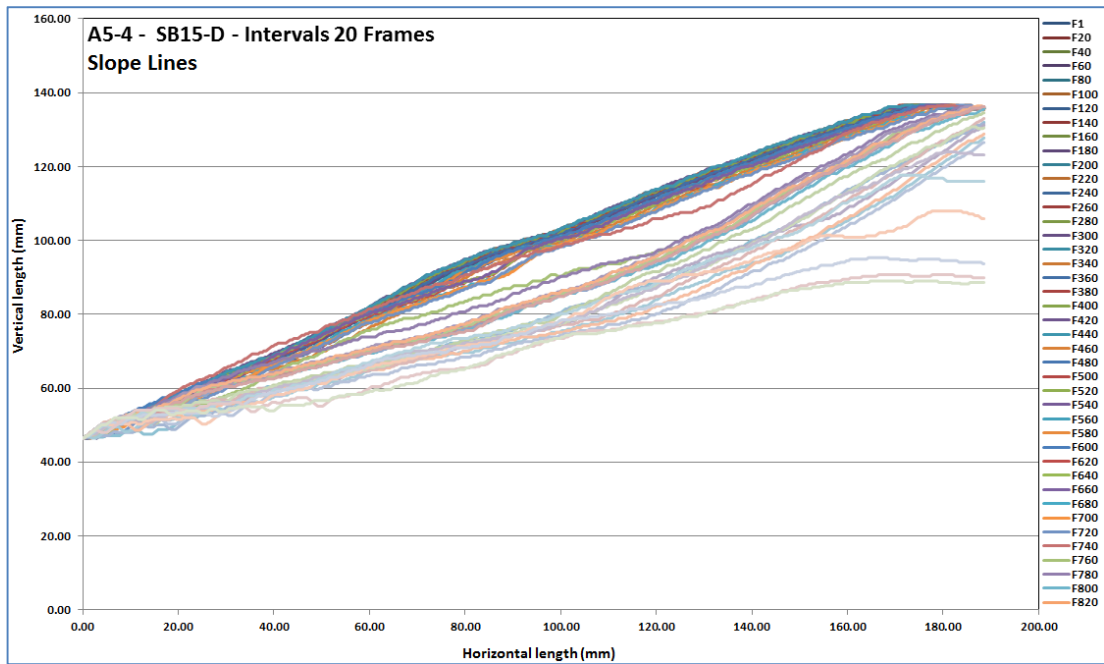


Figure 4-17: Changes in slope geometry for different frames with alignment of 5°

The impact of the frame numbers on slope inclination under alignment of 5° is presented in Figure 4-17, which illustrates there is a relative difference between all curves. However, the slope angle continuously decreases when the frame number steadily increases.

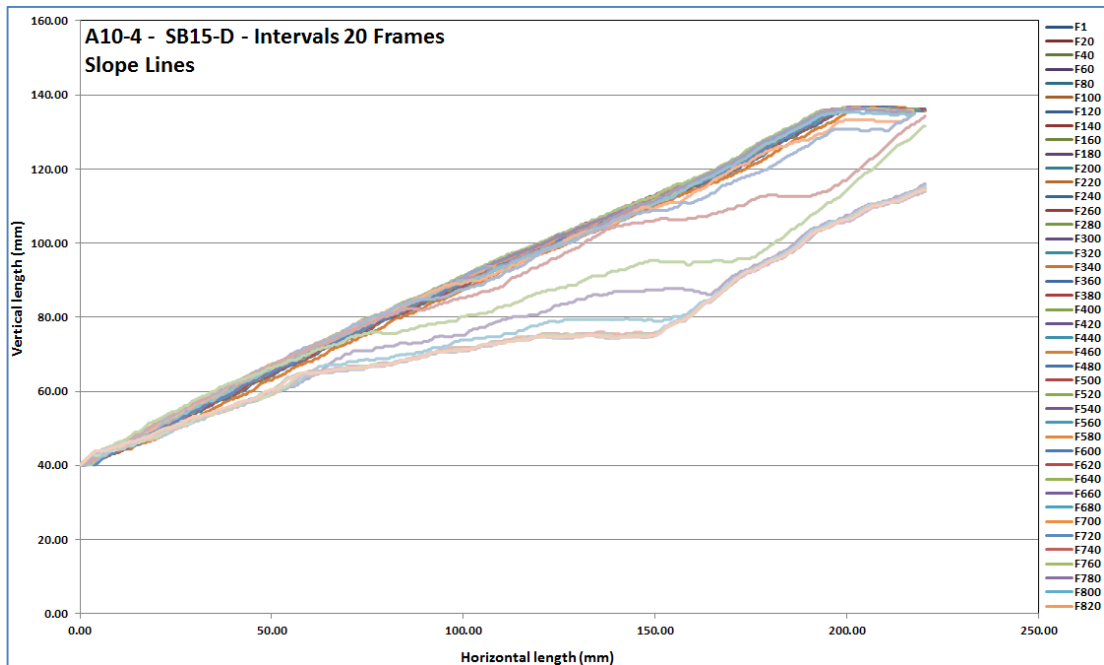


Figure 4-18: Changes in slope geometry for different frames with alignment of 10°

Figure 4-18 illustrates how the slope angle changes when the frame number increases or decreases, with the lines relatively coinciding in lower frame numbers.

#### 4.1.5. SB20-D:(A0-5, A5-5, A10-5)

By addition of 20% bentonite, the laboratory tests are repeated under the identical conditions to above tests, and the results are presented in the following part.

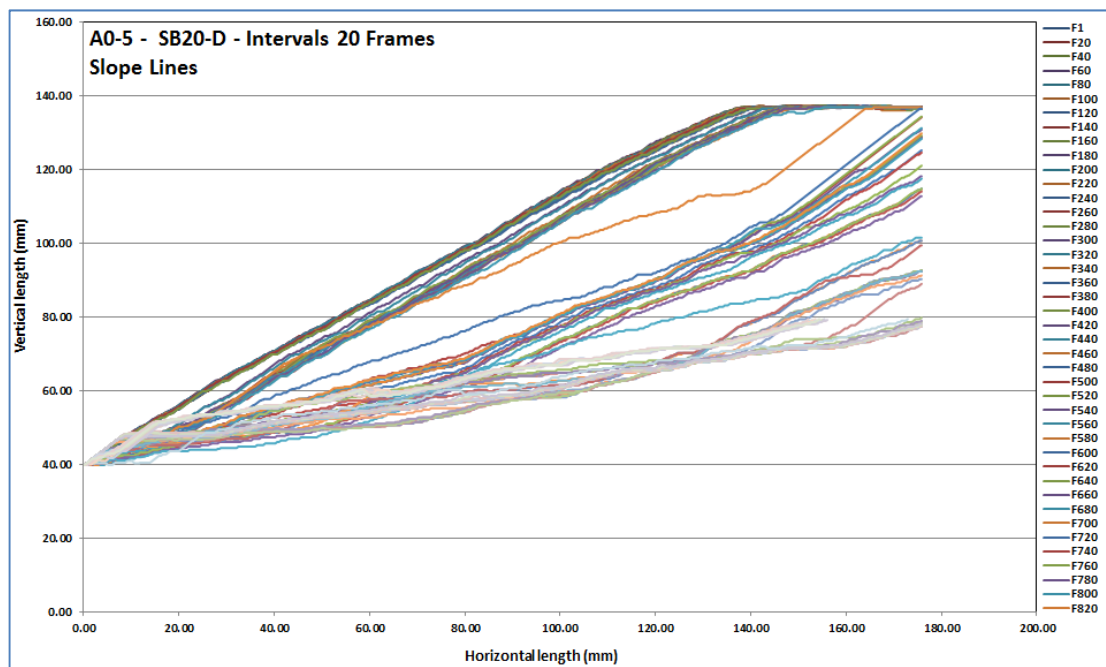


Figure 4-19: Changes in slope geometry for different frames with intervals of 20 frames

Figure 4-19 shows the changes in slope inclination when the frame numbers vary systematically, which illustrates that the slope inclination quickly decreases as the frame number increases.



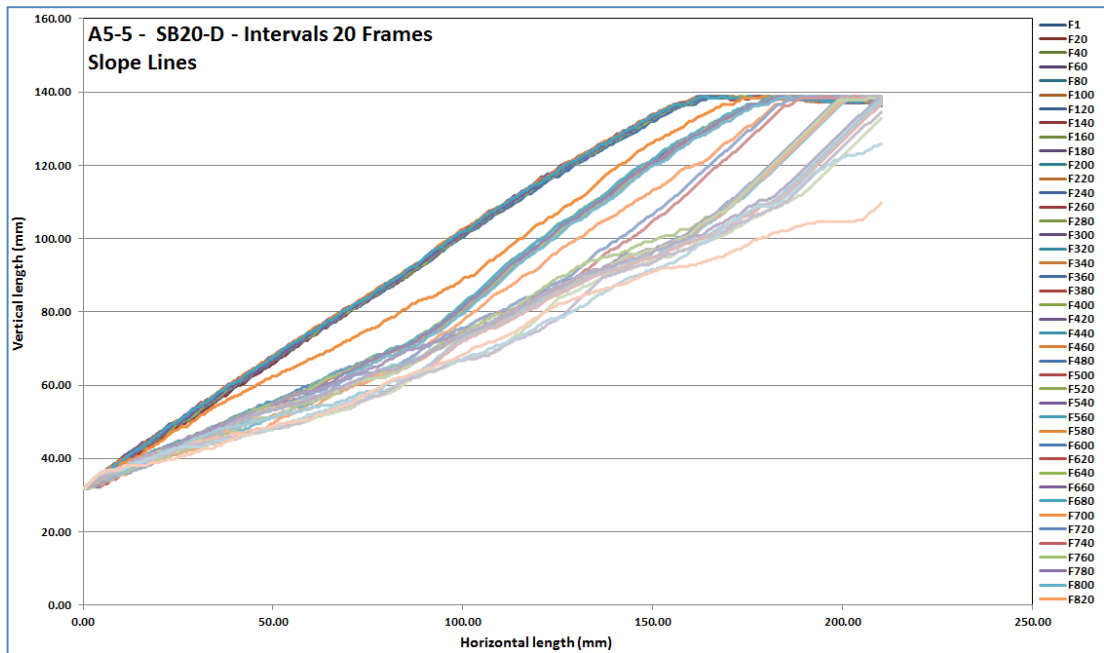


Figure 4-20: Changes in slope geometry for different frames with alignment of 5°

Figure 4-20 reflects how changes in slope inclination are influenced by the frame numbers under alignment of 5°. From the figure, it is obvious that there is a convergence among the curves with increase in the frame number.

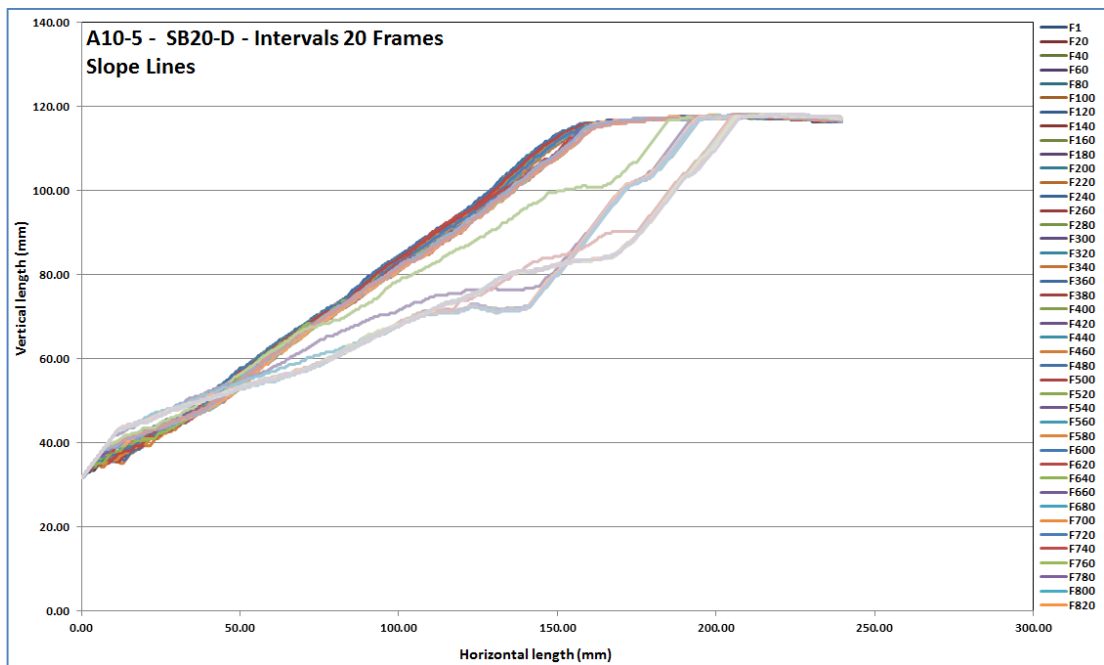


Figure 4-21: Changes in slope geometry for different frames with alignment of 10°

The impact of the frame number on the slope inclination under alignment of 10° is shown in Figure 4-21, which illustrates that a decrease in the frame number leads to an increase in the slope inclination.

## 4.2. Tests Conducted with the Same Alignment and Different Ingredients

In this section, the results from Figure 4-1 to Figure 4-21 are reproduced according to their batching proportions or ingredient contents. Thus, by changing the composition of the test samples, a new set of analysis are obtained for the slopes as follows:

### 4.2.1. A0-1,2,3,4,5: (S, SB5 , SB10, SB15, SB20 – D)

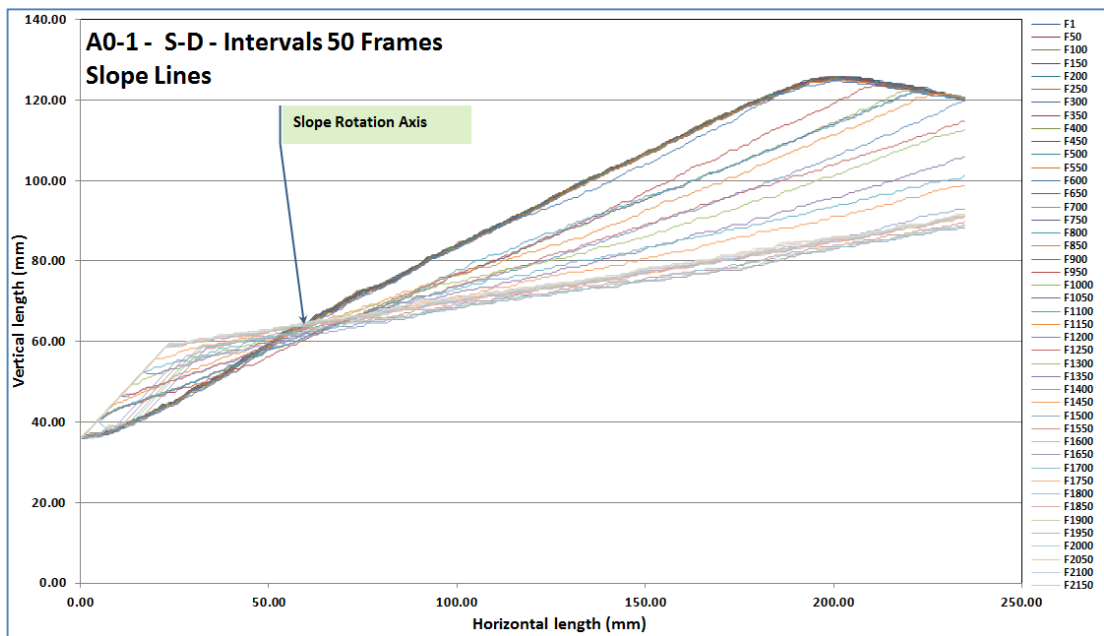


Figure 4-22: Changes in slope geometry for different frames with intervals of 50 frames

The effect of the frame number on the slope angle is presented in Figure 4-22 with intervals of 50 frames, which shows that the lines are distributed uniformly and differences between lines are not significant. However, this result does not occur by increasing the percentage of bentonite in the sample, as presented in the following figures.

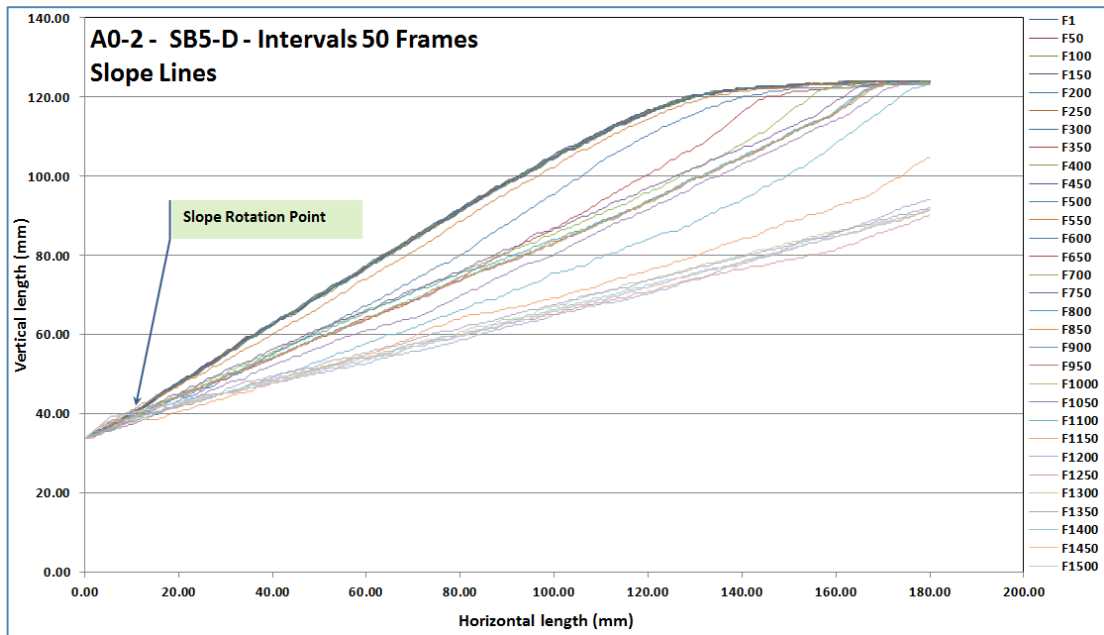


Figure 4-23: Changes in slope geometry for different frames with 5% bentonite

The changes in slope angle with the frame number are shown in Figure 4-23, which illustrates a convergence between the lines because of the slip surfaces with increase in the frame number. This convergence tends to shift upward from 0% bentonite to 10% bentonite as illustrated in Figure 4-24.

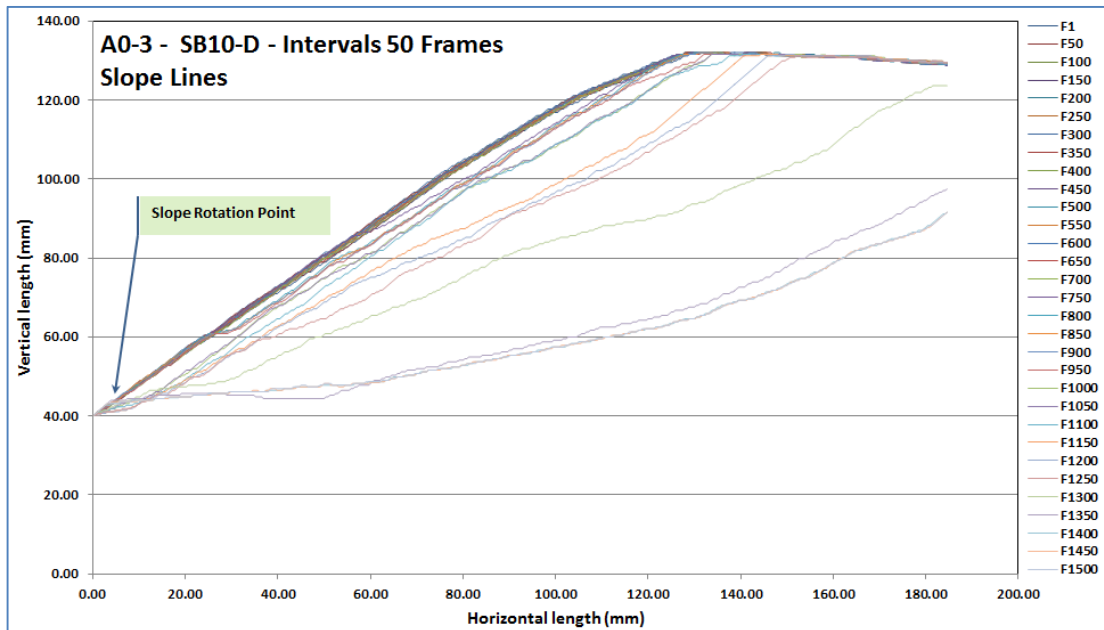


Figure 4-24: Changes in slope geometry for different frames with 10% bentonite

Figure 4-24 depicts the changes in slope stability with the frame numbers under the addition of 10% bentonite, which shows that there is a significant difference between the lines.

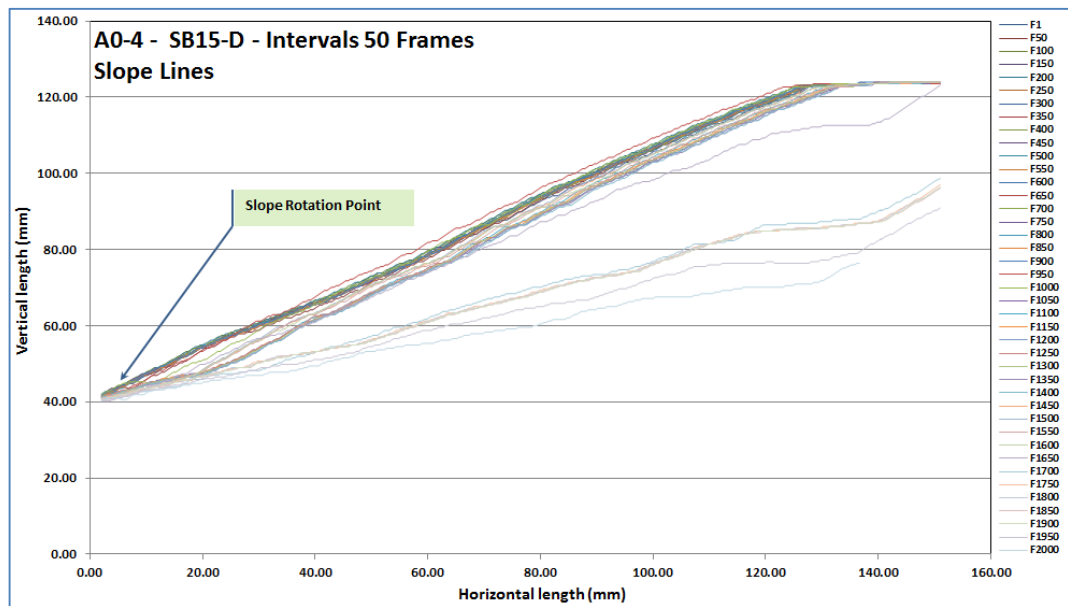


Figure 4-25: Changes in slope geometry for different frames with 15% bentonite

The effect of the frame number on the slope inclination is depicted in Figure 4-25, which shows there is an outstanding convergence among all curves with increasing frame number. However, the slope angle decreases as the frame number increases.

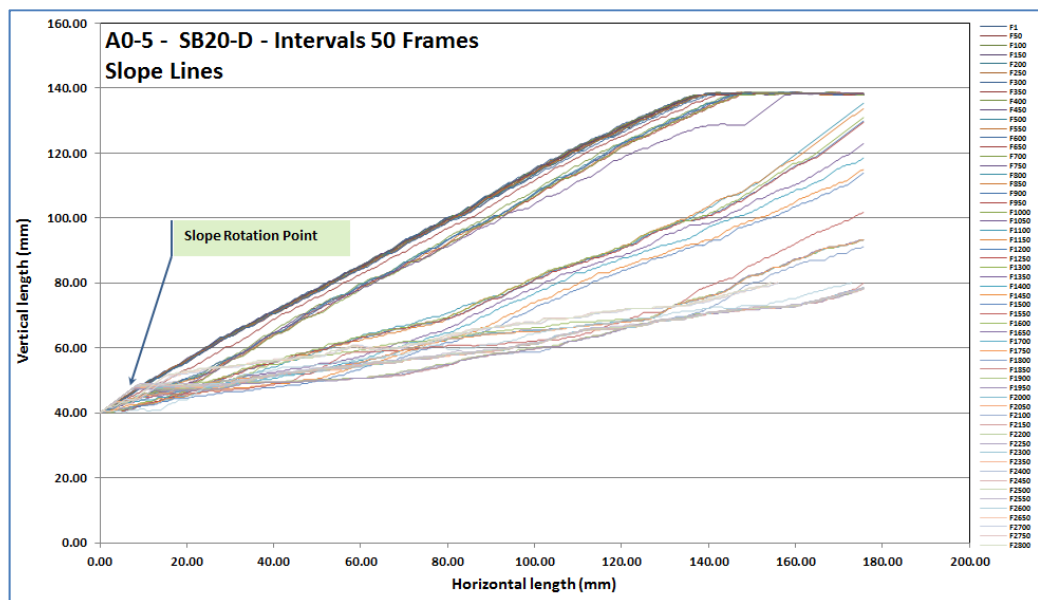


Figure 4-26: Changes in slope geometry for different frames with 20% bentonite

Figure 4-26 reflects the changes in slope stability when the frame number varies, which illustrates that in the zero bentonite treatment there is a relative difference among all curves. From this figure, the slope angle decreases when the frame number increases.

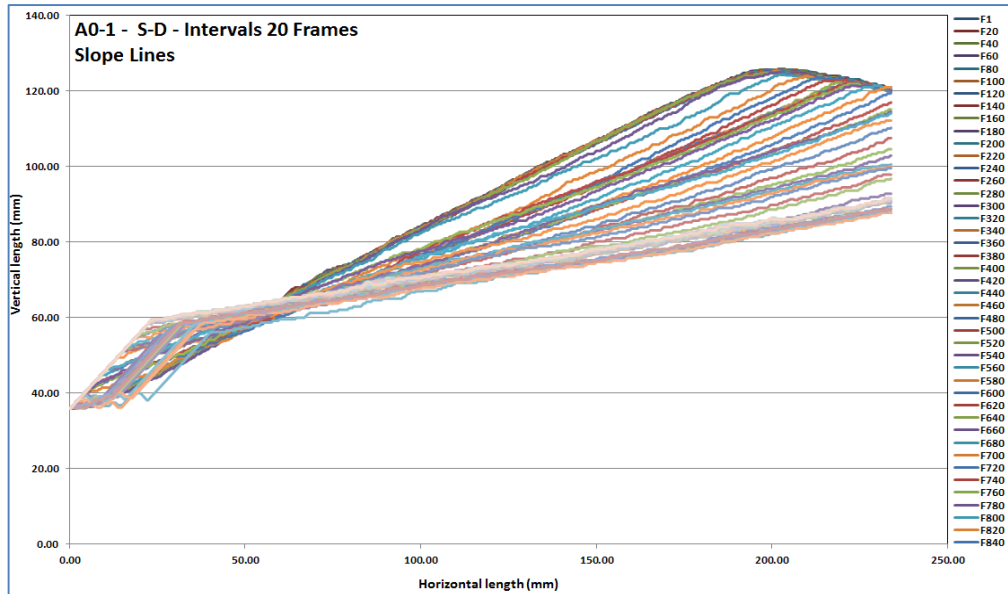


Figure 4-27: Changes in slope geometry for different frames with alignment of 20 frames

The impact of the slope angle on the frame number is shown in Figure 4-27, which demonstrates that with increasing frame number, the slope angle decreases. However, there is a reverse relationship between the frame number and slope inclination.

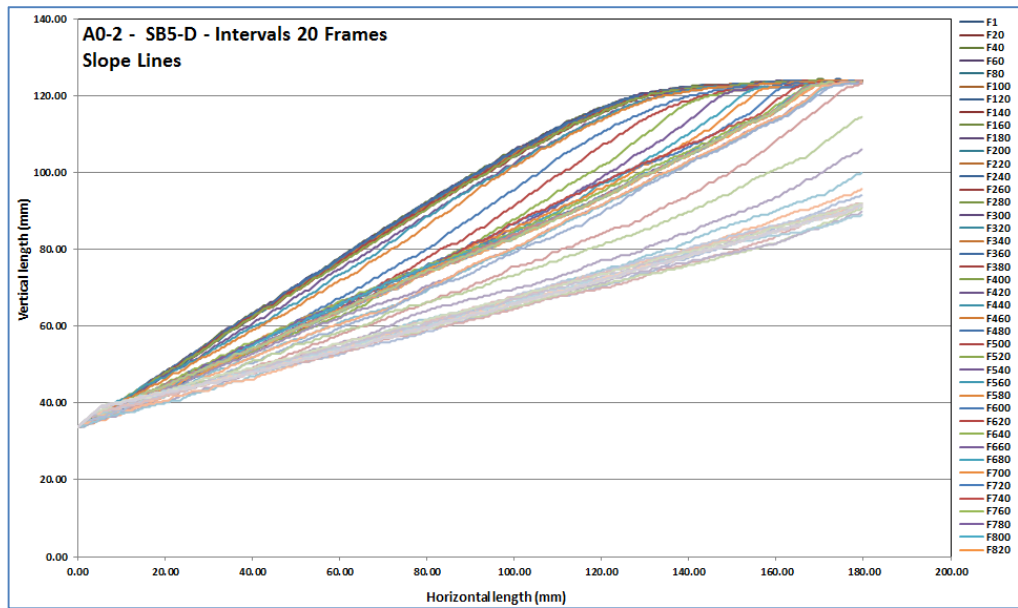


Figure 4-28: Changes in slope geometry for different frames with 5% bentonite

The impact of the frame number on slope inclination is shown in Figure 4-28, which demonstrates a convergence between all curves resulted from the slip surfaces with increasing frame number. However, the results are still in agreement with those of previous tests.

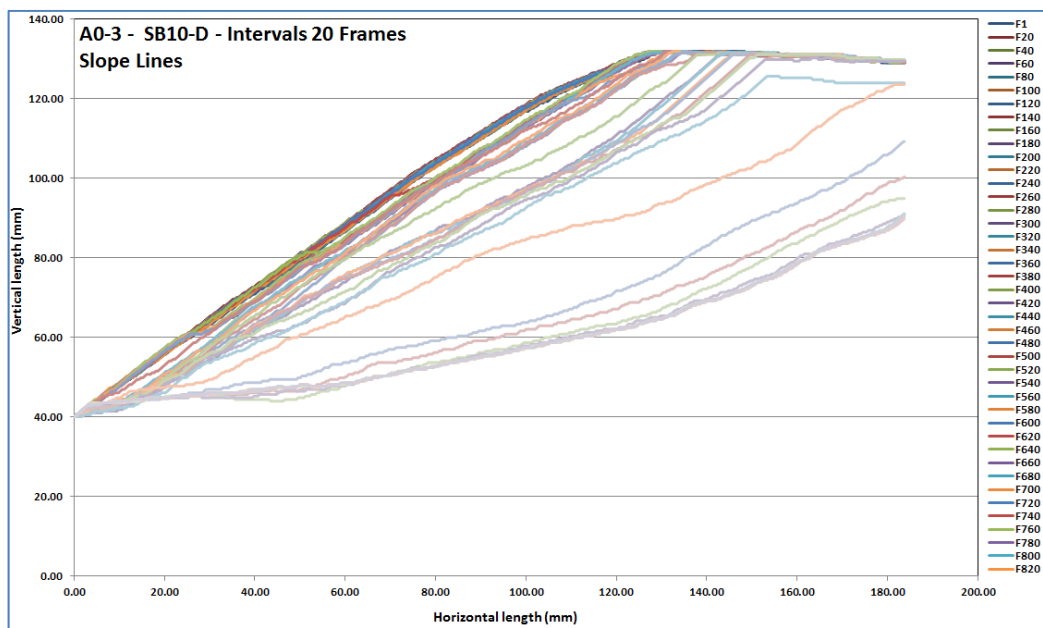


Figure 4-29: Changes in slope geometry for different frames with 10% bentonite

Figure 4-29 depicts several curves extracted from the slip surfaces captured by the camera. The results show that there is a substantial difference between the lines.

However, the figure confirms that the relationship between the slope angle and frame number is a reverse function.

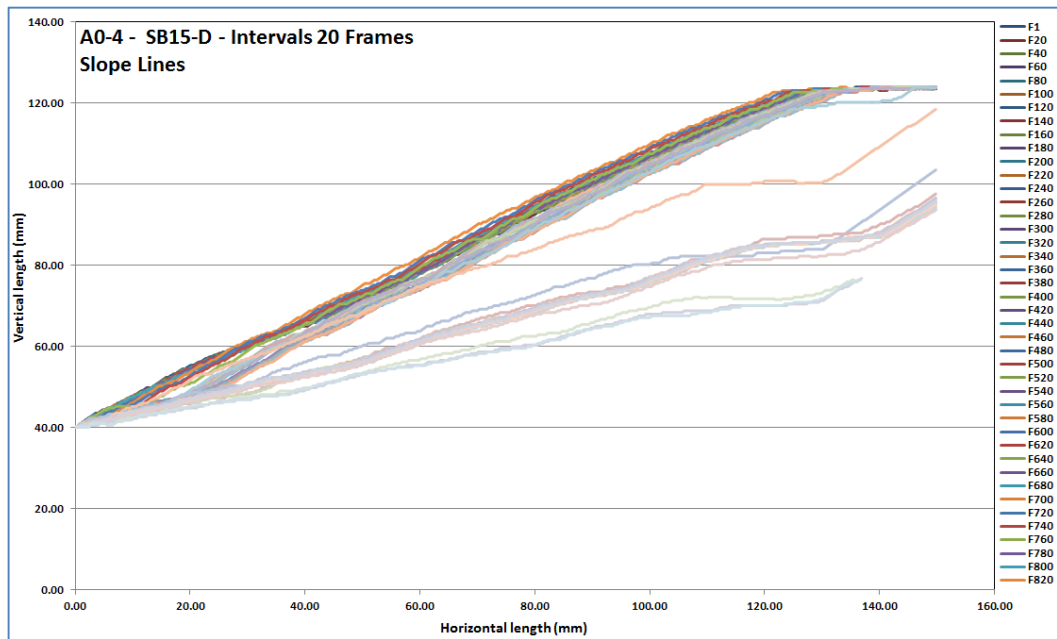


Figure 4-30: Changes in slope geometry for different frames with 15% bentonite

The effect of the frame number on slope angle by adding 15% bentonite is shown in Figure 4-30, which depicts a convergence between all curves with increasing frame number, i.e. with steadily increasing the frame number, the slope angle gradually decreases.

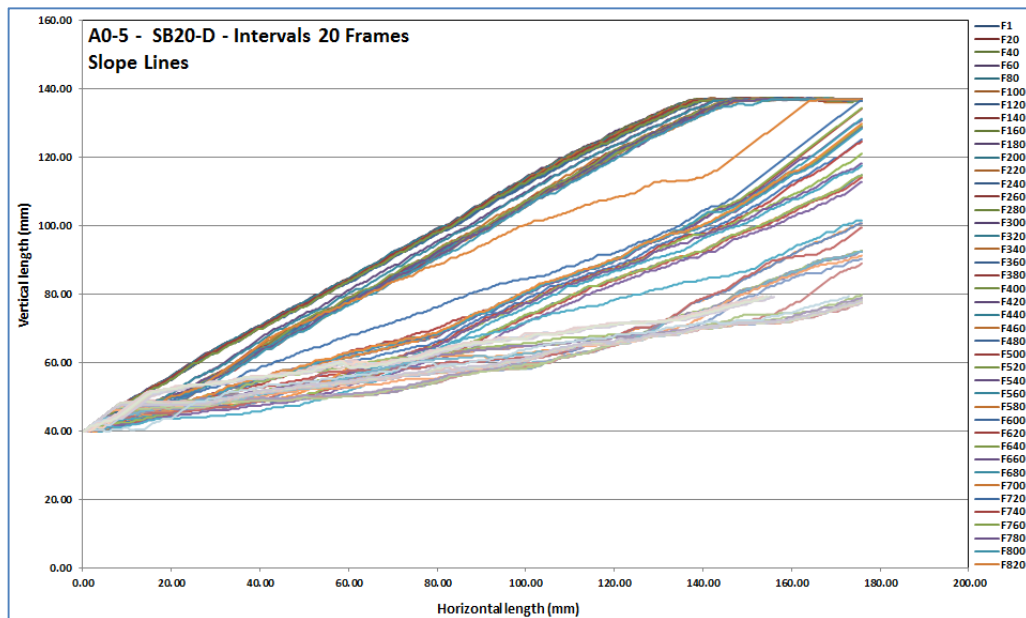


Figure 4-31: Changes in slope geometry for different frames with 20% bentonite

Figure 4-31 shows how the slope stability varies when the frame number changes, which demonstrates that the results are in line with the previous ones, i.e. when the frame number increases, the slope angle decreases.

#### 4.2.2. A5-1,2,3,4,5: (S, SB5 , SB10, SB15, SB20 – D)

By addition of bentonite, a set of tests were conducted to understand how the composition affects slope stability. The test results are presented in the following section.

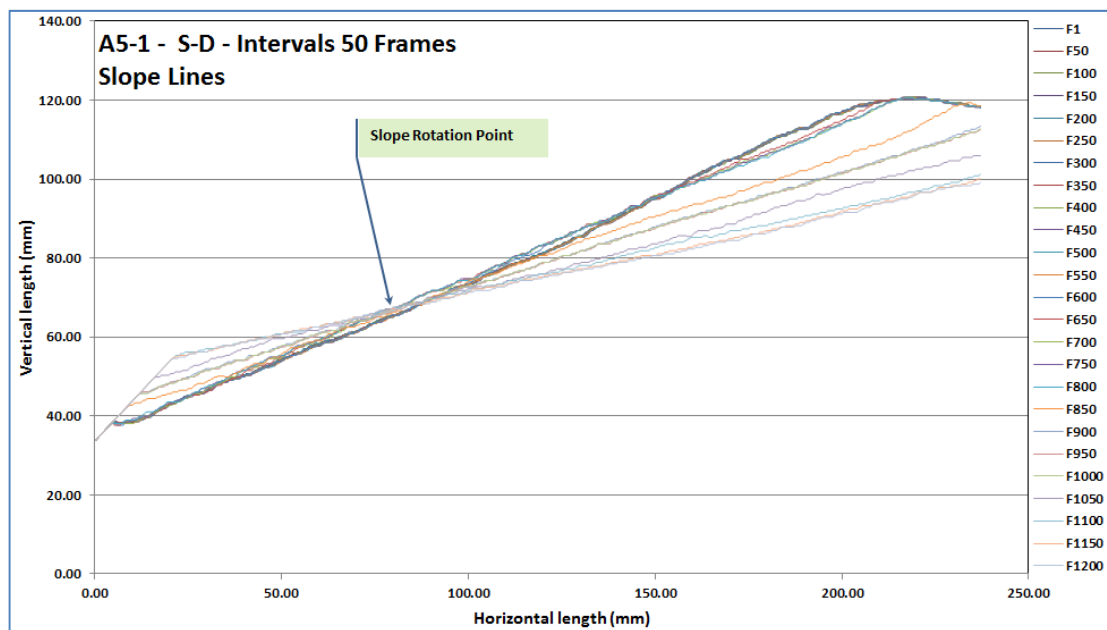


Figure 4-32: Changes in slope geometry for different frames with alignment of 5°

Figure 4-32 depicts the relationship between the slope angle and the frame number and shows that the slope inclination drops when the frame number increases. From the figure, a slight difference between all curves can be observed.



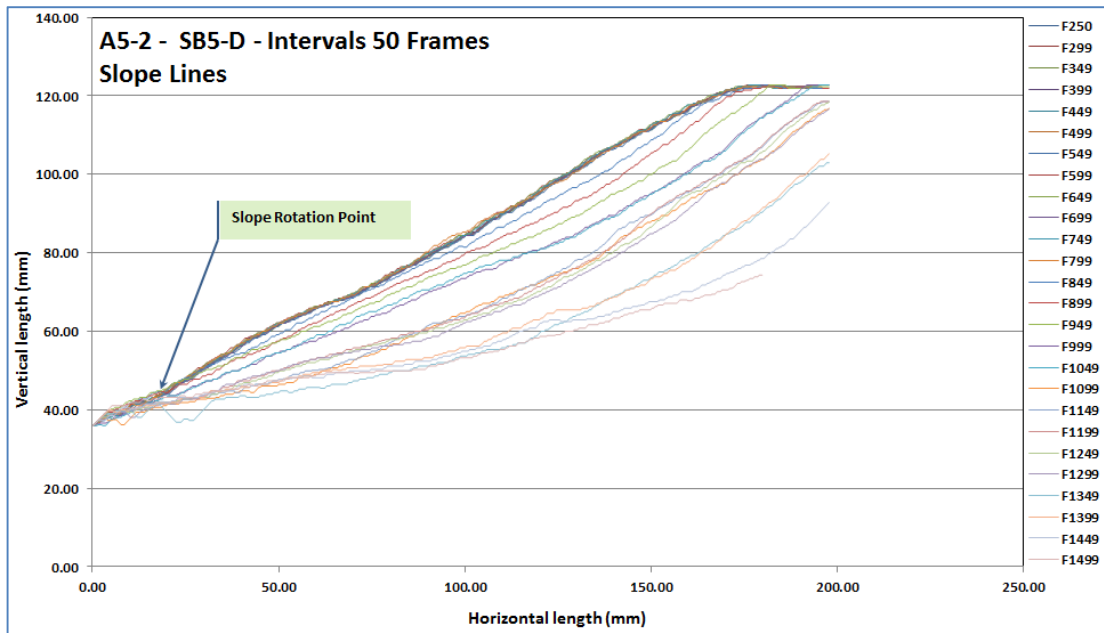


Figure 4-33: Changes in slope geometry for different frames with intervals of 50 frames

Figure 4-33 shows how the changes in the frame number vary the slope angle; therefore, progressive increase in frame number leads to a gradual decrease in slope inclination.

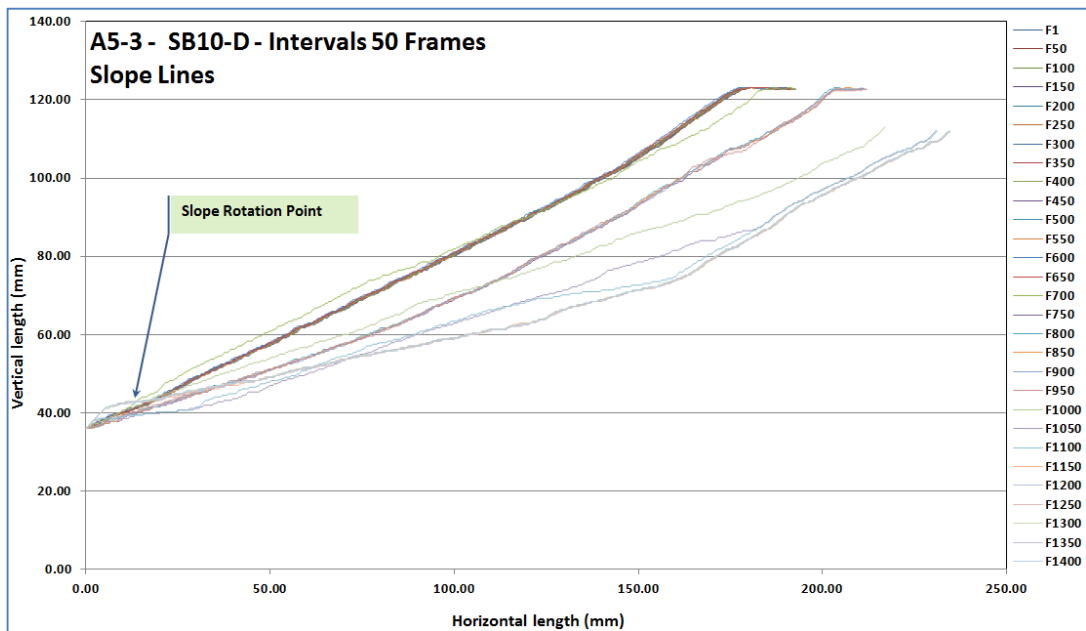


Figure 4-34: Changes in slope geometry for different frames with 10% bentonite

The changes in the slope angle with the frame number are graphically shown in Figure 4-34, which illustrates a convergence between all curves with increasing

frame number. However, the relationship between the slope angle and frame number is a reverse function.

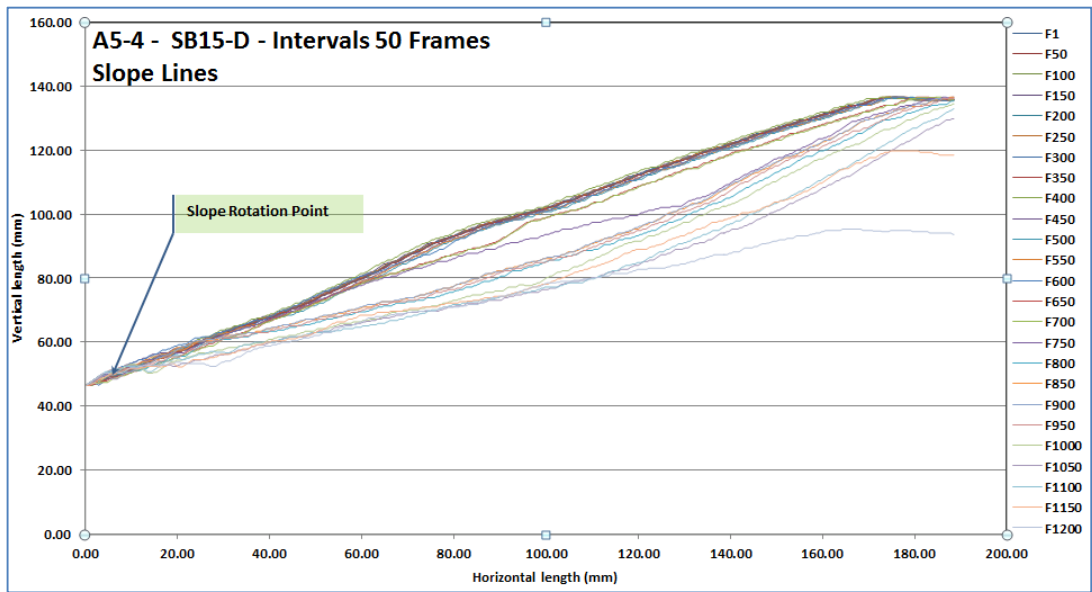


Figure 4-35: Changes in slope geometry for different frames with 15% bentonite

The impact of the frame number on slope inclination with addition of 15% bentonite with intervals of 50 frames is presented in Figure 4-35. From the figure, it is obvious that all curves are converged at a certain point on the left hand side of the figure.

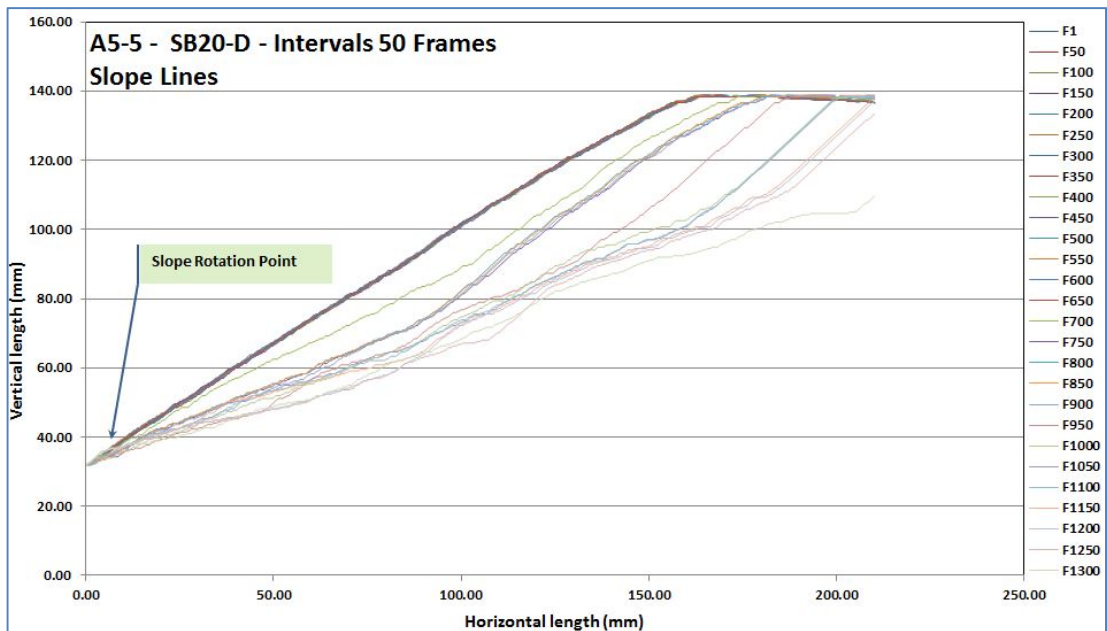


Figure 4-36: Changes in slope geometry for different frames with 20% bentonite

Figure 4-36 shows how a decrease in the frame number leads to an increase in the slope inclination. From the figure, there is a convergence between all curves with increasing frame number.

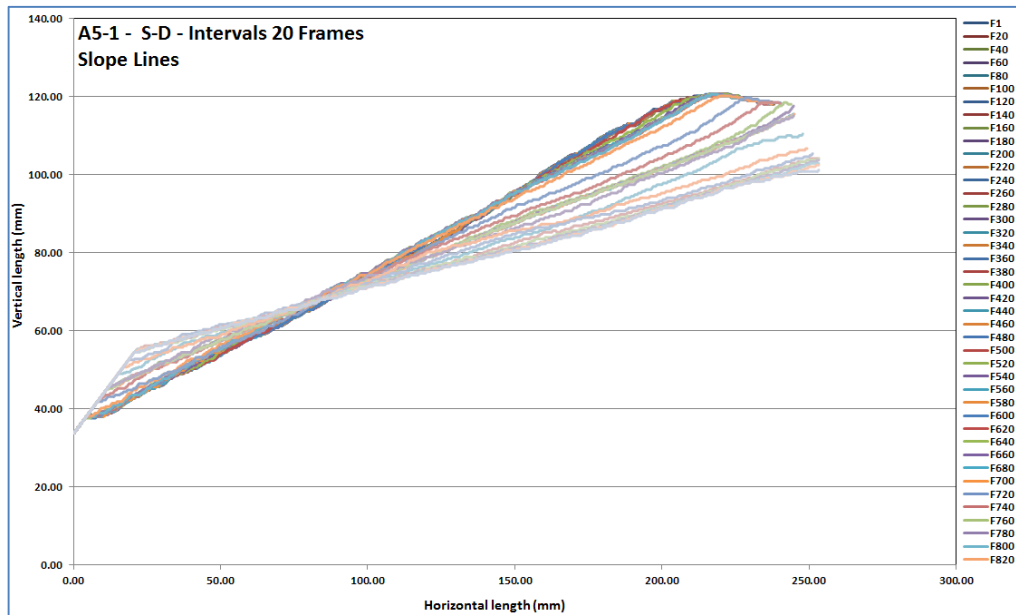


Figure 4-37: Changes in slope geometry for different frames with intervals of 20 frames

The relationship between the frame number and the slope inclination under intervals of 20 frames is presented in Figure 4-37, which shows only slight differences between all curves.

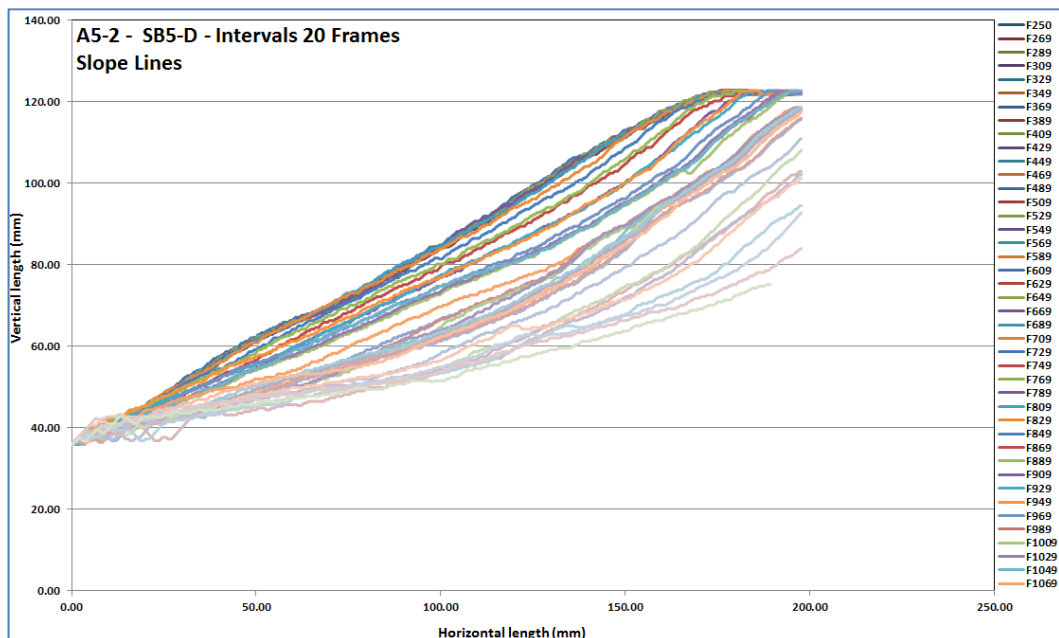


Figure 4-38: Changes in slope geometry for different frames with 5% bentonite

The changes in the slope inclination with the frame number are shown in Figure 4-38, which illustrates that the slope angle increases when the frame number decreases.

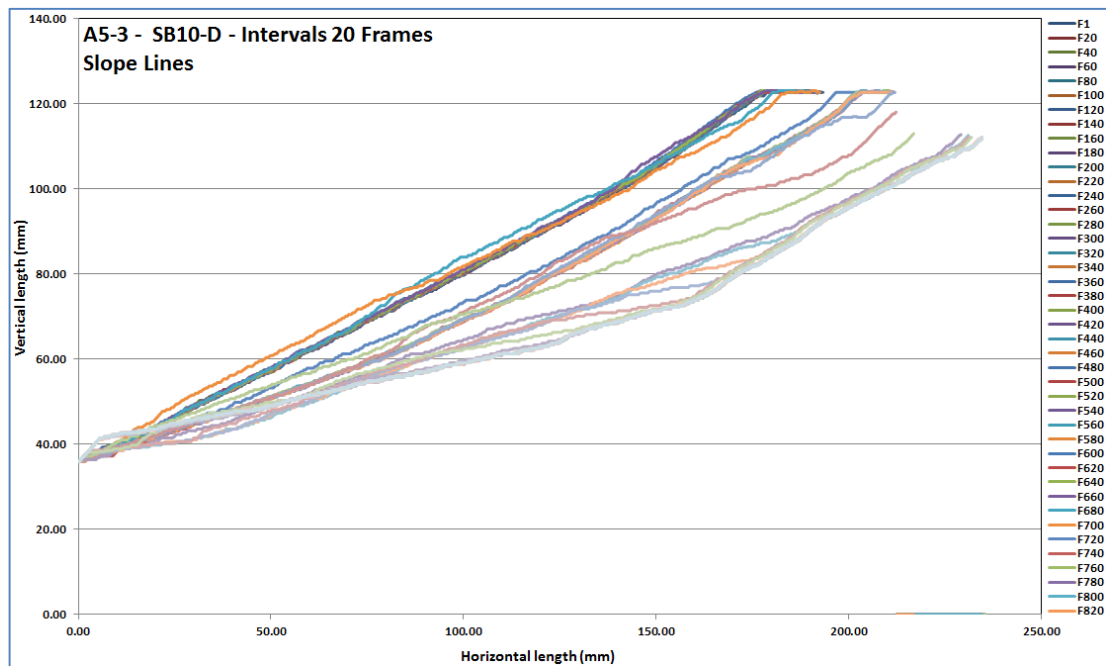


Figure 4-39: Changes in slope geometry for different frames with 10% bentonite

The effect of the frame number on the slope inclination with the addition of 10% bentonite is depicted in Figure 4-39, which illustrates that an increase in frame number leads to a decrease in slope inclination.

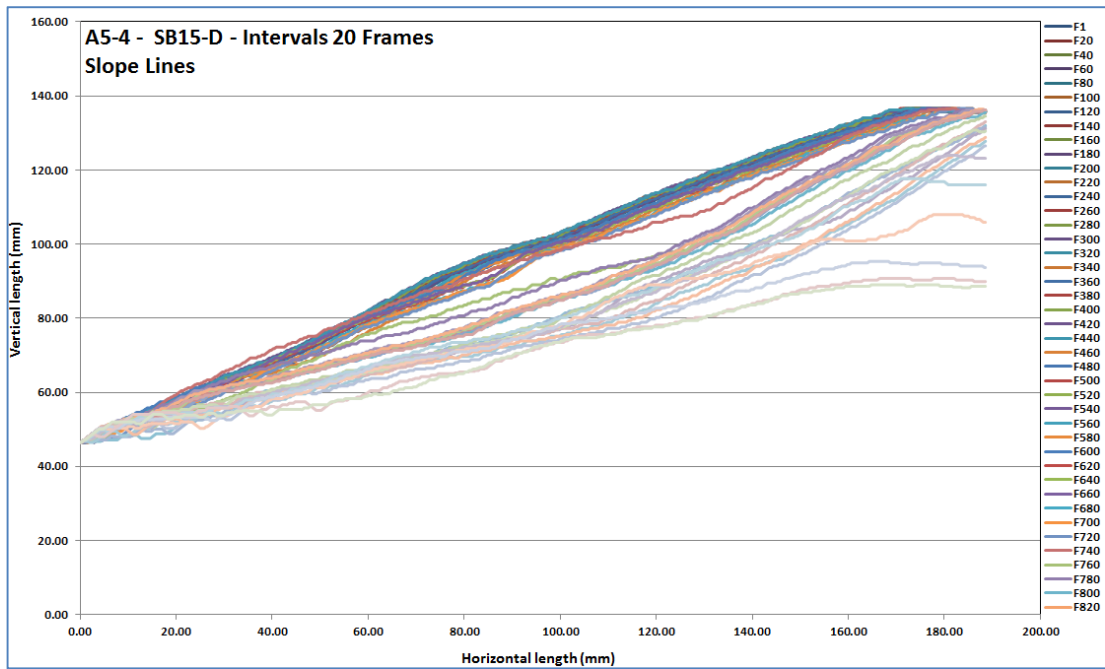


Figure 4-40: Changes in slope geometry for different frames with 15% bentonite

Figure 4-40 shows how the changes in the frame numbers vary the slope inclination by the addition of 15% bentonite and confirms that the relationship between the slope angle and frame number is a reverse function.

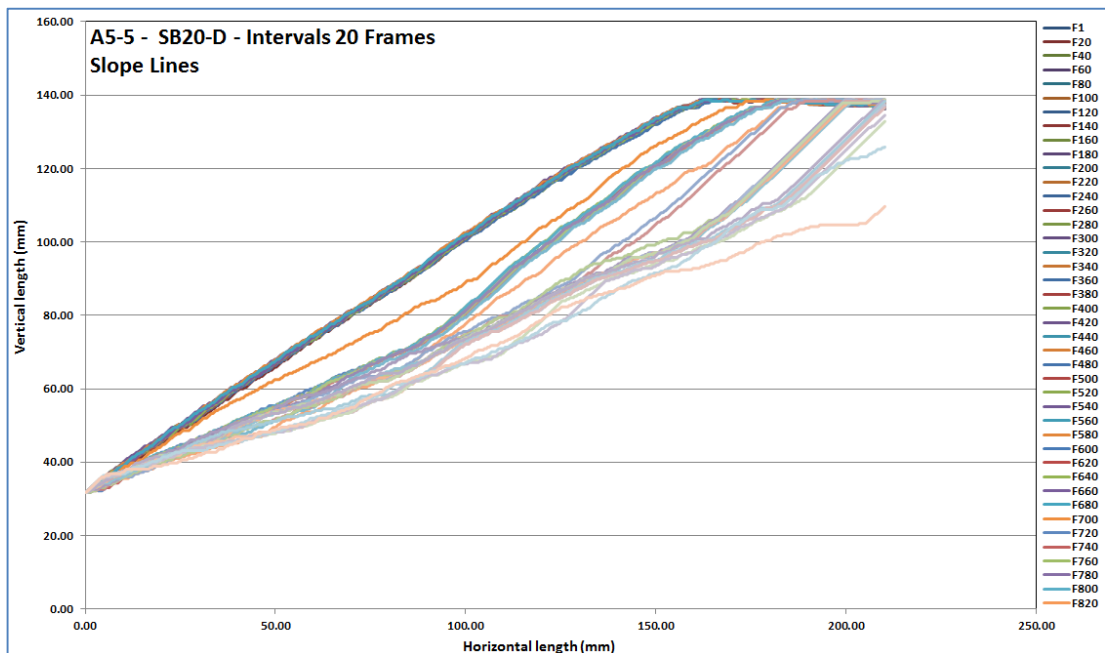


Figure 4-41: Changes in slope geometry for different frames with 20 % bentonite

The changes in the slope angle with varying the frame number under intervals of 20 frames are shown in Figure 4-41, which illustrates a gradual increase in the frame numbers leads to a continuous decrease in the slope inclination.

#### 4.2.3. A10-1,2,3,4,5: (S, SB5 , SB10, SB15, SB20 – D)

By addition of bentonite in different percentages to the saturated soil, several tests were conducted to find how an increase of 5° changes the slope stability.

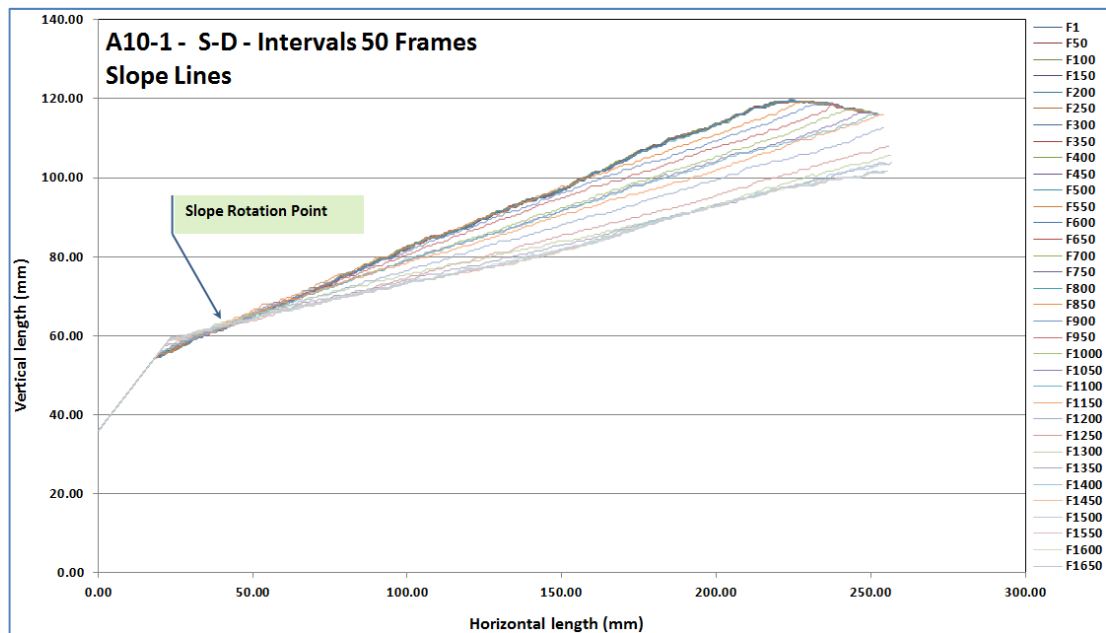


Figure 4-42: Changes in slope geometry for different frames with alignment of 10 percent

Figure 4-42 shows how a progressive increase in the frame number leads to a gradual decrease, and demonstrates only a slight difference between all curves.

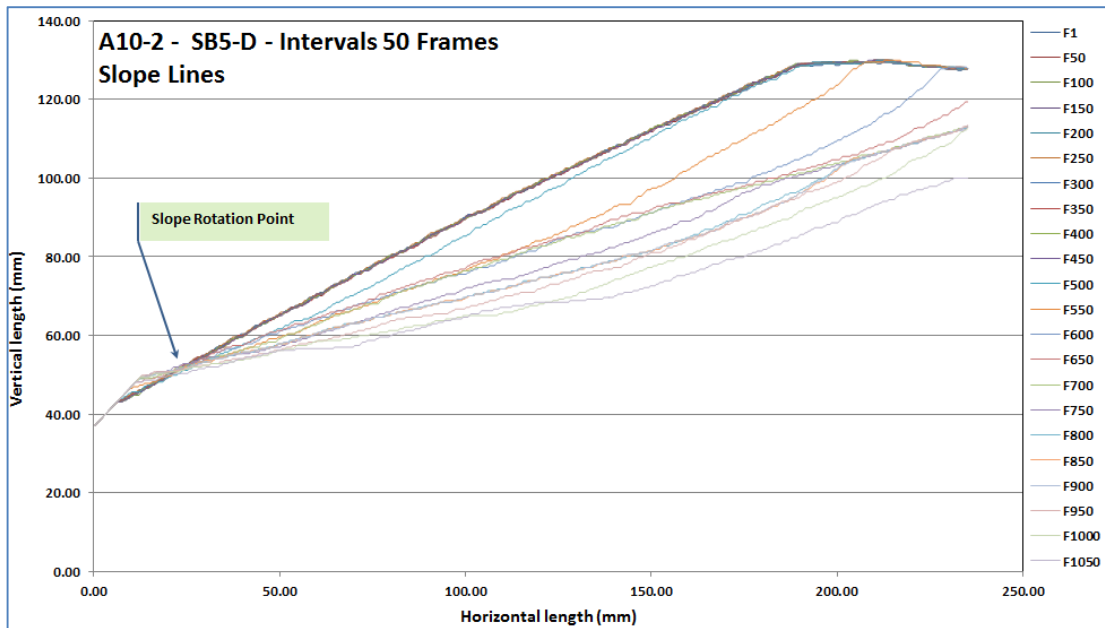


Figure 4-43: Changes in slope geometry for different frames with 5% bentonite

Figure 4-43 shows the behaviour of the slope angle when the frame number changes, which reveals a convergence between all curves with increasing frame numbers.

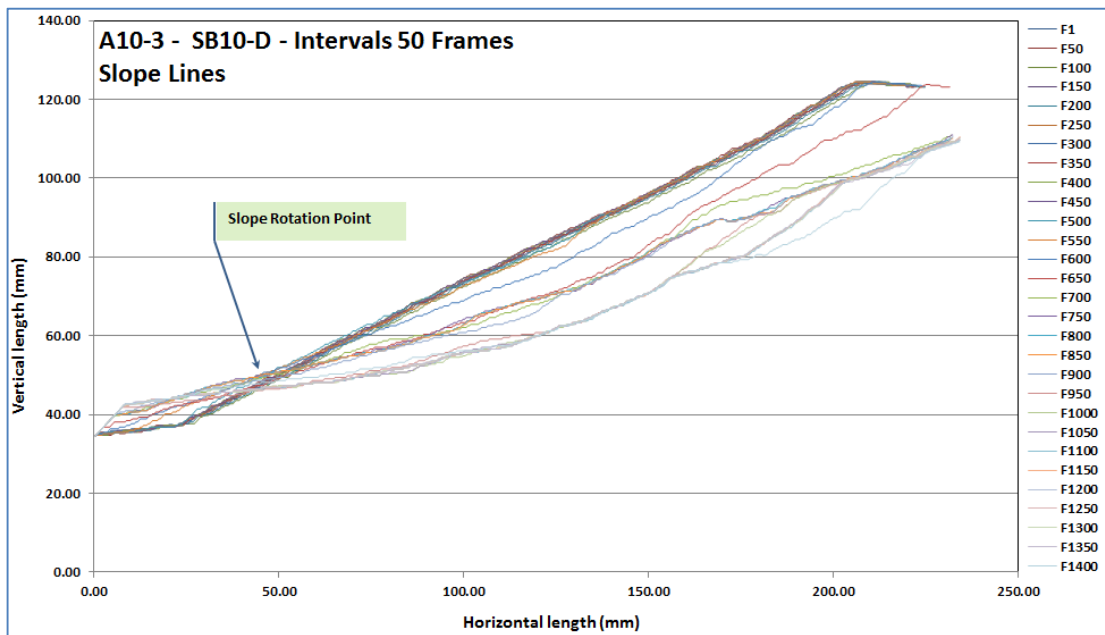


Figure 4-44: Changes in slope geometry for different frames with 10% bentonite

Figure 4-44 depicts how the slope angle changes when the frame number varies with a composition of 10% bentonite. This figure shows that the obtained results are in agreement with those of the previous tests.

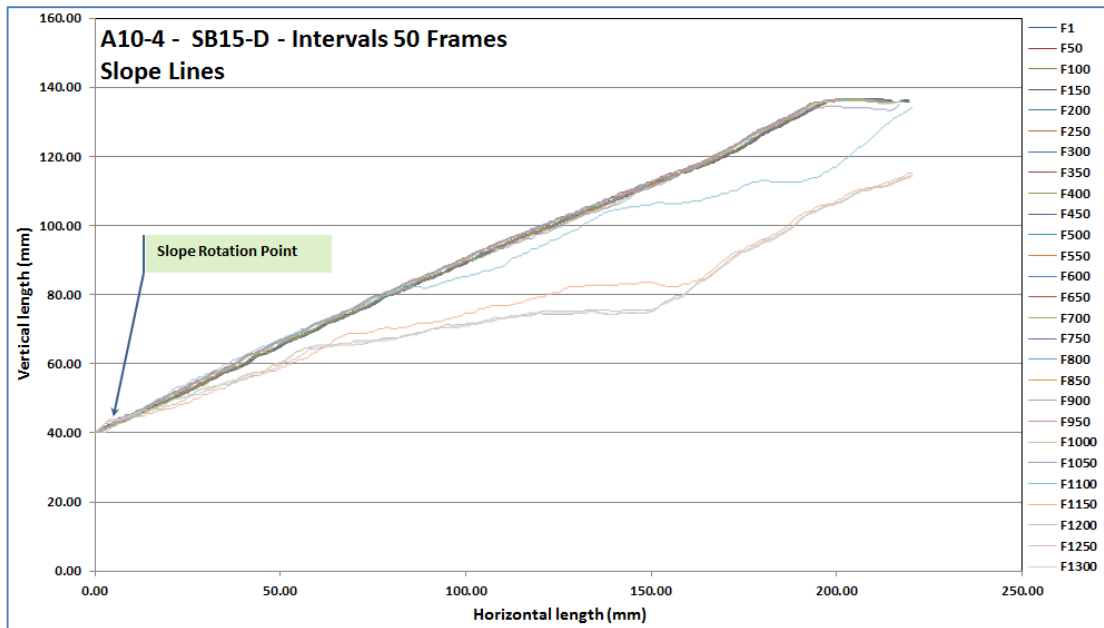


Figure 4-45: Changes in slope geometry for different frames with 15% bentonite

Figure 4-45 depicts how the changes in the frame number can vary the slope angle with the addition of 15% bentonite. From the figure, it can be seen that a decrease in the frame number leads to an increase in the slope inclination.

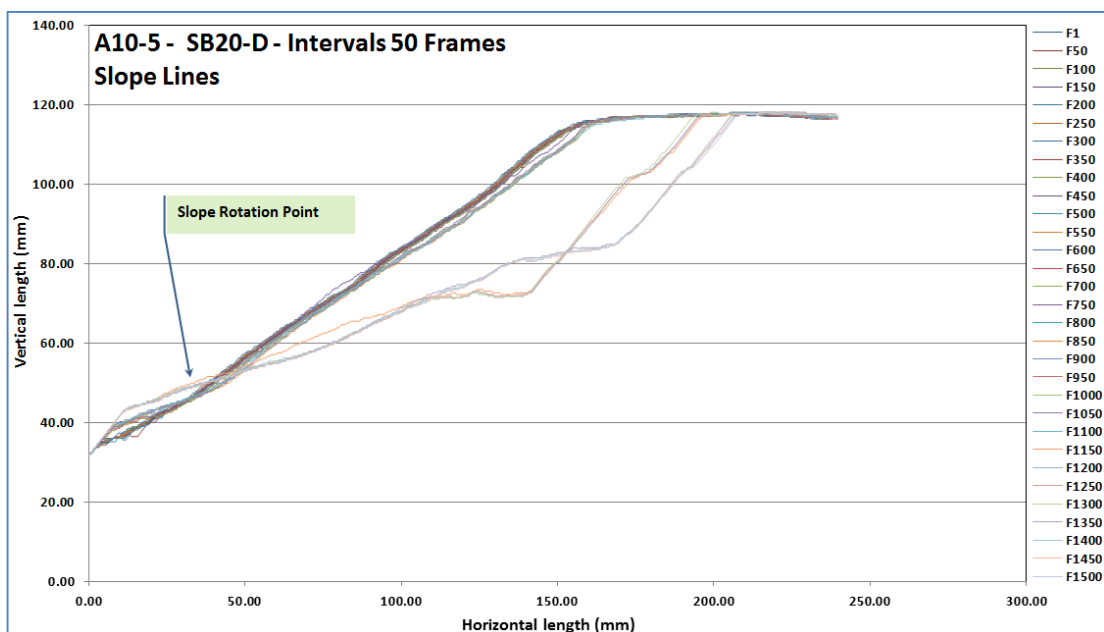


Figure 4-46: Changes in slope geometry for different frames with 20% bentonite



The changes in the slope stability for several frame numbers with the addition of 20% bentonite are shown in Figure 4-46, which confirms that there is a reverse relationship between the slope inclination and frame number.

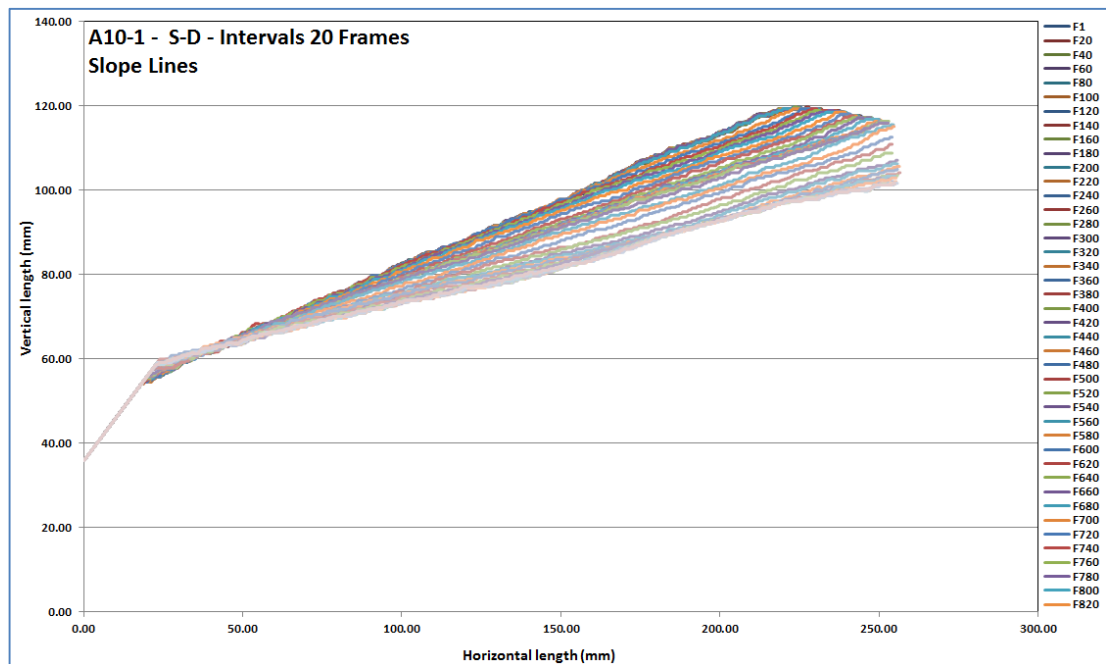


Figure 4-47: Changes in slope geometry for different frames with intervals of 20 frames

Figure 4-47 shows how a decrease in the frame number leads to an increase in the slope angle. This figure demonstrates that there is a convergence between all curves with increasing frame number.

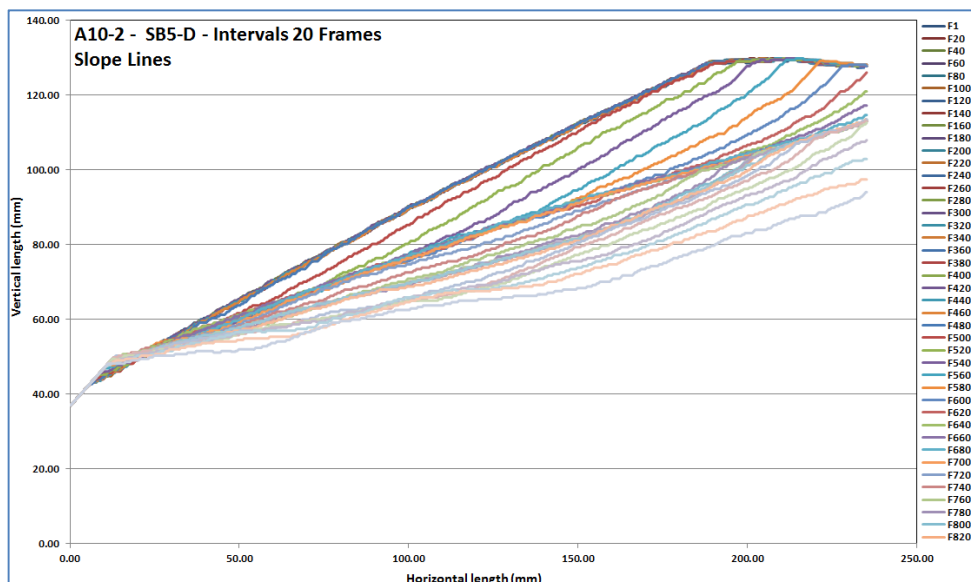


Figure 4-48: Changes in slope geometry for different frames with 5% bentonite

Figure 4-48 depicts all curves resulting from the slip surfaces are relatively different and with an increase in the frame number, the slope angle decreases. This figure shows that there is a convergence between all curves with decreasing slope angle.

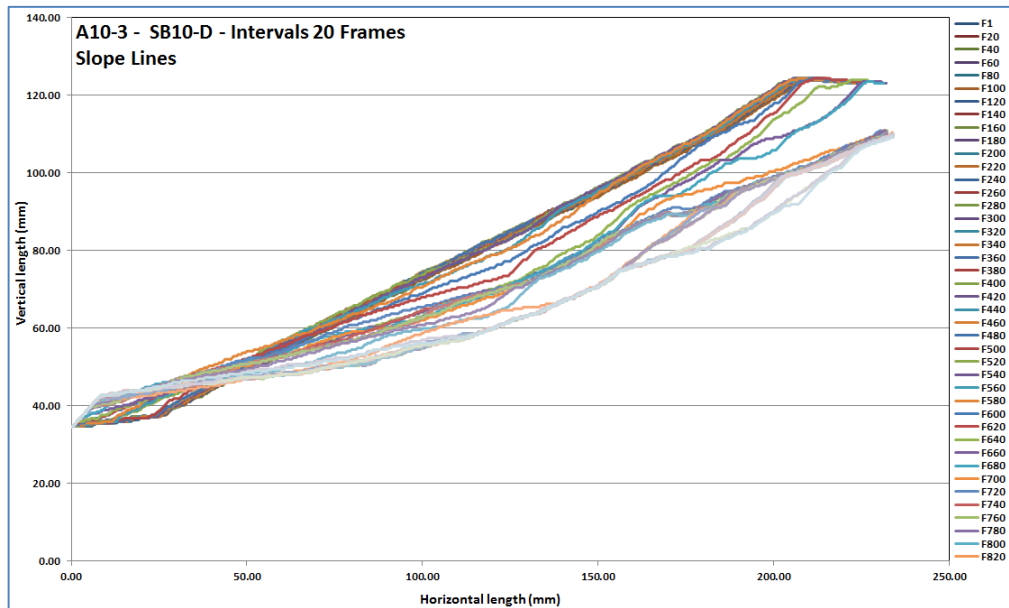


Figure 4-49: Changes in slope geometry for different frames with 10% bentonite

Figure 4-49 shows that the pattern between the frame number and the slope inclination is a linear relationship. Therefore, progressive increase in the frame number leads to a continuous decrease in the slope angle.

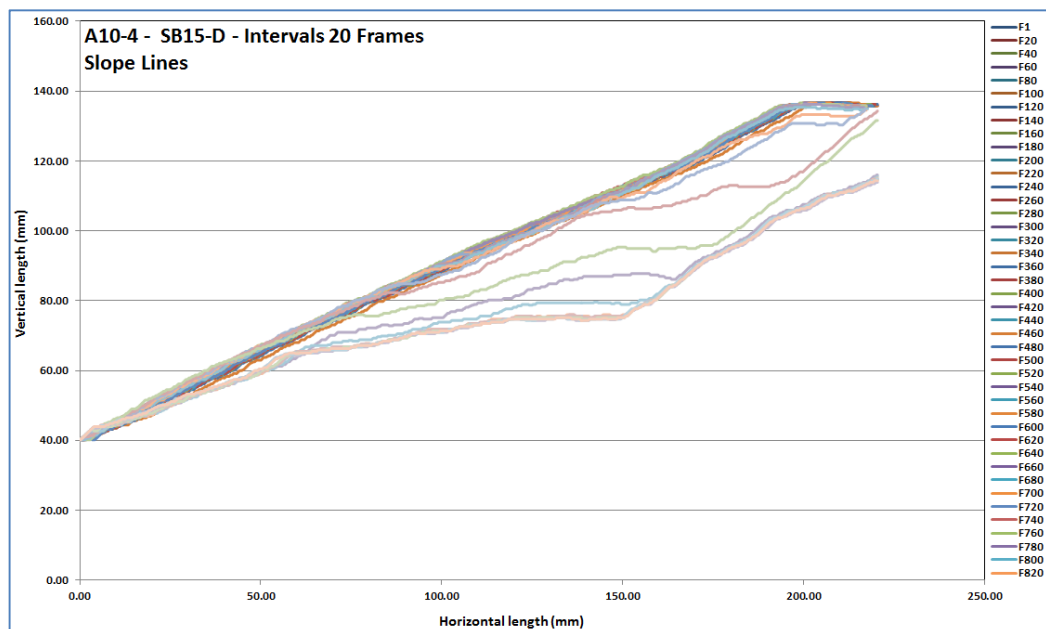


Figure 4-50: Changes in slope geometry for different frames with 15% bentonite

The effects of the frame number on the slope inclination are graphically depicted in Figure 4-50, which shows a convergence between all curves with decreasing the slope inclination.

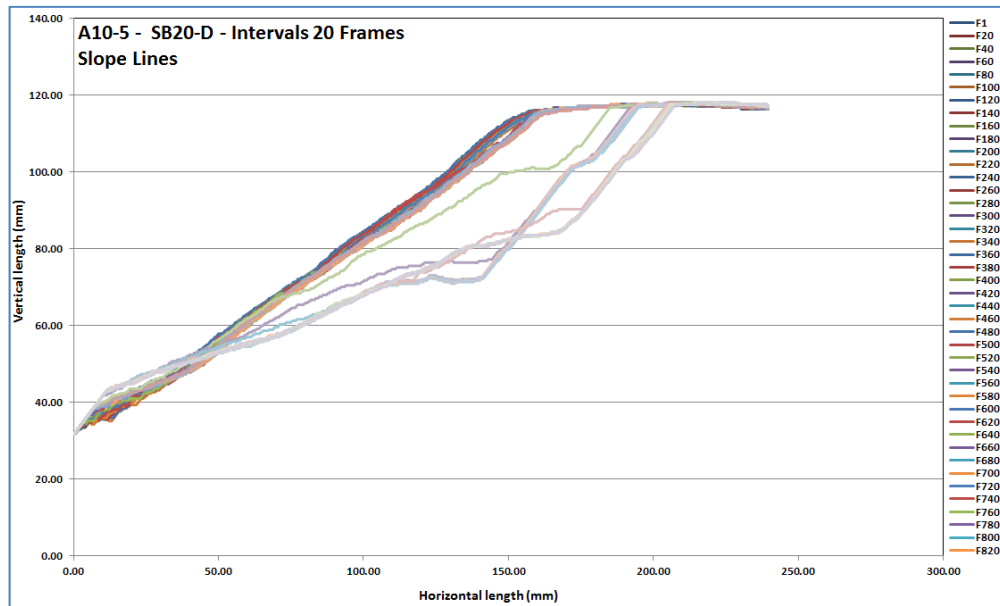


Figure 4-51: Changes in slope geometry for different frames with 20% bentonite

Figure 4-51 presents how the slope inclination changes when the frame number varies and shows a relative difference between all curves resulting from the slip surfaces. However, a decrease in the slope inclination results from an increase in the frame number.

### 4.3. Summary of Results from Image Processing

Bentonite was added to the samples to replicate fine content effects when analysing slope stability. From the results obtained above, by adding bentonite, the slope stability decreased significantly. For example, at 5° alignment, the stability of soil with 5% bentonite, soil with 10% bentonite, and soil with 15% bentonite steadily decreased. The decrease in the slope inclination can be directly attributed to the increase in the volume of bentonite. As presented in the figures, the slope stability curves shifted downwards with an increase in bentonite content. Because soil displacement varies with composition, an important design problem in slope stability analysis is soil decomposition.

From these results, it can be concluded that a soil with no bentonite is more stable than with bentonite. As the bentonite content increases the stability of the slope decreases. Whereas, the least stable slope belongs to the sample with the soil and the least alignment. For all curves resulting from the image processing technique, the slope stability decreased with frame numbers. Therefore, the potential for slope stability decreases when frame number increases. Therefore, the results indicate that slope stability is a function of the frame number in addition to the degree of composition.

The alignment varied from 0° to 15°, with this variable being slightly less significant for changes in the slopes, with the effect of alignment on slope stability is negligible. For smaller intervals, the numbers of frames are associated with more detail and information. Over different test designs, intervals of 20 frames were found to be the best for analysis.

#### **4.4. SPSS Analysis Results**

After the primary image processing analyses of the test results, the outputs were entered in the database for SPSS analysis. This technique helps to locate jump locations in an analytical logic and to avoid visual errors in identifying first failure locations. For example, a typical test (A0-1 - S-D - intervals of 20 frames) is presented below.

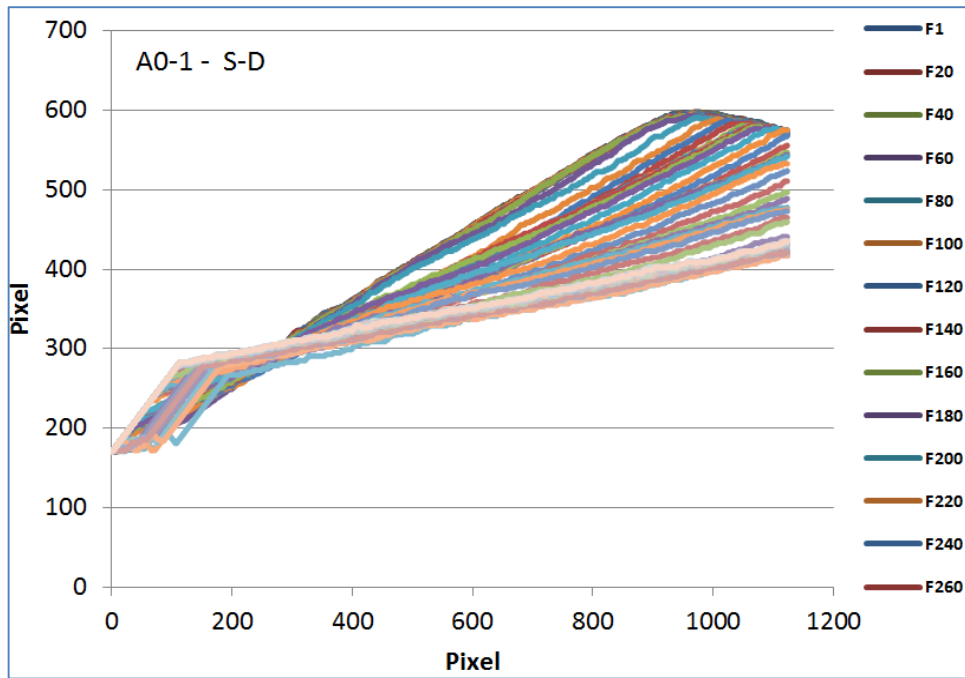


Figure 4-52: Changes in slope geometry for different frames with intervals of 20 frames

Figure 4-52 shows how the behaviour of the slope angle changes when the frame number varies and presents a range of 114 frames, from F1 to F260, with intervals of 20 frames. In a visual check, some initial micro failures can be seen, as depicted in Figure 4-53. In this research, the micro failures are neglected.

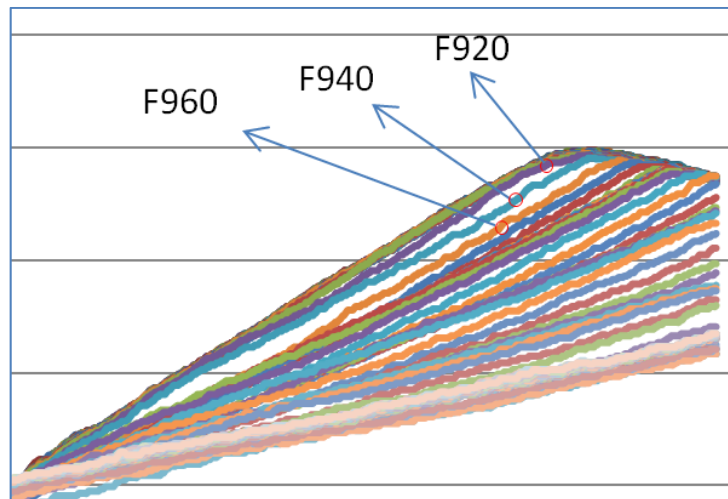


Figure 4-53: Micro failures

For purpose of analysing and classifying the data, the homogeneous properties of various image features were categorised into classes. The K-Mean cluster method, a data-partitioning and iterative algorithm as presented in Appendix B, was applied to

separate the frames logically. The results obtained from the K-Mean cluster method are sorted as listed in Table 4-1 as shown in coloured yellow blue and brown.

**Table 4-1 : K-Mean cluster analysis**

Cluster Category	Cluster Number in SPSS	Frame No.
5	1	F1
5	2	F20
5	3	F40
5	4	F60
5	5	F80
5	6	F100
5	7	F120
5	8	F140
5	9	F160
5	10	F180
5	11	F200
5	12	F220
5	13	F240
5	14	F260
5	15	F280
5	16	F300
5	17	F320
5	18	F340
5	19	F360
5	20	F380
5	21	F400
5	22	F420
5	23	F440
5	24	F460
5	25	F480
5	26	F500
5	27	F520
5	28	F540
5	29	F560
5	30	F580
5	31	F600
5	32	F620
5	33	F640
5	34	F660
5	35	F680

Cluster Category	Cluster Number in SPSS	Frame No.
5	36	F700
5	37	F720
5	38	F740
5	39	F760
5	40	F780
5	41	F800
5	42	F820
5	43	F840
5	44	F860
5	45	F880
5	46	F900
4	47	F920
9	48	F940
9	49	F960
1	50	F980
1	51	F1000
1	52	F1020
1	53	F1040
1	54	F1060
1	55	F1080
1	56	F1100
1	57	F1120
1	58	F1140
1	59	F1160
8	60	F1180
8	61	F1200
8	62	F1220
8	63	F1240
8	64	F1260
8	65	F1280
8	66	F1300
8	67	F1320
6	68	F1340
6	69	F1360
6	70	F1380
6	71	F1400
6	72	F1420
6	73	F1440
6	74	F1460

Cluster Category	Cluster Number in SPSS	Frame No.
10	75	F1480
7	76	F1500
2	77	F1520
3	78	F1540
3	79	F1560
3	80	F1580
3	81	F1600
3	82	F1620
3	83	F1640
3	84	F1660
3	85	F1680
3	86	F1700
10	87	F1720
10	88	F1740
10	89	F1760
10	90	F1780
10	91	F1800
10	92	F1820
10	93	F1840
10	94	F1860
10	95	F1880
10	96	F1900
10	97	F1920
10	98	F1940
10	99	F1960
10	100	F1980
10	101	F2000
10	102	F2020
10	103	F2040
10	104	F2060
10	105	F2080
10	106	F2100
10	107	F2120
10	108	F2140
10	109	F2160
10	110	F2180
10	111	F2200
10	112	F2220
10	113	F2240
10	114	F2260



For a better understanding, the clusters are graphically curved as shown in Figure 4-54 to Figure 4-63.

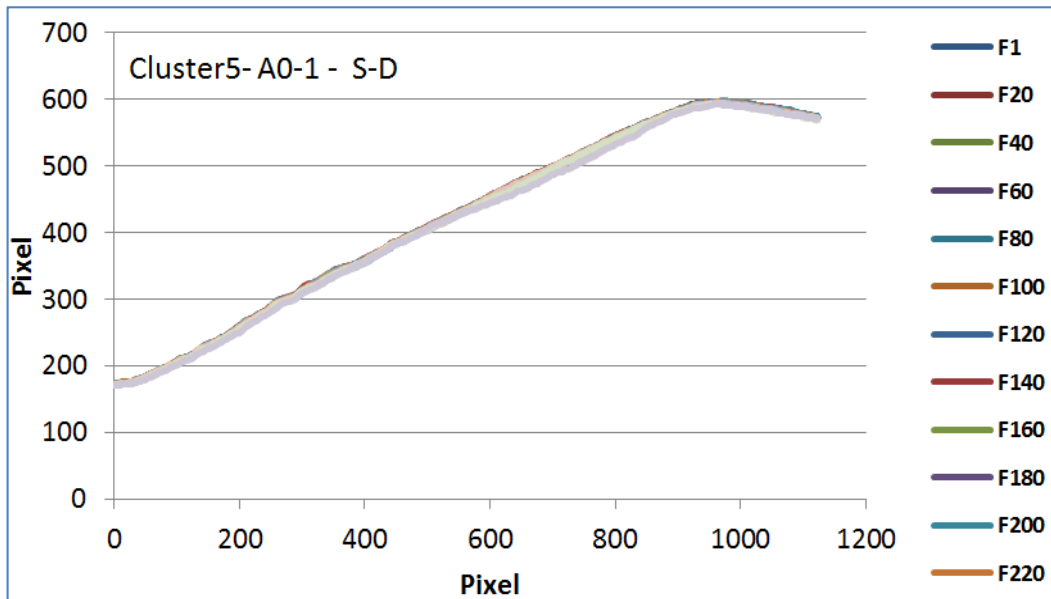


Figure 4-54: Cluster5 - A0-1 - S-D - Intervals of 20 frames

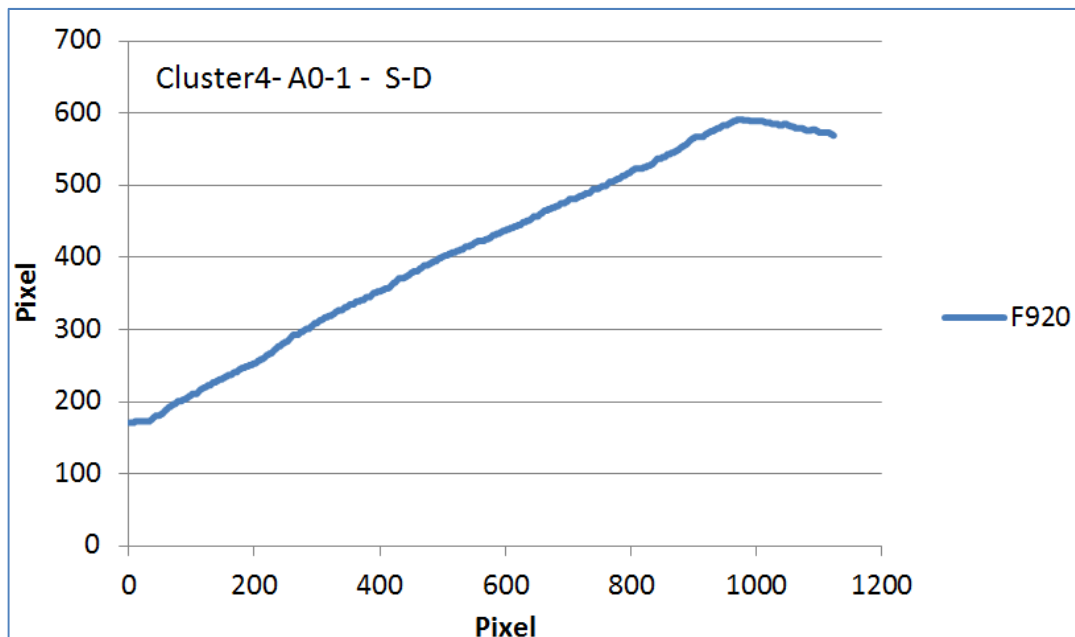


Figure 4-55: Cluster4 - A0-1 - S-D - Intervals of 20 frames

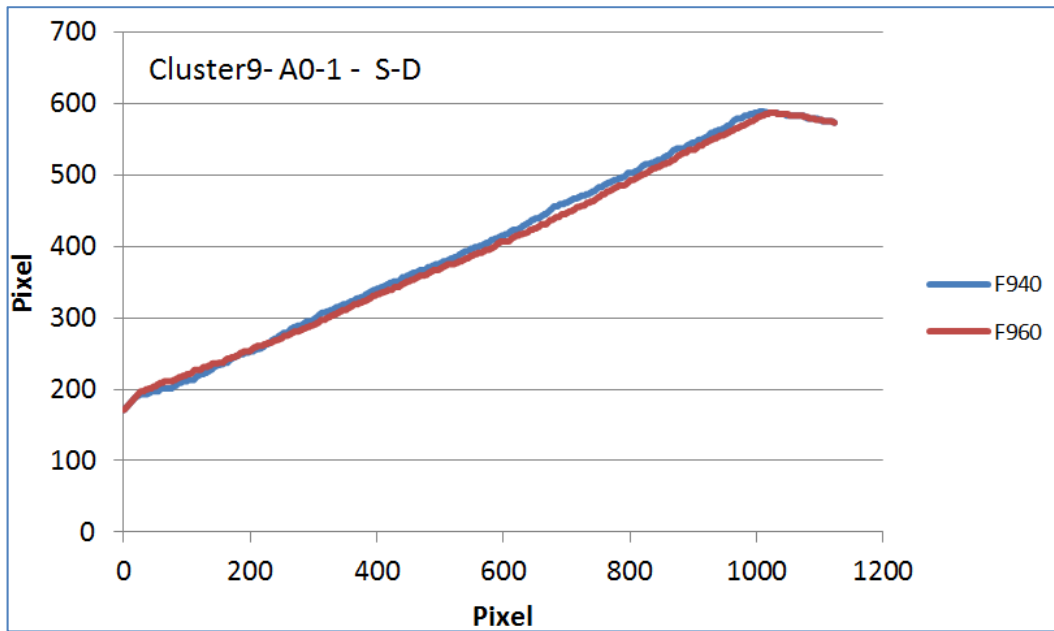


Figure 4-56: Cluster9 - A0-1 - S-D - Intervals of 20 frames

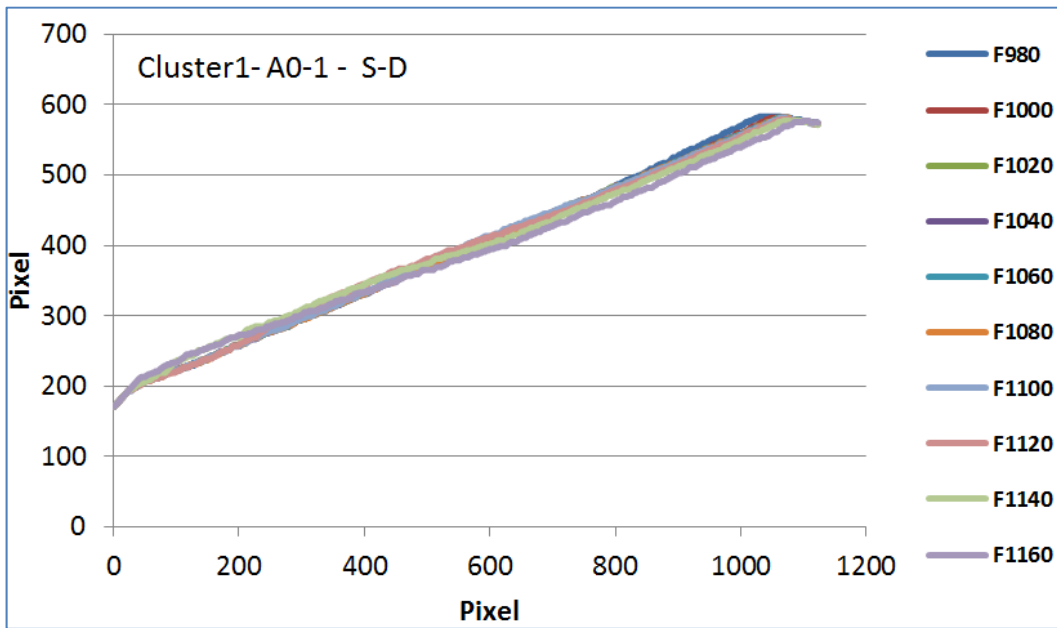


Figure 4-57: Cluster1 - A0-1 - S-D - Intervals of 20 frames

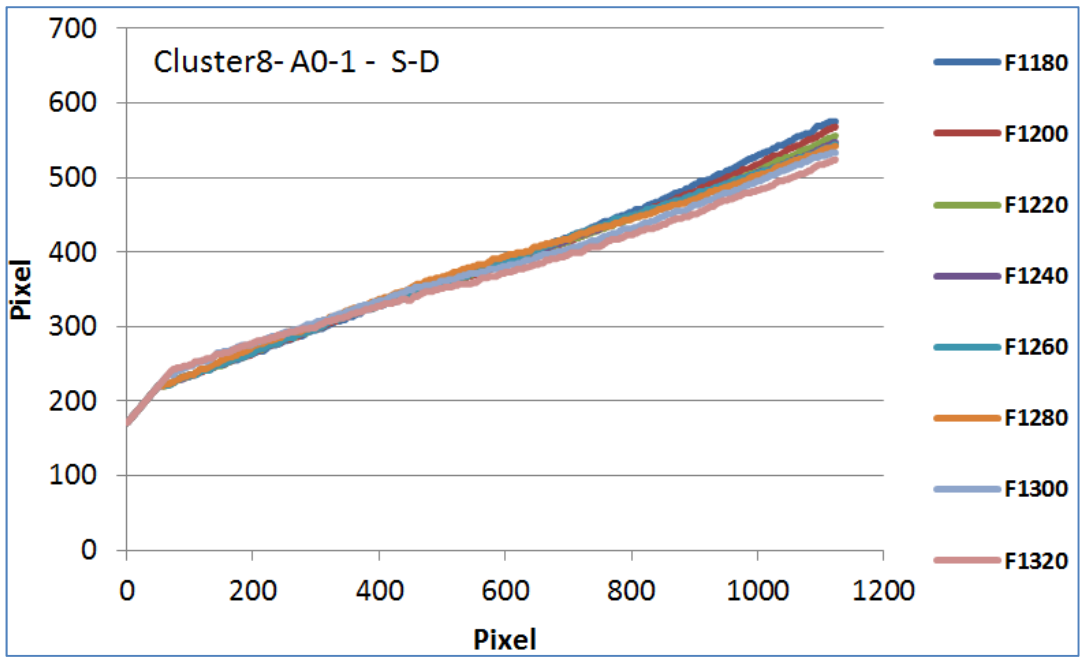


Figure 4-58: Cluster8 - A0-1 - S-D - Intervals of 20 frames

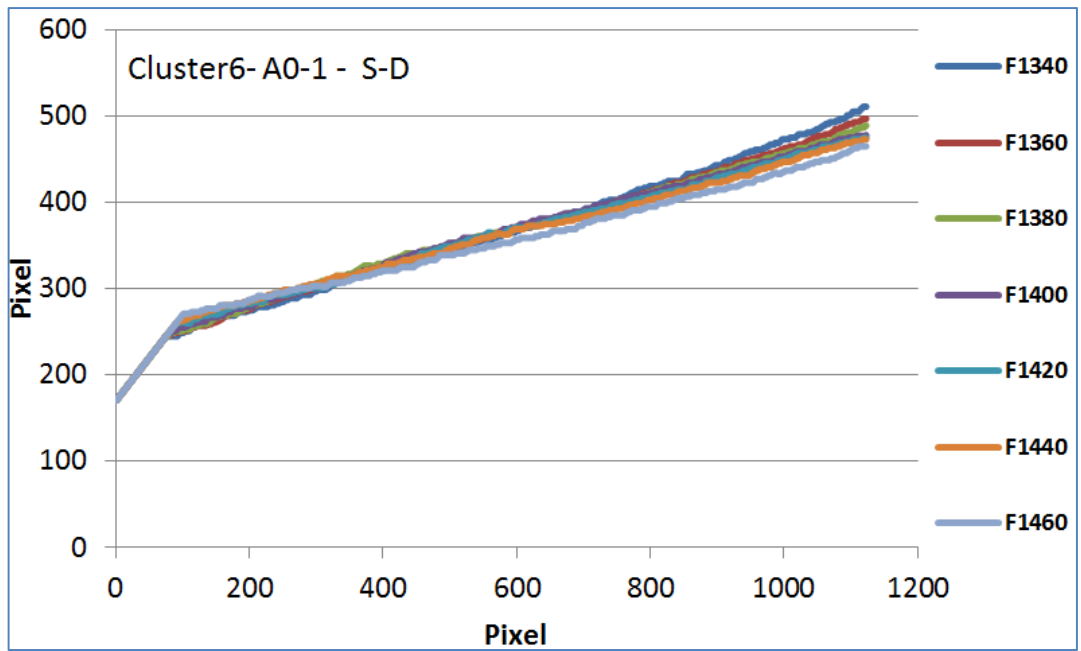


Figure 4-59: Cluster6 - A0-1 - S-D - Intervals of 20 frames

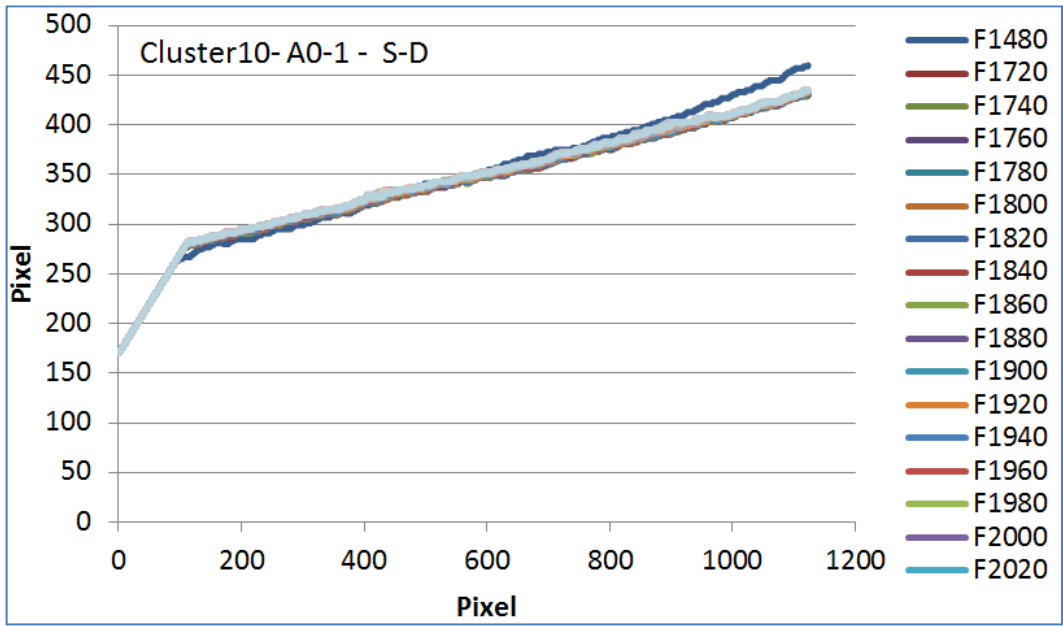


Figure 4-60: Cluster10 - A0-1 - S-D - Intervals of 20 frames

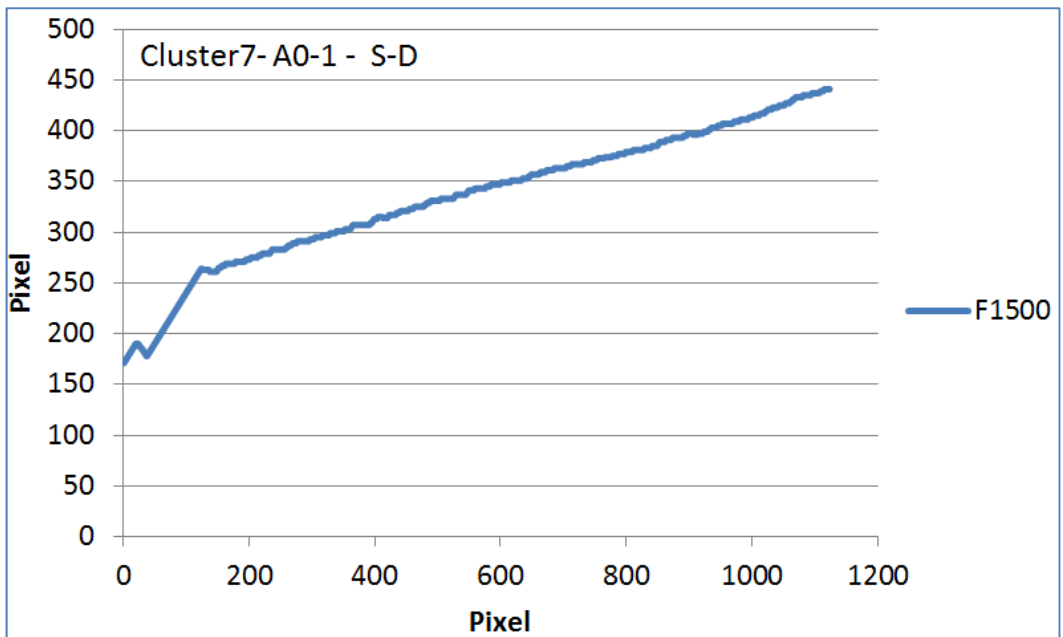


Figure 4-61: Cluster7 - A0-1 - S-D - Intervals of 20 frames

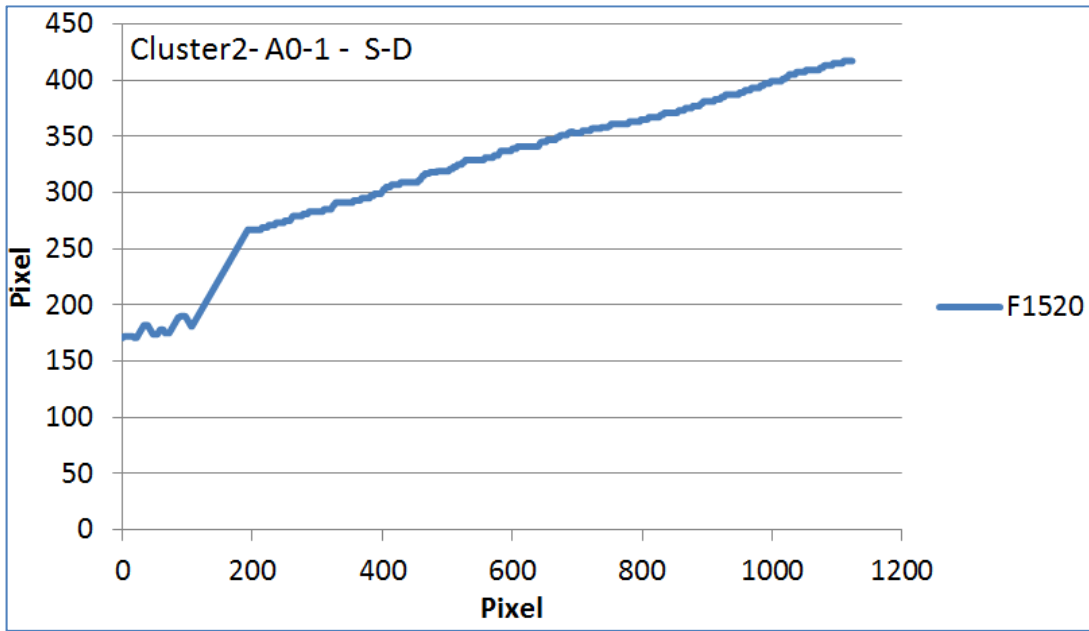


Figure 4-62: Cluster2 - A0-1 - S-D - Intervals of 20 frames

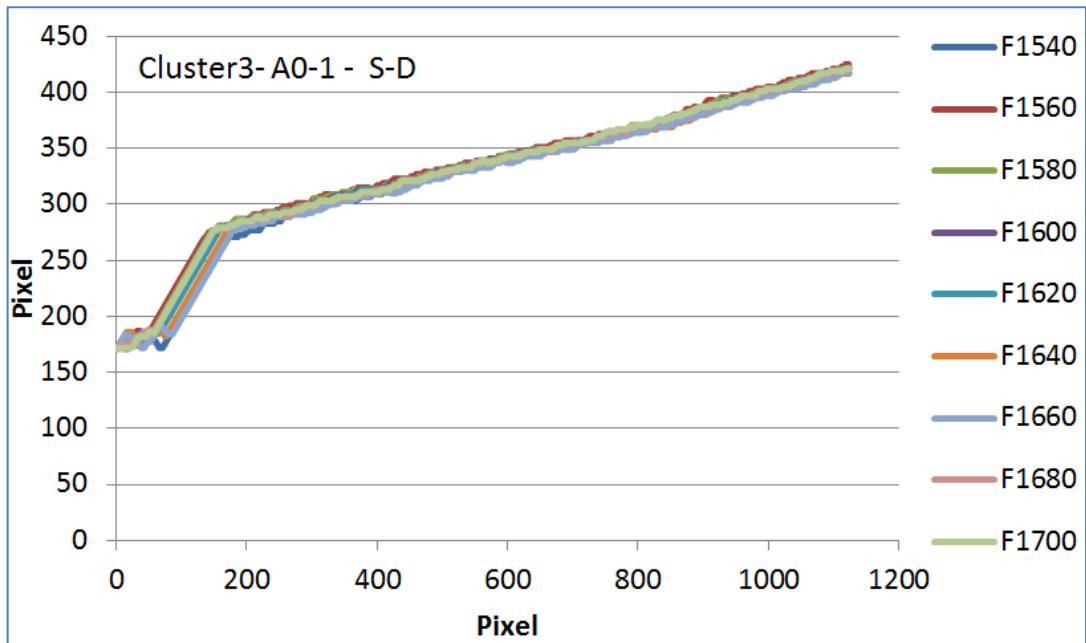

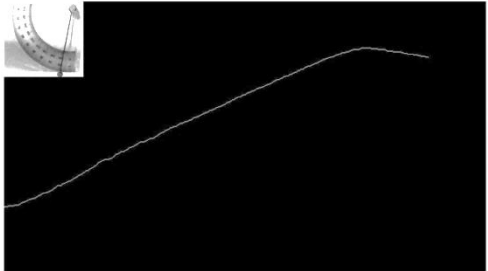
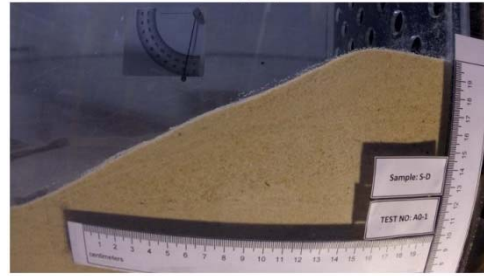
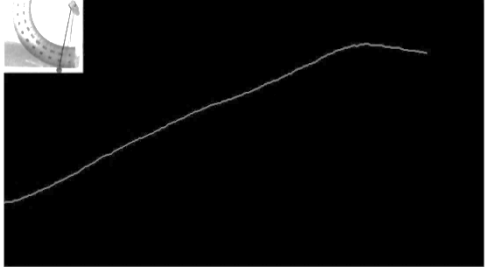


Figure 4-63: Cluster3 - A0-1 - S-D - Intervals of 20 frames

## 4.5. Calculation of Inclination and Maximum Vertical Displacement Speed

In this section, for calculation of inclination and maximum vertical displacement, two frame numbers (F840 and F900) were utilised as shown in Figure 4-64. The outputs of the two frame numbers under different slope angles are presented in Table 4-2.

**Table 4-2: The conversion of the frame numbers F840 and F900 to a monochrome plan**

Frame 840 (Tank slope = 8°)	Frame 840 (Tank slope = 8°)
	
Frame 900 (tank slope = 9°)	Frame 900 (Tank slope = 9°)
	

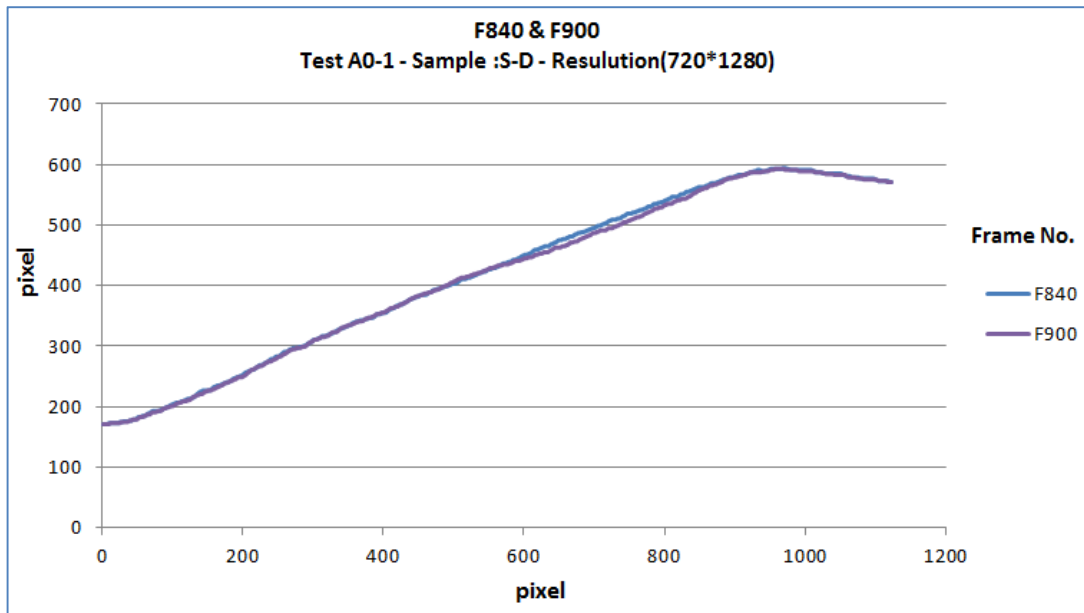


Figure 4-64: Test A0-1 - S-D - output graph of F840 and F900

To compare the two frame numbers (F840 and F900), a section of the line was separated to analyse the outputs as shown in Figure 4-64, with additional information presented in Figure 4-65.

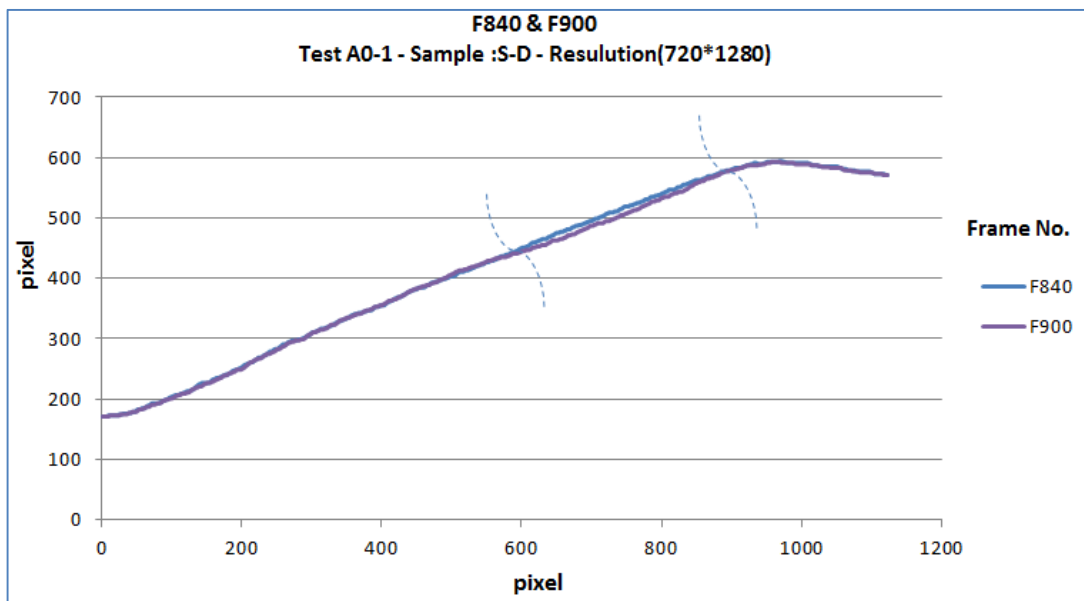


Figure 4-65: Test A0-1 - S-D - output graph of F840 and F900- the selected area to compare

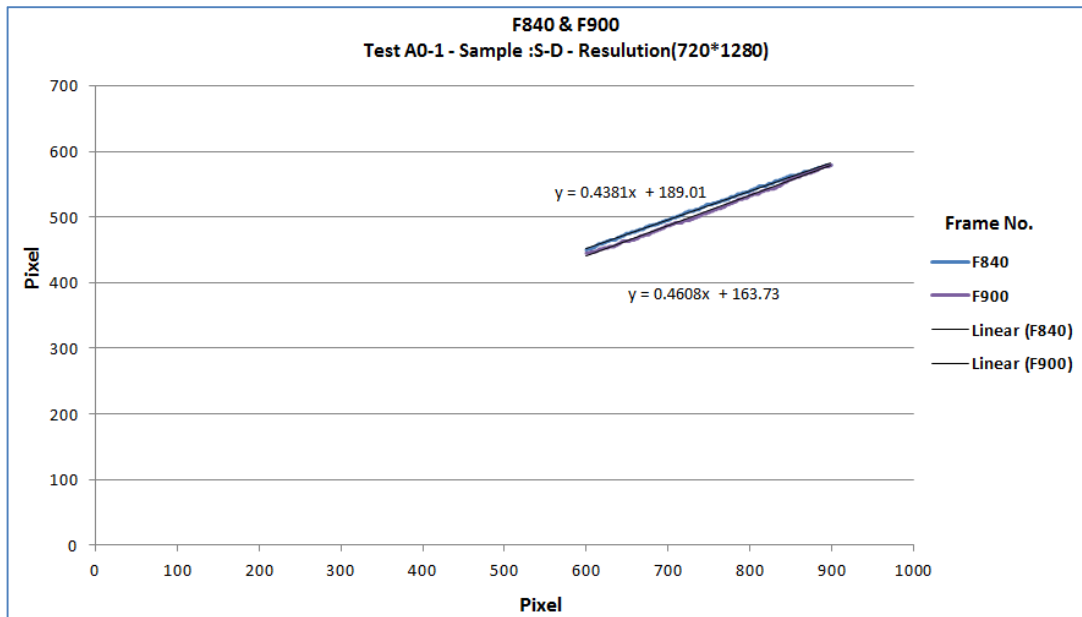


Figure 4-66: Test A0-1 - S-D - output graph of F840 and F900 - line equation

It was necessary to convert pixels to millimetre dimensions before conducting the tests. Two vertical and horizontal rulers were installed to compute the vertical and horizontal displacement (Figure 4-66). The conversion rate for y- axis and x-axis is 4.75 and 4.8, respectively. For example, to convert a 10-pixel displacement on the y-axis to a standard millimetre unit, it is necessary to divide 10 by 4.75 ( $10 \div 4.75 = 2.1\text{mm}$ ). Detailed information on the displacement is presented in Table 4-3 and Figure 4-67.



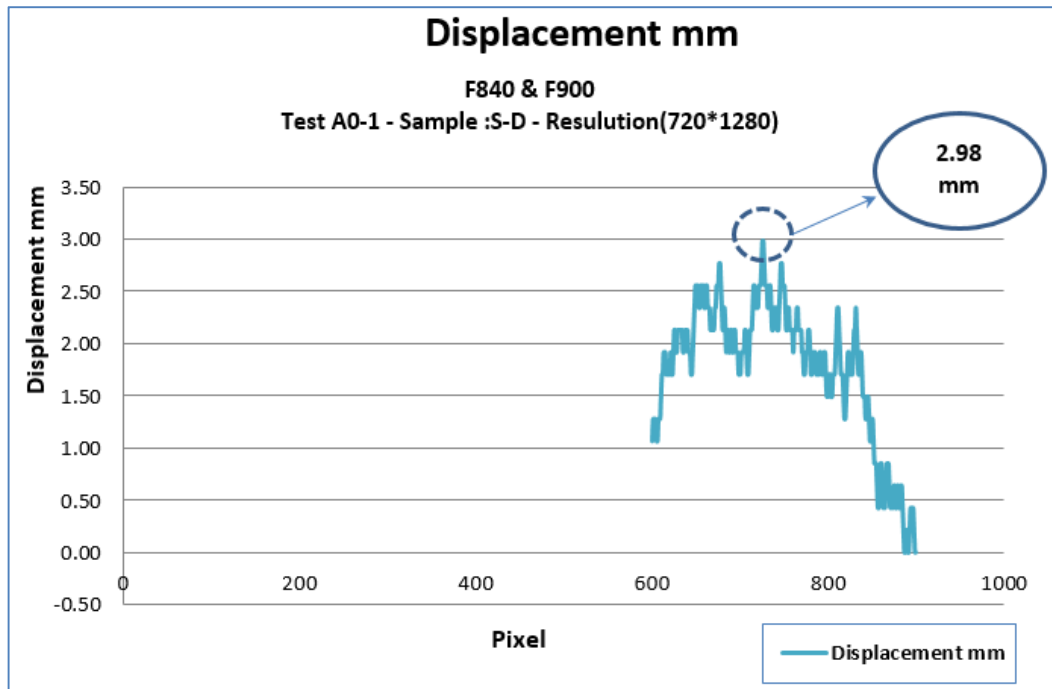


Figure 4-67: Test A0-1 - S-D - output graph F840 and F900- Displacement mm

Table 4-3: Calculation of inclination and maximum vertical displacement speed

Frame No.	Tan(Alpha)	Slope Angle	Slope Angle	Unit
F840	0.438	0.413 (Radian)	23.66	Degree
F900	0.461	0.431(Radian)	24.74	Degree
<b>Results of Calculation</b>				
Delta Slope (Slope variation)			1.08	Degree
Delta Time[(900-840)/59]Second			1.02	Sec
Slope Speed= Delta Slope/Delta Time			1.064	Degree/Sec
Max Displacement Speed = 2.98mm/Delta Time			2.93	Mm/Sec
Average Displacement Speed = 1.76mm/Delta Time			1.73	Mm/Sec

#### **4.6. Interpretation**

In this section, all previous findings are evaluated in more detail, with the movements and their rates shown as time passes and the results presented in two graphs for each test treatment.

In the following figures, the first double vertical axis line graph shows the slope angle (Deg) as indicated on the left y-axis, the angular velocity (Delta slope/Sec) shown on the right y-axis and the time (Sec) is considered on the x-axis. The main first and second peaks named Jump1 and Jump2, respectively, are shown.

The second graph illustrates the relationship between the FOS indicated on the y-axis and time (Sec) on the x-axis. (FOS calculated according to equation 2-4)

According to the legends, slope angle and FOS are described by the solid lines and a dotted line depicts the angular velocity.

Data is selected from tank rotation moving from start time until highest degree stop time.

### Test A0-1 Sample S-D

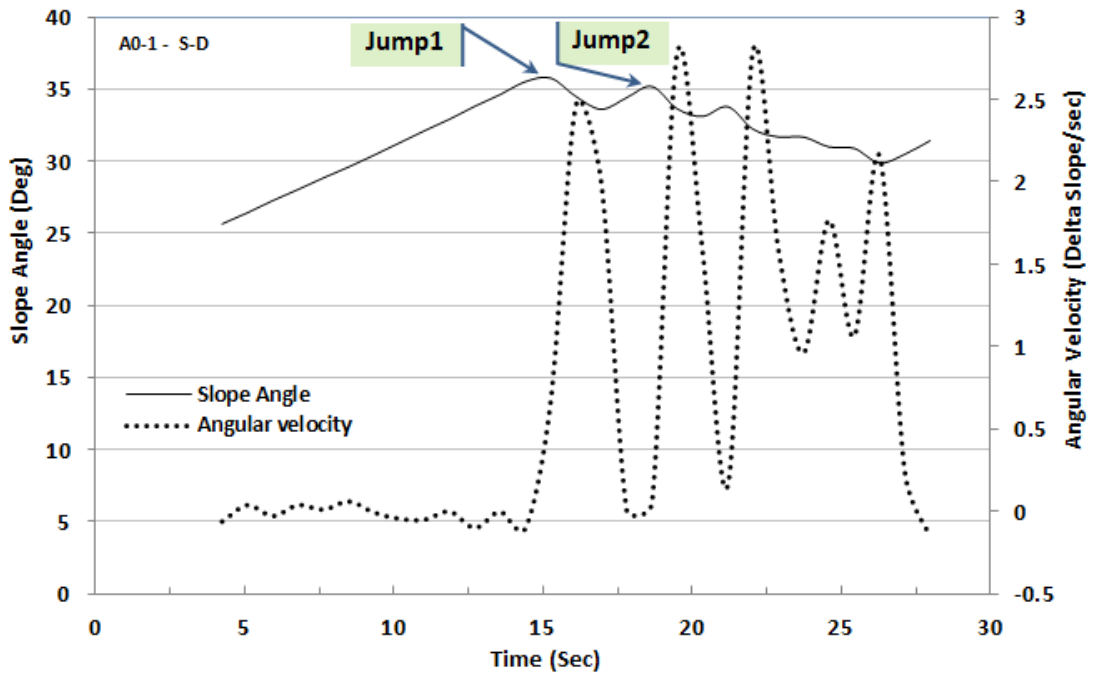


Figure 4-68: Variation of slope angle and angular velocity with time for test: A0-1, sample: S-D

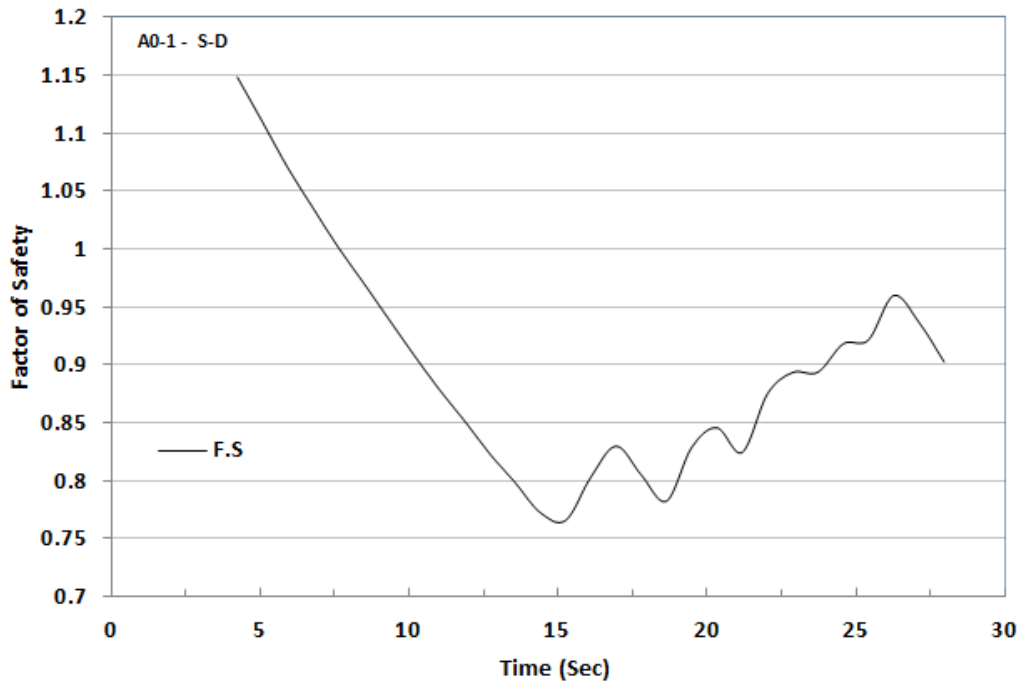


Figure 4-69: Variation of factor of safety(FOS) with time for test: A0-1, sample: S-D

### Test A0-2 Sample SB5-D

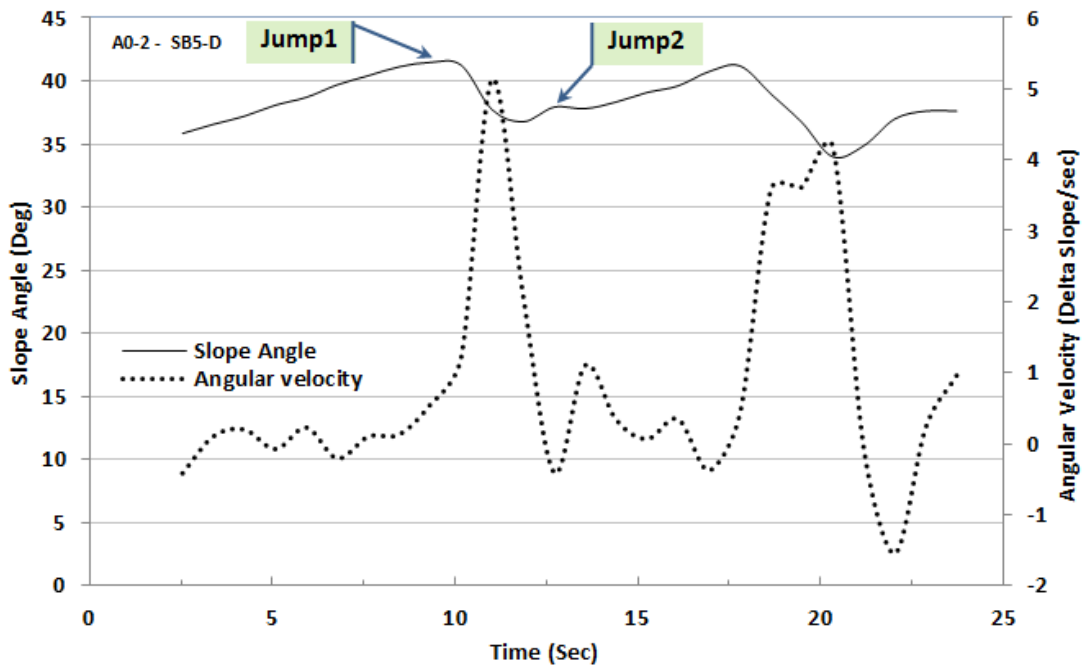


Figure 4-70: Variation of slope angle and angular velocity with time for test: A0-2, sample: SB5-D

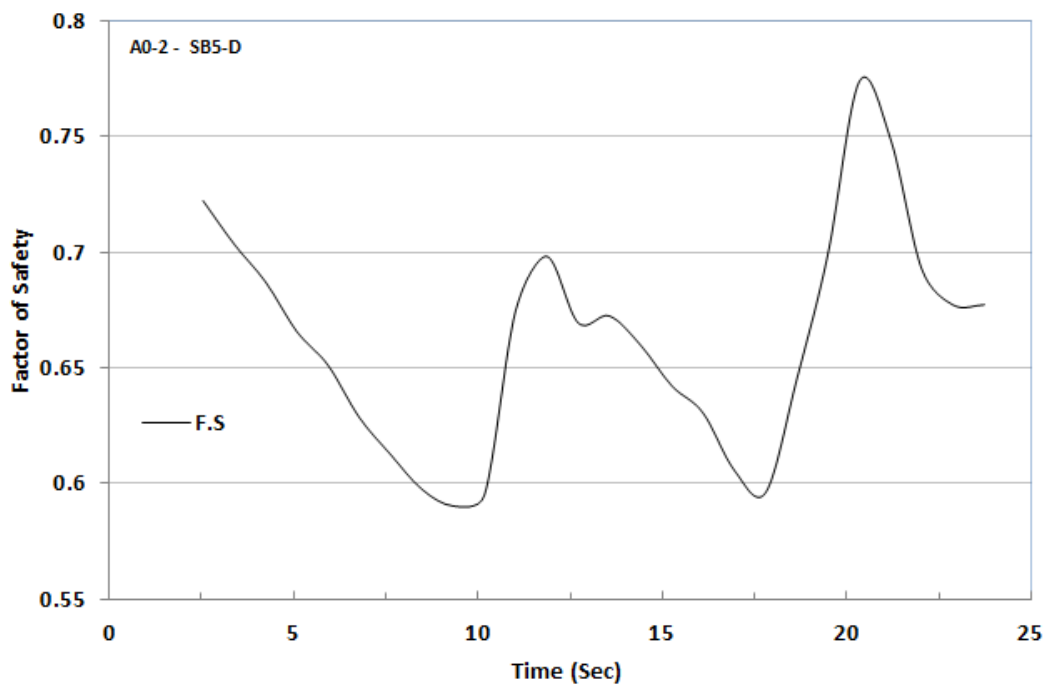


Figure 4-71: Variation of factor of safety(FOS) with time for test: A0-2, sample: SB5-D

**Test A0-3 Sample SB10-D**

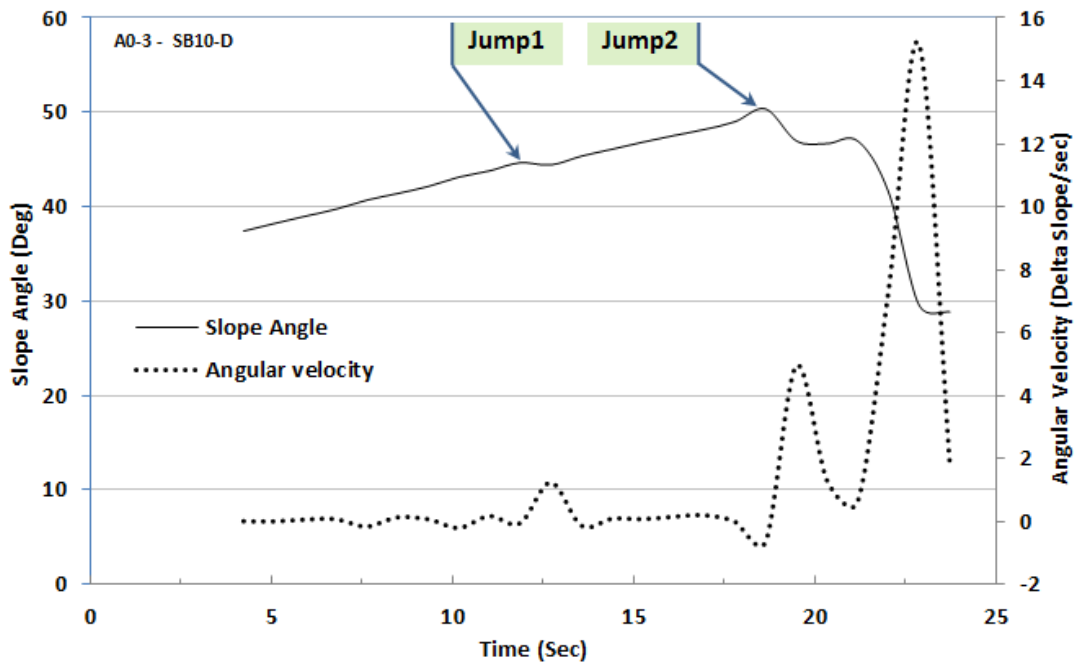


Figure 4-72: Variation of slope angle and angular velocity with time for test: A0-3, sample: SB10-D

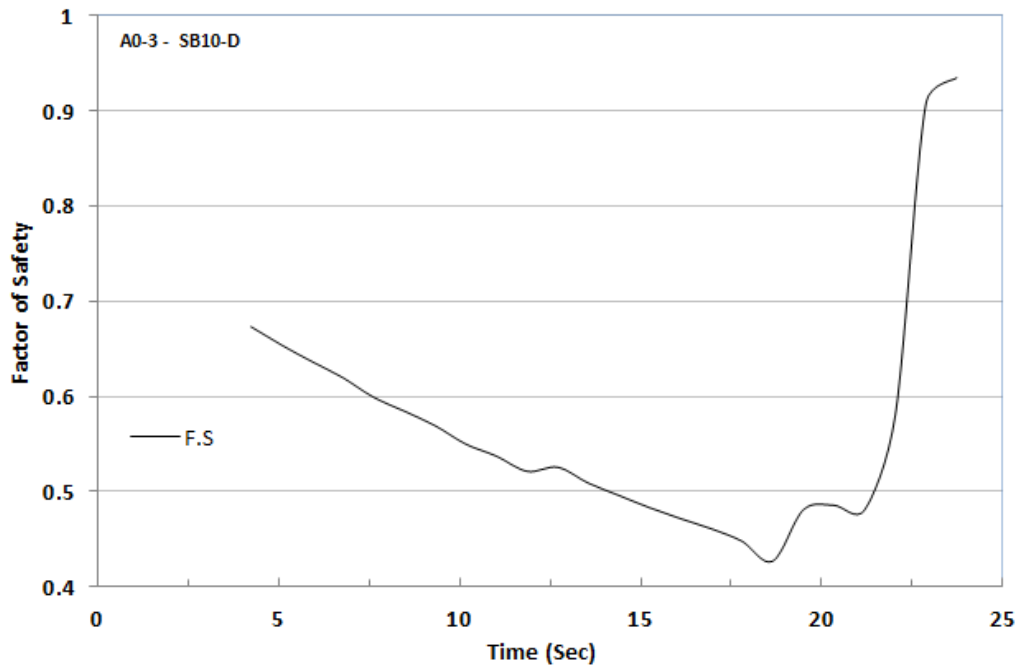


Figure 4-73: Variation of factor of safety(FOS) with time for test: A0-3, sample: SB10-D

**Test A0-4 Sample SB15-D**

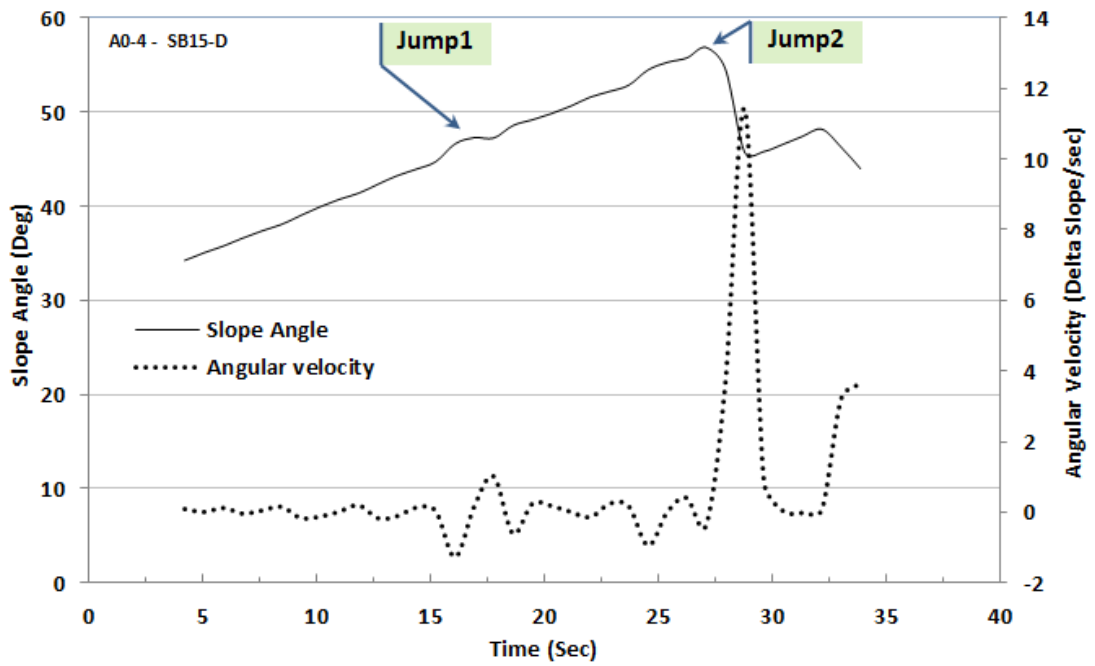


Figure 4-74: Variation of slope angle and angular velocity with time for test: A0-4, sample: SB15-D

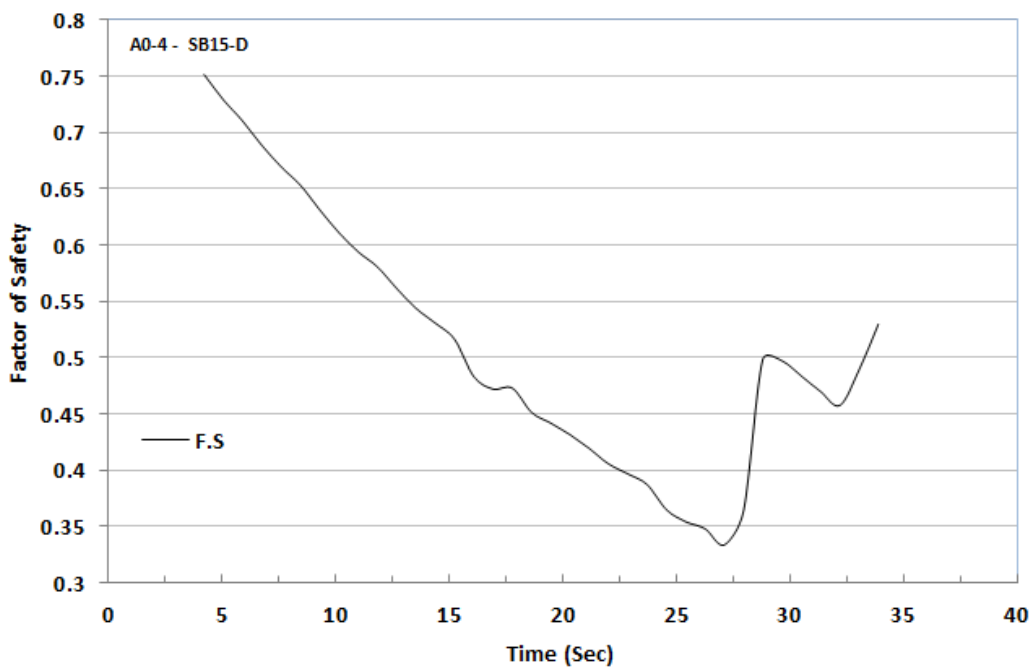


Figure 4-75: Variation of factor of safety(FOS) with time for test: A0-4, sample: SB15-D

**Test A0-5 Sample SB20-D**

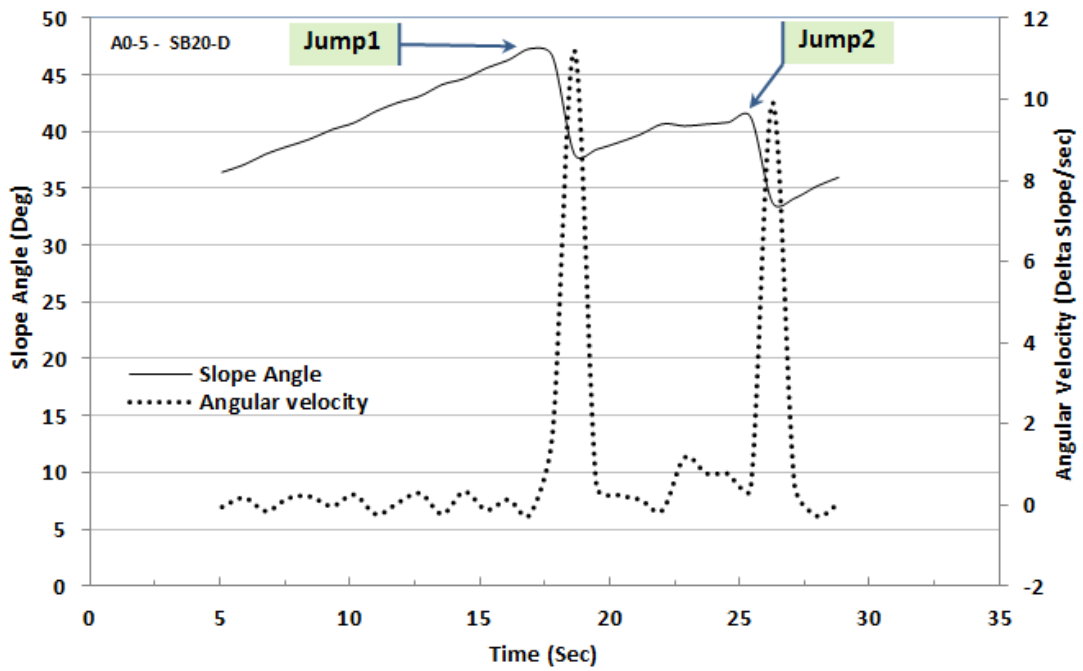


Figure 4-76: Variation of slope angle and angular velocity with time for test: A0-5, sample: SB20-D

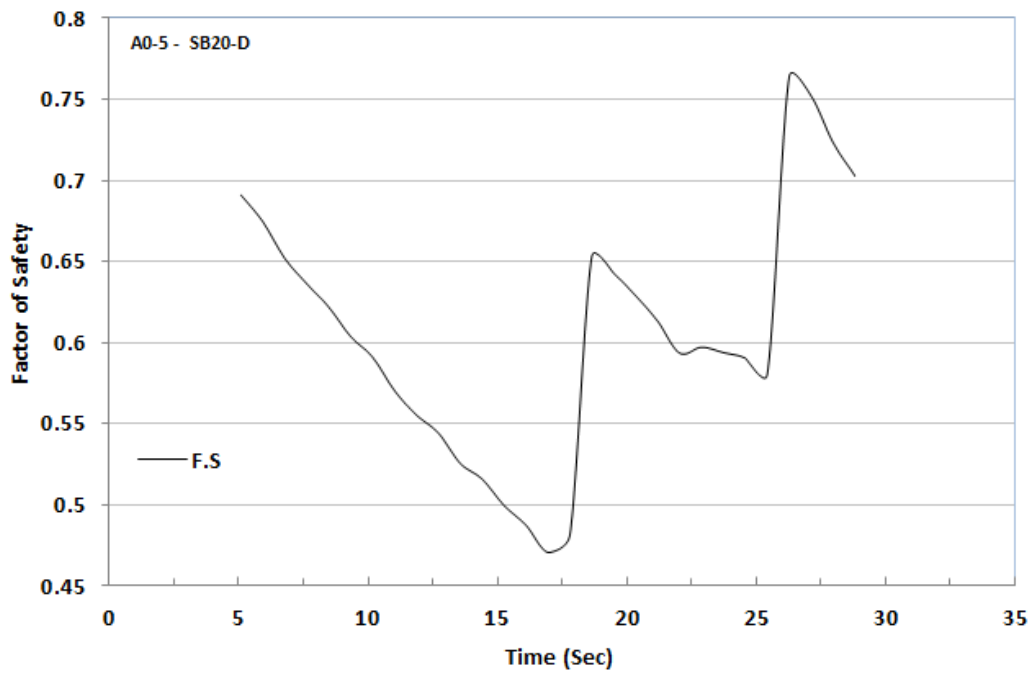


Figure 4-77: Variation of factor of safety(FOS) with time for test: A0-5, sample: SB20-D

### Test A5-1 Sample S-D

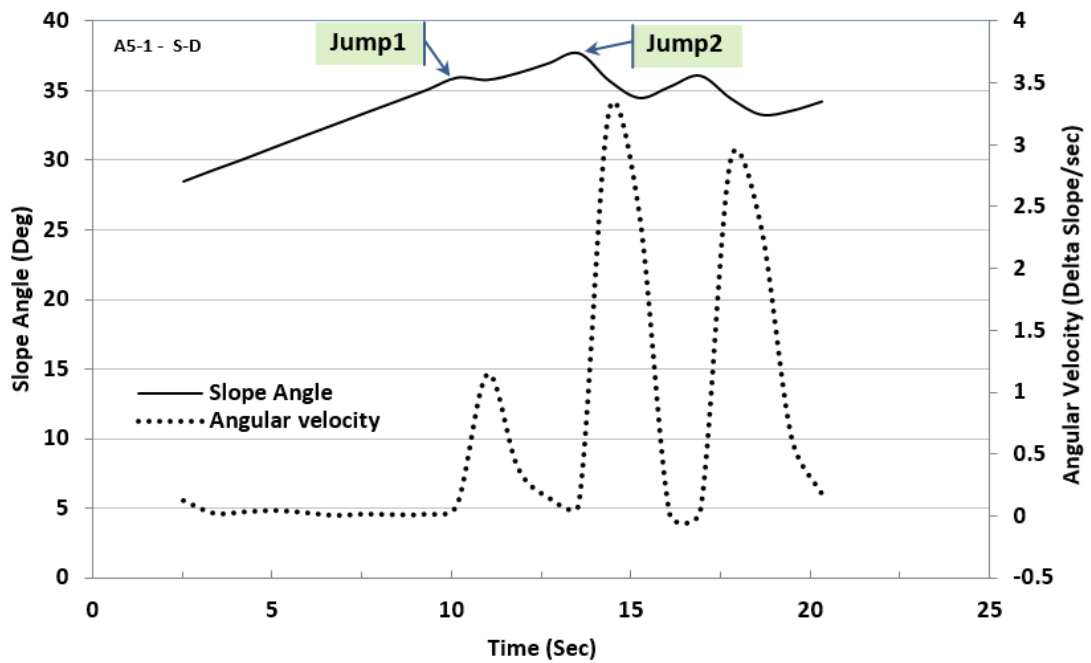


Figure 4-78: Variation of slope angle and angular velocity with time for test: A5-1, sample: S-D

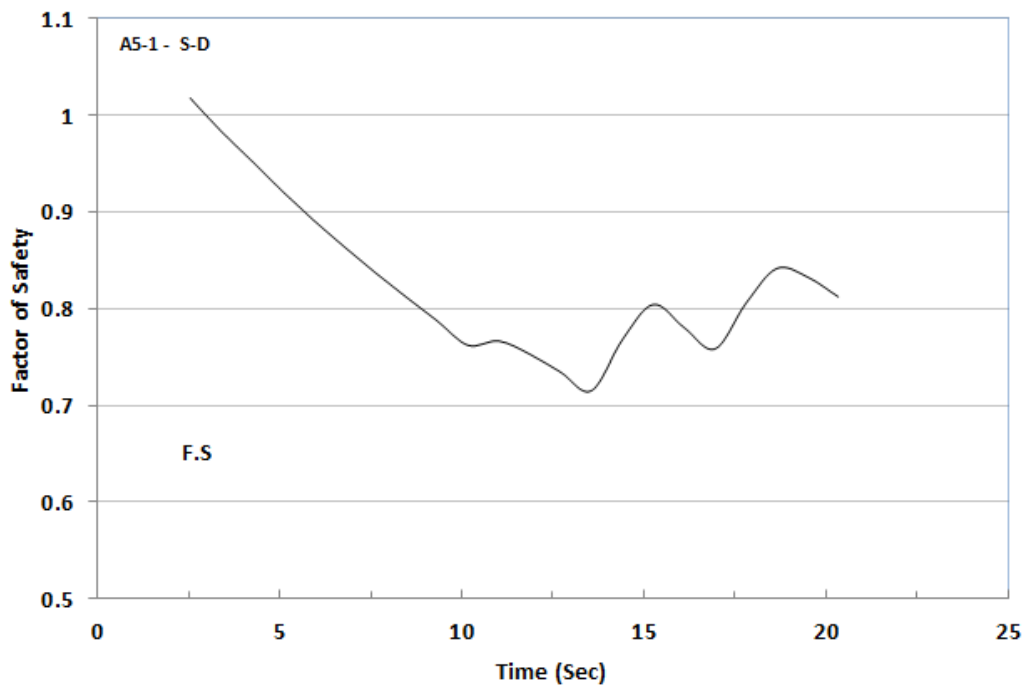


Figure 4-79: Variation of factor of safety(FOS) with time for test: A5-1, sample: S-D



### Test A5-2 Sample SB5-D

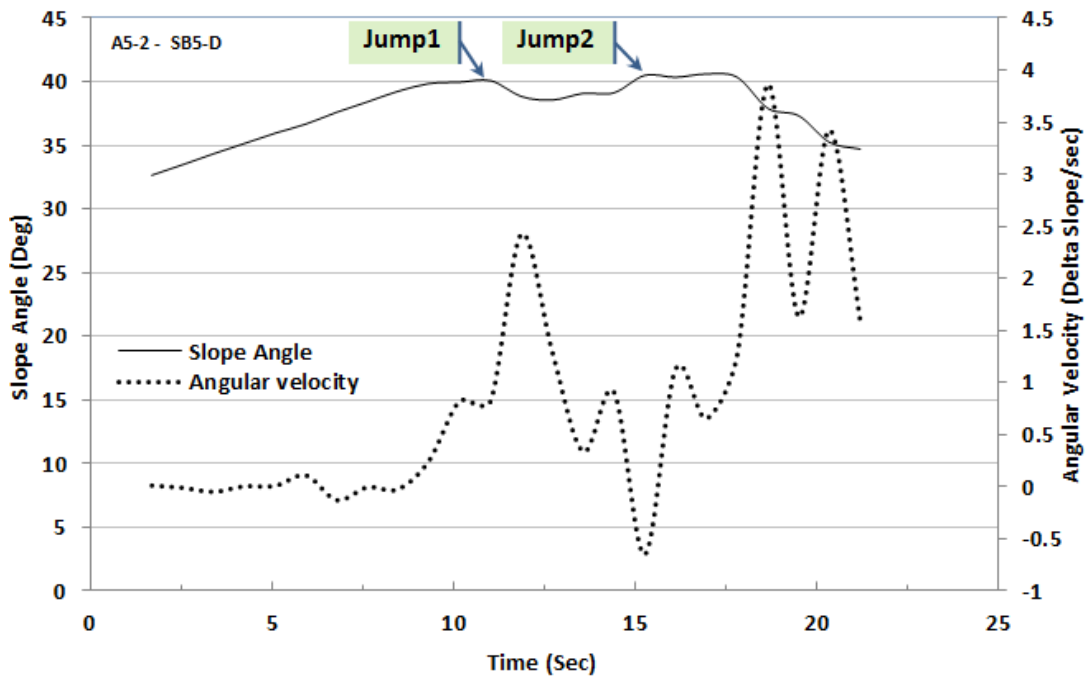


Figure 4-80: Variation of slope angle and angular velocity with time for test: A5-2, sample: SB5-D

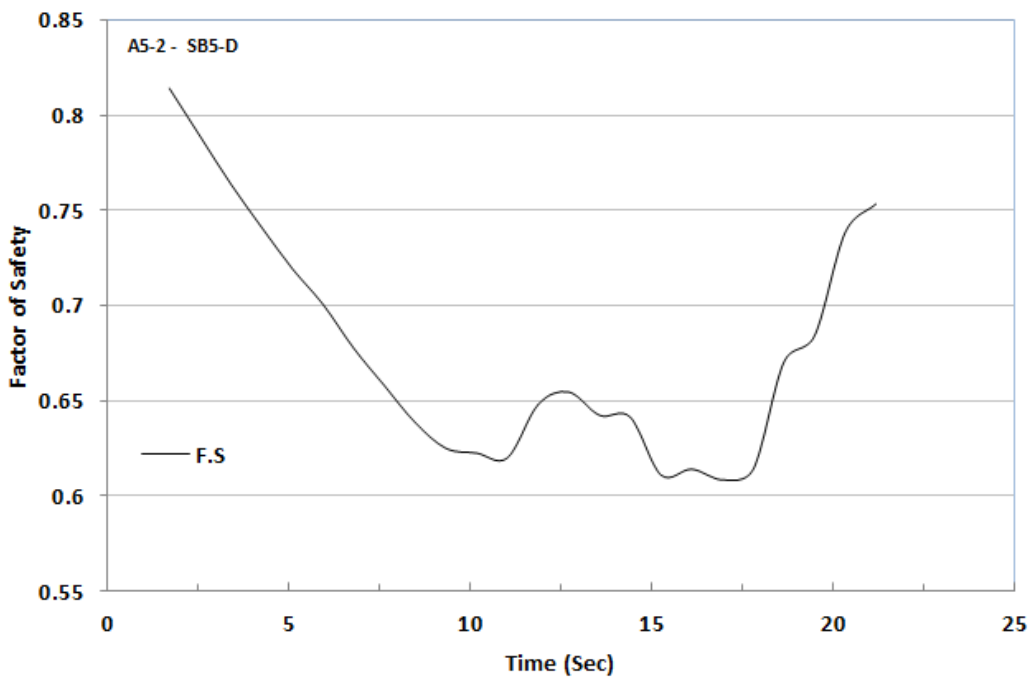


Figure 4-81: Variation of factor of safety(FOS) with time for test: A5-2, sample: SB5-D

**Test A5-3 Sample SB10-D**

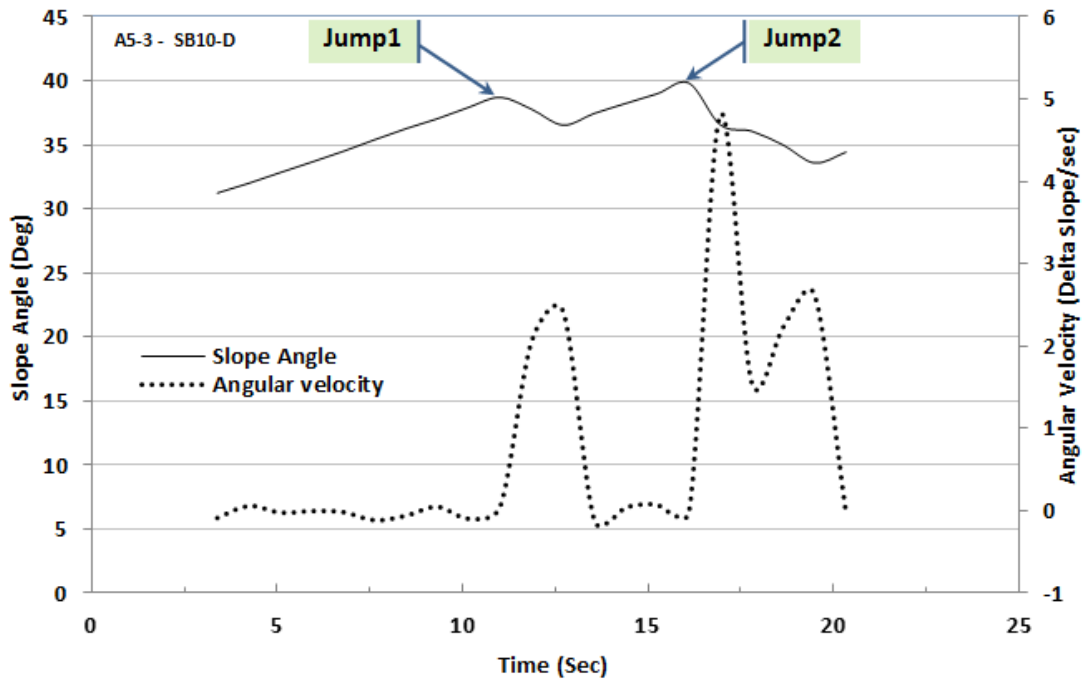


Figure 4-82: Variation of slope angle and angular velocity with time for test: A5-3, sample: SB10-D

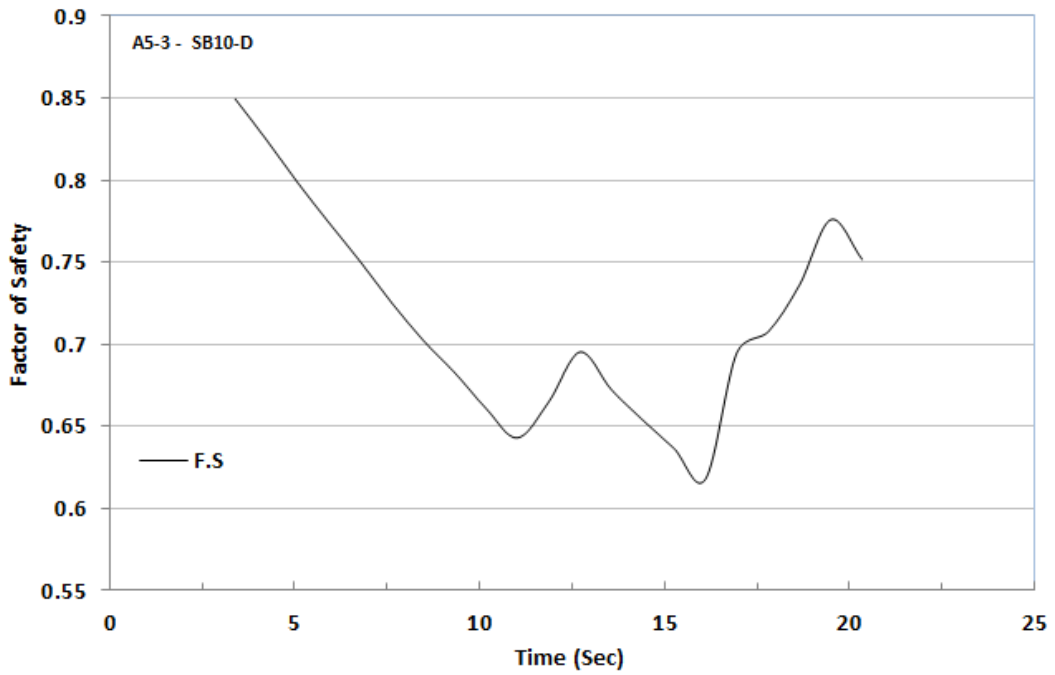


Figure 4-83: Variation of factor of safety(FOS) with time for test: A5-3, sample: SB10-D

### Test A5-4 Sample SB15-D

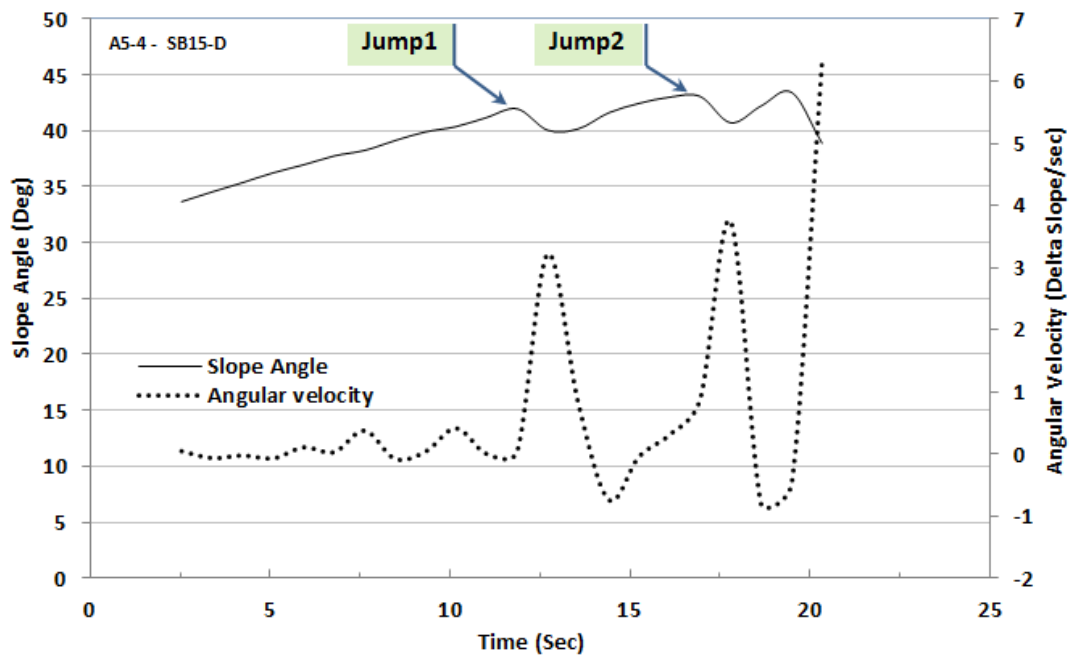


Figure 4-84: Variation of slope angle and angular velocity with time for test: A5-4, sample: SB15-D

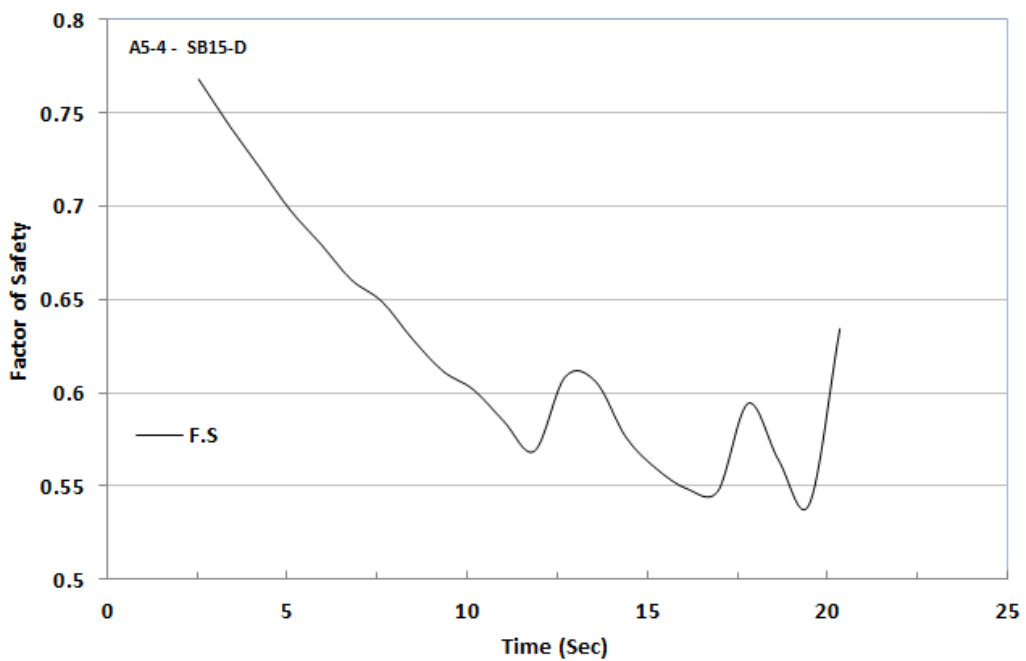


Figure 4-85: Variation of factor of safety(FOS) with time for test: A5-4, sample: SB15-D

### Test A5-5 Sample SB20-D

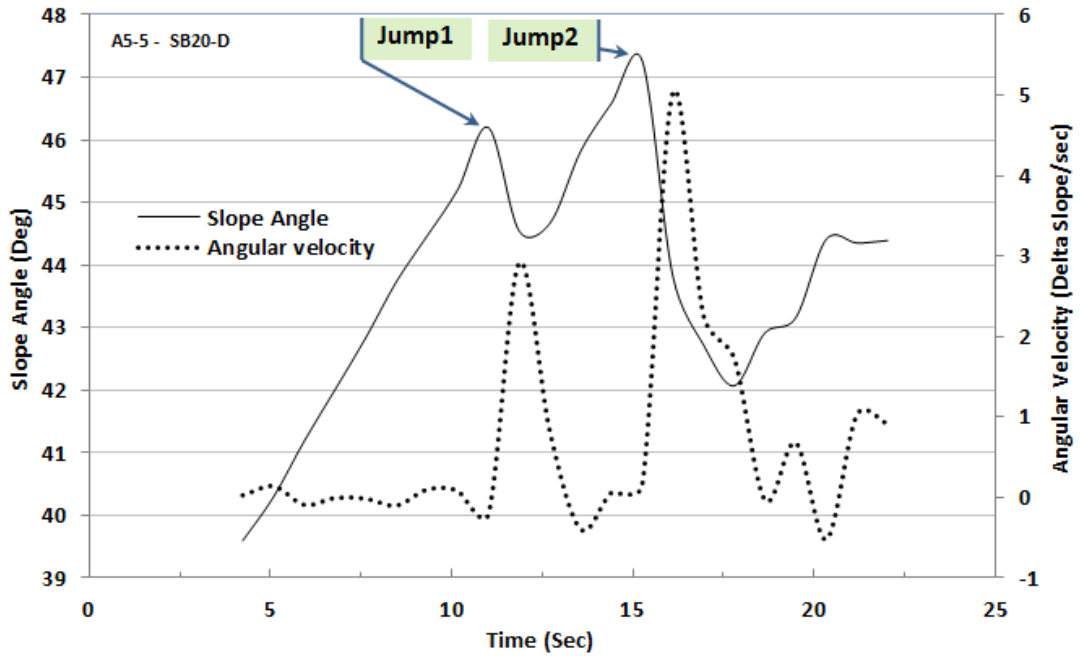


Figure 4-86: Variation of slope angle and angular velocity with time for test: A5-5, sample: SB20-D

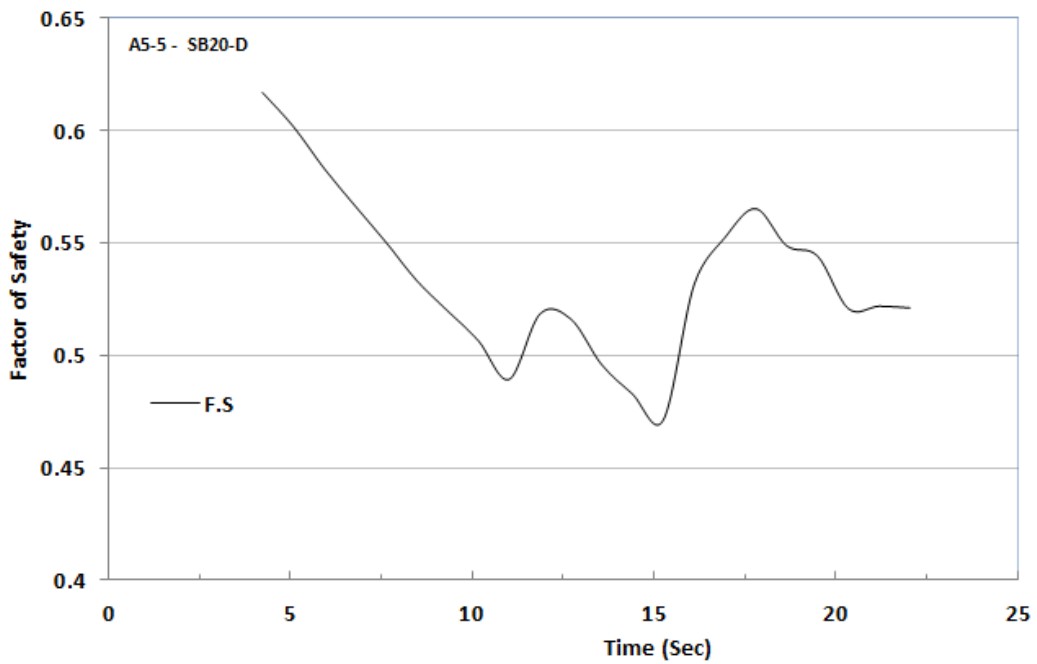


Figure 4-87: Variation of factor of safety(FOS) with time for test: A5-5, sample: SB20-D

### Test A10-1 Sample S-D

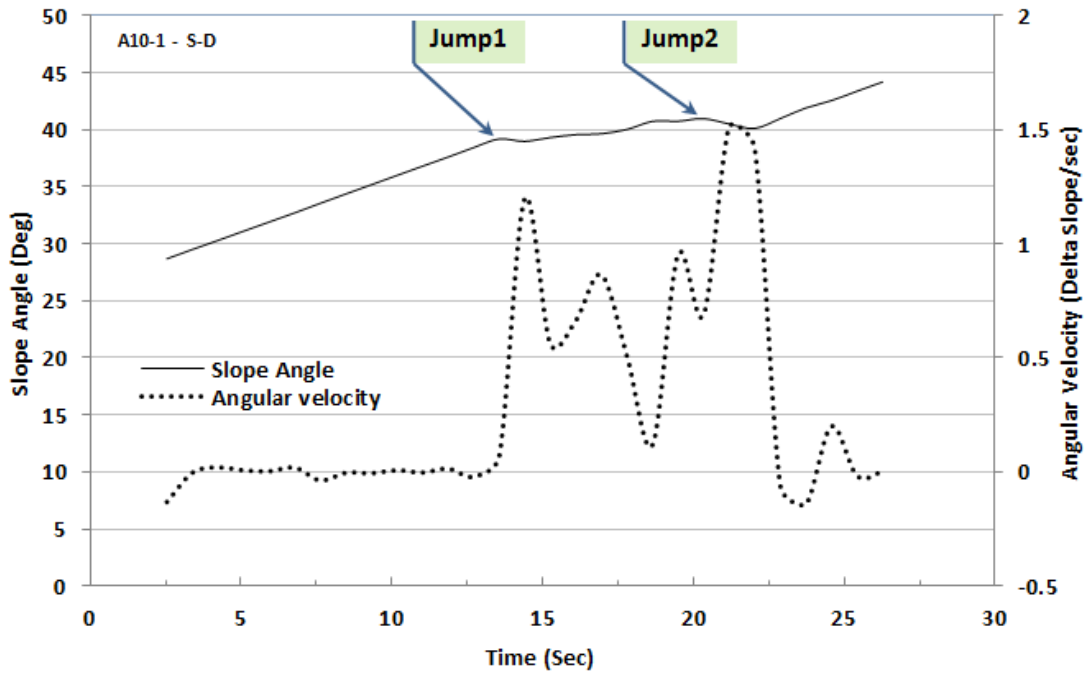


Figure 4-88: Variation of slope angle and angular velocity with time for test: A10-1, sample: S-D

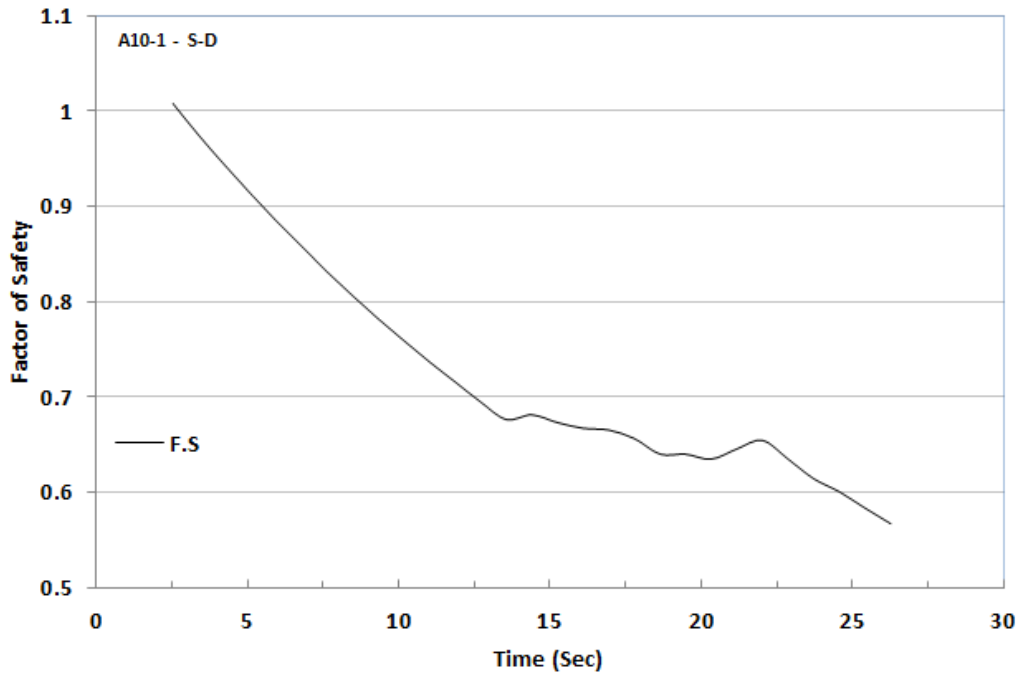


Figure 4-89: Variation of factor of safety(FOS) with time for test: A10-1, sample: S-D

### Test A10-2 Sample SB5-D

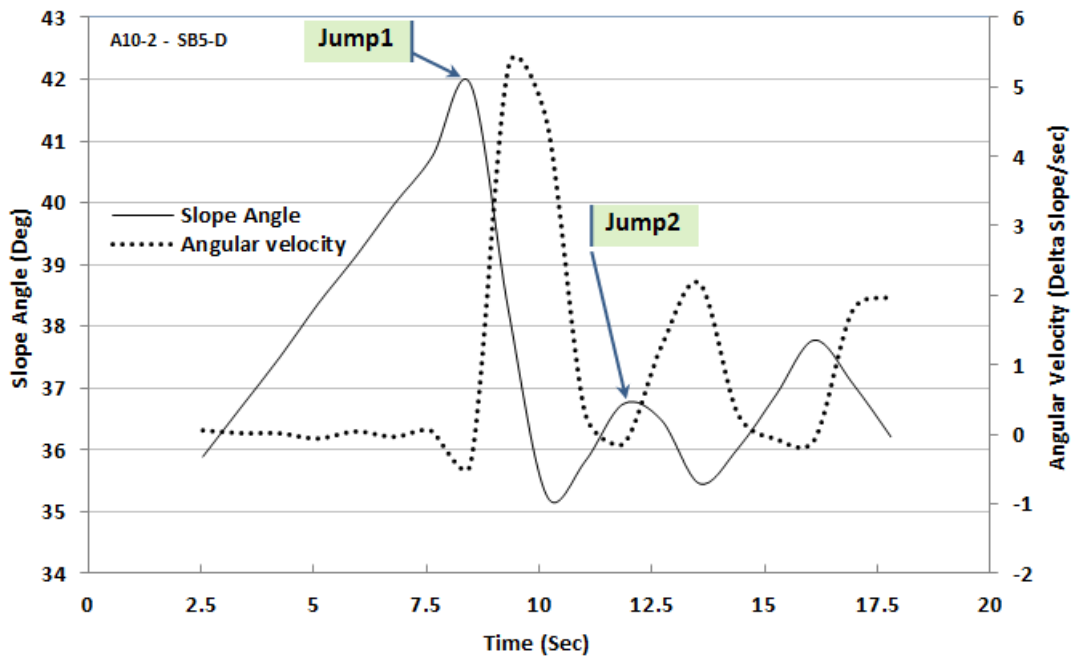


Figure 4-90: Variation of slope angle and angular velocity with time for test: A10-2, sample: SB5-D

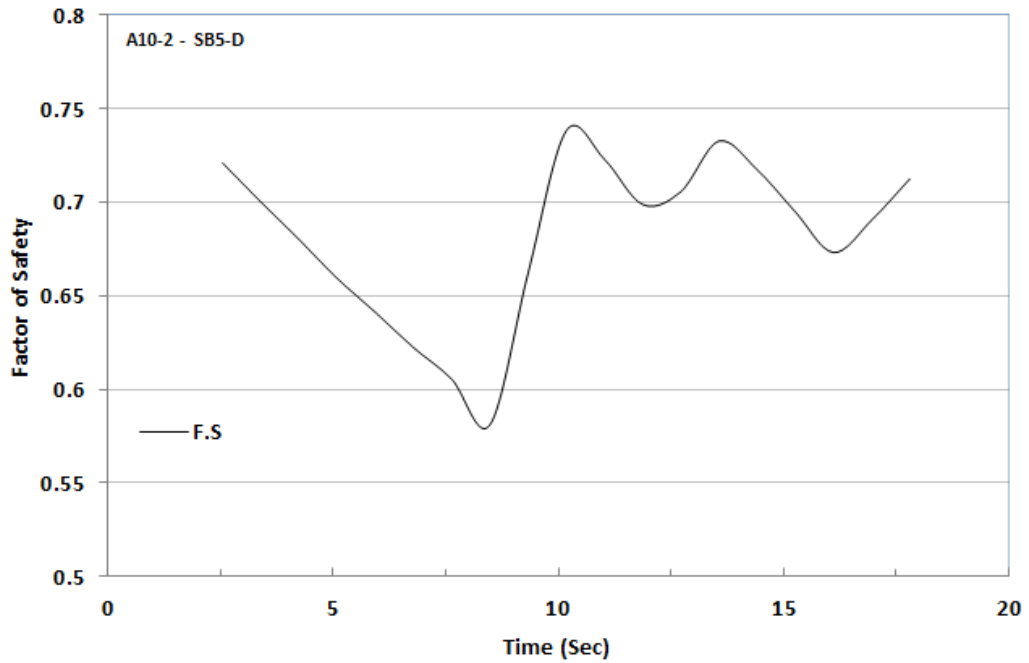


Figure 4-91: Variation of factor of safety(FOS) with time for test: A10-2, sample: SB5-D

### Test A10-3 Sample SB10-D

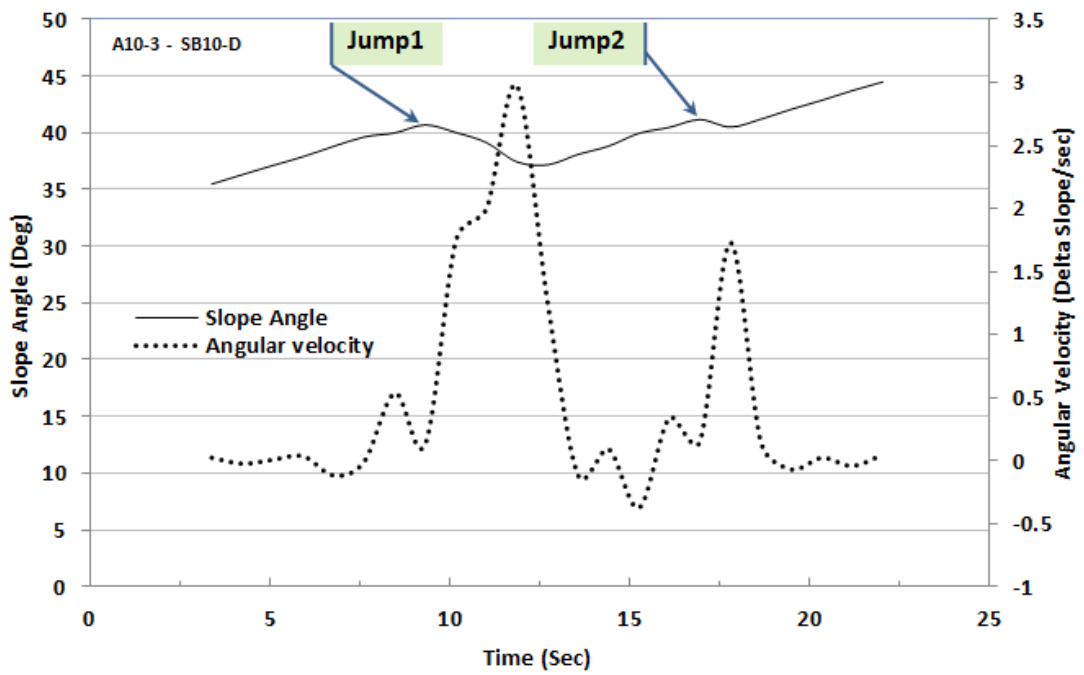


Figure 4-92: Variation of slope angle and angular velocity with time for test: A10-3, sample: SB10-D

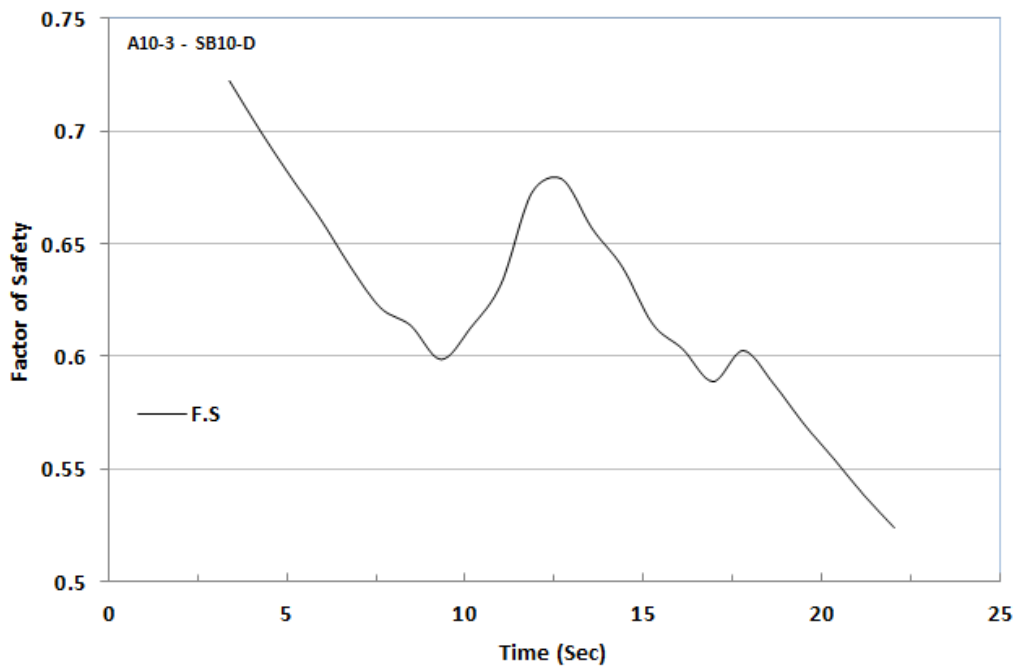


Figure 4-93: Variation of factor of safety(FOS) with time for test: A10-3, sample: SB10-D

### Test A10-4 Sample SB15-D

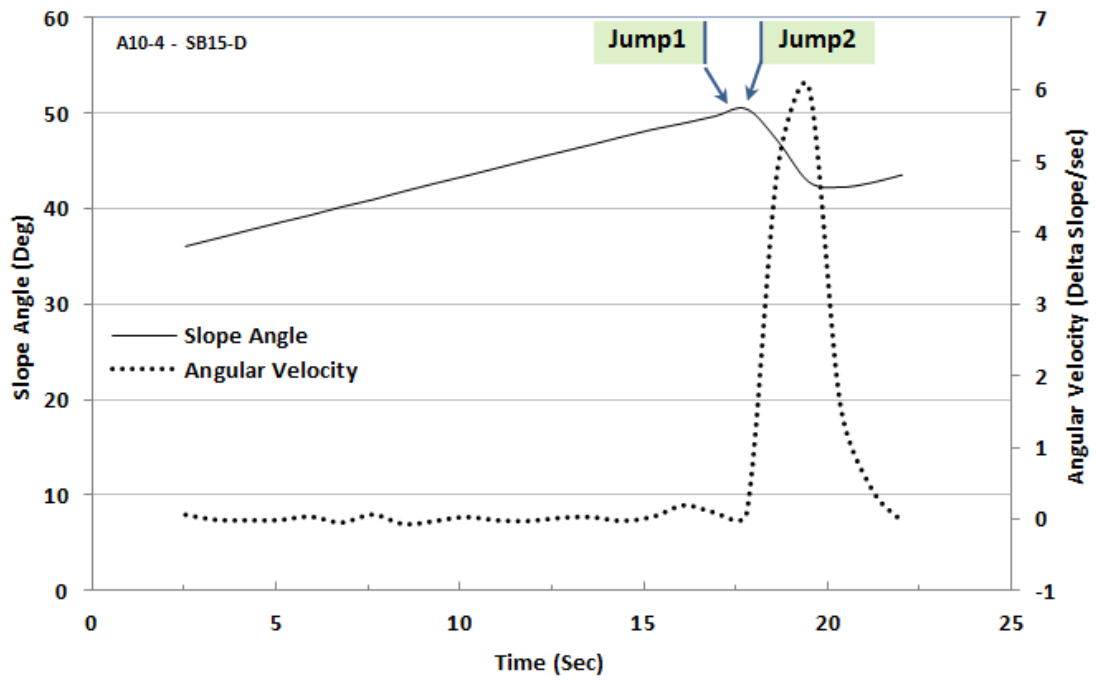


Figure 4-94: Variation of slope angle and angular velocity with time for test: A10-4, sample: SB15-D

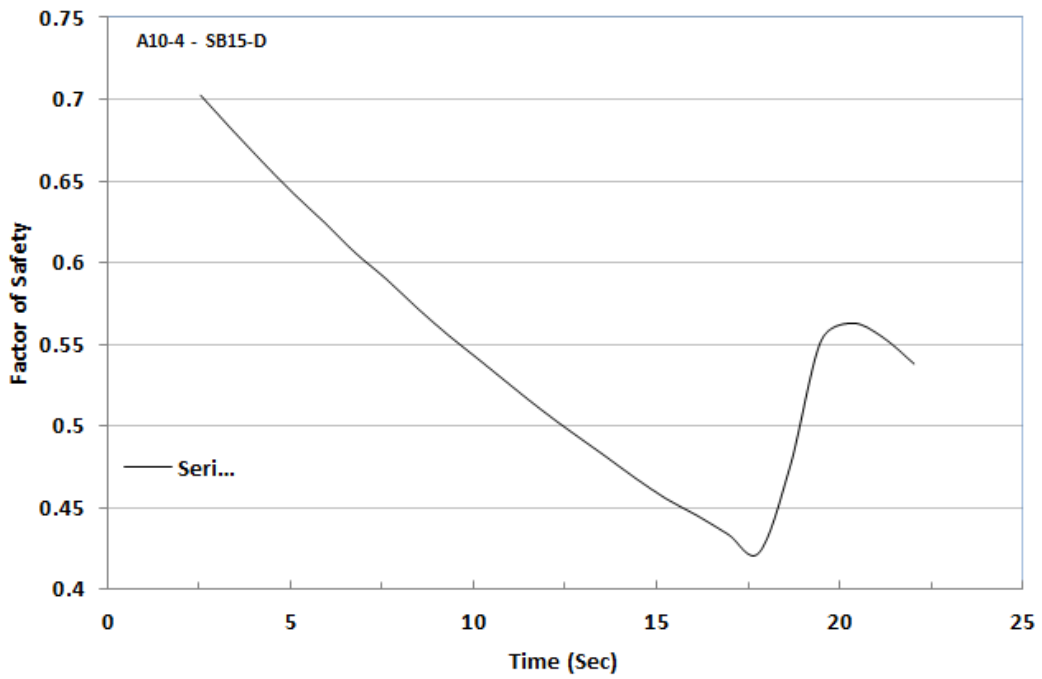


Figure 4-95: Variation of factor of safety(FOS) with time for test: A10-4, sample: SB15-D



### Test A10-5 Sample SB20-D

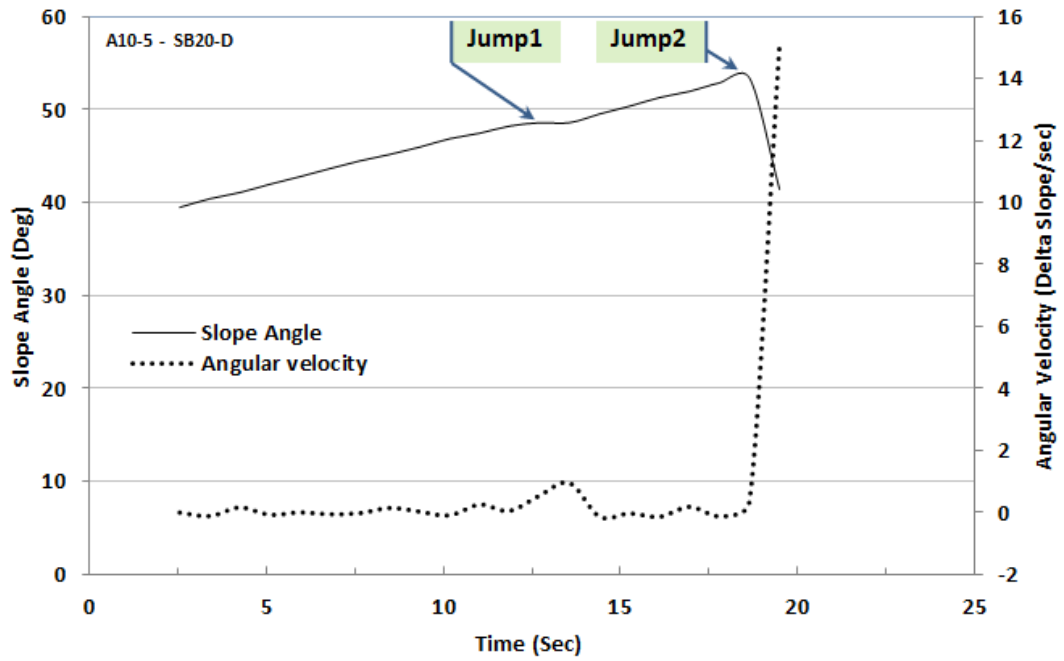


Figure 4-96: Variation of slope angle and angular velocity with time for test: A10-5, sample: SB20-D

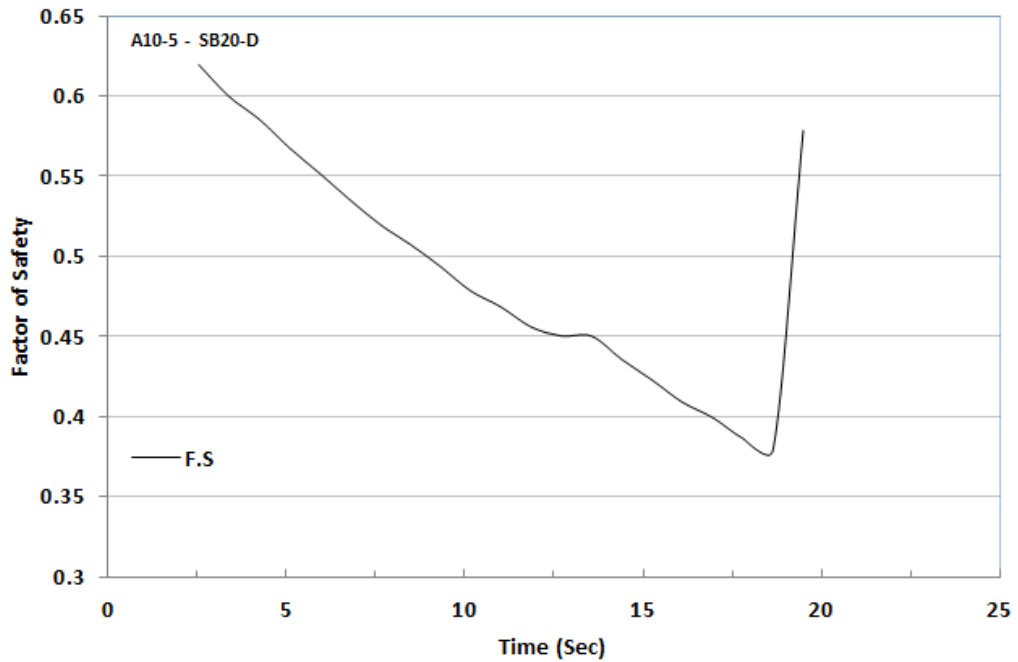


Figure 4-97: Variation of factor of safety(FOS) with time for test: A10-5, sample: SB20-D

### **Test A0-1 Sample S-D**

Figure 4-68, which was monitored between 4.2 and 27.9 seconds, illustrates how slope angle rises steadily before Jump1 or the first failure threshold. After that, the slope angles starts to decrease in an oscillating manner. The velocity of the slope is nearly constant about zero before the failure threshold but dramatically increases to nearly 2.4 deg/sec corresponding to yielding of slope. This graph also shows a fall in slope angle simultaneously there is an upward trend in velocity in both Jump1 and Jump2.

Figure 4-69 represents how FOS changes according to the relationship noted in equation 2-6. It decreases until failure threshold is reached at 15.3 seconds, which coincides with Jump1 in angular velocity; however, it increases again at 18.6 seconds, which surprisingly coincides with Jump2 in angular velocity.

### **Test A0-2 Sample SB5-D**

Figure 4-70, which was monitored between 2.5 and 23.7 seconds, represents a moderate rise in slope angle until 9.3 seconds when Jump1 occurs. Then the slope angle decreases slowly and has a slight noticeable peak at Jump2. The angular velocity fluctuates and increases dramatically within 11 seconds. By contrast, it drops significantly. Immediately after Jump1 and Jump2, two bumps are easily seen in angular velocity at 11 s and 13.5 seconds, respectively.

Figure 4-71 reveals that FOS decreases sharply to a minimum point of 0.59, which coincides with Jump1, then it increases to 0.7, and then again decreases to 0.67, which coincides with Jump2.

### **Test A0-3 Sample SB10-D**

Figure 4-72, which was monitored between 4.2 and 23.7 seconds, shows a very smooth increase in slope angle including Jump1, which is small yet still observable. Although it then slowly decreases, the slope angle continues to increase until Jump2 at 18.6 seconds. The angular velocity has steady fluctuations, with it increasing to

12.7 seconds, and then decreasing, with the lowest point in angular velocity occurring at exactly the same time as Jump2 at 18.6 seconds.

Figure 4-73 illustrates that the FOS has a downward trend until 11.9 seconds, which occurs at the same time as Jump1. The FOS then increases, but decreases again until it reaches the most minimum point (0.43), which coincides with Jump2 in the slope angle.

#### **Test A0-4 Sample SB15-D**

Figure 4-74 shows that the slope angle has an upward trend and has two jumps at 16.4 and 27.1 seconds, respectively, and then decreases after Jump2. Conversely, angular velocity reveals many fluctuations until 16.4 seconds, when it decreases, although it again demonstrates different fluctuations afterwards. This continues until it increases abruptly at 28.8 seconds. The most minimum point of angular velocity in all these fluctuations occurs at the same time as Jump1. Both factors were monitored between 4.2 and 33.8 seconds.

Figure 4-75 demonstrates a downward trend. This decrease continues until 0.47, coinciding with Jump1, but then has a small increase, after which it retains its downward trend until it reaches the most minimum point (0.33) coinciding with Jump2.

#### **Test A0-5 Sample SB20-D**

Figure 4-76 demonstrates continual increases until 19.9 seconds when Jump1 occurs, after which it decreases then increases again gradually until 25.4 seconds when Jump2 occurs. Conversely, angular velocity has two dramatic jumps, with both occurring immediately after Jump1 and Jump2 in slope angle. This line graph shows data that was monitored from 5 until 28.8 seconds.

Figure 4-77 depicts continual decreases in the FOS until reaching the most minimum point (0.47), which coincides with Jump1. Although it increases suddenly, it decreases again to 0.58, which is exactly when Jump2 in slope angle occurs.

### **Test A5-1 Sample S-D**

Figure 4-78, which represents data monitored from 2.5 until 20.3 seconds, shows a steady increase in slope angle until reaching Jump1 at 10.2 seconds. It then decreases, however, this decrease does not last long; it increases again soon after and reaches Jump2 at 13.5 seconds. The angular velocity decreases and then remains almost stable until it increases sharply at 11.9 seconds. Then, it has two more rapid changes, one of which reaches the peak at 14.4 seconds.

Figure 4-79 illustrates the FOS having a decrease until 0.76, after which it increases. Then, it decreases again until the most minimum point at 0.71, with the FOS again increasing afterwards. The two minimum points in angular velocity occur at the same time as Jump1 and Jump2.

### **Test A5-2 Sample SB5-D**

Figure 4-80 shows increase in slope angle in which Jump1 occurs at 11 seconds, after which it shows slight changes until Jump2 at 15.3 seconds. Angular velocity increases sharply at 11.9 seconds (immediately after Jump1 in slope angle), and then shows rapid changes. Surprisingly, the most minimum of angular velocity occurs at the same time as Jump2 in the slope angle. Both of these factors were monitored from 1.7 to 21.2 seconds.

Figure 4-81 reveals that the FOS declines until it reaches 0.62, which is the same time as Jump1. After increasing for a while, it decreases again to 0.61, which coincides with Jump2 in slope angle.

### **Test A5-3 Sample SB10-D**

Figure 4-82 shows continual rise in slope angle until it reaches 11 seconds when Jump1 occurs, after which it decreases again, then increases and reaches the maximum at 16.1 seconds when Jump2 occurs. Angular velocity changes only slightly, increasing at 12.7 seconds immediately after Jump1 and when the slope

angle has dropped. Angular velocity reaches the maximum point at 16.4 seconds, right after Jump2.

Figure 4-83 represents a sudden decrease in the FOS. This decrease continues until 0.64, coinciding with Jump1, after which it increases, then decrease again and reaches its minimum point at 0.63, coinciding with Jump2.

#### **Test A5-4 Sample SB15-D**

Figure 4-84 illustrates a gradual increase in slope angle. These factors were monitored from 2.5 to 20.3 seconds. Jump1 occurs at 11.8 seconds, yet it decreases again, and then Jump2 occurs at 16.9 seconds. Angular velocity experiences a considerable increase immediately following Jump1 and Jump2.

Figure 4-85 depicts significant decreases in the FOS until it first minimum of 0.57, which corresponds with Jump1. The second FOS minimum at 0.54 coincides with Jump2 in slope angle.

#### **Test A5-5 Sample SB20-D**

Figure 4-86 reveals a sudden increase in slope angle until Jump1 occurs at 11 seconds, after which it decrease but then increases again until it reaches 15.2 seconds when Jump2 occurs. Then it decreases rapidly. Angular velocity has two main jumps, each occurring after the jumps in slope angle, i.e. increases in velocity occurred during decreases in slope angle. Both slope and angular velocity were recorded between 4.2 and 22 seconds.

Figure 4-87 reveals a decrease in FOS. Two main minimum points, occurring at 0.49 and 0.47, are shown, with the first one coinciding with Jump1, and the second one with Jump2.

### **Test A10-1 Sample S-D**

Figure 4-88 shows a constant increase in slope angle where the two main jumps occur at 13.5 and 20.3 seconds. Conversely, angular velocity decreases at exactly in the same time as the slope angle increases. Angular velocity does have two main increases (both occurring immediately after each increase in slope angle), one at 14.40 seconds and the other at 12.1 seconds, which is the maximum point.

Figure 4-89 shows a constant decrease in FOS, which drops to 0.67 at Jump1 and 0.63 at Jump2.

### **Test A10-2 Sample SB5-D**

Figure 4-90 reveals rapid waves in both slope angle and angular velocity. Slope angle reaches its maximum point at 8.4 seconds, then decreases and increases again when Jump2 occurs at 11.9 seconds. Angular velocity remains constant until it increases suddenly immediately after Jump1 at 9.3 seconds. After this, it decreases and then increases again to 13.5 seconds, which is exactly after Jump2. Both of these factors were recorded between 2.5 and 17.8 seconds.

Figure 4-91 illustrates a downward trend in the FOS as it reaches its minimum point at 0.58 coinciding with Jump1. After that, it increases dramatically, which occurs as the slope angle decreases, and then decreases to 0.69, which coincides with Jump2 in the slope angle.

### **Test A10-3 Sample SB10-D**

Figure 4-92 shows an increase in slope angle that continues until 9.3 seconds when Jump1 occurs. Then it decreases briefly, and then increases again until it reaches 16.9 seconds when Jump2 happens. Angular velocity has many fluctuations. However, it has two main jumps at 11.8 and 17.8 seconds. The first jump occurs immediately after Jump1 in slope angle, and the second jump occurs immediately after Jump2. These data were recorded between 3.4 and 22 seconds.

Figure 4-93 depicts a sudden decrease in the FOS until it reaches 0.59 coinciding with Jump1, then increases briefly and decreases again; reaching 0.58 before its next increase. This second minimum point coincides with Jump2 in the slope angle.

#### **Test A10-4 Sample SB15-D**

Figure 4-94 shows a constant increase in the slope angle, with Jump1 and Jump2 occurring at 17.7 and 18.6 seconds that are very close to each other. Conversely, there is almost a plateau in angular velocity until it increases abruptly at 19.5 seconds. This increase occurs immediately after Jump2. Only one jump in angular velocity coincides with Jump1 and Jump2 occurring very close together. These data were recorded between 2.5 and 22 seconds.

Figure 4-95 reveals a constant decrease in FOS until reaching its minimum point at 0.42, which coincides with Jump2 in slope angle.

#### **Test A10-5 Sample SB20-D**

Figure 4-96 illustrates a gradual increase in slope angle, although there is not a big jump, Jump1 is still noticeable at 12.7 seconds just before a slow decrease. The slope angle then increases again until it reaches the maximum at 18.6 second, after which it decreases. Angular velocity has a plateau until a slight increase at 13.5 seconds, which occurs immediately after Jump1. It then decreases and fluctuates but increases dramatically at 19.11 seconds. These factors were monitored between 2.5 and 19.49 seconds.

Figure 4-97 depicts the FOS decreasing sharply. It then reaches 0.45, which coincides with Jump1 after which it slightly increases before decreasing again and reaches the minimum point at 0.37, which coincides with Jump2.

Figure 4-98 illustrates the variations of the FOS for Jump1 and Jump2 versus bentonite content. As can be seen, Jump1 and Jump2 have nearly identical

behaviour with regard to bentonite changes, i.e. they both decrease with increased bentonite concentration in an approximately steady manner.

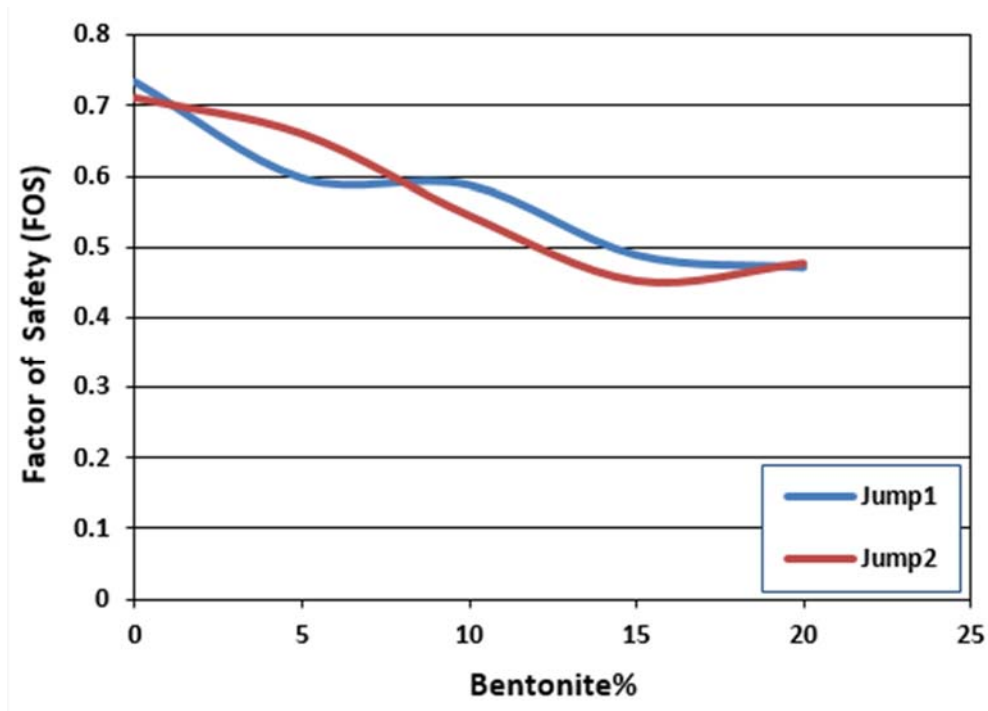


Figure 4-98: Variation of median (FOS) of jumps with bentonite content for all samples

The common points from Figure 4-68 to Figure 4-97 are listed below:

- There are direct relationships between slope angle, angular velocity and FOS during each test.
- At each main jump, there is a maximum resistance against movements while showing minimum safety factors.
- Immediately following the main jumps, there is a dramatic increase in angular velocity of movements.
- There is always FOS retrieval after the main jumps. FOS values ranged from 0.3 to 0.7 while failures were not initiated. Therefore, slopes can resist against movements even for FOS less than one.
- There is a relatively steady decrease in FOS trend with bentonite content, i.e. bentonite decreases FOS of slopes and does not help stability of slopes when they are dry and loose.



## **5. SUMMARY AND CONCLUSIONS**

The main aim of this research was to evaluate the application of an image processing technique, particle image velocimetry (PIV), for slope stability analysis. The analysis was implemented with emphasis on shallow slope failures in dry and loose sands including wide range fine contents. The primary reason for considering the PIV technique is the need for development of a powerful technique that can quantify soil slope stability and result in a graph for reflecting the information in the frame of a graphical analysis.

The method was clearly described in Chapter 2, and the soil sample preparation and apparatus manufacturing was presented in Chapter 3. Chapter 4 illustrated how the slope stability can change when the composition of the soil content varies with the addition of bentonite, and discusses the observed features of planar slope stability and their effective components by means of PIV and statistical analyses.

The results of image processing and the SPSS analysis reveal how shallow slopes behave in real time, which is hard to distinguish with other stability methods as explained in Chapter 2. Failure thresholds and velocity of movements were clearly obtained, which are necessary for detailed studies. The shape of failures and their geometrical characteristics were obtained, which is one advantage of using the PIV application. The relationship between FOS and fine content were also qualified, and utilization of SPSS analysis helps clarify and display the main failure surfaces, which are hard to distinguish with other methods. Moreover, this analysis reveals the details of slopes and micro slopes more efficiently. A schematic view of research output is presented in Figure 5-1.

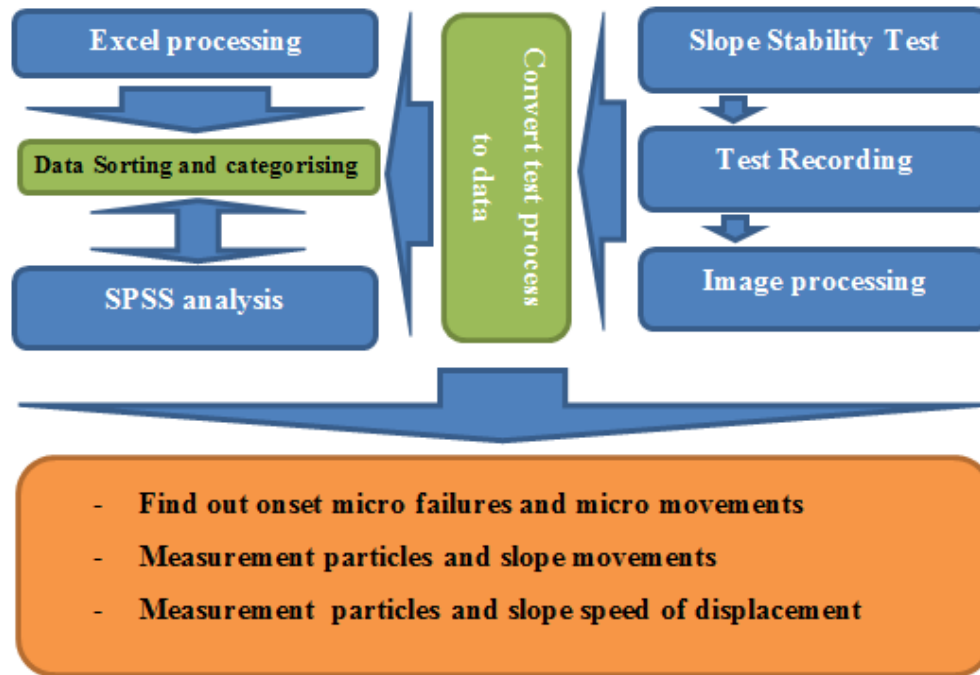


Figure 5-1: A schematic view of research output procedures

In this thesis, the following research findings were accomplished: (i) the effect of the percentage of bentonite on slope stability, (ii) development of a graphical model for slope stability analysis, (iii) influence of the alignment on surface failure, and (iv) the features of failures. The main results are summarized below:

### 5.1. Influence of Bentonite

In this research, the influence of bentonite on the soil slope stability was evaluated, with the bentonite content ranging from 0 to 20%. For different alignments, the slope angle was investigated. The bentonite contents steadily increased for all slope angles and the results are graphically shown. The results revealed that bentonite or dirtiness is not helpful for sandy slopes when they are dry and loose, i.e. planar failures are more unstable with increasing fine particle content in sand.

## **5.2. Benefits of PIV Method**

By evaluation of the surface lines extracted from images, it is clear that the mode of failure is a planar failure in a rotational manner. This does not comply with transitional failure mechanisms described in different literature.

Based on the results obtained from the laboratory experiments, the following results can be highlighted:

- PIV can be efficiently employed to analyse slope stability in the form of 2D analyses.
- PIV delivers real time changes in slope stability analyses in terms of velocities, safety factors and distribution of failure surfaces.
- When modeling 2D soil slopes, PIV provides a more suitable failure mechanism in comparison with that of conventional techniques.
- According to the complexity of the soil composition that can influence slope stability, conventional techniques are not capable of modelling the complexity involved in the process of movements.
- Based on the obtained results, the significant movement velocity of the slope occurs with reduction of safety factors with a delay of a few seconds after failure.
- From the research analysis, it can be inferred that increases in bentonite content negatively impacts dry slopes. Therefore, considerable increase in the percentage of bentonite has a significant decrease in the slope stability.
- 2D analysis of the PIV technique is superior to the conventional methods because of its versatility and capabilities.

## **5.3. Planar Failure Features**

It is discovered that shallow failures in loose sands or clayey sands do not have transitional or planar failure patterns. They have more rotational trends around an axis located on the slope face between toes to one third of its length. It should be noted that this type of slope resists against loading to some extent and show high velocity of movements about 2–4 deg/s when they are approaching failure.

## **6. RECOMMENDATIONS**

This research evaluates the potential of the PIV method for slope stability analysis.

From the results obtained, further studies are required to:

- confirm the accuracy of the approach for other soil compositions,
- conduct field research experiments to confirm the observed failure characteristics seen in the laboratory,
- complete the results by verification of slopes including other coarse material,
- confirm the results obtained for soil with different moisture contents,
- evaluate the impact of water flow, saturation or vibrations on slope stability,
- compare the results obtained in a 2D space with those in a 3D space,
- evaluate the yield results to substantiate the capability of the developed approach for the assessment of slope stability, and investigate other non-plastic soil effects.

Automatic electrical winch with a recordable speed, glass container, camera with a high resolution and flexible mount, a dark space with a manageable lightness helps to increase quality and accuracy.

With a combination of MATLAB and SPSS analysis in the form of a newly designed software program, the subject of probabilistic and statistical slope stability analyses can be conjugated.

## **7. REFERENCES**

- Abaqus/CAE User's Guide (6.14). (2016). Retrieved from <http://abaqus.software.polimi.it/v6.14/books/usi/default.htm>
- Abramson, L. W. (2002). *Slope stability and stabilization methods*: John Wiley & Sons.
- Adam, J., Urai, J. L., Wieneke, B., Oncken, O., Pfeiffer, K., Kukowski, N., & Schmatz, J. (2005). Shear localisation and strain distribution during tectonic faulting—new insights from granular-flow experiments and high-resolution optical image correlation techniques. *Journal of Structural Geology*, 27(2), 283-301. <http://dx.doi.org/http://dx.doi.org/10.1016/j.jsg.2004.08.008>
- Adhikary, D., Dyskin, A., & Jewell, R. (1996). *Numerical modelling of the flexural deformation of foliated rock slopes*. Paper presented at the International journal of rock mechanics and mining sciences & geomechanics abstracts
- Adrian, R. J. (1991). Particle-imaging techniques for experimental fluid mechanics. *Annual review of fluid mechanics*, 23(1), 261-304.
- Agam, M., Hashim, M., Murad, M., & Zabidi, H. (2016). Slope Sensitivity Analysis Using Spencer's Method in Comparison with General Limit Equilibrium Method. *Procedia Chemistry*, 19, 651-658.
- Akhtar, K. (2011). *Three dimensional slope stability analyses for natural and manmade slopes*: University of Illinois at Urbana-Champaign.
- Anastasopoulos, I., Gazetas, G., Bransby, M., Davies, M., & El Nahas, A. (2007). Fault rupture propagation through sand: Finite-element analysis and validation through centrifuge experiments. *Journal of Geotechnical and Geoenvironmental Engineering*, 133(8), 943-958.
- Ata, A. A., Salem, T. N., & Elkhawas, N. M. (2015). Properties of soil–bentonite–cement bypass mixture for cutoff walls. *Construction and Building Materials*, 93, 950-956. <http://dx.doi.org/http://dx.doi.org/10.1016/j.conbuildmat.2015.05.064>
- Baba, H. O., & Peth, S. (2012). Large scale soil box test to investigate soil deformation and creep movement on slopes by Particle Image Velocimetry (PIV). *Soil and Tillage Research*, 125(0), 38-43. <http://dx.doi.org/http://dx.doi.org/10.1016/j.still.2012.05.021>
- Baligh, M. M., & Azzouz, A. S. (1975). End effects on stability of cohesive slopes. *Journal of Geotechnical and Geoenvironmental Engineering*, 101(ASCE# 11705 Proceeding)
- Barends, F. B. J. (2011). *Geotechnical Engineering: Proceedings of the 21st European Young Geotechnical Engineers' Conference Rotterdam*. Amsterdam: Amsterdam : IOS Press.
- Biodata - Dr.D.J.Petley. (2016). Retrieved from [http://www.geoeng.iwhr.com/ENGLISH1/software\\_download.htm](http://www.geoeng.iwhr.com/ENGLISH1/software_download.htm)
- Bishop, A. W. (1955). The use of the Slip Circle in the Stability Analysis of Slopes. *Géotechnique*, 5, 7-17. Retrieved from <http://www.icevirtuallibrary.com/content/article/10.1680/geot.1955.5.1.7>
- Bobet, A. (2010). Numerical methods in geomechanics. *The Arabian Journal for Science and Engineering*, 35(1B), 27-48.

- Botero-Jaramillo, E., Romo, M. P., Méndez, B., & Marengo, H. (2014). Use of the Distinct Element Method as a Tool to Detect Stability Problems in Deep Spillway Excavations. *Tecnología y Ciencias del Agua*, *V(4)*, 187-196.
- Bridgwater, J. (2012). Mixing of powders and granular materials by mechanical means—A perspective. *Particuology*, *10(4)*, 397-427.  
<http://dx.doi.org/http://dx.doi.org/10.1016/j.partic.2012.06.002>
- Cameron, S. M. (2011). PIV algorithms for open-channel turbulence research: Accuracy, resolution and limitations. *Journal of Hydro-environment Research*, *5(4)*, 247-262.  
<http://dx.doi.org/http://dx.doi.org/10.1016/j.jher.2010.12.006>
- CandecAD. (2016). Retrieved from <http://candecad.com/candecad.php>
- Cavoundis, S. (1987). On the ratio of factors of safety in slope stability analyses. *Geotechnique*, *37(2)*
- Chen. (1975). *Limit analysis and soil plasticity*: Elsevier.
- Chen, Kuo, K. J., Chen, Y.-N., & Ku, C.-W. (2011). Model tests for studying the failure mechanism of dry granular soil slopes. *Engineering Geology*, *119(1)*, 51-63. <http://dx.doi.org/10.1016/j.enggeo.2011.02.001>
- Cheng, Y.M., Lansivaara, T., & Siu, J. (2008). Impact of convergence on slope stability analysis and design. *Computers and Geotechnics*, *35(1)*, 105-113.  
<http://dx.doi.org/http://dx.doi.org/10.1016/j.compgeo.2007.02.011>
- Cheng, Y.M., Lansivaara, T., Baker, R., & Li, N. (2013). Use of internal and external variables and extremum principle in limit equilibrium formulations with application to bearing capacity and slope stability problems. *Soils and Foundations*, *53(1)*, 130-143.
- Cheng, Y. M., & Lau, C. K. (2008, Dec 2008). Slope stability analysis and stabilization; new methods and insight. *Scitech Book News*, *32*.
- Chugh, A. (1986). Variable factor of safety in slope stability analysis. *Geotechnique*, *36(1)*, 57-64.
- Collin, A. (1846). *Recherches experimentales sur les glissements spontanés des terrains argileux, accompagnées de considerations sur quelques principes de la mecanique terrestre par Alexandre Collin*: Carilian-Goeury.
- Computational Infrastructure for Geodynamics :: Software. (2016). Retrieved from [https://geodynamics.org/cig/software/specfem3d\\_geotech/](https://geodynamics.org/cig/software/specfem3d_geotech/)
- Conti, R., & Viggiani, G. M. (2013). A new limit equilibrium method for the pseudostatic design of embedded cantilevered retaining walls. *Soil Dynamics and Earthquake Engineering*, *50*, 143-150.
- CRISP Geotechnical Finite Element Analysis Software. (2016). Retrieved from <http://www.mycrisp.com/>
- Cundall, P. (1971). *A computer model for simulating progressive large-scale movements in block rock mechanics*. Paper presented at the Proc. Symp. Int. Soc. Rock Fracture. Nancy, France, 1, 8-17
- Dejong, J. T., White, D. J., & Randolph, M. F. (2006). *Microscale observation and modeling of soil-structure interface behavior using particle image velocimetry*. *Soils and Foundations*, *46(1)*, 15-28.  
<http://dx.doi.org/10.3208/sandf.46.15>

- Dijkstra, J., White, D.J., & Gaudin, C. (2013). Comparison of failure modes below footings on carbonate and silica sands. *International journal of physical modelling in geotechnics*, 13(1), 1-12.
- Donald, I. B., & Chen, Z. (1997). Slope stability analysis by the upper bound approach: fundamentals and methods. *Canadian Geotechnical Journal*, 34(6), 853-862. Retrieved from <http://www.nrcresearchpress.com/doi/pdf/10.1139/t97-061>
- Drucker, D.C., Greenberg, H.J., & Prager, W. (1951). The safety factor of an elastic plastic body in plane strain. *Transactions of the ASME, Journal of Applied Mechanics*, , 73, 371.
- Duncan, J. (1996). State of the Art: Limit Equilibrium and Finite-Element Analysis of Slopes. *Journal of Geotechnical Engineering*, 122(7), 577-596. [http://dx.doi.org/doi:10.1061/\(ASCE\)0733-9410\(1996\)122:7\(577\)](http://dx.doi.org/doi:10.1061/(ASCE)0733-9410(1996)122:7(577))
- Duncan., J. M., Wright, S. G., & Brandon, T. L. (2014). *Soil strength and slope stability*: John Wiley & Sons.
- Dynamic Earthquake Analysis with QUAKE/W - GEO-SLOPE International Ltd. (2016). Retrieved from <http://www.geo-slope.com/products/quakew.aspx>
- Eid, H. T. (2014). Stability charts for uniform slopes in soils with nonlinear failure envelopes. *Engineering Geology*, 168, 38-45.
- Engineering Consulting | Geotechnical Software | Earth Resources | An Itasca International Company. (2016). Retrieved from <http://www.itascacg.com/>
- Fellenius, W. (1936). *Calculation of the stability of earth dams*. Paper presented at the Transactions of the 2nd congress on large dams, Washington, DC
- GALENA - Slope Stability Analysis. (2015). Retrieved from <http://www.galenasoftware.com/>
- Gao, Y., Wu, D., & Zhang, F. (2015). Effects of nonlinear failure criterion on the three-dimensional stability analysis of uniform slopes. *Engineering Geology*, 198, 87-93.
- Gao, Y., Yang, S., Zhang, F., & Leshchinsky, B. (2016). Three-dimensional reinforced slopes: Evaluation of required reinforcement strength and embedment length using limit analysis. *Geotextiles and Geomembranes*, 44(2), 133-142.
- Gaskell Concrete Sand Technical Data Sheet. (2014) Western Australia: (Rocla Quarry Products Pty Ltd).
- Geocentrix ReActiv - overview. (2015). Retrieved from <http://www.geocentrix.co.uk/reactiv/overview.html>
- GeoPIV-RG. (2016). Retrieved from <http://www.geopivrg.com/>
- Geosysta. (2015). Software and Equipment Publications. Retrieved from <http://www.geotechpedia.com/Software/Category>
- Geotechnical Software - 3D Slope Stability – Geotechnical Software for a 3D World. (2016). Retrieved from <http://tagasoft.com/>
- Geotechnical Software GEO5 | Fine. (2016). Retrieved from <http://www.finesoftware.eu/geotechnical-software/>
- GGU-STABILITY - Slope failure calculations and soil nailing. (2016). Retrieved from [http://www.ggu-software.com/software/ggu-computation/stability/stability\\_slope\\_failure.html](http://www.ggu-software.com/software/ggu-computation/stability/stability_slope_failure.html)

- GIGER, M. W., & KRIZEK, R. J. (1975). Stability analysis of vertical cut with variable corner angle. , *15*(2), 63-71.
- Gonzalez, R. C., & Woods, R. E. (2008). Digital image processing (Third Edition). *Nueva Jersey*,
- GoogleMaps. (2016). Gaskell Ave. Retrieved from <https://www.google.com.au/maps/place/Gaskell+Ave,+Lexia+WA+6079/@-31.7845843,115.9469321,673m/data=!3m1!1e3!4m5!3m4!1s0x2a32b38a83d cc4e1:0x19f11937787a9507!8m2!3d-31.7862736!4d115.946385>.
- Griffiths, D., & Fenton, G. A. (2004). Probabilistic slope stability analysis by finite elements. *Journal of Geotechnical and Geoenvironmental Engineering*, *130*(5), 507-518.
- GSTABL7 with STEDwin » Gregory Geotechnical. (2016). Retrieved from <https://www.gregeo.com/software/gstabl7-with-stedwin/>
- Hannachi, S., Benia, R., Belouar, M., & Belouar, A. (2015). Probability Analysis of Slope Stability Analysis. *Abstract of Applied Sciences and Engineering*, *5*(5)
- Hashemi, M. A., Massart, T. J., Salager, S., Herrier, G., & François, B. (2015). Pore scale characterization of lime-treated sand–bentonite mixtures. *Applied Clay Science*, *111*, 50-60.  
<http://dx.doi.org/http://dx.doi.org/10.1016/j.clay.2015.04.001>
- Hero3 Black edition (2014). Retrieved from <http://gopro.com/support/product-manuals-support>
- Hoek, E., & Bray, J. D. (1981). *Rock slope engineering*: CRC Press.
- Hossain, M.S., Fourie, A. (2013). Stability of a strip foundation on a sand embankment over mine tailings. *Geotechnique*, *63*(8), 641-650.
- Hossain, M.S., Hu, Y., Randolph, M., & White, D. (2005). Limiting cavity depth for spudcan foundations penetrating clay. *Géotechnique*, *55*(9), 679-690.
- Hsü, K. J. (1975). Catastrophic debris streams (sturzstroms) generated by rockfalls. *Geological Society of America Bulletin*, *86*(1), 129-140.
- Huang, M., Wang, H., Sheng, D., & Liu, Y. (2013). Rotational–translational mechanism for the upper bound stability analysis of slopes with weak interlayer. *Computers and Geotechnics*, *53*, 133-141.
- Hungr, O. (1987). An extension of Bishop's simplified method of slope stability analysis to three dimensions. *Géotechnique*, *37*(1), 113-117.  
<http://dx.doi.org/doi:10.1680/geot.1987.37.1.113>
- Hungr, O., Salgado, F., & Byrne, P. (1989). Evaluation of a three-dimensional method of slope stability analysis. *Canadian Geotechnical Journal*, *26*(4), 679-686.
- Hutchinson, J., & Sarma, S. (1985). Discussion on 3-Dimensional Limit Equilibrium Analysis fo Slopes. Vol. 35, pp. 215-216.
- IBM. (2013). IBM SPSS Statistics for Windows, Version 22.0: IBM Corp Armonk, NY.
- Itasca Consulting Group, I., An Itasca International Company. (2015). Engineering Consulting - Geotechnical Software - Earth Resources Retrieved from <http://www.itascacg.com/>
- Jähne, B. (2004). Practical handbook on image processing for scientific and technical applications.



- Jähne, B. (2005). Digital image processing, 6th revised and extended edn. Springer, Verlag Berlin Heidelberg.
- Jain, A. K. (1989). *Fundamentals of Digital Image Processing*: Prentice-Hall, Inc.
- Janbu, N. (1954). *Application of composite slip surfaces for stability analysis*. Paper presented at the Proc. European Conf. on Stability of Earth Slopes, Stockholm, 1954
- Janbu, N. (1973). Slope Stability Computations. *Embankment-Dam Eng*, 47-86. Retrieved from <http://www.scopus.com/inward/record.url?eid=2-s2.0-0015754056&partnerID=40&md5=c92b0d8562974648c128e953790a7386>
- Jiang, X.-y., Cui, P., & Liu, C.-z. (2016). A chart-based seismic stability analysis method for rock slopes using Hoek-Brown failure criterion. *Engineering Geology*, 209, 196-208.
- Kawai, T. (1978). New discrete structural models and generalization of the method of limit analysis. *Finite elements in nonlinear mechanics*, 885-906.
- Kovesi, P. D. (2000). MATLAB and Octave functions for computer vision and image processing. Retrieved from <http://www.peterkovesi.com/matlabfns/>
- Krahn, J. (2003). The 2001 RM Hardy Lecture: The limits of limit equilibrium analyses. *Canadian Geotechnical Journal*, 40(3), 643-660.
- Leynaud, D., & Sultan, N. (2010). 3-D slope stability analysis: a probability approach applied to the nice slope (SE France). *Marine Geology*, 269(3), 89-106.
- Lim, K., Li, A., & Lyamin, A. (2015). Three-dimensional slope stability assessment of two-layered undrained clay. *Computers and Geotechnics*, 70, 1-17.
- LimitState:GEO - Geotechnical Analysis Software | LimitState. (2016). Retrieved from <http://www.limitstate.com/geo>
- Lingxi, Q., & Xiong, Z. (1995). Rigid finite element and its applications in engineering. *Acta Mechanica Sinica*, 11(1), 44-50.
- Liu, F.T., Fan, Y.-H., & Yin, J.-H. (2011). The use of QP-free algorithm in the limit analysis of slope stability. *Journal of computational and applied mathematics*, 235(13), 3889-3897.
- Liu, F.T., & Zhao, J. (2013). Limit analysis of slope stability by rigid finite-element method and linear programming considering rotational failure. *International Journal of Geomechanics*, 13(6), 827-839.
- Low, B. K. (2003). Practical Probabilistic Slope Stability Analysis. Proceedings, Soil and Rock America 2003, 12th Panamerican Conference on Soil Mechanics and Geotechnical Engineering and 39th U.S. Rock Mechanics Symposium, held in M.I.T., Cambridge, Massachusetts, Verlag Glückauf GmbH Essen, (pp. 2777-2784).
- Lu, N., & Kaya, M. (2013). A drying cake method for measuring suction-stress characteristic curve, soil-water-retention curve, and hydraulic conductivity function. *Geotechnical Testing Journal*, 36(1) <http://dx.doi.org/10.1520/GTJ20120097>
- Lu, L., Wang, Z. J., Song, M. L., & Arai, K. (2015). Stability analysis of slopes with ground water during earthquakes. *Engineering Geology*, 193, 288-296. <http://dx.doi.org/http://dx.doi.org/10.1016/j.enggeo.2015.05.001>

- Lutton, R. J. (1970). Rock slope chart from empirical slope data. *Trans. Society of Mining Engineers, AIME*, 247, 160-162.
- Maleki Javan, M. R., Kilanehei, F., & Mahjoob, A. (2015). Rock Slope Stability Analysis Using Discrete Element Method. *International Journal of Transportation Engineering*, 2(3), 199-212.
- Material Safety Data Sheet Sibleco Bentonite Group 2 (2010): (SIBELCO Australia).
- Merati, A., Ghasemzadeh, H., & Astaneh, S.M. (2015). Determining Slope Stability by Rigid Finite Element Method and Limit Analysis Methods. *Novel Applied Sciences* 4(5), 579-589.
- Mickovski, S. B., Bransby, M. F., Bengough, A. G., Davies, M. C. R., & Hallett, P. D. (2010). Resistance of simple plant root systems to uplift loads.(Report). *Canadian Geotechnical Journal*, 47(1), 78.
- midas GTS NX | Geotechnical Analysis New Experience. (2016). Retrieved from [http://en.midasuser.com/product/gtsnx\\_overview.asp](http://en.midasuser.com/product/gtsnx_overview.asp)
- Mitre Software Corporation. (2016). Retrieved from <http://www.mitresoftware.com/prod01.htm>
- Moosavi, M., Yarahmadi, A.R., & Bakhshi, H.R. (2009). 3d numerical slope stability analysis of west wall of sarcheshmeh mine utilizing a distinct element method. *Journal of faculty of engineering (university of Tehran)* 43(3), 311-324.
- Morgenstern, N.R. (1992). Evaluation of slope stability – a 25 year perspective : Morgenstern, N R Proc Conference Stability and Performance of Slopes and Embankments II, Berkeley, 29 June–1 July 1992V1, P1–26. Publ New York: ASCE, 1992 (ASCE Special Geotechnical Publication No 31). *International Journal of Rock Mechanics and Mining Sciences & Geomechanics Abstracts*, 30(3), A195. [http://dx.doi.org/http://dx.doi.org/10.1016/0148-9062\(93\)93166-U](http://dx.doi.org/http://dx.doi.org/10.1016/0148-9062(93)93166-U)
- Morgenstern, N.R., & Price, V.E. (1965). The analysis of the stability of general slip surfaces. *Geotechnique*, 15(1), 79-93.
- Nian, T.-K., Jiang, J.-C., Wang, F.-W., Yang, Q., & Luan, M.-T. (2016). Seismic stability analysis of slope reinforced with a row of piles. *Soil Dynamics and Earthquake Engineering*, 84, 83-93. <http://dx.doi.org/http://dx.doi.org/10.1016/j.soildyn.2016.01.023>
- Oasys Software (2015). Retrieved from <http://www.oasys-software.com/>
- Peth, S., Nellesen, J., Fischer, G., & Horn, R. (2010). Non-invasive 3D analysis of local soil deformation under mechanical and hydraulic stresses by  $\mu$ CT and digital image correlation. *Soil and Tillage Research*, 111(1), 3-18. <http://dx.doi.org/http://dx.doi.org/10.1016/j.still.2010.02.007>
- PLAXIS - Essential for geotechnical professionals. (2016). Retrieved from <http://www.plaxis.nl/>
- Pulat, H. F. (2009). *An experimental and analytical study of various soil slopes in laboratory conditions*. Master of Science in Civil Engineering İzmir Institute of Technology
- Raffel, M. (2007). *Particle Image Velocimetry : A Practical Guide / by Markus Raffel, Christian E. Willert, Steve T. Wereley, Jürgen Kompenhans*. Berlin, Heidelberg: Berlin, Heidelberg : Springer Berlin Heidelberg.

- Resnick, G. S., & Znidarčić, D. (1990). Centrifugal Modeling of Drains for Slope Stabilization. *Journal of Geotechnical Engineering*, 116(11), 1607-1624. [http://dx.doi.org/doi:10.1061/\(ASCE\)0733-9410\(1990\)116:11\(1607\)](http://dx.doi.org/doi:10.1061/(ASCE)0733-9410(1990)116:11(1607))
- ReSSA (3.0). (2016). Retrieved from <https://www.geoprograms.com/ressaindex.htm>
- Scheidegger, A. E. (1973). On the prediction of the reach and velocity of catastrophic landslides. *Rock mechanics*, 5(4), 231-236.
- Schroeder, A., & Willert, C. E. (2008). *Particle Image Velocimetry New Developments and Recent Applications*. Berlin, Heidelberg: Springer Berlin Heidelberg. *Topics in Applied Physics*, Retrieved from <http://link.lis.curtin.edu.au/cgi-bin/gw?url=http://dx.doi.org/10.1007/978-3-540-73528-1>
- Scientific Software Group. (2015). Retrieved from <http://www.scientificsoftwaregroup.com/>
- Shamekhi, E., & Tannant, D. D. (2015). Probabilistic assessment of rock slope stability using response surfaces determined from finite element models of geometric realizations. *Computers and Geotechnics*, 69, 70-81. <http://dx.doi.org/http://dx.doi.org/10.1016/j.compgeo.2015.04.014>
- Shamsabadi, A., Xu, S.-Y., & Taciroglu, E. (2013). A generalized log-spiral-Rankine limit equilibrium model for seismic earth pressure analysis. *Soil Dynamics and Earthquake Engineering*, 49, 197-209. <http://dx.doi.org/http://dx.doi.org/10.1016/j.soildyn.2013.02.020>
- Shen, B., Stephansson, O., Einstein, H. H., & Ghahreman, B. (1995). Coalescence of fractures under shear stresses in experiments. *Journal of Geophysical Research- All Series-*, 100, 5975-5990.
- Shen, J., Karakus, M., & Xu, C. (2013). Chart-based slope stability assessment using the Generalized Hoek–Brown criterion. *International Journal of Rock Mechanics and Mining Sciences*, 64, 210-219. <http://dx.doi.org/http://dx.doi.org/10.1016/j.ijrmms.2013.09.002>
- Shen, H., & Abbas, S. M. (2013). Rock slope reliability analysis based on distinct element method and random set theory. *International Journal of Rock Mechanics and Mining Sciences*, 61, 15-22. <http://dx.doi.org/http://dx.doi.org/10.1016/j.ijrmms.2013.02.003>
- Shou, K.-J., & Wang, C.-F. (2003). Analysis of the Chiufengershan landslide triggered by the 1999 Chi-Chi earthquake in Taiwan. *Engineering Geology*, 68(3–4), 237-250. [http://dx.doi.org/http://dx.doi.org/10.1016/S0013-7952\(02\)00230-2](http://dx.doi.org/http://dx.doi.org/10.1016/S0013-7952(02)00230-2)
- Slide. (2016). Retrieved from <https://www.rocscience.com/rocscience/products/slide>
- Slope Stability Analysis. Clara-W software. (2016). Retrieved from <http://www.clara-w.com/>
- Slope stability - XSLOPE - Civil Engineering - The University of Sydney. (2016). Retrieved from <http://sydney.edu.au/engineering/civil/research/scigem/software/xslope/index.shtml>.
- Slope Stability Analysis with SLOPE/W. (2016). Retrieved from <http://www.geo-slope.com/products/slopew.aspx>

- Soil and Water Engineering - Modeling Software. (2015). Retrieved from <http://forest.moscowfsl.wsu.edu/>
- SoilVision Systems - Geotechnical Finite Element Software - SVSLOPE®. (2016). Retrieved from <https://www.soilvision.com/products/svoffice5/svslope/>
- Spencer, E. (1967). A Method of analysis of the Stability of Embankments Assuming Parallel Inter-Slice Forces. *Geotechnique*, 17(1), 11-26. <http://dx.doi.org/10.1680/geot.1967.17.1.11>
- Springman, S., Laue, J., & Seward, L. (2010). *Physical Modelling in Geotechnics*: CRC Press.
- SSAP2010 (rel. 4.7.2 - 2016). (2016). Retrieved from <http://www.ssap.eu/>
- STABL -Slope Stability Analysis Software. (2016). Retrieved from <https://engineering.purdue.edu/STABL/>
- Stamhuis, E. J. (2006). Basics and principles of particle image velocimetry (PIV) for mapping biogenic and biologically relevant flows. *Aquatic Ecology*, 40(4), 463-479. <http://dx.doi.org/DOI.10.1007/s10452-005-6567-z>
- Stankovic, J. N., Filipovic, S., Rajkovic, R., Obradovic, L., Marinkovic, V., & Kovacevic, R.,. (2013). Risk and reliability analysis of slope stability deterministic and probabilistic method. *Trends in the Development of Machinery and Associated Technology*, 17, 97-100
- Stark, T. D., & Eid, H. T. (1998). Performance of three-dimensional slope stability methods in practice. *Journal of Geotechnical and Geoenvironmental engineering*, 124(11), 1049-1060.
- StrataSlope System - Geogrid. (2016). Retrieved from <http://www.geogrid.com/en-us/products/strataslope-system/>
- Take, W. A., & Bolton, M. D. (2011). Seasonal ratcheting and softening in clay slopes, leading to first-time failure. *Geotechnique*, 61(9), 757-769. <http://dx.doi.org/10.168/geot.9.P.125>
- Tang, G.-p., Zhao, L.-h., Li, L., & Yang, F. (2015). Stability charts of slopes under typical conditions developed by upper bound limit analysis. *Computers and Geotechnics*, 65, 233-240. <http://dx.doi.org/http://dx.doi.org/10.1016/j.compgeo.2014.12.008>
- Taylor, D. W. (1937). *Stability of earth slopes* (Vol. 24): Boston Society of Civil Engineers.
- Tejchman, J. (2010). Finite element investigations of granular material behaviour during cyclic wall shearing under a constant normal stiffness condition.(Report). *Canadian Geotechnical Journal*, 47(9), 985.
- Tschuchnigg, F., Schweiger, H. F., & Sloan, S. W. (2015). Slope stability analysis by means of finite element limit analysis and finite element strength reduction techniques. Part I: Numerical studies considering non-associated plasticity. *Computers and Geotechnics*, 70, 169-177. <http://dx.doi.org/http://dx.doi.org/10.1016/j.compgeo.2015.06.018>
- Wei, W. B., Cheng, Y. M., & Li, L. (2009). Three-dimensional slope failure analysis by the strength reduction and limit equilibrium methods. *Computers and Geotechnics*, 36(1-2), 70-80. <http://dx.doi.org/http://dx.doi.org/10.1016/j.compgeo.2008.03.003>

- White, D.J., Take, W., & Bolton, M. (2001). *Measuring soil deformation in geotechnical models using digital images and PIV analysis*. Paper presented at the 10th International Conference on Computer Methods and Advances in Geomechanics, Tucson, Arizona
- White, D.J., Take, W., & Bolton, M. (2003). Soil deformation measurement using particle image velocimetry (PIV) and photogrammetry. *Geotechnique*, 53(7), 619-631.
- Wijewickreme, D., Karimian, H., & Honegger, D. (2009). Response of buried steel pipelines subjected to relative axial soil movement.(Report). *Canadian Geotechnical Journal*, 46(7), 735.
- Win, P. (2012). *Study on Model test about the Stability of Slopes due to Rainfalls*. T. U. o. A. a. Technology. Retrieved from [http://www.tuat.ac.jp/~folens/report/pdf/intern\\_winwin\\_2012aug.pdf](http://www.tuat.ac.jp/~folens/report/pdf/intern_winwin_2012aug.pdf)
- Wong, L. S., Hashim, R., & Ali, F. (2013). Utilization of sodium bentonite to maximize the filler and pozzolanic effects of stabilized peat. *Engineering Geology*, 152(1), 56-66. <http://dx.doi.org/http://dx.doi.org/10.1016/j.enggeo.2012.10.019>
- Wu, G. (2013). Wutec Geotechnical International - Design, Application of Geotechnical Software. Retrieved from <http://www.wutecgeo.com/versat-2d.aspx>
- Xiao, Yan, L., & Cheng, Z. (2011). A method combining numerical analysis and limit equilibrium theory to determine potential slip surfaces in soil slopes. *Journal of Mountain Science*, 8(5), 718-727. <http://dx.doi.org/10.1007/s11629-011-2070-2>
- XSTABL home page. (2016). Retrieved from <http://www.xstabl.com/>
- Yang, X.-g., & Chi, S.-c. (2013). Upper bound finite element analysis of slope stability using a nonlinear failure criterion. *Computers and Geotechnics*, 54, 185-191. <http://dx.doi.org/http://dx.doi.org/10.1016/j.compgeo.2013.06.007>
- Zace Services Ltd ZSoilPC software for geotechnics and geomechanics (2016). Retrieved from <http://www.zsoil.com/>
- Zhang. (1999). Slope stability analysis based on the rigid finite element method. *Géotechnique*, 49(5), 585-593. <http://dx.doi.org/doi:10.1680/geot.1999.49.5.585>
- Zhang, & Qian. (1993). Rigid finite element and limit analysis. *Acta Mechanica Sinica*, 9(2), 156-162.
- Zhao, L.-H., Cheng, X., Zhang, Y., Li, L., & Li, D.-J. (2016). Stability analysis of seismic slopes with cracks. *Computers and Geotechnics*, 77, 77-90. <http://dx.doi.org/http://dx.doi.org/10.1016/j.compgeo.2016.04.007>
- Zhou, X. P., & Cheng, H. (2013). Analysis of stability of three-dimensional slopes using the rigorous limit equilibrium method. *Engineering Geology*, 160, 21-33. <http://dx.doi.org/http://dx.doi.org/10.1016/j.enggeo.2013.03.027>
- Zhou, X. P., & Cheng, H. (2014). Stability analysis of three-dimensional seismic landslides using the rigorous limit equilibrium method. *Engineering Geology*, 174, 87-102. <http://dx.doi.org/http://dx.doi.org/10.1016/j.enggeo.2014.03.009>

Zhou, X. P., & Cheng, H. (2015). The long-term stability analysis of 3D creeping slopes using the displacement-based rigorous limit equilibrium method. *Engineering Geology*, 195, 292-300.  
<http://dx.doi.org/http://dx.doi.org/10.1016/j.enggeo.2015.06.002>

## 8. APPENDIX

### Appendix A - MATLAB Code

```
function soil(f1, f2, delta)

    % Set up default argument values
    if ~exist('f2', 'var'), f2 = f1; end
    if ~exist('delta', 'var'), delta = 1; end

    % Image processing parameters. These may need to be changed if
the rig
    % setup or lighting changes.

    % The figure number to use when displaying processed image
frames
    figNo = 1;

    % Colour difference threshold (in Lab space) for deciding if a
pixel is soil
    % or not. If background areas start being marked as soil try
decreasing
    % this value, If 'holes' appear in the soil try increasing it.
thresh = 15;

    % Weights to apply to the Lightness, a and b colour values when
determining
    % the colour difference. Here the weighting for lightness is
low so that we
    % are not so influenced by lighting variations in the image.
LabWeight = [0.2, 1, 1];

    % Structuring element for morphological close/open operation.
Increase
    % the radius if you get 'holes' in the soil, though you may want
to try
    % increasing 'thesh' a little first
se = strel('disk', 5);

    %% Open the video file (Edit to change the video file used)
vidFile = 'M1.MP4';

    vid = VideoReader(vidFile);
    nFrames = get(vid, 'NumberOfFrames');
    fprintf('Video has %d frames\n', nFrames);

    % Ensure f2 is not greater than the number of frames
f2 = min(f2, nFrames);

    % Read the first frame so that we can determine the image size
im = read(vid, f1);
[rows, cols, chan] = size(im);
```

```

    % Define mask area so that we can eliminate soil boundaries that
    are not
    % of interest. The values below will need to be altered if the
    camera or
    % rig configuration is changed.
    [x,y] = meshgrid(1:cols, 1:rows);
    mask = (y < 550 & x < 900) | (y < 350 & x < 1128);
    figure(100), imshow(mask), title('Mask image')

    % Define inclinometer region, again these may need to be changed
    if the
    % rig setup is changed.
    inc_rrng = 10:210; % Range of row values
    inc_crng = 315:525; % Range of columns

    % Get the user to select a rectangle of soil so that we can
    determine its
    % colour values.
    fprintf('Select a region of soil\n');
    figure(101), imshow(im);
    title('Select a rectangular region of soil', 'FontSize', 18)
    cr = imcrop;

    % Convert the soil region RGB values to Lab colour space
    lab = rgb2lab(cr);

    % Find median L, a and b colour values of the cropped soil
    region
    soilLAB = zeros(1,3);
    for c = 1:3
        tmp = lab(:,:,c);
        soilLAB(c) = median(tmp(:));
    end

    fprintf('Soil region Lab values: L = %.3f  a = %.3f  b =
    %.3f\n', ...
           soilLAB(1), soilLAB(2), soilLAB(3));

    % The main loop that processes the movie frames

    for f = f1:delta:f2
        im = read(vid, f); % Read the frame
        lab = rgb2lab(im); % and convert to Lab colour space

        % Extract subimage of inclinometer from the L channel,
        normalise its
        % range and multiply by 255 for future placement in the
        final image.
        incl = normalise(lab(inc_rrng, inc_crng, 1));

        % Compute weighted colour difference from the reference
        'soil colour'
        % for all pixels in Lab space
        labdiff = zeros(rows,cols);
        for c = 1:3

```



```

        labdiff = labdiff + (LabWeight(c)*(lab(:,:,c)-
soilLAB(c))).^2;
    end
    labdiff = sqrt(labdiff);

    % Generate a binary image representing the soil. This
corresponds to
    % all regions where the colour difference is less than
'thresh'.
    soil = labdiff < thresh;

    % Perform morphological close-open to remove small holes and
isolated
    % regions in the binary image
    soil = imopen(imclose(soil, se),se);

    % Find the perimeter of the soil region. This returns a
binary image
    % with pixels set to 1 on the perimeter.
    perim = bwperim(soil);

    % Mask out the region of interest of the soil perimeter
(Ignore the
    % boundaries with the rulers and labels.
    perim = perim & mask;

    % Cast the perimeter image from 'logical' to type 'double'
so that we
    % can insert a greyscale image of the inclinometer into it.
    perim = double(perim);

    % Extract an edgelist of pixels
    elist = edgelist(perim);
    %Find the longest edgelist and assume it is the surface
profile
    maxlen = 0;
    for n = 1:length(elist)
        len = length(elist{n});
        if len > maxlen
            edgelist = 720 - elist{n};
            maxlen = len;
        end
    end

    % Save edgelist to a file
    % create a folder for this video if it does not already
exist
    foldername = [vidFile '_output'];
    if ~exist(foldername,'dir'), mkdir(foldername), end
    outfile = sprintf('%s/%5d.xls',foldername,f);
    xlswrite(outfile,edgelist);

    % Insert the inclinometer subimage at the top left corner
    perim = implace(perim, incl, 0, 0);

```

```
        % Display the processed image and set the image title to  
correspond  
        % to the frame number  
        figure(figNo), imshow(perim)  
        set(figNo,'name', sprintf('    Frame %d', f));  
        pause(.01);  
    end
```

**Appendix B- SPSS output for test: A0-1 and sample: S-D, for intervals of 20 frames**

Cluster Membership		
Case Number	Cluster	Distance
1	5	47.853
2	5	40.215
3	5	55.977
4	5	52.169
5	5	41.562
6	5	50.506
7	5	59.753
8	5	52.540
9	5	48.288
10	5	48.665
11	5	42.502
12	5	40.744
13	5	53.043
14	5	52.084
15	5	47.370
16	5	62.300
17	5	50.992
18	5	47.120
19	5	35.134
20	5	51.473
21	5	47.283
22	5	29.628
23	5	36.782
24	5	29.018
25	5	33.091
26	5	24.318
27	5	26.447
28	5	23.450
29	5	25.897
30	5	25.981
31	5	28.560
32	5	28.637
33	5	47.405
34	5	35.513
35	5	64.864

36	5	43.614
37	5	55.053
38	5	60.760
39	5	48.681
40	5	56.285
41	5	66.554
42	5	53.387
43	5	88.394
44	5	82.508
45	5	71.740
46	5	209.694
47	4	.000
48	9	146.403
49	9	146.403
50	1	189.770
51	1	93.455
52	1	82.562
53	1	84.594
54	1	86.025
55	1	84.917
56	1	118.396
57	1	174.703
58	1	245.455
59	1	385.303
60	8	394.944
61	8	221.514
62	8	92.969
63	8	96.571
64	8	122.707
65	8	178.984
66	8	277.270
67	8	495.866
68	6	330.504
69	6	174.649
70	6	120.407
71	6	99.805
72	6	93.266
73	6	168.132
74	6	388.479
75	10	339.624

76	7	.000
77	2	.000
78	3	200.487
79	3	186.772
80	3	129.072
81	3	66.206
82	3	47.829
83	3	139.860
84	3	222.222
85	3	101.641
86	3	96.795
87	10	96.475
88	10	94.030
89	10	80.808
90	10	89.133
91	10	75.894
92	10	70.754
93	10	63.795
94	10	52.652
95	10	49.522
96	10	44.342
97	10	42.511
98	10	36.795
99	10	34.901
100	10	28.267
101	10	28.874
102	10	27.490
103	10	30.725
104	10	39.202
105	10	43.365
106	10	63.337
107	10	73.599
108	10	75.861
109	10	75.037
110	10	77.082
111	10	76.354
112	10	71.598
113	10	70.616
114	10	63.735

## Appendix C – Material Specifications

### C-1.Sand Specification



**Rocla Quarry Products Pty Ltd**  
 130 Fawntleroy Avenue  
 Redcliffe, W.A. 6104  
 Tel.: +61 8 9475 2500  
 Fax.: +61 8 9477 2633  
[www.rocla.com.au](http://www.rocla.com.au)

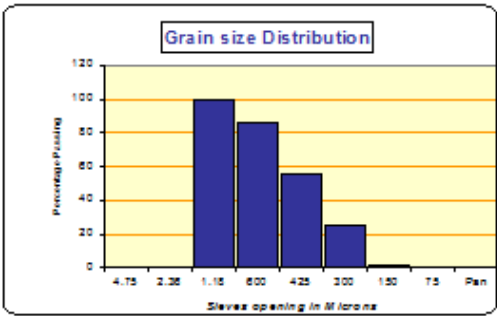
#### Technical Data Sheet

#### Gaskell Concrete Sand

<b>PHYSICAL PROPERTIES</b> (Average of previous 12 months)		<b>PHYSICAL PROPERTIES</b> (Average of previous 12 months)	
Particle Density - SSD Basis.....	2.61 t/m3	Alkali Reactivity At - 10 days...	0.01
- Dry Basis.....	2.59 t/m3	(CSIRO) Mortar Bar - 22 days...	0.07
Water Absorption	0.8 %	Attenburg Consistency Limits	
Dry Density - Maximum.....	1.86 t/m3	- Liquid Limits.....	Not Obtainable
- Minimum.....	1.56 t/m3	- Plastic Limit.....	Non Plastic
Sodium Sulphate Soundness....	0.1 %	- Plasticity Limit.....	Non Plastic
Light Particles.....	<1	- Linear Shrinkage.....	0.0 %
Sugar.....	Absence	Material Finer than 2 micron.....	.2 %
Clay and Fine Silt.....	3 %	Acid Soluble Salts - Cl.....	< 0.01 %
Gross Moisture Content.....	3.2 %	- SO4.....	0.03 %
Fineness Modulus.....	1.9	Organic Impurities (OVI).....	Pass

#### SIEVE ANALYSIS

Average of Previous 12 months		
Sieve opening in $\mu\text{m}$	% Passing	Specification Limits
4.75mm		100
2.36mm		95 – 100
1.18mm	100	90 – 100
600 $\mu\text{m}$	86	72 – 100
425 $\mu\text{m}$	55	
300 $\mu\text{m}$	25	17 – 37
150 $\mu\text{m}$	1.7	0 – 7
75 $\mu\text{m}$	0.1	0 – 5
Pan	0	
Clay and Fine Silt (Quick Set)	3	<= 4



N1 – This is a subjective test. The level of uncertainty for the test cannot be estimated.

PACKAGING = Bulk

STORAGE AND STABILITY = Store the product in the closed original packaging at ambient temperature and protect from humidity.

All information in this publication is in accordance with our present experience and knowledge. However, since we have no influence on the way in which our products are treated and used, we cannot take any responsibility in this respect.

May 2014

Member of Rocla Industries Group

## C-2. Bentonite Specification



# Material Safety Data Sheet

## SIBELCO BENTONITE GROUP 2

**Infosafe™** LPU5P **Issue Date** September 2010 **Status** ISSUED by **BS: 1.10.9**  
**No.** SIBELCO

**Classified as hazardous according to criteria of NOHSC**

### 1. IDENTIFICATION OF THE MATERIAL AND SUPPLIER

**Product Name** SIBELCO BENTONITE GROUP 2

**Product Code**

**Company Name** SIBELCO AUSTRALIA LIMITED

**Address** 49-55 Woodlands Drive Braeside  
Vic 3195

**Emergency Tel.** 1800 638 556

**Telephone/Fax Number** Tel: (03)9586 5400  
Fax: (03)9586 5413

**Recommended Use** Oil well drilling fluids; cement slurries for oil well casings; bonding agent in foundry sands and pelletising of iron ores; sealant for canal walls and dams; thickener in lubricating greases and fire proofing compositions; cosmetics; decolourising agent; filler in ceramics; refractories; paper coatings; asphalt modifier; polishes and abrasives; food additive; catalyst support; pelletising additive for stock food preparations.

<b>Other Names</b>	<b>Name</b>	<b>Product Code</b>
	SM23	
	SM72	
	TRUBOND SM23	
	TRUBOND SM72	
	ACTIVEBOND 23	
	ACTIVEBOND 25	
	ACTIVEGEL 53	
	ACTIVEGEL 150	
	CRESSFEED	

## 2. HAZARDS IDENTIFICATION

---

<b>Hazard Classification</b>	HAZARDOUS SUBSTANCE. NON-DANGEROUS GOODS.  Hazard classification according to the criteria of NOHSC. Dangerous goods classification according to the Australia Dangerous Goods Code.
<b>Risk Phrase(s)</b>	R48/20 Harmful: danger of serious damage to health by prolonged exposure through inhalation.
<b>Safety Phrase (s)</b>	S22 Do not breathe dust. S38 If insufficient ventilation, wear suitable respiratory equipment.

---

## 3. COMPOSITION/INFORMATION ON INGREDIENTS

---

<b>Ingredients</b>	<b>Name</b>	<b>CAS</b>	<b>Proportion</b>
	Smectite	12199-37-0	60-100 %
	Albite		<2 %
	Quartz (crystalline silica)	14808-60-7	<11 %
<b>Other Information</b>	The respirable fraction of free crystalline silica is less than 4%.		

---

## 4. FIRST AID MEASURES

---

<b>Inhalation</b>	If inhaled, remove affected person from contaminated area. Keep at rest until recovered. If symptoms persist seek medical attention.
<b>Ingestion</b>	Do not induce vomiting. Wash out mouth thoroughly with water. If symptoms develop seek medical attention.
<b>Skin</b>	Wash affected area thoroughly with soap and water. If symptoms develop seek medical attention.
<b>Eye</b>	If in eyes, hold eyelids apart and flush the eyes continuously with running water. Continue flushing for several minutes until all contaminants are washed out completely. If symptoms develop and persist seek medical attention.
<b>First Aid Facilities</b>	Eyewash and normal washroom facilities.
<b>Advice to Doctor</b>	Treat symptomatically.

---

## 5. FIRE FIGHTING MEASURES



---

<b>Suitable Extinguishing Media</b>	Use appropriate fire extinguisher for surrounding environment.
<b>Hazards from Combustion Products</b>	Under fire conditions this product may emit toxic and/or irritating fumes and gases.
<b>Specific Hazards</b>	This product is non combustible.
<b>Precautions in connection with Fire</b>	Fire fighters should wear Self-Contained Breathing Apparatus (SCBA) operated in positive pressure mode and full protective clothing to prevent exposure to vapours or fumes.
<b>Unsuitable Extinguishing Media</b>	Do not use water jets.

---

## 6. ACCIDENTAL RELEASE MEASURES

---

<b>Emergency Procedures</b>	Increase ventilation. Evacuate all unprotected personnel. Wear sufficient respiratory protection and full protective clothing to prevent exposure. Sweep up material avoiding dust generation or dampen spilled material with water to avoid airborne dust, then transfer material to a suitable container. Wash surfaces well with soap and water. Seal all wastes in labelled plastic containers for subsequent recycling or disposal. Dispose of waste according to the applicable local and national regulations. If contamination of sewers or waterways occurs inform the local water authorities and EPA in accordance with local regulations.
-----------------------------	---

---

## 7. HANDLING AND STORAGE

---

<b>Precautions for Safe Handling</b>	Use only in a well ventilated area. Keep containers sealed when not in use. Prevent the build up of dust in the work atmosphere. Avoid inhalation of dust, and skin or eye contact. Maintain high standards of personal hygiene i.e. Washing hands prior to eating, drinking, smoking or using toilet facilities.
<b>Conditions for Safe Storage</b>	Store in a cool, dry, well-ventilated area, out of direct sunlight and moisture. Store in labelled, corrosion-resistant containers. Keep containers tightly closed. Store away from bases, water and other incompatible materials. Have appropriate fire extinguishers available in and near the storage area. Ensure that storage conditions comply with applicable local and national regulations.

---

## 8. EXPOSURE CONTROLS/PERSONAL PROTECTION

---

<b>National</b>	No exposure value assigned for this specific material by the
-----------------	--

<b>Exposure Standards</b>	National Occupational Health and Safety Commission (NOHSC), Australia. However, the available exposure limits for ingredients are listed below:  National Occupational Health And Safety Commission (NOHSC), Australia Exposure Standards: Substance TWA STEL ppm mg/m <sup>3</sup> ppm mg/m <sup>3</sup> Dust - 10 - - Crystalline silica - 0.1 - - TWA (Time Weighted Average): The average airborne concentration of a particular substance when calculated over a normal eight-hour working day, for a five-day week. STEL (Short Term Exposure Limit): The average airborne concentration over a 15 minute period which should not be exceeded at any time during a normal eight-hour workday.
<b>Biological Limit Values</b>	No biological limits allocated.
<b>Engineering Controls</b>	Provide sufficient ventilation to keep airborne levels below the exposure limits. Where dust is generated, particularly in enclosed areas, and natural ventilation is inadequate, a local exhaust ventilation system is required.
<b>Respiratory Protection</b>	If engineering controls are not effective in controlling airborne exposure then an approved respirator with a replaceable dust/particulate filter should be used. Reference should be made to Australian/New Zealand Standards AS/NZS 1715, Selection, Use and Maintenance of Respiratory Protective Devices; and AS/NZS 1716, Respiratory Protective Devices, in order to make any necessary changes for individual circumstances.
<b>Eye Protection</b>	Safety glasses with side shields or chemical goggles should be worn. Final choice of appropriate eye/face protection will vary according to individual circumstances. Eye protection devices should conform with Australian/New Zealand Standard AS/NZS 1337 - Eye Protectors for Industrial Applications.
<b>Hand Protection</b>	Wear gloves of impervious material. Final choice of appropriate gloves will vary according to individual circumstances i.e. methods of handling or according to risk assessments undertaken. Reference should be made to AS/NZS 2161.1: Occupational protective gloves - Selection, use and maintenance.
<b>Body Protection</b>	Suitable protective workwear, e.g. cotton overalls buttoned at neck and wrist is recommended. Industrial clothing should conform to the specifications detailed in AS/NZS 2919: Industrial clothing.

---

## 9. PHYSICAL AND CHEMICAL PROPERTIES

---

<b>Appearance</b>	Light pink, off white impalpable powder or granules
<b>Odour</b>	No distinct odour
<b>Melting Point</b>	Not available
<b>Boiling Point</b>	Not applicable
<b>Solubility in</b>	Insoluble. Forms colloidal suspensions in water, with strong

<b>Water</b>	thixotropic properties.
<b>Specific Gravity</b>	3.30
<b>pH Value</b>	8-10 (20% aqueous slurry)
<b>Vapour Pressure</b>	Not applicable
<b>Vapour Density (Air=1)</b>	Not applicable
<b>Flash Point</b>	Not applicable
<b>Flammability</b>	Non-combustible solid
<b>Auto-Ignition Temperature</b>	Not applicable
<b>Flammable Limits - Lower</b>	Not applicable
<b>Flammable Limits - Upper</b>	Not applicable

---

## 10. STABILITY AND REACTIVITY

---

<b>Chemical Stability</b>	Stable under normal conditions of storage and handling.
<b>Conditions to Avoid</b>	Not available
<b>Incompatible Materials</b>	Not available
<b>Hazardous Decomposition Products</b>	Under fire conditions this product may emit toxic and/or irritating fumes and gases.
<b>Hazardous Polymerization</b>	Will not occur.

---

## 11. TOXICOLOGICAL INFORMATION

---

<b>Toxicology Information</b>	No toxicity data available for this product.
<b>Inhalation</b>	Inhalation of product dust may cause irritation of the nose, throat and respiratory system.
<b>Ingestion</b>	Ingestion of this product may irritate the gastric tract causing nausea and vomiting. When ingested, bentonite can swell several times in volume and can produce intestinal obstruction.
<b>Skin</b>	May be irritating to skin. The symptoms may include redness, itching and swelling.

<b>Eye</b>	May be irritating to eyes. The symptoms may include redness, itching and tearing.
<b>Chronic Effects</b>	Repeated exposure to respirable crystalline silica dust may lead to silicosis, or other serious delayed lung injury. The onset of silicosis is usually slow and lung damage may occur even when no symptoms or signs of ill-health have occurred. Silicosis can develop to a more serious degree even after exposure has ceased, and may also lead to other diseases including heart disease and scleroderma
<b>Carcinogenicity</b>	The product contains a small proportion of respirable crystalline silica as quartz (<4%). Crystalline Silica (respirable size <= 7 µm) has been classified by the International Agency for Research on Cancer (IARC) as Carcinogenic to Humans (Group 1).

---

## 12. ECOLOGICAL INFORMATION

---

<b>Ecotoxicity</b>	No ecological data are available for this material.
<b>Persistence / Degradability</b>	Not available
<b>Mobility</b>	Not available
<b>Environment Protection</b>	Prevent this material entering waterways, drains and sewers.

---

## 13. DISPOSAL CONSIDERATIONS

---

<b>Disposal Considerations</b>	Dispose of waste according to applicable local and national regulations.
--------------------------------	--

---

## 14. TRANSPORT INFORMATION

---

<b>Transport Information</b>	Not classified as Dangerous Goods according to the Australian Code for the Transport of Dangerous Goods by Road and Rail. (7th edition)
------------------------------	---

---

## 15. REGULATORY INFORMATION

---

<b>Regulatory Information</b>	Classified as Hazardous according to criteria of National Occupational Health & Safety Commission (NOHSC), Australia. Not classified as a Scheduled Poison according to the Standard for the Uniform Scheduling of Drugs and Poisons (SUSDP).
<b>Poisons Schedule</b>	Not Scheduled
<b>Hazard Category</b>	Harmful

---

## 16. OTHER INFORMATION

---

**Date of  
preparation or  
last revision  
of MSDS**

MSDS Reviewed: September 2010  
Supersedes: December 2008

**Contact  
Person/Point**

Emergency Advice: ACOHS ERS - 1800 638 556 (24 Hours)

**PLEASE NOTE:**

The information contained herein is based on data available to Sibelco Australia Limited from both our own technical sources and from recognised published references and is believed to be both accurate and reliable. Sibelco Australia Limited has made no effort to censor nor to conceal deleterious aspects of this product. Since we cannot anticipate or control the many different conditions under which this information and our products may be used, each user should review these recommendations in the specific context of the intended application and confirm whether they are appropriate. It is therefore recommended that you undertake your own risk assessment in relation to your method of handling and proposed use of this product. Sibelco Australia Limited accepts no liability whatsoever for damage or injury caused from the use of this information or of suggestions contained herein.

---

End of MSDS

---

(C) Copyright ACOHS Pty Ltd

Copyright in the source code of the HTML, PDF, XML, XFO and any other electronic files rendered by an Infosafe system for Infosafe MSDS displayed is the intellectual property of Acohs Pty Ltd.

Copyright in the layout, presentation and appearance of each Infosafe MSDS displayed is the intellectual property of Acohs Pty Ltd.

The compilation of MSDS's displayed is the intellectual property of Acohs Pty Ltd.

Copying of any MSDS displayed is permitted for personal use only and otherwise is not permitted. In particular the MSDS's displayed cannot be copied for the purpose of sale or licence or for inclusion as part of a collection of MSDS without the express written consent of Acohs Pty Ltd.

Print Date: 05/07/2011

BS: 1.10.9

## Appendix D – Test Report Sheet

### Report Sheet

Test Code: \_\_\_\_\_ Date: / /

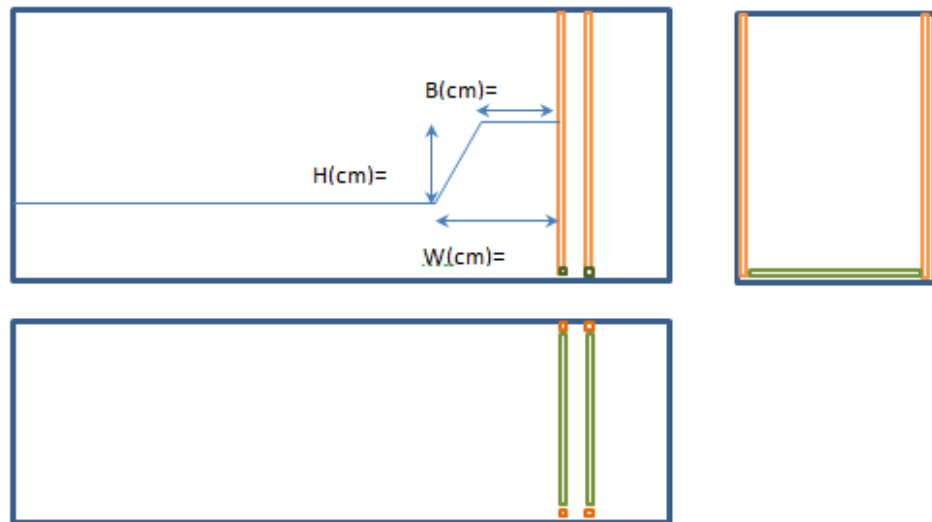
Sample Code: \_\_\_\_\_ File Name: \_\_\_\_\_

Time Start: : : Finish: : : :

Test Type: Saturation  Moving up

Container angle before test: ..... ° (Degree)

Material: Soil: % ..... Bentonite: % ..... Water: % .....



Note:

.....

.....

.....

.....

<p>Test Code:  A0, A5, A10, S - 1, 2, 3...  A0: Start align in 0° - A5: Start in 5°  A10: Start in 10° - S: Saturated</p>	<p>Sample Code:  S,SB5,SB10 - D,W5,W10  S: Sand - SB5: Sand+Bentonite%5  SB10: Sand+Bentonite%10 - D:Dry  W5: Water%5 – W10: Water%10</p>
---	---